5-2023

Functions Of The Trna Splicing Endonuclease And Other Adventures In Rna Processing

Jennifer Hurtig

Ambro van Hoof

Functions of the tRNA splicing endonuclease and other adventures in RNA processing

by

Jennifer E. Hurtig

APPROVED:

_____
Ambro van Hoof, Ph.D.
Advisory Professor

_____
Kevin Morano, Ph.D.

_____
Nayun Kim, Ph.D.

_____
Nicholas DeLay, Ph.D.

_____
Neal Waxham, Ph.D.

APPROVED:

_____
Dean, The University of Texas
MD Anderson Cancer Center UTHealth Graduate School of Biomedical Sciences

Functions of the tRNA splicing endonuclease and other adventures in RNA processing

A

Dissertation

Presented to the Faculty of

The University of Texas

MD Anderson Cancer Center UTHealth

Graduate School of Biomedical Sciences

in Partial Fulfillment

of the Requirements

for the Degree of

Doctor of Philosophy

by

Jennifer E. Hurtig
Houston, Texas

May, 2023

Acknowledgements

Of course I must thank my advisor Ambro van Hoof for allowing me to research in his lab. I have been a very demanding student both emotionally and scientifically and Ambro has taken all of it in stride. I cannot count the number of times Ambro has had to talk me down from some type of panic including but not limited to AI taking my job, never finding a job, not being able to spell, and having the worst blots of anyone in the world. I will forever cherish the memories and lessons from my time as his mentee.

My lab members are the absolute best. LeeAnn is my ray of sunshine, Sayef strokes my ego constantly, and Catherine keeps me entertained. They are, of course, all superstars smarter than me and I can't wait to work for one of them. I will miss them and the fantastically strange work environment we have created. Sarah Lach has become one of my best friends and an honorary van Hooligan. Thanks for all the support, fun, and super random facts.

Past lab members including Minseon Kim and Jill Losh have given me so much guidance and encouragement. Jill Losh has become like a big sister to me with our weekly trips to the dog park turning into me venting while she patiently listens and encourages. Her dog, Lucy, is often more excited to see me than my own dog which is so sweet. Luisa Orlando kept me sane during the whole COVID pandemic. We had some great laughs and some epic cries.

The MMG department and MID program are truly amazing. This department definitely has the best mentors, and all the students feel like friends. No one is more deserving of the department chair position than Mike Lorenz as I know he will make the department even more awesome. Carolyn Parker is truly an amazing multi-tasker. She helps us with literally anything from administration to personal. She also feeds us so she has all of our hearts. Poor Justin

Mayberry must deal with me far too often. His kindness, patience, and humor are something I hope no one will ever take for granted.

I must thank my past mentors who have gotten me to this point. James West saw how desperate I was to have a shot at making it into research and helped me get an internship here at UT Health. Without that internship I would have never had a chance at being accepted to graduate school. He was always honest with me about my numerous flaws and helped me realize my strengths and how to utilize them. Kevin Morano allowed me into his lab that summer where I basically just took up space while running horrendous Western blots for Dr. West. His recommendation got me to this point. I hope neither of them regret taking a chance on me and that I can make them proud in the future. Brian Carlson helped me realize that I wanted to do research. He was always over complementary even telling me I could teach if I wanted. Without his encouragement, I never would have applied to graduate school.

My parents have of course been supportive both emotionally and financially. They have also given me space when I needed it including while writing this thesis which I appreciate more than they know. Though they have no clue what I do, they always act interested and supportive and say how proud they are. They also brag about me to friends and neighbors which is really cute. Even when others say that I will not be a 'real doctor' they stick up for me.

My partner Tony Weber is my rock. Thank you for letting me be myself, giving me unconditional support, and letting me watch *Bob's Burgers* so many times we probably both have the episodes memorized.

Lastly, my pets are my life. I left my precious Speedy-bump in Ohio with my parents but he is in my heart every moment. Along this journey, I lost my dear, sweet Moxie cat to kidney failure at the age of 14. I will never forgive myself but I hope she was happy with the 5

years we had together. Since her passing, we adopted Dax who is an utterly bizarre, little monster but makes up for it with all her cuddles and kisses. I work so I can afford nice things for Eevee. She runs the house and we just live in it. Thanks for always wagging your tail when I come home. It makes me feel like I am wanted even after a bad day. I could really do without the hair pulling though.

Functions of the tRNA splicing endonuclease and other adventures in RNA processing

Jennifer E. Hurtig

Advisory Professor: Ambro van Hoof, Ph.D.

The tRNA splicing endonuclease (TSEN), has been studied for over three decades for its function in tRNA splicing. However, this enzyme has other functions that are just beginning to be characterized. Mutations in TSEN cause the neuronal disease pontocerebellar hypoplasia (PCH) that is characterized by atrophy of the cerebellum and pons, overall developmental failure, and usually results in death before adolescence. How mutations in TSEN cause these neuronal defects and disease is not understood. In yeast, TSEN has another essential function that is independent of tRNA splicing and is still unknown. In this thesis I strived to understand the other function of the TSEN complex. TSEN has one mRNA target in yeast which led me to the hypothesis that TSEN could cleave other mRNAs. I used Parallel Analysis of RNA Ends (PARE) to identify other mRNA substrates of TSEN. I found TSEN cleaves a subset of mRNAs that encode mitochondrial localized proteins. In vivo and in vitro analysis determine TSEN recognizes an A before its cleavage sites. We identified some sequence and localization requirements for TSEN targets but it is likely other factors play a role in substrate recognition such as structure of the mRNA target. Overall we used PARE to identify a novel endonuclease decay pathway, termed TED, in which TSEN can degrade a select group of mRNAs. Yeast genetic screens were used to complement our RNAseq approach to finding the other essential function of TSEN. A spontaneous suppressor screen identified mutations in Dbr1 as suppressors of only the other essential function a mutant sen2. Because mutations in Dbr1 could only complement a partially functional TSEN complex and the catalytic activity of Dbr1 must be lost for this suppression, we propose that Dbr1 and TSEN complete for a common substrate. Through RNAseq, we discovered that loss of the other essential function

of TSEN triggers the Gcn4 response. This response is protective in our sen2 mutant and when Dbr1 is mutated in addition to sen2, the Gcn4 response is reduced as TSEN now has no competition for substrate to perform its essential function. As TSEN is involved in mRNA decay through the TED pathway, I wondered what enzymes could be involved in the degradation of these cleavage products. To investigate this, we used PARE to define targets of the exonuclease Dxo1 and the kinase Trl1. This revealed Dxo1 can “nibble” downstream of endonuclease cleavage and decapping but that its main function is in processing the 25S’ to the 25S rRNA in the cytoplasm. Trl1 can also act downstream of endonuclease decay in the TED pathway by phosphorylating the 5’ end of TSEN cleavage products. Though the other essential function of TSEN remains elusive, this research uncovered the participation of TSEN in mRNA decay and the functions of downstream enzymes as well as the identification of a potential competitor, Dbr1.

Table of Contents

Table of Figures

Table of Tables

1) Introduction

Introduction to RNA processing

RNA is the mediator between DNA and protein, genotype and phenotype, the intermediary molecule in the central dogma. The diversity of life can only partially be explained by differences at the genomic level. The expression level of genes and their splicing variants contribute to the heterogeneity of life. In addition to mRNAs, non-coding RNAs such as miRNAs, tRNAs and others influence levels of RNA and proteins and ultimately the phenotypic outcome. To further underscore the impact of RNA, the RNA world hypothesis posits that RNA molecules were the catalyst of life itself as they code genetic information and can perform chemical reactions (Joyce, 1989). A reflection of this RNA world may be that key reactions central to life, such as splicing and translation, are still catalyzed by RNA. As RNA is so critical, its regulation through RNA processing and degradation are highly complex and regulated. RNA processing and degradation pathways control the birth and death of RNA, respectively and are ancient and essential processes that occur throughout the three domains of life. Pre-mRNAs can go through three major steps of RNA processing, 5' capping, 3' polyadenylation, and splicing. 5' 7-methyl-guanosine caps are added to the pre-mRNA to prevent the newly synthesized mRNA from being degraded as well as aid in its export to the ribosomes in the cytoplasm. The 3' poly(A) tail is a series of adenosine bases added to the pre-mRNA which, like the cap, protects the RNA from degradation and may play a role in translation efficiency of the mRNA.

Splicing; diverse mechanisms to remove introns from mRNAs and ncRNAs

The third subprocess pre-mRNAs can undergo is splicing in which the intronic sequences, interspersed between coding region, are removed from the RNA. Typically, more complex eukaryotes such as humans and plants have larger genomes with more introns and

splicing events especially when compared to bacteria and single-cell fungi. Alternative splicing allows several isoforms to be produced from a single RNA and creates proteins with different functions originating from the same gene. Splicing is one way viruses can diversify their transcriptomes. Viruses produce the necessary proteins to invade and hijack the replication machinery of the host cell from a relatively small pool of RNAs with some viral genomes being less than 2 kb. Splicing can generate diverse viral machinery by creating several distinct proteins from the same sequence.

In eukaryotes, the majority of mRNA splicing is conducted by the multi-subunit protein-RNA complex, the spliceosome (reviewed in Matera and Wang, 2014). The RNA components of the spliceosome, snRNAs, allow the spliceosome to target the intron/exon junction. Several types of proteins are also associated with the spliceosome including helicases and WD box proteins that regulate the structure of the RNA. The splicing reaction is then catalyzed by the RNA-protein complexes U6, U2, and U5 which, in brief, allow the 2' hydroxyl of the intron to attack the 5' splice site, forming a loop. The now free 3' hydroxyl of the 5' exon then attacks the 3' splice site, resulting in the ligation of the two exons and release of the looped intron. This creates the mature spliced mRNA and a lariat intron (Matera and Wang, 2014). It is worth noting that the degradation of these lariat introns is also important. Dbr1, or the lariat debranching enzyme, is a phosphodiesterase that opens the ring-like structure of the intron which allows it to be degraded (Chapman and Boeke, 1991; Khalid et al., 2005).

There are several examples of non-spliceosomal splicing that take place in both non-coding RNAs and mRNAs. Group I and II introns are self-catalyzing, forming ribozymes that enable similar transesterification reactions that occur during spliceosomal splicing, although group I introns require attack by a guanosine cofactor rather than the 2' hydroxyl of the intron. Though group II introns are found in bacteria and organelles of eukaryotes and archaea, group I can also be found in the nuclear genomes of eukaryotes (Saldanha et al., 1993).

Non-spliceosomal splicing can also be catalyzed by endoribonuclease proteins, enzymes that cleave within an RNA sequence, and ligases that join the two exons together. All eukaryotes have tRNAs with introns that are spliced out through endonuclease cleavage and ligation. The tRNA spicing endonuclease (TSEN) cleaves at either end of the intron while a tRNA ligase fuses the two exons together. Though TSEN is conserved between fungi and metazoans, the identity and mechanisms of the ligase differs between the fungal ligase, Trl1, and RtcB of metazoans and bacteria (see Table 1.1 for list of ribonucleases) (Abelson et al., 1998). Endonucleases can also catalyze splicing of mRNAs, with the best example being cleavage of *HAC1* by the endonuclease Ire1 in yeast (Gonzalez et al., 1999; Sidrauski and Walter, 1997). During normal or stressless conditions, the *HAC1* transcript is unspliced and the full-length RNA is targeted for degradation rather than translation. During the unfolded protein response (UPR), Ire1, located on the membrane of the ER, responds to unfolded proteins by forming a dimer. The Ire1 homodimer then cuts either side of the intron within *HAC1* mRNA (Cherry et al., 2019; Gonzalez et al., 1999; Sidrauski and Walter, 1997). Similar to tRNA processing, the enzyme Trl1 or RtcB ligates the two ends of the exons (Cherry et al., 2019; Kosmaczewski et al., 2014; Sidrauski et al., 1996). Instead of being degraded, this spliced transcript is then translated into a transcription factor that upregulates many factors involved in the stress response (Chapman and Walter, 1997; Mori et al., 1996). This process is conserved between yeast and humans as human IRE1 excises the intron from *XBP1* mRNA and the exons are then ligated together by RTCB (Kosmaczewski et al., 2014; Lee et al., 2002). Though there are fewer examples of atypical splicing compared to events catalyzed by the spliceosome, both contribute to cellular processes and survival.

Eukaryotic RNA degradation is catalyzed by a large number of diverse ribonucleases

RNA processing is a complex set of mechanisms that creates and protects the mature RNA; however, degradation of RNA is also an essential process with many moving parts.

When an RNA is aberrant, damaged, or no longer useful, it must be degraded. RNA degradation is involved in maintaining the steady state level of RNA and a key mechanism in transcription regulation. RNA can be degraded by three classes of RNases. Exonucleases remove one base at a time from either the 5’ or 3’ end of the RNA and are responsible for the majority of RNA degradation. However, endonucleases can also participate in RNA degradation as internal cleavage of an RNA can initiate decay of the resulting products by other RNases. Though mRNA decay occurs both in the cytoplasm and nucleus, the major pathways for bulk mRNA decay occur in the cytoplasm while nuclear decay is more associated with quality control (Garneau et al., 2007). Table 1.1 provides an overview of some of the major proteins that contribute to RNA processing and decay.

Table 1.1: RNA processing enzymes and their functions

Enzyme Yeast/HUMAN	Family/Function	Characterized Roles
CLP1	Kinase	Part of human TSEN, phosphorylates pre-tRNA, 3' end processing
Cue2/N4BP2	Endo	Cleaves aberrant RNAs where ribosomes have stalled
Dbr1	phosphodiesterase	Linearizes lariat introns
Dcp1/2	Decapping	Removes canonical caps from mRNAs
DXO	5' to 3' Exo	Removes 5' hydroxyls, phosphates, and non-canonical caps
Dxo1	Decapping and Exo?	Non-canonical decapping, possible exonuclease
EndA (archaea)	Endo	Endonuclease, archaeal predecessor of TSEN
Hac1/XBP1	Transcription factor	Regulates the UPR, cleaved by Ire1
Ire1	Endo	Removes intron from *HAC1* to activate UPR
Rai1	Decapping	Removes non-canonical or incomplete caps
Rat1/XRN2	5' to 3' Exo	Primary nuclear 5' to 3' exonuclease
Rrp44/DIS3	3' to 5' exo and endo	Primary 3' to 5' exonuclease, catalytic subunit of the RNA exosome
RTCB	Ligase	tRNA ligase, also ligates *XBP1* exons
Ski complex	Helicase/cofactor	Cofactor of cytoplasmic exosome, aids in non-stop decay
SMG6	Endo	Cleaves aberrant RNA during no-go decay
Tpt1	phosphotransferase	Removes 2' phosphate from pre-tRNA
Trl1	Kinase/ligase/ phosphodiesterase	Ligase for tRNA and Hac1 splicing, kinase activity in No-go decay
TSEN complex	Endo	Removes introns from pre-tRNAs
Xrn1	5' to 3' Exo	Primary cytoplasmic 5' to 3' exonuclease

5’ to 3’ RNA decay

5’ to 3’ exonuclease degradation is the dominant pathway for eukaryotic mRNA turnover. First, the cap added during mRNA maturation which protects the RNAs from degradation must be removed. Decapping requires a variety of enzymes and accessory proteins (Coller and Parker, 2004). The canonical decapping enzyme is Dcp2 which is conserved between yeast and humans and essential in the former (Kim and van Hoof, 2020). In vitro, this enzyme has activity on m7G 5’ caps but in vivo, co-factors such as Dcp1, Edcs, and Lsms, are required to stimulate decapping activity (Wurm and Sprangers, 2019). Although Dcp2 is the canonical decapping enzyme, other enzymes can perform similar functions. Dcp2 is a member of the NUDIX hydrolase superfamily and like Dcp2, some other enzymes from this family also catalyze decapping (Kramer and McLennan, 2019). In addition, other families of decapping enzymes have been identified including the Rai1/Dxo1/DXO family that removes a variety of 5’ ends from RNAs. Most eukaryotic genomes encode a single family member, but *Saccharomyces cerevisiae* and the close relative *K. lactis* have two paralogs. Though in vitro data has defined some of the varying functions of these enzymes across species, in vivo information on most of the individual members and their unique functions is lacking. For example, the *K. lactis* Rai1 can remove non-canonical 5’ cap such as FAD, CoA, NAD, unmethylated, or incomplete caps, none of which are substrates of the major decapping enzyme Dcp2 (Chang et al., 2012). The human DXO enzyme can remove these non-canonical caps but can also remove 5’ hydroxyls and 5’ monophosphates from uncapped ends, blurring the line between decapping enzymes and 5’ exonucleases (Doamekpor et al., 2020a, 2020b). Cellular localization of the family members within a species may also be important in determining their function. DXO and Din1 are the only family members in human and *S. pombe*, respectively, and are primarily nuclear (Shobuike et al., 2001; Xue et al., 2000) while the *S. cerevisiae* paralogs Rai1 and Dxo1 are nuclear and cytoplasmic, respectively (Chang

et al., 2012; Huh et al., 2003; Krzyszton et al., 2012). The function of *S. cerevisiae* Dxo1 is largely uncharacterized though in vitro work with *K. lactis* Dxo1 showed the enzyme has exonuclease activity and the capacity to remove some types of caps (Chang et al., 2012). Despite similar in vitro findings, the difference in localization between Rai1 and Dxo1 suggests they have their own unique functions and substrates. Deciphering the roles of individual proteins in the Rai1/Dxo1/DXO family will lead to insight about the evolution of these enzymes as well as potentially novel players and pathways in RNA decay and processing.

Both the canonical and noncanonical decapping enzymes produce RNAs with a 5' monophosphate, which makes the transcript a target for 5' to 3' RNA decay. 5' to 3' decay of uncapped mRNAs is primarily mediated by Xrn1, the major cytoplasmic 5' to 3' exonuclease (Garneau et al., 2007; Larimer and Stevens, 1990). Deletion of Xrn1 in yeast results in slow growth (Larimer and Stevens, 1990), while in humans XRN1 is likely essential (Jones et al., 2013; Newbury and Woollard, 2004; Takaoka et al., 2021), highlighting the importance of this pathway. Xrn1 has a nuclear homolog, Rat1 (XRN2 in humans) which is essential in yeast (Johnson, 1997). Rat1 is involved in rRNA processing as well as RNA quality control (Krzyszton et al., 2012). Both Xrn1 and Rat1 have high activity on 5' monophosphates but some functional groups like 5' hydroxyls and triphosphates are not a preferred substrate of Xrn1 and are trimmed or fully degraded by other enzymes (Garneau et al., 2007; Jinek et al., 2011; Nagarajan et al., 2013).

3' to 5' RNA decay

Exonucleases that remove bases from the 3' to 5' direction also contribute to RNA decay. The major enzyme responsible for this pathway is the RNA exosome. The RNA exosome is composed of nine protein subunits which make up a cap and barrel structure (Chlebowski et al., 2013; Schneider and Tollervey, 2013; Wasmuth and Lima, 2012). The RNA is threaded through the cap and barrel towards the catalytic subunit Rrp44. Some RNA can

bypass the barrel structure and still be degraded by Rrp44 though this appears to be less productive (Delan-Forino et al., 2017). The RNA exosome has many different cofactors that vary based on its localization and function. Among these cofactors are the RNA helicases Ski2 and Mtr4. Both the RNA exosome and its cofactors are widely conserved throughout eukaryotes. In yeast, the RNA exosome and many of its nuclear cofactors such as Mtr4, are essential as its role in rRNA processing is indispensable (Allmang et al., 1999a, 1999b; Mitchell et al., 1997). In the cytoplasm, the yeast RNA exosome is often associated with the Ski complex. The Ski complex is composed of two Ski8 subunits that associate with Ski2, the active helicase subunit, and Ski3 (Anderson and Parker, 1998). Ski7 then binds to the cap of the RNA exosome and anchors the Ski complex to the RNA exosome. Although the cytoplasmic RNA exosome plays an important role in RNA surveillance and mRNA decay (Frischmeyer et al., 2002; Januszyk and Lima, 2014; van Hoof et al., 2002; Wasmuth and Lima, 2012), the redundancy with the more efficient 5' to 3' degradation pathways allow RNA degradation even when the exosome is inactivated. However, when Xrn1 is deleted or impaired, the Ski complex and therefore the cytoplasmic exosome activity becomes essential. Thus, as long as either the major 3' to 5' or 5' to 3' exonuclease is active in the cytoplasm, the cell can survive, but loss of both pathways is lethal (Johnson and Kolodner, 1995). As previously stated, the RNA exosome seems to play a larger role in RNA quality control than in steady state maintenance of RNA levels. For example, in non-stop decay, the ribosome fails to identify a stop codon and eventually the ribosomes stall on the mRNA (Schaeffer and van Hoof, 2011; Schmid and Jensen, 2008; van Hoof et al., 2002). The C-terminal region of Ski7 is required to recognize this stall and directs the RNA exosome to the non-stop transcript for decay of the RNA, and release of the stalled ribosome.

Endonuclease mediated decay

Though degradation from either the 5’ or 3’ end of the RNA are common pathways for RNA turnover, emerging studies suggest endonucleases also play a role in RNA decay. One example of this is the endonuclease Ire1, which cleaves within some RNAs to initiate their degradation. As previously discussed, Ire1 activates the UPR through atypical splicing in which Ire1 cuts on either side of the HAC1 intron (Gonzalez et al., 1999; Sidrauski and Walter, 1997). However, Ire1 can also perform RNA degradation during the UPR. In a process termed RIDD (Regulated Ire1 Dependent Decay), Ire1 cleaves a subset of mRNAs based on sequence and proximity to the ER (Dufey et al., 2020; Hollien et al., 2009; Hollien and Weissman, 2006; Mishiba et al., 2013; Moore and Hollien, 2015; Tam et al., 2014). The pieces of these RNAs are then degraded by Xrn1 and the RNA exosome. RIDD likely occurs in the cell at basal levels but increases upon detection of unfolded proteins (Dufey et al., 2020; Hollien and Weissman, 2006; Mishiba et al., 2013; Moore and Hollien, 2015; Tam et al., 2014). Interestingly, the two functions of Ire1, RIDD and *HAC1* splicing, can both be UPR dependent but are hypothesized to lead to different survival outcomes (Tam et al., 2014). Splicing of *HAC1* mRNA and the downstream impact of the active Hac1 transcription factor, may promote cell survival during the UPR while RIDD prompts apoptosis (Tam et al., 2014). The mechanism by which Ire1 determines which function to perform is still unclear. Though RIDD has been well defined in *S. pombe* and metazoan cells, some RIDD-like targets have been posited in *S. cerevisiae*, including Dap2 and Mat-α though these results have not been reproducible in vivo (Tam et al., 2014). At least in vitro, human IRE1 recognizes a stem-loop with the sequence CUGCAG (Moore and Hollien, 2015). Ire1 is an endonuclease, that similarly to TSEN, produces a 5’ hydroxyl and 2’3’ phosphate (Gonzalez et al., 1999; Shigematsu et al., 2018). During RIDD, the cleavage products of Ire1 must be degraded by an exonuclease although it is still unclear how the resulting 5’ hydroxyl and 2’3’ phosphate are resolved to be degraded by Xrn1 and the RNA exosome, respectively (Hollien and Weissman, 2006).

Endonuclease decay is also involved in surveillance and disposal of aberrant RNAs. In metazoans, an endonuclease initiates nonsense-mediated decay (NMD) that occurs when a premature stop causes ribosomes to terminate while translating the RNA (Lykke-Andersen et al., 2014). The terminating ribosomes are recognized by UPF1 which recruits the endonuclease SMG6. SMG6 cleaves the RNA near the premature termination codon to initiate RNA decay and recycling of ribosomes through the ribosomal quality control pathway (RQC) (Eberle et al., 2009; Huntzinger et al., 2008; Schmidt et al., 2015). The cleavage products of SMG6 are then degraded, primarily by Xrn1 and the RNA exosome. Endonucleases also participate in No-Go decay and Non-stop decay, aberrant RNA decay pathways that occur when ribosomes stall during elongation (Powers et al., 2020). This can lead to ribosomes piling up behind one another and cause ribosomal collisions which the cell senses to triggers aberrant RNA decay mechanisms. Ubiquitin ligases such as yeast Hel2, detect the collided ribosomes and mark them for dissociation from the RNA and recycling (Matsuo et al., 2017). As for the mRNA, an endonuclease, Cue2 in yeast, recognizes ubiquitinated ribosomes and cleaves the mRNA to begin degradation by exonucleases (D'Orazio et al., 2019).

One interesting endonuclease was discovered over a decade ago, but its function still remains uncharacterized. The catalytic subunit of the RNA exosome, Rrp44, not only has exonuclease activity but also endonuclease activity (Lebreton et al., 2008; Schaeffer et al., 2009; Schneider et al., 2009). Rrp44 has a PIN domain that is conserved between yeast and humans. This domain has been shown to have *in vitro* endonuclease activity; however, bona fide in vivo targets have yet to be identified. Microarray analysis and CRAC (in vivo crosslinking of protein-RNA complexes) of endonuclease mutant strains revealed no significant transcriptomic changes or targets, respectively (Schneider et al., 2012; Tsanova et al., 2014). Mutations that inactivate the PIN domain in yeast are not lethal just as inactivation

of the exonuclease activity of Rrp44 is not lethal. However, mutation of both the exo- and endo- domains are lethal (Lebreton et al., 2008; Schaeffer et al., 2009; Schneider et al., 2009). It has also been shown that either domain can perform non-stop decay while only the exonuclease domain seems to be involved in normal mRNA decay (Schaeffer and van Hoof, 2011). Despite its conservation, in vitro activity, and synthetic lethality with the exo- domain, the function of the endonuclease domain in RNA processing and decay is still unknown. There are still many endonucleases with unknown functions to characterize.

In many, perhaps all, of these cases, endonuclease cleavage is followed by Xrn1-mediated 5' to 3' decay. Interestingly, some endonucleases including Ire1 and Cue2 produce a product with a 5' hydroxyl termini during cleavage, that are not preferred substrates for Xrn1 (Gasse et al., 2015; Gonzalez et al., 1999; Ho et al., 1990; Shigematsu et al., 2018). In yeast, Trl1 phosphorylates Cue2 products to a 5' phosphate which is then rapidly degraded by Xrn1 (Navickas et al., 2020). The human homolog of Cue2, N4BP2, also produces a fragment with a 5' hydroxyl, but humans lack Trl1 and thus, there must be other enzymes that act on 5' hydroxylated RNAs (Nicholson-Shaw et al., 2022). The endonucleases that produce 5' hydroxyls also produce 2'3' cyclic phosphates on the 5' cleavage product. It is unknown if the RNA exosome can efficiently degrade these ends. The human Angel1 enzyme acts as a cyclic phosphodiesterase and opens the 2'3' cyclic phosphate ring, which has been proposed to allow degradation by the RNA exosome (Nicholson-Shaw et al., 2022). Angel1 is a member of the Exonuclease Endonuclease Phosphatase (EEP) family which has family members in yeast, Ngl2 and Ngl3. These proteins are thought to be 3' exonucleases, but their ability to hydrolyze 2'3' cyclic phosphates has not been tested (Faber et al., 2002; Feddersen et al., 2012).

Overview and evolution of TSEN

Though TSEN has been extensively studied for its role in tRNA splicing, it also participates in mRNA decay. Before this is discussed, I will further explore the TSEN complex and its canonical function.

tRNA introns can be found in all three domains of life. The function of these introns is still not fully understood but their conservation suggests that they perform some function. In yeast, ten different tRNAs are encoded by intron-containing genes or gene families (with up to ten members per family). One study created ten different strains with each one lacking all of the introns for a specific tRNA family (Hayashi et al., 2019). They found these tRNA introns were not essential for yeast viability under normal conditions but some intronless tRNAs lead to cold sensitive, slow growing, or respiratory defective mutants suggesting there is a physiological role for tRNA introns (Hayashi et al., 2019). There are some tRNA modifications that depend on the presence of the intron, including formation of the pseudouridines in tRNA Tyr(GUA) and Ile(UAU) and methylation of a cytosine in Leu(CAA) (Johnson and Abelson, 1983; Strobel and Abelson, 1986; Szweykowska-Kulinska et al., 1994). The enzymes that modify these residues (Pus7, Pus1, and Trm4) are thought to recognize the pre-tRNA structure. Without the intron, these modifications do not occur. This can affect decoding fidelity, leading to incorrect incorporation of amino acids into proteins (Hayashi et al., 2019; Schmidt and Matera, 2020). Overall, we currently know tRNA introns are important for some modifications and regulation, though more research is needed in this area.

As the presence of tRNA introns is highly conserved, so is the machinery to remove them. TSEN is a highly conserved, essential complex consisting of four subunits. Two subunits, Sen2 and Sen34 are catalytic subunits while Sen15 and Sen54 are structural (Hayne et al., 2022b; Rauhut et al., 1990; Trotta et al., 1997). Although the four subunits are distinct, they are very distantly related and have a similar structure. It has been proposed that Sen54

and Sen2 form a dimer while Sen15 and Sen34 form a separate dimer that can then associate together to form the full heterotetramer (Li et al., 1998; Trotta et al., 1997). The catalytic subunits of TSEN, Sen2 and Sen34, must cooperate to cleave the 5' and 3' end of the intron, respectively (Greer et al., 1987; Reyes and Abelson, 1988; Trotta et al., 1997), with Sen2 contributing important catalytic subunits for 5' cleavage and Sen34 contributing to RNA binding. Surprisingly, the reverse does not appear to be true, as residues of Sen2 are dispensable for Sen34 cleavage in vitro (Trotta et al., 2006).

Homologs of TSEN can be found throughout eukaryotes and even archaea. In archaea, the TSEN homolog is EndA and by examining the subunit composition and structure of EndA, we can begin to imagine how the modern eukaryotic TSEN complex originated (Yoshihisa, 2014). EndA can be arranged in α4, where the homotetramer is made of the same subunit although in two different conformations. Two of the subunits take on a catalytic fold, while the other two are inactive/structural (Figure 1.1). EndA can also have a $(\alpha\beta)_2$ homodimer of heterodimers arrangement consisting of two types of subunits, a catalytic (α) and structural (β) subunit that form two heterodimers which associate to form the tetramer (Yoshihisa, 2014). One can easily imagine how EndA is the basis for the eukaryotic TSEN complex. Duplication could have made two copies of the genes encoding the catalytic and structural subunits. Overtime these genes evolved to form four distinct subunits making a αβγδ complex, like the yeast and human TSEN complexes. The αβγδ TSEN form is often referred to as eukaryotic TSEN but may only occur in unikonta (a group that contains animals, fungi and Amoebozoa), but not in early diverging eukaryotes such as plants and parasites.

As archaeal and eukaryotic TSENs share structural similarities, they also share some aspects of substrate recognition. EndA has been shown to recognize a bulge-helix-bulge secondary structure within the pre-tRNA (Fujishima and Kanai, 2014; Yoshihisa, 2014). A similar structure is often found in the intron containing anti-codon loop in unikonta TSEN

substrates. In vitro, introducing a bulge-helix-bulge into a non-tRNA RNA was sufficient for TSEN cleavage (Fruscoloni et al., 2001). TSEN can also cleave a hybrid pre-tRNA substrate with sequences and features from archaea demonstrating their conservation (Fabbri et al., 1998). Though EndA and TSEN share this basic structural recognition, how TSEN cleaves at the splice sites involves more complex mechanisms and even measurements.

TSEN substrate recognition, catalysis, and structure

In eukaryotes, tRNA introns are found in the anticodon loop and begin at the second nucleotide downstream of the anticodon. Two bases upstream of the anticodon is position CP1 or the A position (Figure 1.2) (Baldi et al., 1992; Bufardeci et al., 1993; Negri et al., 1997). This A site base-pairs with the I site located three bases downstream of the 3' cleavage site. The A site is a pyrimidine in all yeast and human pre-tRNAs, and this seems important for 5' splice site recognition. Therefore, the I site must be a purine to allow base-pairing which is especially important for Sen34 cleavage at the 3' splice site (Baldi et al., 1992; Bufardeci et al., 1993; Negri et al., 1997). Position CP2, the first base of the 3' exon, is important for binding of TSEN (Baldi et al., 1992). The position of these bases relative to the anticodon and splice sites is conserved throughout eukaryotic intron-containing tRNAs, demonstrating the importance these positions have on the ability of TSEN to recognize the tRNA substrate. As such, a ruler mechanism has been proposed by which Sen54 "measures" the position of the 5' splice site to allow correct cleavage by Sen2 (Calvin and Li, 2008; Chatterjee et al., 2018; Phizicky and Hopper, 2010). The length of the anticodon stem as well as the position of CP1 two bases upstream of the anticodon, allow correct alignment of TSEN so Sen2 can cleave five bases downstream of the CP1 site. Thus sequence, secondary structure, and tertiary structure all play a role in eukaryotic TSEN recognition of intron containing tRNAs substrates.

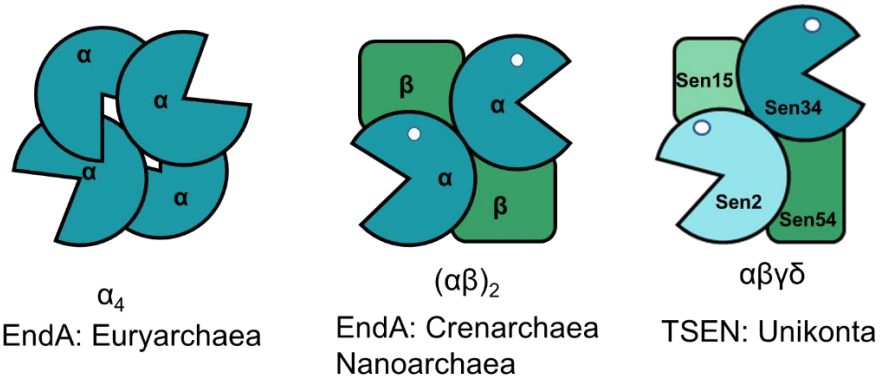

Figure 1.1: Subunit composition of TSEN homolog, EndA, and eukaryotic TSEN.

EndA can be made of four of the same subunits, a homotetramer. There can also be two different subunits in which one is structural and one is catalytic. A duplication in these genes likely resulted in the four distinct subunits of the eukaryotic TSEN (Yoshihisa, 2014).

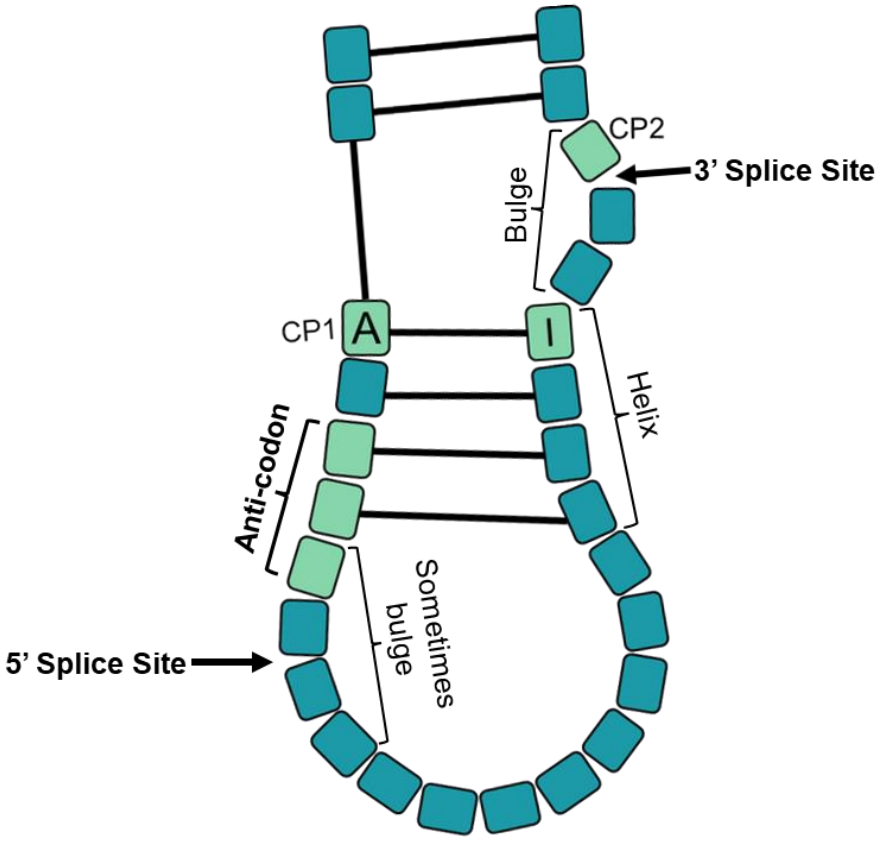

Figure 1.2: Elements recognized by eukaryotic TSEN complex.

Compared to archaea, which generally recognize a bulge-helix-bulge structure, eukaryotic TSEN has additional criteria for substrates (Yoshihisa, 2014). First, five bases upstream of the 5' splice site is base CP1 (Baldi et al., 1992; Bufardeci et al., 1993; Negri et al., 1997). This base forms the A-I pair and creates a structure that resembles a bulge-helix-bulge, though it can be largely more relaxed. CP2 is recognized by TSEN and occurs just downstream of the 3' splice site. The I site which is the other element for base pairing, is 3 bases upstream of CP2 (Baldi et al., 1992; Bufardeci et al., 1993; Negri et al., 1997).

To examine the catalysis of eukaryotic TSEN on pre-tRNA, we turn to the yeast enzyme. In yeast, it has also been found that the two catalytic subunits may have a shared active site (Trotta et al., 2006). Sen2 has an active site histidine (His297) that is essential for 5' cleavage. Likewise, Sen34 has an active site histidine (His217) that is required for 3' cleavage. In vitro data suggests that residues from Sen34, (Arg243 and Trp271), contribute to 5' cleavage by Sen2 (Trotta et al., 2006). Based on similarity to the archaeal enzyme, Arg243 and Trp271 are thought to stack with the base of nucleotide -2. Additionally, the active site histidine also stacks on the base at +1. This cooperative triad is thought to aid in the positioning of Sen2 to allow cleavage at the proper splice site. However, the reverse does not appear to be true for Sen2. When equivalent residues of Sen2 (Arg321 and Trp348) are mutated, in vitro data shows no effect on 3' cleavage by Sen34 (Trotta et al., 2006). Therefore, it appears that Sen34 relies strictly on the bulge-helix-bulge and A-I pairing to position itself correctly for cleavage of the pre-tRNA without influence from Sen2 (Hayne et al., 2022b, 2022a; Sekulovski et al., 2022). Outside of positioning, the basic cleavage reactions of Sen2 and Sen34 on tRNA are the same. Three residues on each catalytic subunit participate in their respective splice site cleavage (Figure 1.3). A tyrosine residue (Sen2-Tyr289, Sen34-Tyr209) acts as a general base and deprotonates the 2' hydroxyl of the ribose (Calvin and Li, 2008; Li et al., 1998). This results in a 2'O^- which acts as a nucleophile and attacks the phosphate group that makes up the RNA backbone. This forms an unstable negatively charged pentavalent transition state which is stabilized by a positively charged lysine residue (Sen2-Lys328, Sen34-Lys250) (Calvin and Li, 2008; Li et al., 1998). Finally, the active site histidine acts as a general acid donating a hydrogen to an oxygen molecule of the phosphate backbone, which then acts as the leaving group. This results in a 3' fragment with a 5' hydroxyl and a 5' fragment with a 2'3' cyclic phosphate (Ho et al., 1990; Peebles et al., 1983).

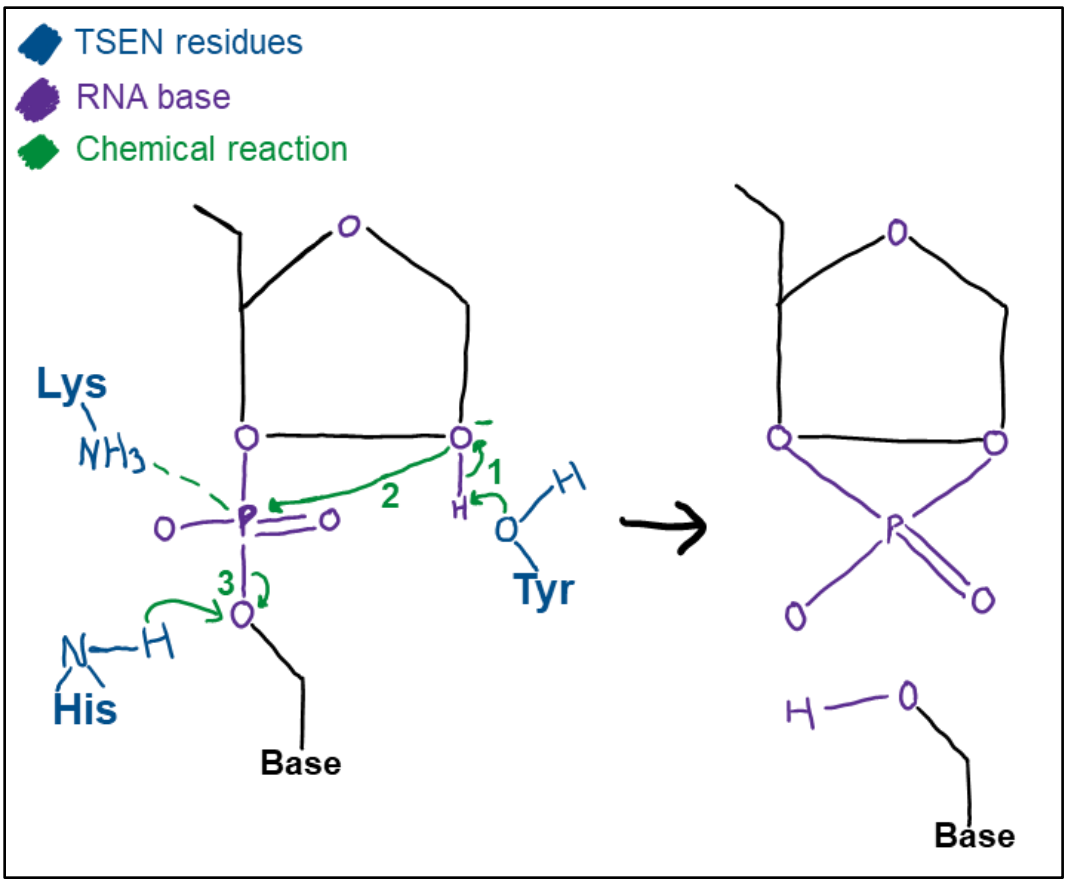

Figure 1.3: General mechanism of TSEN catalyzed tRNA cleavage.

In the first step (1), the tyrosine residue of Sen2 or Sen34 acts as a nucleophile and deprotonates the 2' hydroxyl of the ribose. (2) The negatively charged oxygen then attacks the phosphate backbone. This negatively charged transition state is stabilized by a lysine residue of the catalytic Sen subunits. (3) The active site histidine acts as an acid and donates a hydrogen to the oxygen on the phosphate backbone (Calvin and Li, 2008; Li et al., 1998). This then acts as a leaving group and breaks the phosphate backbone ultimately resulting in a ribonucleotide with a 2'3' phosphate and a one with a 5' hydroxyl (Ho et al., 1990; Peebles et al., 1983).

Although the yeast TSEN structure has not been solved, recently two cryo-EM structures were published of human TSEN (Hayne et al., 2022a; Sekulovski et al., 2022). From these studies, we can confirm some of the previous yeast data as well as gain insight into human TSEN. Both structures were solved with the Arg(TCT), the pre-tRNA with the smallest intron, docked within the complex. The data agree with the previously posited idea that TSEN34 and TSEN15 and TSEN2 and TSEN54 form dimers via interaction at the C terminal β-strand (Li et al., 1998; Trotta et al., 1997). In computer simulations, TSEN15 could disassociate from the complex. This small subunit has a highly negative charge and has been found to form a homodimer with itself in human cells (Song and Markley, 2007). TSEN34 seems to interact extensively with TSEN54 and TSEN2 where they interface near the active site for 3' splicing. The 3' splice site was well resolved and depends on the A-I helix formation which also aids in the bulge-helix-bulge (or loop) formation. The structures also provide more evidence for the ruler mechanism of TSEN54 as the N-terminal region of this subunit has the most interactions with pre-tRNA. TEN54 interacts with the acceptor stem and D-arm of the tRNA which helps position and anchor the substrate within the complex. Although the 3' splice site had enlightening resolution, the 5' splice site could not be clearly resolved. This is likely due to the site being more dynamic and less structured. This could be to allow non-tRNA substrates to enter the complex and be cleaved.

Subcellular localization of the TSEN complex is debated and possibly dependent on the organism. In yeast, the complex is localized to the outside of the mitochondria, facing the cytoplasm (Yoshihisa et al., 2007, 2003). However, pre-tRNAs are primarily processed in the nucleus and therefore, intron containing pre-tRNAs must be shuttled, primarily by Los1, to the cytoplasm to be cleaved by TSEN (Chatterjee et al., 2018). After ligation in the cytoplasm, some of the spliced tRNAs are not ready to be charged as they are still missing crucial modifications. For example, Trm5-catalyzed m1G37, a step in wybutosine synthesis, only

occurs in the nucleus and after a tRNA has been spliced (Chatterjee et al., 2018; Hopper, 2013; Ohira and Suzuki, 2011). Therefore, the spliced tRNA must be reimported to the nucleus, modified, and then re-exported to the cytoplasm for charging. This means the pre-tRNA is made and partially processed in the nucleus, transported to the cytoplasm for cleavage, imported back into the nucleus for further modification, and then exported again to be used in translation (Chatterjee et al., 2018; Hopper, 2013; Ohira and Suzuki, 2011; Takano et al., 2005). The inefficient transportation of pre-tRNAs suggests TSEN may have another important task to perform in the cytoplasm. This leads to the hypothesis that TSEN has other functions in the cytoplasm outside of tRNA processing. Even more striking, pre-tRNA export may be conserved in humans. Until recently, the human TSEN complex was thought to be localized to the nucleus (Paushkin et al., 2004), but new evidence suggests that TSEN is likely localized to the cytoplasm like yeast TSEN (Akiyama et al., 2022). In HeLa cells, it was also found that tRNAs can be imported back into the nucleus especially during times of stress (Schwenzer et al., 2019). Therefore, the re-import could also be common between yeast and humans and be a means of quality control and translational regulation. The conservation of TSEN localization and potential pathways for tRNA nuclear re-import point to TSEN having some other essential function in the cytoplasm that has made it a staple cytoplasmic enzyme.

Partners of TSEN

TSEN alone is not sufficient for yeast tRNA splicing. TSEN cleavage on either side of the intron results in a 2’3’ cyclic phosphate and 5’ hydroxyl which must then be ligated to form the spliced tRNA (Greer et al., 1987; Ho et al., 1990; Reyes and Abelson, 1988; Trotta et al., 1997). Trl1 performs three different reactions to complete ligation of the pre-tRNA (Figure 1.4) (Greer et al., 1983; Peebles et al., 1979; Phizicky et al., 1992; Wu and Hopper, 2014). Trl1 acts as a kinase and phosphorylates the 5’ hydroxyl of the intron, allowing its degradation by Xrn1, and the 3’ exon to a 5’ phosphate. Trl1 also uses its phosphodiesterase activity to open

the 2’3’ cyclic phosphate and create a 2’ phosphate and 3’ hydroxyl. Finally, Trl1 ligates the exons together using its ligase domain. Another enzyme, Tpt1 removes the remaining 2’ phosphate to complete the spliced tRNA (Culver et al., 1997; Wu and Hopper, 2014). This multistep ligation is referred to as ‘heal-and-seal’, as the ends must be processed or ‘healed’ before they are able to be ligated or ’sealed’ (Wu and Hopper, 2014).

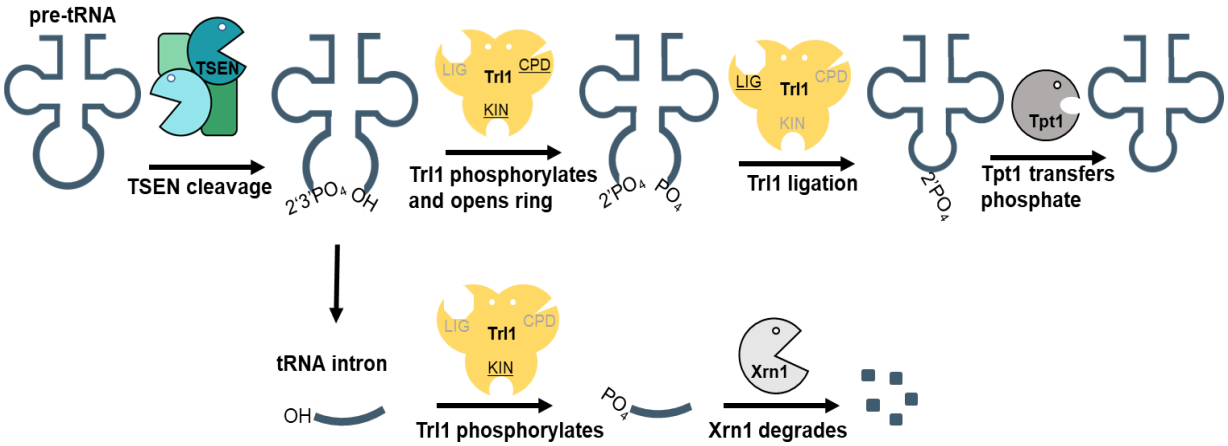

Figure 1.4: The heal-and-seal ligation pathway.

TSEN cleavage results in a 2'3' cyclic phosphate ring that Trl1 opens to a 3' hydroxyl and 2' phosphate with a cyclic-phosphodiesterase domain. On the other exon, TSEN leaves a 5' hydroxyl which is phosphorylated by the kinase domain of Trl1. Trl1 can then join the 5' phosphate and 3' hydroxyl as a ligase. The remaining 2' phosphate is removed by the phosphotransferase Tpt1. The excised intron is also phosphorylated by Trl1 which allows its degradation by Xrn1.

In metazoans, there may be two ways to splice tRNAs, a well characterized one-step ligation, which is predominant, and possibly a heal-and-seal pathway. In the one-step ligation pathway, RTCB directly ligates the 2'3' phosphate to the 5' hydroxyl created by TSEN cleavage with no intermediate enzymes or functional groups needed (Desai et al., 2014; Popow et al., 2011). In *C. elegans*, RtcB is an essential enzyme but can be deleted if artificial intronless tRNA genes are expressed, showing that the direct ligation pathway is the main tRNA ligation pathway (Kosmaczewski et al., 2014). The heal-and-seal pathway may use CLP1, a kinase, phosphorylating the 5' hydroxyl to a 5' phosphate. CLP1 has been found to be a stable component of the human TSEN complex and is often co-purified with subunits of the TSEN complex (Hayne et al., 2022a; Karaca et al., 2014; Paushkin et al., 2004; Ramirez et al., 2008; Sekulovski et al., 2022; Weitzer et al., 2015). Complete tRNA ligation would also require an enzyme that opens the 2'3' cyclic phosphate and a ligase that acts on 3' hydroxyls and 5' phosphates. Angel1/2 are candidates for processing the 2'3' phosphate. Recent studies have shown Angel1/2 could be involved in human pathways such as ribosome-stalled mRNA decay and *XBP1* splicing which are similar to the functions Trl1 performs in yeast (Nicholson-Shaw et al., 2022; Pinto et al., 2020). It is possible these enzymes also act on the 2'3' phosphate of tRNA as when Angel2 was perturbed, defects in pre-tRNA processing were observed (Pinto et al., 2020). However, an alternative hypothesis is that CLP1 end processing actually inhibits ligation by RTCB, acting as a regulator of RTCB (Hayne et al., 2020). Despite this, studies have shown CLP1 mutants with impaired kinase activity do have pre-tRNA splicing defects (Karaca et al., 2014; Ramirez et al., 2008). CLP1 is also associated with the 3' mRNA cleavage and polyadenylation machinery, indicating a role in not only tRNA but mRNA processing as well (Monaghan et al., 2021; Paushkin et al., 2004). However, CLP1 is not known to have a catalytic role in cleavage and polyadenylation. Whether human TSEN, like its binding partner CLP1, has other targets remains to be seen.

Other functions of TSEN

TSEN can perform functions outside of tRNA splicing including mRNA processing and degradation. EndA in archaeal species such as *Sulfolobus* was found to cleave the intron from the mRNA *cbf5* which is necessary to produce the mature Cbf5 protein (Yoshinari et al., 2006, 2005). The *cbf5* pre-mRNA has a secondary structure similar to the bulge-helix-bulge (BHB) motif of pre-tRNAs but more relaxed. A trend the authors noted is that most of these species have at least two different subunits of EndA (i.e. $(\alpha\beta)_2$) and hypothesize that this form of EndA may have less stringent requirements for substrate recognition (Yokobori et al., 2009; Yoshinari et al., 2006, 2005). This shows even the ancestral TSEN complex can recognize substrates other than pre-tRNAs. In many archaeal species, rRNAs also have a BHB domain. In *Haloferax volcanii,* the rRNA precursor contains two BHB motifs that span the 16S and 23S precursors (Schwarz et al., 2020). If EndA in this species is depleted, these rRNA precursors accumulate indicating EndA is necessary for correct rRNA processing. Additionally, this study also identified a novel mRNA with a BHB in its 5' UTR. EndA from *H. volcanii* was able to cleave this substrate in vitro (Schwarz et al., 2020). Together, these results demonstrate that archaeal TSEN (EndA) can cleave rRNAs and mRNAs in addition to its canonical tRNA substrate.

Eukaryotic TSEN also has targets other than pre-tRNA. One study showed that introducing a bulge-helix-bulge structure into an mRNA was sufficient for *Xenopus* TSEN to cleave this non-tRNA substrate in vitro (Fabbri et al., 1998). This further suggests TSEN could have targets besides pre-tRNAs. This proved to be true as yeast TSEN was found to cleave *CBP1* mRNA in vivo. Tsuboi and colleagues discovered 5' and 3' cleavage products of *CBP1* mRNA that, when TSEN was impaired, were no longer seen (Tsuboi et al., 2015). Importantly, this cleavage is dependent on the mitochondrial targeting sequence of Cbp1. Cbp1 is involved in the production of cytochrome B and as such localizes to the mitochondria (Islas-Osuna et

al., 2002). Often such proteins are imported co-translationally suggesting the *CBP1* mRNA localizes to the mitochondrial surface, making it spatially feasible for TSEN and *CBP1* to interact (Golani-Armon and Arava, 2016). Similarly, mutating a small region of Sen54 that results in mislocalization of the TSEN complex abolished the cleavage (Tsuboi et al., 2015). These results indicate that part of the mRNA substrate specificity of TSEN is explained by co-localization of the mRNA and enzyme. One region within *CBP1* that is essential for TSEN cleavage was predicted to form a stem-loop structure. Although the structure does not obviously resemble a pre-tRNA, it could be important for substrate recognition (Tsuboi et al., 2015). While archaeal EndA can splice *cbf5* mRNA*,* Tsuboi showed that *CBP1* mRNA is likely degraded downstream of TSEN cleavage as the 5' and 3' fragments are stabilized by cytoplasmic exosome (*ski7*Δ*)* and *xrn1*Δ mutations, respectively. This suggests TSEN participates in mRNA decay and could have other targets.

This discovery generated many open questions about the mechanism and targets of the TSEN complex. Sen2 and Sen34 act cooperatively in tRNA splicing in that they cleave either side of the intron, and Sen34 residues seem to contribute to 5' cleavage by Sen2 (Greer et al., 1987; Reyes and Abelson, 1988; Trotta et al., 2006, 1997). *CBP1* has several cut sites, but it is unknown which subunit of TSEN cleaves which sites and if the same residues and catalytic mechanisms are involved (Tsuboi et al., 2015). After TSEN cleaves *CBP1*, it likely produces a 5' hydroxyl and 2'3' cyclic phosphate as is the case with pre-tRNAs. We know the 3' fragment is eventually degraded by Xrn1 (Tsuboi et al., 2015), but Xrn1 has been shown to strongly prefer 5' monophosphate substrates over 5' hydroxyls (Johnson, 1997; Nagarajan et al., 2013). This suggests that some enzyme may need to convert the TSEN product into a 5' monophosphate RNA before Xrn1 can act. Similarly, the 5' fragment is known to be degraded by the RNA exosome, but whether it can directly degrade from the 2'3' cyclic phosphate end or needs another enzyme to convert this is also unknown.

Along with the known functions of TSEN in tRNA processing and *CBP1* degradation, we know that yeast TSEN must have another essential function independent of tRNA processing. The Hopper lab re-localized pre-tRNA splicing to the nucleus (Figure 1.5) (Dhungel and Hopper, 2012). To accomplish this, they added nuclear localization signals to the TSEN subunits and deleted Los1, which prevents intron containing pre-tRNAs from being exported to the cytoplasm. They found when TSEN was localized to the nucleus with unspliced tRNAs, TSEN was active and produced mature tRNAs that were correctly exported to the cytoplasm for translation. Despite tRNA processing appearing normal by all metrics examined, the cells were still dead when the nuclear localized subunits were expressed and the mitochondrially localized TSEN was repressed (Dhungel and Hopper, 2012). They also expressed a Sen2 H297A catalytic mutant in the cytoplasm to determine if this would complement the nuclear localized TSEN mutant and promote cell survival. However, this cytoplasmic catalytic mutant was not able to rescue the nuclear localized TSEN mutant (Dhungel and Hopper, 2012). This research shows that TSEN has another essential function in the cytoplasm and is dependent on its catalytic activity but independent of tRNA processing.

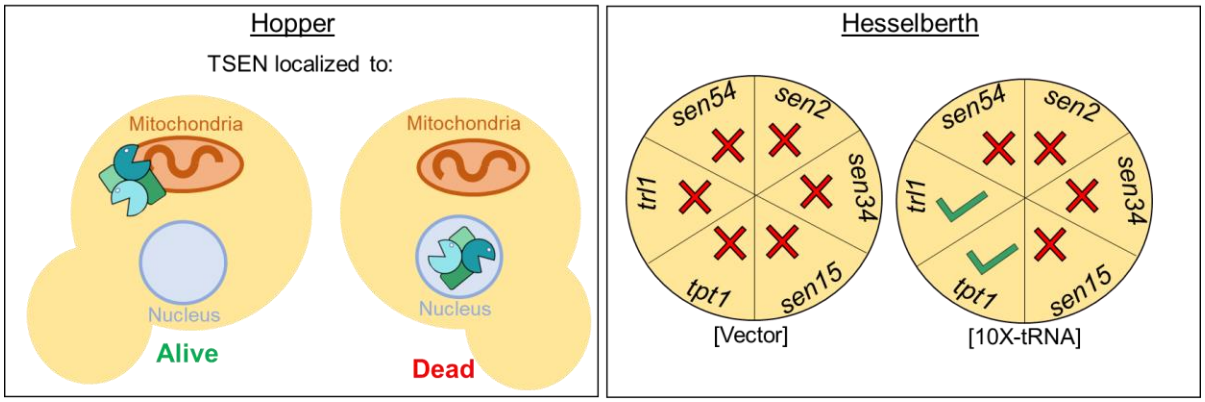

Figure 1.5: Summary of evidence that yeast TSEN has another essential function.

Left panel: The Hopper lab localized tRNA splicing from the mitochondrial surface to the nucleus. In doing so, they saw that pre-tRNAs were spliced to mature tRNAs efficiently. Despite this, when cytoplasmic TSEN was depleted leaving only the nuclear TSEN, the yeast were still dead even with proper tRNA splicing (Dhungel and Hopper, 2012). Right panel: The Hesselberth lab designed a plasmid of tRNAs with their introns already removed, bypassing the need for tRNA splicing. This plasmid suppresses the lethality of tRNA ligation mutants (*trl1*Δ and *tpt1*Δ) but the TSEN complex remained essential (Cherry et al., 2018).

Research from the Hesselberth lab also suggests TSEN has a tRNA-independent essential function (Figure 1.5). They bypassed the need for tRNA splicing using a plasmid expressing intronless tRNAs. This intronless tRNA plasmid restored viability to tRNA ligation mutants, *trl1*Δ *and tpt1*Δ*,* but not to TSEN mutants (Cherry et al., 2018). That Trl1 and Tpt1 were no longer essential with the intronless-tRNA plasmid suggests the tRNA splicing pathway is successfully bypassed but despite this, all four subunits of TSEN were still essential. Taken together, these data suggest the TSEN complex must have another essential function, independent of tRNA splicing that relies on the complex being catalytically active in the cytoplasm. Despite these clues, this function is still unidentified.

TSEN and human disease

Pontocerebellar hypoplasia (PCH), a condition characterized by both underdevelopment and degeneration of the cerebellum and often, the pons, can be caused by mutations in the human TSEN complex (Battini et al., 2014; Bierhals et al., 2013; Breuss et al., 2016; Budde et al., 2008; Cassandrini et al., 2010; Namavar et al., 2011a; Sepahvand et al., 2020; van Dijk et al., 2018). Most mutations associated with PCH are in RNA production or processing enzymes. Interestingly, mutations in the TSEN associated kinase, CLP1, can also cause PCH (Karaca et al., 2014; Monaghan et al., 2021; Schaffer et al., 2014). It has been proposed that some of the PCH mutations in TSEN could affect association of CLP1 with the complex (Hayne et al., 2022a; Sekulovski et al., 2022). As previously discussed, CLP1 does not seem to majorly contribute to tRNA splicing and instead has other functions in mRNA processing. In contrast, mutations in other tRNA ligation enzymes such as Archease, DDX1, and RTCB have not been shown to cause PCH while mutations in other mRNA processing genes like those encoding subunits of the RNA exosome and TOE1 do cause PCH (Cassandrini et al., 2010; Namavar et al., 2011a; van Dijk et al., 2018). In addition, the phenotype of PCH is severe especially when compared to the rather mild effect PCH

associated CLP1 mutations have on mature tRNA formation (Weitzer et al., 2015). Together, these observations suggest the tRNA splicing function of TSEN may not fully explain the PCH phenotype. Identifying the unknown functions of TSEN could give us insight into this human disease.

PCH cases range widely in severity, symptoms, and neuronal morphology. Classic features associated with most cases of PCH include severe intellectual disability, central motor impairments and seizures. Imaging often reveals progressive microcephaly and deterioration of the cerebellum and pons (Cassandrini et al., 2010; Namavar et al., 2011a; van Dijk et al., 2018). The lifespan of patients also varies but most cases result in death, usually due to respiratory failure, well before adulthood. Recently and likely due to the increased frequency of genome sequencing, a few patients with remarkably mild cases have been identified who have survived into their late teens or even early 30s (Chen et al., 2022; Mu et al., 2021; Rong et al., 2022). PCH is an autosomal recessive disease and relatively rare with only hundreds of cases reported since the early 1900s. The frequency of PCH is unknown with a vague estimation of less than 1:200,000 (Sánchez-Albisua et al., 2014). However, this disease is likely more common than the number of cases that are actually diagnosed. The broadness of the symptoms makes this condition difficult to diagnose without whole genome sequencing. Also, because of the severity of the disease it is likely that many potential patients are never born due to miscarriages. Because PCH is recessive and rare, homozygous mutations are often the result of consanguineal procreation, a practice that is common in some parts of the world. An estimated 1 billion people make up cultures that prefer consanguineal marriages (Cassandrini et al., 2010; Hamamy, 2012; Namavar et al., 2011a; van Dijk et al., 2018). Heterozygous mutations between non-consanguine parents have also accounted for many and the most severe cases of PCH. There are now two exceptionally rare cases of a

patient inheriting two copies of a PCH allele from one parent (uniparental disomy) (Sakamoto et al., 2022; Slavotinek et al., 2020).

At the time of writing, 17 types of PCH have been described that vary by mutations and severity of symptoms (omim.org). PCH type 1 is most frequently caused by mutations in the RNA exosome with the majority affecting subunits EXOSC3 and EXOSC8; however, recently mutations in EXOSC9, EXOSC5, EXOSC2 have been reported (Bizzari et al., 2019; Boczonadi et al., 2014; Burns et al., 2018; Mu et al., 2021; Slavotinek et al., 2020; van Dijk et al., 2018; Xue Yang et al., 2020). As previously mentioned, the RNA exosome is the major 3' to 5' exonuclease in both the nucleus and cytoplasm and performs a variety of cellular functions. Spinal motor neurodegeneration resulting in spinal muscular atrophy (SMA) is unique to PCH1 (van Dijk et al., 2018). These mutations in the RNA exosome have been predicted to affect RNA binding, subunit stability, and overall complex stability, though the specific function of the RNA exosome that is affected in PCH is still unknown (Bizzari et al., 2019; Boczonadi et al., 2014; Burns et al., 2018, 2018; Slavotinek et al., 2020). PCH7 is caused by mutations in TOE1, a deadenylation factor that allows removal of the polyA tail on snRNAs (Chen et al., 2022; Lardelli et al., 2017). Some studies have shown mutations in TOE1 resulted in incomplete 3' end maturation of snRNAs. Mutations in CLP1 cause PCH10 that results in severe developmental delay, facial dysmorphism, and atrophy of the ventral pons and brainstem (Karaca et al., 2014; Monaghan et al., 2021; Schaffer et al., 2014; van Dijk et al., 2018). Unexpectedly, the cerebellar decay is less severe in this type (van Dijk et al., 2018). The R140H founder mutation in CLP1 is predicted to disrupt the kinase activity from the yeast structure. tRNA processing and association with the TSEN complex was found to be affected in patient fibroblasts (Monaghan et al., 2021). However, the 3' RNA end processing function of CLP1 was not assessed, raising questions about which CLP1 functions

are responsible for PCH. In addition, recent literature suggests CLP1 plays a relatively small role in tRNA splicing compared to the one-step RTCB ligation (Hayne et al., 2020).

PCH2 is the most common form of PCH (Cassandrini et al., 2010; Namavar et al., 2011a; van Dijk et al., 2018). The most common cases are the result of a founder mutation in TSEN54, A307S which results in the classical “dragonfly” pattern where the cerebral hemispheres are severely affected but the vermis remains relatively intact (Budde et al., 2008; Namavar et al., 2011a). This mutation in combination (heterozygous) with splicing variants, premature stop, or other loss of function mutations in TSEN54 cause types 4 and 5 of PCH (Battini et al., 2014; Budde et al., 2008; Namavar et al., 2011b, 2011a). These are very severe cases of PCH where survival beyond the prenatal stage is rare, and those who survive to neonates, must be on ventilators and die shortly after. Though less common, mutations in TSEN2, 15, and 34 have been reported to cause PCH 2. Three different mutations in TSEN15 were found across four different patients in three different families (Breuss et al., 2016). All these amino acid substitutions resulted in reduced tRNA splicing. Two mutations that occurred in the core of the protein are predicted to disrupt the subunit stability and as such, the levels of TSEN15 were reduced. The third mutation appears to disrupt interaction with the complex as less of the other subunits were pulled down with this mutant TSEN15 (Breuss et al., 2016). At least four patients have been identified with mutations in TSEN2 (Bierhals et al., 2013; Namavar et al., 2011a). Functional studies have not been performed on these variants and as such it is unknown if tRNA splicing or RNA processing was affected. Only one patient has been identified with a homozygous mutation in TSEN34 (Namavar et al., 2011a). The molecular consequence of this mutation has also not been studied.

As previously stated, the vast majority (over 90%) of PCH2 cases are linked to mutations in TSEN54. Based on the current knowledge of the complex, I would like to present several speculations for the inequality in disease associated mutations in the subunits. First,

the most common mutation associated with PCH2 is the TSEN54 pA307S. The majority of these patients were found in one study that sequenced a population with this founder mutation (Budde et al., 2008). Not only can this founder mutation explain the disparity but also sample bias can arise from sequencing a specific population. Second, TSEN54 is the largest subunit of the complex and does not have a catalytic site. I therefore speculate that there are more residues that can be mutated without completely abolishing activity of the TSEN complex. In contrast, there are only a few known mutations in TSEN2 and TSEN34 that result in PCH (Namavar et al., 2011a). Mutations in these subunits would need to straddle a fine line where they are pathogenic but do not completely disrupt their functions that would surely prevent a live birth. Accordingly, in the recent human structures of TSEN, the TSEN34 and TSEN2 PCH mutations were not near catalytic sites but instead appeared to be at binding interfaces, potentially weakening the interaction between subunits (Hayne et al., 2022a; Sekulovski et al., 2022). The TSEN54 mutations mapped on the structure also likely affect binding interfaces and potentially TSEN54 stability in the more severe cases. Interestingly, the A307S mutation of TSEN54 was unable to be mapped on the structure as it is located in an intrinsically disordered region.

In summation, PCH is a rare, recessive, often fatal condition that is characterized by atrophy and developmental failure of the cerebellum and often pons. Though having a wide range of symptoms and severity, most mutations are related to RNA processing (Cassandrini et al., 2010; Namavar et al., 2011a; van Dijk et al., 2018). Many questions remain about PCH including how similar the types are to one another. Do different mutations lead to the same molecular changes that present this phenotype or are the subtypes all different on a molecular level and should be characterized as separate diseases? Mutations in all subunits of the human TSEN complex including CLP1 can cause PCH2 but mutations in TSEN54 result in more severe types 4 and 5. Do mutations in the RNA exosome which cause PCH1 lead to

similar molecular consequences or is the mechanisms completely independent but leads to a similar phenotype? The limited studies suggest modest defects in mature tRNA. However, if this was the case, one would expect mutations in RTCB and other tRNA ligation machinery to also cause PCH. These studies do indicate a buildup of tRNA precursors that some speculate may be toxic in developing neurons (Karaca et al., 2014; Weitzer et al., 2015). Other possibilities behind the molecular mechanism of PCH need to be explored, including the involvement of another unknown TSEN function. Taken together, I speculate that TSEN could have other functions in humans, similar to its yeast homolog, that are independent of tRNA processing and that this function contributes to the PCH phenotype.

Goals of this thesis

The goal of this dissertation was to define novel targets and functions of the TSEN complex. I also sought to identify how TSEN cleavage products are degraded as these products are not known substrates of the major exonucleases. I used PARE (Parallel Analysis of RNA Ends), a specialized type of RNA-seq, to determine unknown mRNA targets of TSEN (German et al., 2009, 2008; Harigaya and Parker, 2012). I also sought to uncover the other essential function of TSEN using classical yeast genetics. Both high-copy and spontaneous suppressor screens were used to find mutations that could compensate for a conditional TSEN mutant. I used an intronless-tRNA plasmid to differentiate between tRNA splicing dependent and independent functions. Once I identified TSEN targets, I investigated their degradation using PARE. We made mutations in two potential candidates, Dxo1 and Trl1 to determine if in their absence, Xrn1 was still able to degrade the TSEN cleavage products. Along the way, we discovered a novel function for *Saccharomyces cerevisiae* Dxo1 in rRNA processing and identified new targets of Trl1 that could be connected to Ire1 and the unfolded protein response.

2) Methods

Parts of this chapter were taken from my previous publications, Hurtig JE, van Hoof A. Yeast Dxo1 is required for 25S rRNA maturation and acts as a transcriptome-wide distributive exonuclease. RNA. 2022 May;28(5):657-667 and Hurtig JE, Steiger MA, Nagarajan VK, Li T, Chao TC, Tsai KL, van Hoof A. Comparative parallel analysis of RNA ends identifies mRNA substrates of a tRNA splicing endonuclease-initiated mRNA decay pathway. Proc Natl Acad Sci U S A. 2021 Mar 9;118(10):e2020429118 and the submitted paper Hurtig JE, van Hoof A. An unknown essential function of tRNA splicing endonuclease is linked to the integrated stress response and intron debranching. Resubmitted to *Genetics*. Accepted 2023 March 10.

Yeast and plasmids; strain and growth methods

All yeast strains and plasmids are listed in Table 2.1 and 2.2, respectively. All yeast strains used are in BY4741/4742 backgrounds. Yeast were grown in selective SC media (Sunrise Science Products) or YPD. Deletion strains were obtained from the yeast knockout collection (Giaever et al., 2002). Double mutant strains were generated by crossing single mutant strains using standard mating and random spore isolation methods. Transformations of plasmids into yeast strains were done as previously described (Gietz and Schiestl, 2007). To replace the KanMX cassette in deletion mutants with HygMX, strains were transformed with a DNA fragment of the HygMX cassette (pav1158/pAG32) (Goldstein and McCusker, 1999), allowing for homologous recombination between the promoters and 3'UTRs of the cassettes. Yeast gifted or obtained by other means are noted in Table 2.1. Plasmids (Table 2.2) were generated using either traditional cloning with restriction enzymes (NEB) and T4 ligase (NEB) or HiFi Gibson assembly (NEB) unless otherwise noted. PCR to amplify genes for cloning was performed using either Vent (NEB) or Q5 high-fidelity (NEB) polymerase. For expression of TSEN in baculovirus *SEN15* and FLAG-*SEN34* were cloned into pFastBac dual LIC using ligation independent cloning to generate pAV1468. His6-*SEN2* and *SEN54* were cloned into pFastBac dual His6-TEV LIC using ligation independent cloning to generate pAV1467. pFastBac Dual LIC and pFastBac dual His6-TEV LIC cloning vectors were gifts from Scott Gradia (Addgene plasmid # 30121; http://n2t.net/addgene:30121; RRID:Addgene_30121 and Addgene plasmid # 30122; http://n2t.net/addgene:30122; RRID:Addgene_30122)

Both the cloning method and any oligos used to create the constructs are listed in the table. The sequence of the numbered oligos can be found in Table 2.3. Plasmids previously published or gifted from other labs are also noted in Table 2.2. Plasmids were confirmed using

colony PCR with 2X OneTaq Master mix and Sanger sequencing (Genewiz) or whole plasmid sequencing (Plasmidsaurus).

Growth Assays

For growth assays on plates, yeast strains were grown overnight in selective media or YPD and diluted to an OD600 of 0.2 the next day. The cells were then grown to an OD600 of ~ 0.6, spun down, and resuspended in water. The yeast were serially diluted and spotted onto the appropriate media and temperatures. The plates were imaged after 2-5 days of growth.

For growth assays in liquid cultures, yeast strains were grown on selective liquid overnight, diluted to an OD600 of 0.2 the next day, and then grown until they doubled twice. The strains were again diluted to an OD600 of 0.2 in a 96-well plate with YPD. A plate reader was used to measure the OD600 change over 16 hours of growth and doubling times were determined for the exponential growth phase.

Table 2.1: Yeast strains

BY4741	*matA, ura3-Δ0, leu2-Δ0, his3-Δ1, met15-Δ0*
BY4742	*matα, ura3-Δ0, leu2-Δ0, his3-Δ1, lys2-Δ0*
yAV952	*mata ura3-Δ0 leu2-Δ0 his3-Δ1 met15-Δ0 xrn1Δ::NEO*
yAV1705	*mata ura3-Δ0 leu2-Δ0 his3-Δ1 xrn1Δ::NEO rrp44Δ::HYG,* pAV344 *RRP44*
yAV1706	*mata ura3-Δ0 leu2-Δ0 his3-Δ1 xrn1Δ::NEO rrp44Δ::HYG,* pAV503 *rrp44-endo-*
yAV2278	*mata ura3-Δ0 leu2-Δ0 his3-Δ1 xrn1Δ::NEO rrp44Δ::HYG rat1-1,* pAV344 *RRP44*
yAV2281	*mata ura3-Δ0 leu2-Δ0 his3-Δ1 xrn1Δ::NEO rrp44Δ::HYG rat1-1,* pAV503 *rrp44-endo-*
yAV2395	*matA, ura3-Δ0, leu2-Δ0, his3-Δ1, lys2-Δ0, sen2-ts*::*URA3, can1Δ::MFA1pr-HIS3*
yAV2544	*matA*, *ura3-Δ0, leu2-Δ0, his3-Δ1, lys2-Δ0, sen2Δ::NEO,* pAV1270 intronless tRNA, pAV1292 *SEN2*
yAV2659	*matα, ura3-Δ0, leu2-Δ0, his3-Δ1, lys2-Δ0, sen2-ts::URA3*
yAV2666	*matA, ura3-Δ0, leu2-Δ0, his3-Δ1, lys2-Δ0, met15-Δ0, xrn1Δ::NEO, sen2-ts*::URA3
yAV3120	*matA, ura3-Δ0, leu2-Δ0, his3-Δ1, met15-Δ0, xrn1Δ::HYG*
yAV3248	*matα, ura3-Δ0, leu2-Δ0, his3-Δ1, lys2-Δ0, xrn1Δ::HYG,*
yAV3251	*matA, ura3-Δ0, leu2-Δ0, his3-Δ1, met15-Δ0, dxo1Δ::NEO*
yAV3291	*matA, ura3-Δ0, leu2-Δ0, his3-Δ1, lys2-Δ0, met15-Δ0, xrn1Δ::HYG, dxo1Δ::NEO*
yAV3467	*matα, ura3-Δ0, leu2-Δ0, his3-Δ1, lys2-Δ0, sen2-ts::URA3,* pAV1389 intronless tRNAs
yAV3468	*matα, ura3-Δ0, leu2-Δ0, his3-Δ1, lys2-Δ0, sen2-ts::URA3, dbr1-G122D,* pAV1389 intronless tRNAs (spontaneous suppressor colony 3)
yAV3469	*matα, ura3-Δ0, leu2-Δ0, his3-Δ1, lys2-Δ0, sen2-ts::URA3, dbr1-E369X,* pAV1389 intronless tRNAs (spontaneous suppressor colony 4)
yAV3523	*matA, ura3-Δ0, leu2-Δ0, his3-Δ1, met15-Δ, dbr1Δ::NEO*
yAV3525	*matA, ura3-Δ0, leu2-Δ0, his3-Δ1, met15-Δ, dbr1Δ::NEO, sen2-ts::URA3*
yAV3526	*matA, ura3-Δ0, leu2-Δ0, his3-Δ1, lys2-Δ0, dbr1Δ::NEO, sen2-ts::URA3*
yAV3576	*matα, ura3-Δ0, leu2-Δ0, his3-Δ1, dbr1Δ::NEO*
yAV3577	*matA, ura3-Δ0, leu2-Δ0, his3-Δ1, lys2-Δ0, sen2Δ::HYG,* pAV1292 *SEN2*
yAV3662	*matα, ura3-Δ0, leu2-Δ0, his3-Δ1, lys2-Δ0, sen2Δ::HYG, dbr1Δ::NEO,* pAV1292 *SEN2*
yAV3676	*matα, ura3-Δ0, leu2-Δ0, his3-Δ1, met15-Δ, trl1Δ::NEO xrn1Δ::HYG,* pAV1514 *E. coli* RtcB
yAV3679	*matα, ura3-Δ0, leu2-Δ0, his3-Δ1, lys2-Δ0, trl1Δ::NEO,* pAV1514 *E. coli RtcB*
yAV3697	*matα, ura3-Δ0, leu2-Δ0, his3-Δ1, lys2-Δ0, sen2-ts*
yAV3698	*matα*, *ura3-Δ0, leu2-Δ0, his3-Δ1, lys2-Δ0, dbr1Δ::NEO*
yAV3699	*matα*, *ura3-Δ0, leu2-Δ0, his3-Δ1, lys2-Δ0, dbr1Δ::NEO, sen2-ts*
yAV3933	*matA*, *ura3-Δ0, leu2-Δ0, his3-Δ1, met15-Δ0, gcn4Δ::NEO*
yAV3935	*matA*, *ura3-Δ0, leu2-Δ0, his3-Δ1, lys2-Δ0, met15-Δ, sen2-ts::URA3, gcn4Δ::NEO*
yAV4156	*matA, ura3-Δ0, leu2-Δ0, his3-Δ1, lys2-Δ0, ire1Δ::NEO, xrn1::HYG*

Table 2.2: Plasmids

pRS415	*CEN-LEU2*	Sikorski and Hieter 1989
pRS416	*CEN-URA3*	Sikorski and Hieter 1989
pRS423	*2μ-HIS3*	Sikorski and Hieter 1989
pRS425	*2μ-LEU2*	Sikorski and Hieter 1989
pRS426	*2μ-URA3*	Sikorski and Hieter 1989
p180	*GCN4-LacZ-URA3*	Mohanta and Chakrabarti 2021
pAG32	*HygMX cassette*	Goldstein and McCusker, 1999
pAV344	*RRP44-LEU2*	Schaeffer et al., 2009
pAV503	*rrp44-endo- LEU2*	Schaeffer et al., 2009
pAV1247	*pGAL-CBP1-CEN-LEU2*	Sparks et al 1997
pAV1270	Intronless-tRNA-*HIS3*	Cherry *et al*. 2018
pAV1282	*SEN2-LEU2*	Cherry *et al*. 2018
pAV1283	*sen2H297A-LEU2*	Cherry *et al*. 2018
pAV1288	*pGAL-CEN-URA3*	Obtained from the Morano lab (UT Health). *pGAL* inserted at SacI and XbaI cutsites.
pAV1292	*SEN2-CEN-URA3*	Amplified *SEN2* from genomic DNA using oAV1728 and 1729. Cut pRS416 and PCR ends with BamHI and XhoI
pAV1335	*pGAL-CBP1-CEN-URA3*	Amplified pav1247 with oAVs 1700/1716, cut insert and prs416 with SacI and SalI, ligated with T4 ligase
pAV1338	*pGAL-CBP1*-3AC-*CEN-URA3*	Used overlap PCR to introduce 3 A-C mutations in *CBP1*. Cut insert and prs416 with SacI and SalI, ligated with T4 ligase
pAV1389	Intronless-tRNA-2μ-HIS in pRS423	Amplified pAV1270 with oAV1921 and 1922. Cut PCR and pRS423 EcoRI-HF and SacI-HF. The tF(GAA) gene contains an inadvertent mutation changing basepair 4-69 in the acceptor stem from GU to GC, which does not affect function. All findings were confirmed with pAV1699.
pAV1438	*SEN54-2μ-LEU2*	From genomic tiling collection, Jones *et al*. 2008 (Jones et al., 2008)
pAV1467	His-*SEN2* and *SEN54* in pFastBac dual His6-TEV LIC	Constructed by Michelle Steiger
pAV1468	*SEN15* and *SEN34* in pFastBac dual LIC	Constructed by Michelle Steiger
pAV1514	*GPD-E. coli RtcB-LEU2*	Received from Steward Shuman, amplified with oAVs 2074 and 2075 and put in prs425 with GPD promotor
pAV1515	*SEN2-CEN-LEU2*	Amplified *SEN2* from genomic DNA using oAV2087 and 2088. Amplified pRS415 with oAV2054 and 2055.
pAV1522	*Sen2-Y289F-CEN-LEU2*	Cut prs415 with ApaI and SacI, amplified gDNA using oAv2093/2094; oAv2087/2088 to introduce mutation, assembled with Gibson
pAV1523	*Sen2-G293E-CEN-LEU2*	Cut prs415 with ApaI and SacI, amplified gDNA using oAv2092/2091; oAv2087/2088 to introduce mutation, assembled with Gibson
pAV1524	pre-tRNA-Phe	tRNA Phe from yeast with the T7 promoter in a pUC19 vector; BSTNI site at the 3' end of tRNA gene
pAV1528	*CBP1*	CBP1 TSEN substrate with the T7 promoter in a pUC19 vector; DraI site at the 3' end of CBP1
pAV1529	*COQ5*	COQ5 TSEN substrate with the T7 promoter in a pUC19 vector; ApoI site at the 3' end of COQ5
pAV1530	*MIS1*	MIS1 TSEN substrate with the T7 promoter in a pUC19 vector; NcoI site at the 3' end of MIS1

pAV1531	*PKP2*	PKP2 TSEN substrate with the T7 promoter in a pUC19 vector; Ssp1 site at the 3' end of PKP2
pAV1532	*ERV1*	ERV1 TSEN substrate with the T7 promoter in a pUC19 vector; SbfI site at the 3' end of ERV1
pAV1533	Control	CBP1 negative control for TSEN reaction with the T7 promoter in a pUC19 vector
pAV1547	*DBR1-CEN-LEU2*	Amplified DBR1 from genomic DNA using oAV3088 and 3089. Cut PCR and pRS415 with ApaI and SacI-HF
pAV1552	*dbr1N85A-CEN-LEU2*	Cloned using overlap PCR with oAV3086-3089 from genomic DNA. Cut pRS415 and PCR with ApaI and SacI-HF
pAV1560	*Sen2-R321A-CEN-LEU2*	Cut prs415 with ApaI and SacI, amplified Sen2 from gDNA using oAv3126/2098; oAv3127/2097 to introduce mutation, assembled with Gibson
pAV1561	*Sen2-K328A-CEN-LEU2*	Cut prs415 with ApaI and SacI, amplified Sen2 from gDNA using oAv3126/3000; oAv3127/2099 to introduce mutation, assembled with Gibson
pAV1562	*Sen2-W348A-CEN-LEU2*	Cut prs415 with ApaI and SacI, amplified Sen2 from gDNA using oAv3126/3002; oAv3127/3001 to introduce mutation, assembled with Gibson
pAV1563	*Sen2-W370A-CEN-LEU2*	Cut prs415 with ApaI and SacI, amplified Sen2 from gDNA using oAv3126/3004; oAv3127/3003 to introduce mutation, assembled with Gibson
pAV1564	*Sen2-F230C-CEN-LEU2*	Cut prs415 with ApaI and SacI, amplified Sen2 from gDNA using oAv3126/3006; oAv3127/3005 to introduce mutation, assembled with Gibson
pAV1565	*Sen2-Y266C-CEN-LEU2*	Cut prs415 with ApaI and SacI, amplified Sen2 from gDNA using oAv3126/3008; oAv3127/3007 to introduce mutation, assembled with Gibson
pAV1566	*Sen2-P233R-CEN-LEU2*	Cut prs415 with ApaI and SacI, amplified Sen2 from gDNA using oAv3126/3010; oAv3127/3009 to introduce mutation, assembled with Gibson
pAV1613	*TRL1-CEN-HIS3*	Cut prs413 with SacI and SalI, amplified TRL1 from gDNA with oAVs 3191/3192 and inserted to vector using Gibson assembly
pAV1614	*Trl1K404AT405A-CEN-HIS3*	Cut prs413 with SacI and SalI, amplified TRL1 from gDNA using oAv3191/3192 and oAv3185/3186 to introduce mutation. Assembled with Gibson.
pAV1615	*Trl1K425N-CEN-HIS*	Cut prs413 with SacI and SalI, amplified TRL1 from gDNA using oAVs 3191/3192 and oAVs 3183/3184 to introduce mutation. Assembled with Gibson
pAV1633	*DXO1-2μ-URA3*	pRS426 was digested with SacI-HF and SalI-HF and the *DXO1* amplified with oAV3259 and 3260 was inserted using Gibson assembly.
pAV1662	*DBR1-2μ-LEU2*	Cut pAV1547 and pRS425 with ApaI and SacI, ligated with T4 ligase
pAV1685	*pGAL-DBR1-CEN-URA3*	Amplified *DBR1* from genomic DNA using oAV3337 and 3338. Cut pAV1288 with XhoI and XmaI.
pAV1699	Intronless-tRNA-2μ-*HIS3* in pRS423	Amplified insert from pav1270 with oAV1291 and 3344. Cut PCR and pRS423 with SacI-HF and SalI-HF.

Table 2.3: Oligos and siRNAs

oAV224	SCR1_Probe:	GTCTAGCCGCGAGGAAGG
oAV1728	SEN2_F:	TAAGCAGGATCCTCCTTTGTCAATTAGCCCTAAGA
oAV1729	SEN2_R:	TAAGCACTCGAGGATGTTTGGGTGTGGCTCTG
oAV1921	tRNA_prs_F:	AGAGAGAGCTCCCATCTTGGAAGGACCGG
oAV1922	tRNA_prs_R:	AGAGAGAATTCTTTCTTTCTGTATCGC
oAV2054	pRS_F_Gibson:	CGAATTCCTGCAGCCCGG
oAV2055	pRS_R_Gibson:	ATATCAAGCTTATCGATACCGTCGAC
oAV2074	E. coli_RtcB_F:	GAACTAGTGGATCCCCCCGGGATGAATTACGAATTACTGACC
oAV2075	E. coli_RtcB_R:	TTGATATCGAATTCCTGCAGTTATCCTTTTACGCACAC
oAV2087	SEN2_F_Gibson:	GGTATCGATAAGCTTGATATCAAGTTTCCCATTCAGTTC
oAV2088	SEN2_R_Gibson:	CCCCGGGCTGCAGGAATTCGCCTTGTCCCTTCCCTAAATC
oAV2091	SEN2_Y289F_F:	TTCGGCTGCGATTATTTATTATTTAAGAGAGGGCCACATTT
oAV2092	SEN2_Y289F_R:	AAATGGTGGCCCTCTCTTAAATAATAATAATCGCAGCCGAA
oAV2093	SEN2_G292E_F:	ATTATTTATTATATAAGAGAGAGCCACCATTTCAACACGCT
oAV2094	SEN2_ G292E_R:	AGCGTGTTGAAATGGTGGCTCTCTCTTATATAATAAATAAT
oAV2097	SEN2_ R321A_F:	TGGTATTCTAGCATAGCCGCTGTTGTGGGCGGCGCAAAGAA
oAV2098	SEN2_ R321A_R:	TTCTTTGCGCCGCCCACAACAGCGGCTATGCTAGAATACCA
oAV2099	SEN2_ K328A_F:	TTGTGGGCGGCGCAAGGCGACGTTTGTGTTATGCTA
oAV3000	SEN2_ K328A_R:	TAGCATAACACAAACGTCGCCTTTGCGCCGCCCACAA
oAV3001	SEN2_ W348A_F:	AACAGGAAGGCGATAGCACTAGCGAAACAACTTTA
oAV3002	SEN2_ W348A_R:	TAAAGTTGTTTGATTTCGCTAGTGCTATCGCCTCCTGTT
oAV3003	SEN2_ W370A_F:	AAGTATTGTATAAGAGAGCGGTTCCCGGAAGAAATAGAGACTAG
oAV3004	SEN2_ W370A_R:	CTAGTCTCTATTTCTTCCGGGAACCGCTCTCTTATACAATACTT
oAV3005	SEN2_ F230C_F:	TGGAAGCTATGTTTTTAACTTGTGCACTTCCTCTTCTTGACAT
oAV3006	SEN2_ F230C_R:	ATGTCAAGAACAGGAAGTGCACAAGTTAAAAACATAGCTTCCA
oAV3007	SEN2_ Y266C_F:	TTTGTCAGATCATACGTTATATGCCATCACTACAGATCACACGGTT
oAV3008	SEN2_ Y266C_R:	AACCGTGTGATCTGTAGTGATGGCATATAACGTATGATCTGACAAA
oAV3009	SEN2_ P233R_F:	AAGCTATGTTTTTAACTTTTGCACTTCGTGTTCTTGACATATCT
oAV3010	SEN2_ P223R_R:	AGATATGTCAAGAACACGAAGTGCAAAAGTTAAAAACATAGCTT
oAV3086	DBR1_cat_F:	CTACTATTTTTATTGGCGGTGCTCATGAATCGATGAGACATT
oAV3087	DBR1_cat_R:	AATGTCTCATCGATTCATGAGCACCGCCAATAAAAATAGTAG
oAV3088	DBR1_F_SacI:	AAGAAGGAGCTCCCTTCCGTACCTCCAACTGT
oAV3089	DBR1_R_ApaI:	GAAGAAGGGCCCCCCAAACGACAAGACCAAAGT

oAV3126	SEN2_fwd_Gib2	GGCGAATTGGGTACCGGGCCCAAGTTTCCCATTCAGTTC
oAV3127	SEN2_rev_Gib2	AGGGAACAAAAGCTGGAGCTCCTTGTCCCTTCCCTAAATC
oAV3151	tL(CAA)intron:	TTCCCACAGTTAACTGCGGTCAAGATATTT
oAV3152	tW(CCA)intron:	TGCAATCTTATTCCGTGGAATTTCCAAGATTTAA
oAV3166	Mature_tL(CAA):	CGATACCTGAGCTTGAATCAG
oAV3167	Mature_tW(CCA):	TTCGATTTGGAGTCGAAAGCTC
oAV3169	3interm_tL(CAA):	GATACCTGAGTATTCCCACAG
oAV3170	5interm_tL(CAA):	ATATTTCTTGAATCAGGCGCC
oAV3173	3interm_tW(CCA):	CCTTCGATTGCAATCTTATTCCG
oAV3174	5interm_tW(CCA):	GATTTAATTGGAGTCGAAAGCTC
oAV3183	TRL1_D425N_F:	GGGGTCATATTCAAAATAATGATATTACAGGTAAAGATAA
oAV3184	TRL1_D425N_R:	TTATCTTTACCTGTAATATGATTATTTTGAATATGACCCC
oAV3185	TRL1_K404A_F:	TATCAGTTATTGGATGTGGCGCAGCAACAACTTCCCAGACATTA
oAV3186	TRL1_K404A_R:	TAATGTCTGGGAAGTTGTTGCTGCGCCACATCCAATAACTGATA
oAV3191	TRL1_F_3:	TACCGGGCCCCCCCTCGAGGAATGTGGTTAAAACATTATTTCTAG
oAV3192	TRL1_R_3:	AGGGAACAAAAGCTGGAGCTCCAATATATTACTAACCGATACTTTC
oAV3208	SNZ1_Probe:	TGGTACCCTCATTTCCTCAGCAACTT
oAV3259	DXO1_F_Gibson:	TACCGGGCCCCCCCTCGAGGAGAGGTTGTTAGTACCAAC
oAV3260	DXO1_R_Gibson:	AGGGAACAAAAGCTGGAGCTCCTATACTATAAGTTTTGAAGGCCTGAA GACAACATGATATAA
oAV3158	25S'_Probe:	TTTGAGGTCAAACTTTAA
oAV3178	5S rRNA_probe:	GCGTATGGTCACCCACTAC
oAV3337	DBR1_gal416_F:	CTCTAGAACTAGTGGATCCCCATTTTGCTTATGACTAAATTGCGAATT GCTG
oAV3338	DBR1_gal416_R:	ATTGGGTACCGGGCCCCCCCTGCGGTCCCCCACCATTT
oAV3344	tRNA_prs_R2:	AGAGAGTCGACTTTCTTTCTGTATCGC
	siTSEN15 #1	5'CCCUAAGUAUCUAGAAAUG[dT][dT]3' 5'CAUUUCUAGAUACUUAGGG[dT][dT]3'
	siTSEN15 #2	5'CACCCUAAGUAUCUAGAAA[dT][dT]3' 5'UUUCUAGAUACUUAGGGUG[dT][dT]3'
	siTSEN2 #1	5'CGUUAAUGUCUCUAAGGAA[dT][dT]3' 5'UUCCUUAGAGACAUUAACG[dT][dT]3'
	siTSEN2 #2	5'GCUCUAUGGGAAAGGUUAU[dT][dT]3' 5'AUAACCUUUCCCAUAGAGC[dT][dT]3'
	siTSEN34 #1	5'CUGGCAAGUUCGGAGGUGA[dT][dT]3' 5'UCACCUCCGAACUUGCCAG[dT][dT]3'
	siTSEN34 #2	5'GAGGUGACUUCCUGGUCUA[dT][dT]3' 5'UAGACCAGGAAGUCACCUC[dT][dT]3'
	siTSEN54 #1	5'GGAUGUGCAUUAGUGGAUU[dT][dT]3' 5'AAUCCACUAAUGCACAUCC[dT][dT]3'
	siTSEN54 #2	5'CACCUGAAGAGGUUGGGUU[dT][dT]3' 5'AACCCAACCUCUUCAGGUG[dT][dT]3'

	siControl	SIC001 siRNA Universal Negative Control #1 Sigma Proprietary sequence

Yeast RNA and Northerns

RNA extractions of yeast

For experiments utilizing a temperature sensitive strain, yeast were grown overnight at room temperature in selective SC media or YPD. Yeast were then diluted to 0.1 OD600 in 30 ml of media and grown at room temperature for 16 hours. The cells were incubated at 37 °C for 1 hour (to inactivate *sen2-ts* or *rat1-1*). For experiments without temperature sensitive yeast, overnights were grown at 30°C, diluted to an OD600 of 0.2-0.3, and grown until the OD600 reached 0.6 to 1.2. For the Ire1 PARE, cells were treated in mid-log phase with tunicamycin (2.5 µg/ml) or DMSO for 2 hours before being spun down as described in previous literature (Cherry et al., 2019). *S. pombe* wild type and *din1*∆ strains were obtained from Ke Zhang Reid (Wake Forest University). The *S. pombe* were grown overnight, diluted to an OD600 of 0.3, and grown to an OD600 of 0.6-0.8 in YES media at 30°C. All cells were spun down and stored at -80 °C. RNA was extracted using a hot phenol method previously described (He et al., 2008), precipitated with either ethanol or isopropanol, and dissolved in DPEC-treated water. The quality and quantity of the RNA was assessed using a Nanovue spectrophotometer and by running on a denaturing agarose gel.

Northern blotting

10 µg of RNA was suspended in NorthernMax Formaldehyde Load Dye (Ambion) or polyacrylamide load dye (95% formamide, 0.025%SDS, 18 mM EDTA, 0.05% bromophenol blue) prior to being run on an agarose or polyacrylamide gel respectively. The samples were also heated at 65 °C for 15 minutes before loading. Agarose gels were 1.3% agarose formaldehyde and run with MOPS buffer. Polyacrylamide gels were 10-15% polyacrylamide (19:1), 7.8M urea, and run with TBE buffer. The RNA was transferred to Zetaprobe membrane (Bio-Rad) by osmosis (agarose) or voltage transferred in 0.1X TBE (polyacrylamide), UV

crosslinked, and probed with 5' P32 end labeled oligonucleotides. Probe sequences are listed in Table 2.3. Signals were detected using a Typhoon imager (GE Healthcare) and quantitated using ImageQuant software.

RNAseq and bioinformatics

Parallel analysis of RNA Ends RNAseq

PARE analysis for Figure 3.1 was performed essentially as previously described (Nagarajan et al., 2019). For all other figures, PARE was performed by LCScience. These two protocols differ slightly from each other and from the protocol from Harigaya and Parker (Harigaya and Parker, 2012). The three protocols identified essentially the same *CBP1* cleavage sites, indicating that the method is robust to methodological variations. RNA sequencing reads have been deposited in SRA under accession PRJNA663967 (Chapter 3) and PRJNA752382 (Chapter 5).

All data analysis was performed on a freely accessible Galaxy server (usegalaxy.org). Read quality was assessed using "FastQC". "TopHat" was used to map the reads to a genome file that contained the R64 reference genome plus the 2-micron plasmid and known RNA viral elements (L, M, 20S and 23S). TopHat settings allowed introns between 40 to 5000 bases. The resulting BAM alignment files were converted to bedgraphs and bigwig files using "bamCoverage". bamCoverage settings used were normalize to counts per million, Bin size =1 (resulting in single nucleotide resolution), and offset inside each alignment =1 (resulting in only the first nucleotide of each read being counted). bamCoverage was run twice, with each run being specific for one strand of the genome. The resulting bedgraph files contain all the PARE scores. "bigwigCompare" was then used to compute a $\log_2$(fold change) from the bigwig files to generate a bedgraph file with comPARE scores. For each position, a pseudocount of 0.01 was added to avoid dividing by zero. Finally, "Merge BedGraphs" was used to merge the

bedgraph files containing the PARE scores from bamCoverage and the comPARE scores from bigwigCompare. The merged bedgraph file was filtered by PARE score for the *xrn1*Δ or wildtype samples (PARE>1) to filter out low abundance signals. The resulting files were either further filtered by comPARE score to filter out unchanged signals or imported into an excel spreadsheet.

Novagene RNAseq

rRNA was depleted (Zymo-Seq RiboFree Total RNA Library Kit) and the PE150 RNA-seq was performed by Novogene. Results were analyzed using DeSeq2 (Love et al., 2014). Sequencing data from Chapter 4 is available at SRA PRJNA896630.

Dxo1 Sequence analysis

Homologs of ScDxo1 and ScRai1 were identified using BLAST at https://blast.ncbi.nlm.nih.gov/, and at yeastgenome.org. This was supplemented by sequences retrieved from the yeast gene order browser (http://ygob.ucd.ie/). This identified two homologs in most species of Saccharomycetaceae, including *S. cerevisiae*, *S. mikatae*, *S. kudriavzevii*, *S. uvarum*, *Candida glabrata*, *Naumovozyma castellii*, *N. dairenensis*, *Tetrapisispora blattae*, *T. phaffii*, *Vanderwaltozyma polyspora*, *Zygosaccharomyces rouxii*, *Torulaspora delbrueckii*, *Kluyveromyces lactis*, and *Lachancea kluyveri*. Exceptions include *Eremothecium cymbalariae* that has only one gene due to loss of *DXO1* and *Lachancea thermotolerans* that has three genes due to an additional duplication of *DXO1*. Similarly, two homologs were identified in the Saccharomycodaceae *Hanseniaspora osmophila*. In contrast, we could only find one gene in the Phaffomycetaceae *Cyberlindnera jadinii*, *Komagataella phaffii*, and *Wickerhamomyces ciferrii,* the Dipodascaceae *Yarrowia lipolytica*, the Lipomycetaceae *Lipomyces starkeyi* and the Pichiaceae *Ogataea polymorpha.* Some species within the CUG clade also had one gene (*e.g. Candida auris, Clavispora lusitaniae* and

Metschnikowia bicuspidata) while others had two (*e.g. Candida albicans, C. dubliniensis and C. Parapsilosis*), suggesting an independent duplication within this clade. The retrieved sequences where then aligned together with the biochemically and structurally characterized human DXO and *S. pombe* Rai1 proteins with CLUSTAL omega (http://www.clustal.org/omega/).

Other bioinformatic analysis

Sequence logos were generated at https://weblogo.berkeley.edu/logo.cgi and gene ontology analysis was performed at https://yeastgenome.org/. RNA structure was assessed using mFOLD/UNAfold analysis (Zuker, 2003).

Protein purification and in vitro endonuclease assays

Protein purification

The pFastBac-Dual-LIC plasmids carrying *SEN15/FLAG-SEN34* or His6-*SEN2/SEN54* were transformed into DH10Bac competent cells. The recombinant bacmid DNAs isolated from white colonies were confirmed by PCR prior to transfection into Sf9 insect cells. After three rounds of viral amplification, both high-titer baculoviruses that carry *SEN15/FLAG-SEN34* and His6-*SEN2/SEN54* were used to co-infect High-Five cells to overexpress all four TSEN subunits. 60 hours post infection, 300 ml cells were harvested and washed twice by ice-cold PBS. The cells were lysed in buffer A (20 mM HEPES pH 7.5, 150 mM NaCl, 0.1% Triton X-100, 5 mM $MgCl_2$, and 10% Glycerol) with protease inhibitors using a dounce homogenizer on ice. Lysates were clarified by centrifugation at 38,800g for 30 minutes, and the resulting supernatant was incubated with FLAG beads resin (300 µl) for 2 hours at 4 °C. The FLAG beads resin was washed using 6 ml of buffer A for five times (protease inhibitors were included in the first three washes) and then eluted three times using 300 µl of buffer A containing 300 µg/ml FLAG peptide. After analyzed by SDS-PAGE and

western blotting using anti-His and anti-FLAG M2 antibodies to confirm that all four subunits were present, the eluted TSEN complex was dialyzed into buffer A containing 50% glycerol and then stored at -20 °C.

Endonuclease assays

Endonuclease assays were performed at least three times on each of the mRNA substrates, using duplicate preps of independently expressed and purified protein. The templates were PCR amplified from plasmids listed in Table 2.2, with the exception of the 75 nt *CBP1* substrate and the *CBP1-3AC* substrate, which were PCR amplified from genomic DNA instead of plasmids. The PCR products were gel purified and confirmed by sequencing. Transcription reactions were performed using a HiScribe T7 High Yield RNA Synthesis Kit (NEB) in the presence of P^{32} αUTP according to the manufacturer's directions and purified from an 8% polyacrylamide, 7M urea, TBE gel using a Zymo Research ZR small-RNA PAGE Recovery Kit (Zymo research) according to the manufacturer's instructions. Endonuclease reactions contained 20-100 nM RNA, 20 mM HEPES pH7.3, 5 mM $MgCl_2$, 2.4 mM spermidine pH 7.5, 0.1 mM DTT, 0.4% triton X-100, and 100 ng or 1 µg recombinant TSEN. Reactions were incubated for 30 minutes at 30 °C, stopped by addition of an equal volume of 2x polyacrylamide RNA loading dye, heated to 95 °C for 3 minutes and stored on ice before analysis on a 10% polyacrylamide (19:1), 7.8M UREA, TBE gel. The gels were imaged on a Typhoon imager and quantitated using ImageQuant software.

Suppressor Screens and mutant identification

Spontaneous suppressor screen

The random suppressor screen was conducted by growing the *sen2-ts* strain with the intronless tRNA plasmid in SC-HIS at 30 °C. This yeast was grown for a total of 40

generations. Every 10 generations the yeast were diluted to an OD600 of 0.2 and a small amount was plated on SC-HIS at 37 °C to identify colonies with suppressors.

Genomic DNA extraction and SNP analysis

Genomic DNA was extracted from the *sen2-ts* control strain and the two spontaneous suppressor strains with the Epicentre Genomic Extraction kit (Lucigen). The DNA was purified using the DNA Clean and Concentrate kit (Zymo) following RNase A (Qiagen) digestion for 30 minutes at 37 °C. Whole genome sequencing was performed by Novogene. Sequencing reads were aligned with Bowtie2 (Langmead et al., 2009) to the R64-1-1 reference genome and mutations were identified with FreeBayes (Garrison and Marth, 2012), both run at usegalaxy.org. This identified a single high confidence mutation in each of the suppressors.

High-copy suppressor screen

The yeast genome tiling collection (Horizon) library spans 16, 96-well plates. Each well contains *E. coli* with a high copy plasmid with a region of the yeast genome and a *LEU2* selectable marker. *E. coli* from all 96 wells of each plate were pooled together and plasmids were extracted from each pool. One of these plates contains *SEN2* and as such a 17th pool was assembled omitting the *SEN2* well. All 17 pools were transformed into the *sen2-ts* with intronless tRNA strain. Transformations were plated on SC-HIS-LEU at 37 °C. Only two of the 17 pools yielded transformants capable of growing at 37 °C. The plasmids from those colonies were extracted and identified by Sanger sequencing.

Cell culture and MCF7 Western blots

MCF7 and HEK293T cells were maintained in DMEM+10% FBS at 37°C, 5% CO_2. HEK293T DXO-KO cells were gifted by Mike Kiledjian (Rutgers University). HEK cells were

grown to a confluency of 70% and froze at -80 C°. RNA was extracted using RNeasy kit (Qiagin) and eluted in 30 ul of DPEC-treated water. siRNAs were obtained from Sigma and listed in Table 2.3. The Lipofectamine RNAi Max kit (Fisher) was used to transfect siRNAs (400nM) into cells in suspension.

Western blot of MCF7 protein

Protein was extracted after 36 hours and analyzed by Western blotting with the following primary antibodies Anti-TSEN54: Abcam ab178696, Anti-TSEN34: Abcam ab68868, Anti-TSEN2: Proteintech 13103-2-AP, and anti-Actin: ABclonal AC026. We were unable to identify a commercial antibody source that reliably detected TSEN15.

Beta-Galactosidase assay

The β-galactosidase assay was performed similarly to previous literature (Amberg et al., 2006).Yeast were grown overnight and subcultured to an OD600 of 0.3 and grown until mid-log phase. The exact OD600 was recorded. One ml of the yeast culture was pelleted and resuspended in 1 ml of the Z Buffer/BME/SDS solution (Amberg et al., 2006). 50 µl of chloroform was then added and the samples were vortexed. 100 µl of the aqueous phase was then distributed into wells of a 96-well plate. 100 µl of ONPG (4mg/ml ONPG in Z-Buffer) was added to each well. OD420 readings were taken every minute for 15 minutes. Beta-galactosidase activity was measured by finding the slope of the OD420/time and averaged over 3 technical replicates and 4 biological replicates.

3) Comparative parallel analysis of RNA ends identifies mRNA substrates of a tRNA splicing endonuclease-initiated mRNA decay pathway

This chapter was taken from Hurtig JE, Steiger MA, Nagarajan VK, Li T, Chao TC, Tsai KL, van Hoof A. Comparative parallel analysis of RNA ends identifies mRNA substrates of a tRNA splicing endonuclease-initiated mRNA decay pathway. Proc Natl Acad Sci U S A. 2021 Mar 9;118(10):e2020429118. PNAS approval is not needed to include articles in dissertations (www.pnas.org/about/rights-permissions).

Chapter Introduction

RNA degradation is a complex process that requires multiple ribonucleases in every domain of life. These multiple ribonucleases act sequentially on individual mRNA molecules to completely degrade them. Diverse eukaryotes share a conserved cytoplasmic pathway for the degradation of most cellular mRNAs. First, the poly(A) tail is removed by Ccr4/Not and Pan2/3 exoribonuclease complexes. This deadenylation can be followed either by removal of the cap structure by Dcp2 and 5' to 3' digestion by the exoribonuclease Xrn1, or by 3' to 5' digestion by the RNA exosome. In this pathway, removal of the 5' cap and 3' poly(A) tail are rate-limiting and these structures protect mRNAs from degradation by exonucleases. The contributions of each of these ribonucleases to mRNA degradation have been well characterized (Johnson, 1997; Stevens and Poole, 1995; Chlebowski et al., 2013; van Hoof et al., 2002; Januszyk and Lima, 2014; Nagarajan et al., 2013; Wasmuth and Lima, 2012) and Ccr4/Not, Pan2/3, Dcp2, Xrn1 and the RNA exosome are conserved throughout eukaryotes.

Along with digestion from either end, mRNA degradation can be initiated by a variety of endonucleases. These endonuclease-initiated pathways have been less well characterized, may be less extensively conserved, and generally target only a subset of mRNAs. The endonucleases generally cleave at a small number of specific sites within an mRNA target and produce two products: One with a 5' cap, but no 3' poly(A) tail and one that is uncapped but has a poly(A) tail. Because both products lack one protective end, they are then further degraded by the RNA exosome and Xrn1.

One prominent example of endonuclease-initiated mRNA decay is RNAi initiated by the RNA-induced silencing complex (RISC). The core of RISC, conserved in animals, fungi and plants, consists of a small RNA and a catalytic Argonaut subunit. RISC uses the small RNA to recognize complementary mRNAs and cleave them (Pratt and MacRae, 2009). These cleavage products are degraded by Xrn1 and the RNA exosome (Getz et al., 2020; Lima et

al., 2016; Orban and Izaurralde, 2005; Souret et al., 2004). A second example of endonuclease-initiated mRNA decay is cleavage of mRNAs that contain premature stop codons in Metazoa by the SMG6 endonuclease (Eberle et al., 2009; Huntzinger et al., 2008), followed by XRN1 and RNA exosome-mediated degradation of the cleavage products (Huntzinger et al., 2008). A third example of endonuclease-initiated mRNA decay is the Regulated IRE1-Dependent Decay (RIDD) pathway. The endoribonuclease IRE1 is activated when unfolded proteins accumulate in the ER (endoplasmic reticulum), and functions in two ways to restore homeostasis to the ER. First, IRE1 cleaves two sites within the mammalian *XBP-1* mRNA (or the yeast *HAC1* mRNA) to initiate a non-canonical splicing event (Gonzalez et al., 1999; Sidrauski and Walter, 1997). The resulting *XBP-1* (or *HAC1*) mRNA encodes a transcription factor that activates genes integral to protein folding in the ER (Ron and Walter, 2007). The second function of IRE1 is to cleave a number of mRNAs that encode ER-localized proteins (Hollien et al., 2009; Hollien and Weissman, 2006; Kimmig et al., 2012; Mishiba et al., 2013), which functions to reduce the import of newly translated proteins into the ER and therefore the need for protein folding in the ER. Cleavage of mRNAs by IRE1 is also followed by degradation by XRN1 and the RNA exosome (Hollien and Weissman, 2006). Together the increased folding capacity mediated by *XBP-1* splicing and reduced need for folding mediated by RIDD restore homeostasis to the ER. A fourth example of an endonuclease that initiates mRNA decay is the tRNA splicing endonuclease (TSEN), for which we propose the name TED (tRNA Endonuclease-initiated mRNA Decay). The canonical function of TSEN is to cleave pre-tRNAs to initiate the non-spliceosomal splicing of pre-tRNA (Abelson et al., 1998; Rauhut et al., 1990; Trotta et al., 2006). Recently, TSEN was shown to have a second function; it cleaves the yeast *CBP1* mRNA and the resulting cleavage products are degraded by Xrn1 and the RNA exosome (Tsuboi et al., 2015). Genetic evidence suggests that TSEN has a third function, but the nature of this function is unknown (Cherry et al., 2018; Dhungel and Hopper, 2012).

In each of these cases, endonuclease-initiated mRNA decay appears to target a subset of mRNAs, but which mRNAs are targeted and how they are recognized is incompletely understood. One factor that contributes to mRNA specificity of both RIDD and TED is colocalization of the mRNAs and endonucleases. The Ire1 endonuclease of the RIDD pathway is localized on the outside of the ER, facing the cytoplasm (Cox et al., 1993; Mori et al., 1993; Shamu and Walter, 1996). Similarly, TSEN of the TED pathway is localized on the outside of the mitochondria, facing the cytoplasm (Yoshihisa et al., 2007, 2003). Both pathways target mRNAs that are localized to the outside of these same organelles, and the localization of the target mRNAs is at least in part dependent on the co-translational recognition of the signal sequence/transit peptide of the nascent protein (Hollien and Weissman, 2006; Tsuboi et al., 2015). However, not all mRNAs that are localized to the ER or mitochondrial surface are targeted and not all sites within an mRNA are cleaved equally, indicating that other features contribute to the determination of which phosphodiester bonds get cleaved. RIDD, for example, also shows specificity for sequence and structure (Moore and Hollien, 2015). Whether TED is also sequence and/or structure dependent has not been extensively studied. A target structure for *CBP1* was proposed (Tsuboi et al., 2015), but this structure does not appear to be conserved in other *Saccharomyces* species and its importance has not been rigorously tested by compensatory mutations. Our understanding of TED specificity and physiological function is limited, at least in part because only one substrate (*CBP1*) is known.

Parallel Analysis of RNA Ends (PARE) is a useful tool for finding endonuclease targets (German et al., 2009; Harigaya and Parker, 2012; Lykke-Andersen et al., 2014; Schmidt et al., 2015). This method uses T4 RNA ligase to ligate a linker onto the 5’ ends of polyadenylated RNAs with a free 5’ monophosphate. The linker can then be used for library preparation and deep sequencing, which maps the exact 5’ monophosphate end of the RNA.

Intact mRNAs normally have a ^{7m}GpppN cap structure and are therefore not substrates for this ligation. Moreover, any 5' monophosphate mRNAs that arise by either decapping or endonuclease digestion are rapidly degraded by Xrn1. Here we use PARE to identify 5' monophosphate mRNAs present in *xrn1*Δ but that disappear if TSEN is inactivated. The *xrn1*Δ allows the detection of 5' monophosphate intermediates that are normally very transient. Identification of endonuclease sites has been limited by a lack of easily accessible bioinformatics tools. Here we develop a comparative PARE pipeline (comPARE) that can be easily implemented on a public Galaxy server (usegalaxy.org) and does not require any coding. This should make the comPARE analysis method readily accessible to RNA biologists with limited bioinformatics expertise. With this method, we were able to identify novel TED targets, and show that TED has sequence specificity.

Results

PARE sensitively identifies known TSEN cleavage sites in endogenous *CBP1*

When RNA is cleaved by an endonuclease or decapped, a 5' monophosphate is formed on the 3' cleavage product. Some endonucleases directly produce 5' monophosphates, while others produce 5' hydroxyl ends that are subsequently phosphorylated by a polynucleotide kinase. Xrn1 requires a 5' monophosphate for further degradation. PARE takes advantage of this end to ligate an adaptor to cleaved mRNAs (Figure 3.1A) (German et al., 2009). After ligation, the PARE adaptor is used for NGS library generation, which is then sequenced from the adaptor end. Therefore, the first nucleotide in the NGS read precisely corresponds to the first nucleotide in the 5' monophosphate RNA. We initially attempted to use PARE to investigate the endonuclease domain of the RNA exosome (Lebreton et al., 2008; Schaeffer et al., 2009; Schneider et al., 2009). Many targets of the exonuclease activity of the RNA exosome are known but targets of the highly conserved

endonuclease domain have remained elusive. To investigate targets of the RNA exosome endonuclease activity, we used PARE on *xrn1*Δ and *xrn1*Δ *rat1-1* yeast strains. Xrn1 and Rat1 are the major processive 5' exoribonucleases in the cytoplasm and nucleus, respectively (Nagarajan et al., 2013). Thus, these mutations are expected to stabilize most endoribonuclease cleavage products. Previous PARE studies have used *xrn1* single mutants or depletion, and we reasoned that adding *rat1-1* would expand the degradome studies to nuclear events. Other 5' exonucleases (e.g. Dxo1, Rai1, Rrp17, Ysh1) have been found to play minor roles in RNA degradation and do not interfere with PARE (Doamekpor et al., 2020a; Oeffinger et al., 2009; Payea et al., 2020; Xiao-cui Yang et al., 2020). We also included *xrn1*Δ *rrp44-endo*$^{-}$ and *xrn1*Δ *rat1-1 rrp44-endo*$^{-}$ strains that additionally lack the endonuclease activity of the RNA exosome. Each of these strains was used in biological duplicates. Thus, the cytoplasmic degradome was sequenced in four replicates as has been done previously (Harigaya and Parker, 2012). The four replicates of *xrn1*Δ *rat1-1* (with and without *rrp44-endo*$^{-}$) represent the first characterization of the nuclear degradome of *S. cerevisiae*. Unfortunately, we were unable to identify any novel targets of the RNA exosome endonuclease domain, perhaps because it does not cleave any particular site at high frequency. Similarly our previous microarray analysis was also unable to determine genes that were differentially expressed in the absence of the endoribonuclease activity (Tsanova et al., 2014). While analyzing our PARE data we did observe prominent peaks for several known endonuclease cleavage sites, including peaks in *CBP1*, the only known target for TED (Figure 3.1B) (Tsuboi et al., 2015). These *CBP1* peaks were highly reproducible in the eight PARE datasets. We observed the same peaks in *dcp2*Δ *xrn1*Δ PARE data previously published by the Parker lab (Harigaya and Parker, 2012), but not the wild-type control strain from that study (Figure 3.1B). Thus, these peaks do not reflect decapped mRNAs. In contrast, the peaks just upstream of the *CBP1* ORF were absent in the *dcp2*Δ *xrn1*Δ samples and thus reflect decapped mRNAs.

Five TSEN cleavage sites in *CBP1* have previously been identified by primer extension analysis (Tsuboi et al., 2015). The PARE peaks we identified were near, but not exact matches to the primer extension sites (Figure 3.1C). This is at least in part because the previous studies used an overexpressed *CBP1*. When we repeated the PARE analysis upon overexpression of *CBP1*, we also saw slightly different peaks. Specifically, while both endogenous and overexpressed *CBP1* were cleaved after nucleotides 669, 714 and 719 of the coding region, the 714 site was more prominent in endogenous *CBP1* while the 719 site was more prominent after *CBP1* overexpression (SI Appendix Fig. S1 in publication (Hurtig et al., 2021)). Overexpression also resulted in prominent PARE signals at nucleotide 720 and 670 of *CBP1* that were not seen for the endogenous mRNA. These observations confirm that PARE can map endonuclease cleavage sites while avoiding the need to overexpress target RNAs.

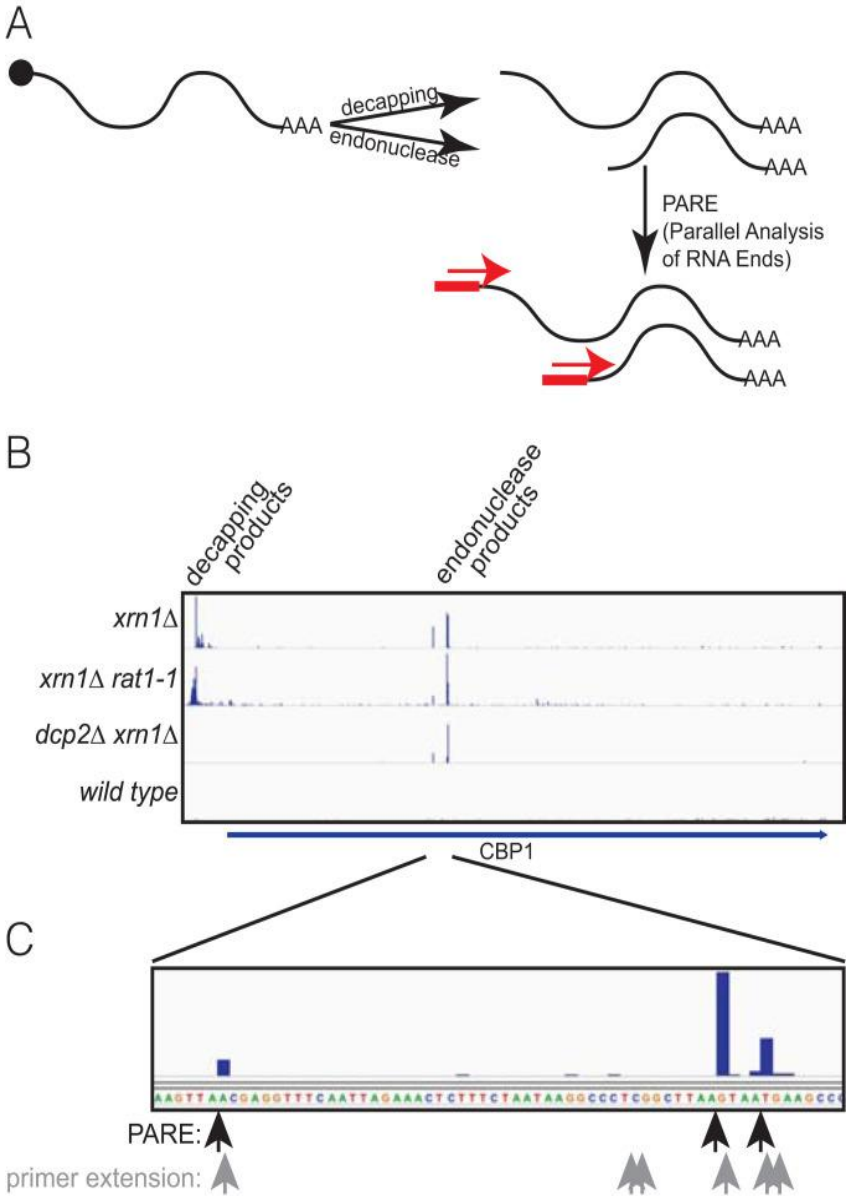
A
AAA
decapping
endonuclease
AAA
AAA
PARE
(Parallel Analysis
of RNA Ends)
AAA
AAA
B
decapping
products
endonuclease
products
xrn1Δ
xrn1Δ rat1-1
dcp2Δ xrn1Δ
wild type
CBP1
C
PARE:
primer extension:

Figure 3.1: PARE detects previously identified cleavage sites within the *CBP1* mRNA.

A). The PARE method is outlined. A linker (red rectangle) is ligated to 5' monophosphates on polyadenylated RNA that result from decapping or endonucleolytic cleavage. Capped (Black circle) RNA is resistant to ligation. This linker is then used in NGS sequencing, resulting in a sequence read (red arrow) that precisely starts at the first nucleotide of the 5' monophosphorylated RNA. **B).** initial PARE analysis for *xrn1*Δ and *xrn1*Δ *rat1-1* strains (top two panels) and published data from *dcp2*Δ *xrn1*Δ and wild-type strains (bottom two panels). Despite differences in the methods, similar endonuclease peaks were identified in all the strains that lacked Xrn1, showing the robustness of the method. **C).** Zoomed in view of the *xrn1*Δ data from B). The major PARE peaks are highlighted (black arrows), as is the previous mapping of cleavage sites by primer extension (grey arrows).

comPARE: A quantitative measure of the dependence of a PARE site on a specific endonuclease

To determine whether the peaks we observed in *CBP1* were indeed produced by TSEN, we generated additional PARE data. We grew an *xrn1*Δ *sen2-ts* strain (carrying a temperature sensitive mutation in TSEN (Ben-Aroya et al., 2008)) and an *xrn1*Δ strain in duplicate at room temperature, incubated all four cultures at 37 °C for one hour to inactivate TSEN, and performed PARE. As shown in Figure 3.2A and consistent with previous data (Reference (Tsuboi et al., 2015) and Figure 3.1), the prominent peaks in the *CBP1* ORF were again detected in the *xrn1*Δ PARE data (top panel), but not in the *xrn1*Δ *sen2-ts* datasets (middle panel). In contrast, the peaks corresponding to decapped *CBP1* mRNA were present in all four datasets. This confirms that TSEN is required for the cleavage of endogenous *CBP1* (Tsuboi et al., 2015).

To develop a bioinformatic approach to identify additional TSEN cleavage sites that is simple to implement, we turned to tools available on a public Galaxy server (usegalaxy.org). Briefly, we first used the Bamcoverage tool to count the number of reads starting at every position in the genome (i.e. at single nucleotide resolution, with no binning). For each sample, this generated a file containing the counts of read 5' ends for each strand of the genome, normalized to total reads mapped (essentially Counts Per Million, CPM, at single nucleotide resolution), which we will refer to as the PARE score. The PARE scores for each nucleotide in *CBP1* are plotted in the top two panels of Figure 3.2A. Second, we used bigwigCompare to divide the number of reads in an *xrn1*Δ sample by the number of reads in the matching *xrn1*Δ *sen2-ts* sample. Essentially, this generated a $\log_2$(fold change) at single nucleotide resolution, which we will refer to as the comPARE score. This comPARE score is plotted along the *CBP1* gene in the third panel of Figure 3.2A. As shown in this panel, the TSEN dependent cleavage sites in *CBP1* have high comPARE scores. In contrast, the decapping products received a

low comPARE score, indicating that they are not affected by the *sen2* mutation. Both Bamcoverage and bigwigCompare output bigwig files which can be visualized directly in IGV (https://software.broadinstitute.org/software/igv/download). Finally, we used the Merge BedGraph files tool to generate one table of 24 million rows (representing nucleotide resolution on both strands of the 12 MB genome) and four columns of PARE scores (from the duplicate *xrn1*Δ and *xrn1*Δ *sen2-ts* samples) and two columns of comPARE scores.

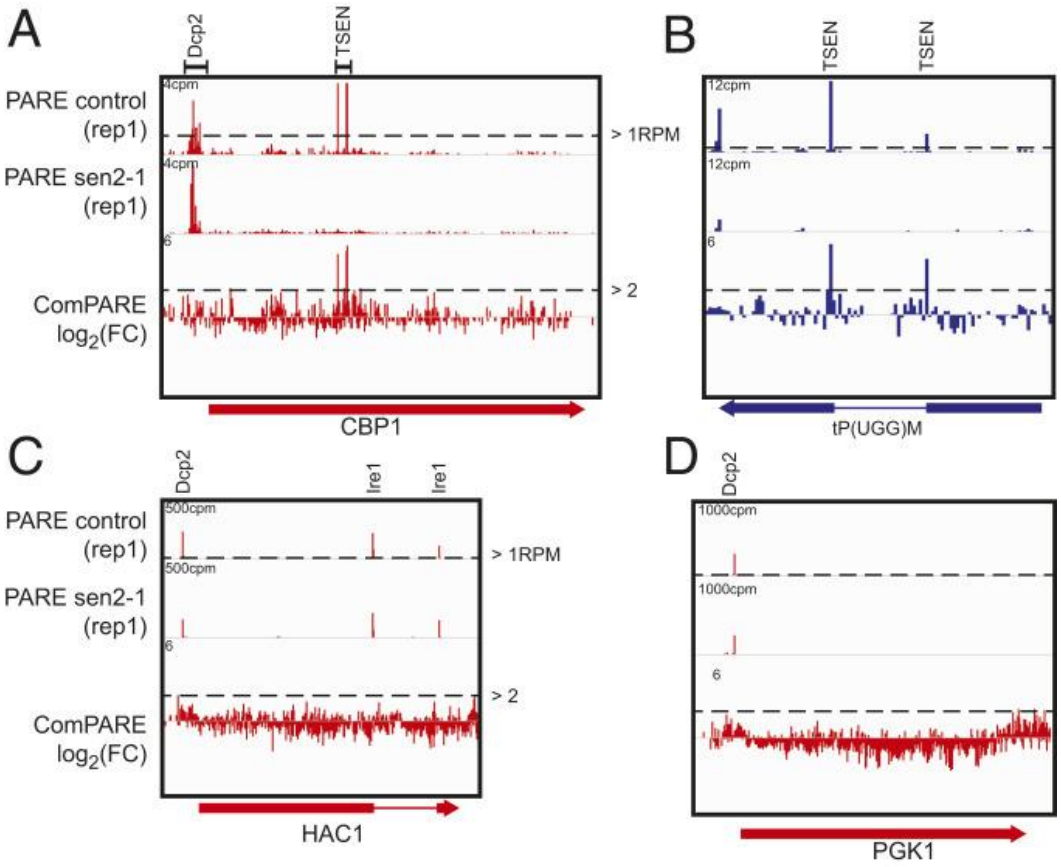
A
Dcp2
TSEN
PARE control (rep1)
PARE sen2-1 (rep1)
ComPARE log2(FC)
4cpm
4cpm
6
> 1RPM
> 2
CBP1
B
TSEN
TSEN
12cpm
12cpm
6
tP(UGG)M
C
Dcp2
Ire1
Ire1
PARE control (rep1)
PARE sen2-1 (rep1)
ComPARE log2(FC)
500cpm
500cpm
6
> 1RPM
> 2
HAC1
D
Dcp2
1000cpm
1000cpm
6
PGK1

Figure 3.2: comparative PARE (comPARE) identifies TSEN-dependent cleavage sites.

A). Cleavage sites in *CBP1* detected in *xrn1*Δ (top panel) are strongly reduced in *sen2-ts xrn1*Δ (middle panel), confirming that TSEN is required for this cleavage. Note that the PARE signals for TSEN products is off the y-axis scale. A scale of 0 to 4 was used to visualize the decapping products. The actual height of the TSEN PARE peaks is listed in SI Appendix Table S1 in the publication (Hurtig et al., 2021). **B).** The cleavage sites in the proline pre-tRNA *tP(UGG)M* detected in *xrn1*Δ are strongly reduced in *sen2-ts xrn1*Δ, confirming that TSEN is required for this cleavage. **C).** The cleavage sites in *HAC1* are similarly detected in *xrn1*Δ and *sen2-ts xrn1*Δ, confirming that TSEN is not required for this Ire1-mediated cleavage. **D).** No significant cleavage sites were detected in the *PGK1* mRNA. This mRNA is normally degraded by Dcp2-mediated decapping and Xrn1-mediated 5' to 3' degradation, but in the *xrn1*Δ strains used here is known to be degraded by the 3' exoribonuclease activity of the RNA exosome.

To assess the viability of comPARE to identify TSEN cleavage sites, we examined the PARE and comPARE scores for known cleavage sites between *xrn1*Δ and *xrn1*Δ *sen2-ts* strains (Figure 3.2). We filtered the data for positions where both *xrn1*Δ PARE scores were larger than 1 (indicated by the dashed line in Figure 3.2). This filters out low level noise and keeps positions that have more than 1 read per million mapped reads. The *CBP1* cleavage sites exceeded this threshold (Figure 3.2A). Although PARE enriches for poly(A)+ RNA, some of the known TSEN sites in tRNA also exceeded this PARE>1 threshold (Figure 3.2B). As an example of sites from another endonuclease, the Ire1 cleavage sites in the *HAC1* mRNA also exceeded PARE>1, even though our samples were not specifically treated to activate Ire1 (Figure 3.2C). In contrast, in an *xrn1*Δ strain the *PGK1* mRNA is degraded by the 3' exoribonuclease activity of the RNA exosome (Anderson and Parker, 1998; Schaeffer and van Hoof, 2011) and reassuringly the *PGK1* ORF did not contain any PARE>1 peaks. Only the *PGK1* decapping peak upstream of the ORF was detected. Thus, the PARE>1 filter appears suitable to reduce low level background noise and reduces the data from 24 million rows to approximately 100,000 rows.

To distinguish TSEN products from those produced by decapping and other endonucleases, we filtered on a comPARE score >2 or <-2 (or a 4-fold change in signal upon TSEN inactivation). A total of 465 positions exceeded this threshold, of which 464 showed a decrease in signal in *sen2-ts*. The only increased signal barely exceeded the comPARE<-2 threshold (Figure 3.3A). The known TSEN sites in *CBP1* and tRNAs exceeded that threshold, but the Ire1 sites in *HAC1* and the decapping sites in *CBP1*, *HAC1*, and *PGK1* did not, reflecting that these sites are not TSEN cleavage sites (bottom panels in Figure 3.2A-D). Many of the top scoring positions were at pre-tRNA splice sites or within ORFs. Limiting the signals to ones that occur at pre-tRNA splice sites or within ORFs reduced the number of positions to 180, all of which were down in the *sen2* mutant (Figure 3.3B). Several of the high scoring

ORFs (including *CBP1* and *PKP2*) contained several cleavage positions (Figure 3.3B). The highest scoring position was one of the known cleavage sites in *CBP1*. Taken together, these results indicate that PARE can reliably identify endonuclease cleavage sites in mRNAs (and pre-tRNAs) expressed at their endogenous level, and that comPARE can identify exact cleavage sites of specific endonucleases such as TSEN.

comPARE identifies a small subset of mRNAs that encode mitochondrial proteins as TED targets

The initial comPARE analysis identified 19 sites in the genome with a comPARE>4 in both replicates. Four cleavage events in *CBP1* (Figure 3.2A) had the first, fourth, tenth and 16th highest comPARE score (average comPARE scores 7.3, 5.7, 5.1, and 4.5, respectively). Four pre-tRNA cleavage sites also had average comPARE>4. We were surprised to detect any tRNA substrates as PARE is designed to identify polyadenylated degradation intermediates that are degraded by Xrn1. The released tRNA exons and introns are not expected to be polyadenylated, the released exons are not stabilized by *xrn1*Δ but instead are rapidly ligated by Trl1 (Abelson et al., 1998; Greer et al., 1983; Peebles et al., 1979), and the released exons and introns are too small for the size selection step in library preparation. Nevertheless, *CBP1* and pre-tRNAs accounted for eight of the top 19 comPARE hits. When examining the read maps of these comPARE hits, peaks are clearly visible in the control and disappear in *sen2-ts* validating our comPARE scores. The other eleven hits included six sites in five other ORFs that encode mitochondrial proteins (Figure 3.3C-F; *COQ5*, *MIS1, PKP2*, *ERV1,* and *YHR033W;* (Dubreuil et al., 2019; Huh et al., 2003; Kumar et al., 2002)), and five intergenic regions. The enrichment for mRNAs localized to the mitochondria is expected as the TSEN complex localizes to the mitochondrial membrane in yeast and this localization has been shown to be required for the other unknown essential function of TSEN (Chatterjee et al., 2018; Dhungel and Hopper, 2012).

To confirm that TSEN is directly cleaving these newly identified mRNAs, we generated *in vitro* transcribed RNAs that span from approximately 60 nts upstream of the PARE site to approximately 60 nts downstream and incubated those RNAs with purified recombinant yeast TSEN. As shown in Figure 3.4, each of the substrates were cleaved by TSEN and produced major products of the expected size (indicated with * in Figure 3.4). Notably, pre-tRNA-Phe (specifically tF(GAA)F) was cleaved more efficiently than the candidate mRNA sites. This preference is expected as *in vivo* TSEN cleaves pre-tRNA to initiate its function, while the mature mRNA is cleaved/degraded slower to allow the functional protein to be translated before the mRNA is cleaved. When compared to each other, the mRNAs were cleaved with different efficiencies, but all were cleaved better than a control mRNA fragment (Figure 3.4). *COQ5* was cleaved least efficiently, perhaps because not all sequence elements required for efficient cleavage are within 60 nts of the main cleavage site (see discussion).

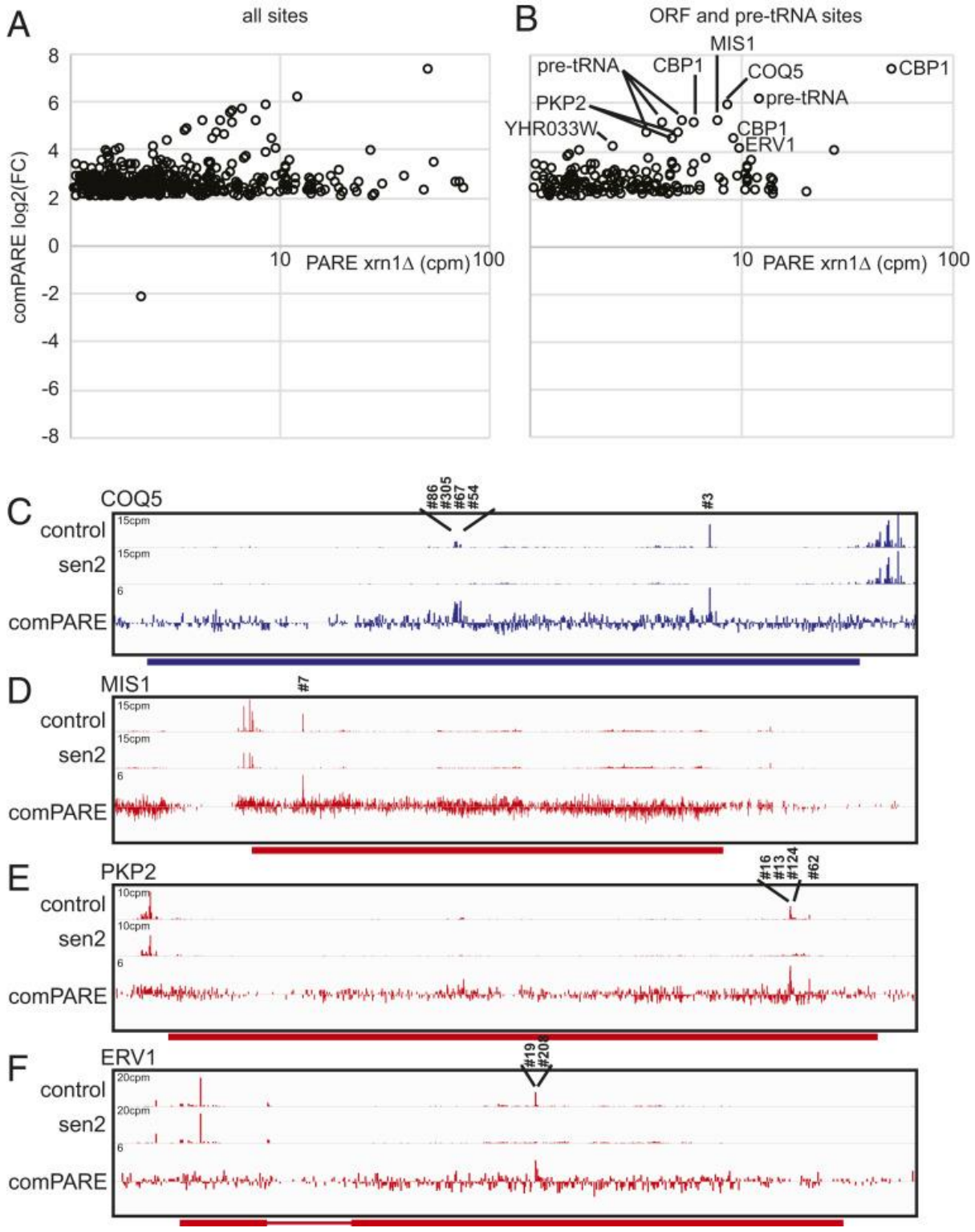
A
all sites
comPARE log2(FC)
8
6
4
2
0
-2
-4
-6
-8
10
PARE xrn1Δ (cpm)
100
B
ORF and pre-tRNA sites
MIS1
pre-tRNA
CBP1
COQ5
CBP1
PKP2
pre-tRNA
YHR033W
CBP1
ERV1
10
PARE xrn1Δ (cpm)
100
C
COQ5
#86
#305
#67
#54
#3
control
sen2
comPARE
15cpm
15cpm
6
D
MIS1
#7
control
sen2
comPARE
15cpm
15cpm
6
E
PKP2
#16
#13
#124
#62
control
sen2
comPARE
10cpm
10cpm
6
F
ERV1
#19
#20
control
sen2
comPARE
20cpm
20cpm
6

Figure 3.3: comPARE reveals previously unknown TSEN-dependent cleavage sites in mRNAs.

A). All 24 million potential sites in the genome were filtered for sites that have PARE score >1 in two biological *xrn1*∆replicates, and a comPARE score either >2 or <-2. This highlights sites that are detectable in *xrn1*∆, but either disappear (comPARE >2) or become more prominent (comPARE <-2) in *xrn1*∆ *sen2-ts*. Plotted is the average PARE score (x-axis) of two biological replicates against the average comPARE score (y-axis) of two biological replicates. Thus, data points towards the right end of the graph reflect 5' monophosphate RNAs that are prominent in *xrn1*∆, while data towards the top reflect 5' monophosphate RNAs that are much less prominent in *xrn1*∆ *sen2-ts*, **B).** as in A, but only data points within ORFs or at pre-tRNA splice sites are included. **C).** TSEN dependent-cleavages in *COQ5* are detected in *xrn1*∆ (top panel), but not in the *xrn1*∆ *sen2-ts* (middle panel), resulting in their high comPARE score (bottom panel). The numbers above each peak indicates their rank in order of comPARE score. For example, the third highest score is for a site in *COQ5*, as are sites ranked 54, 67, 86, and 305. **D)** to **F).** as in C, except that results for *MIS1*, *PKP2* and *ERV1* are shown. Panels C to F show results from one biological replicate. The other replicate showed very similar results as shown in Figure 3.7 and SI Appendix Fig. S3 in publication (Hurtig et al., 2021).

TSEN cleaves mRNAs after specific As.

Upon identification of these novel targets, we sought to identify any similarity between them in terms of sequence or secondary structure that TSEN could use to recognize its substrates. TSEN has been hypothesized to recognize the overall fold of tRNA (Fabbri et al., 1998; Greer et al., 1987; Reyes and Abelson, 1988), and a stem loop structure within *CBP1* (Tsuboi et al., 2015). In addition, TSEN in Archaea and eukaryotes recognizes a ~4bp helix to identify its tRNA targets (Baldi et al., 1992; Fabbri et al., 1998). However, secondary structure prediction revealed no obvious structural similarities between the newly identified targets, CBP1, and/or tRNAs. Secondary structure prediction remains a challenging problem, and future studies are needed to determine whether these TSEN substrates share a similar structure that TSEN recognizes.

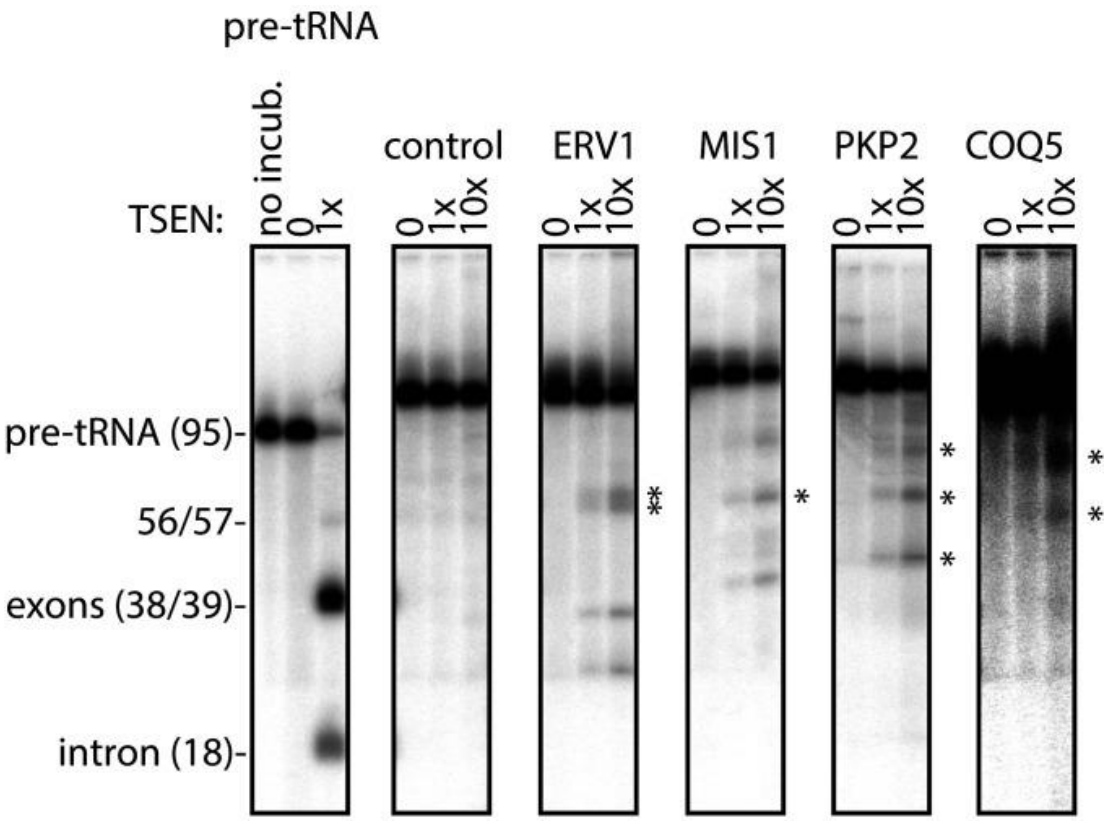

Substrate	size	expected products
pre-tRNA	95	39 + 38 + 18
control	128	N/A
ERV1	122	62 + 60
MIS1	123	62 + 61
PKP2	137	75 + 62 (+40 + 35)
COQ5	129	73 + 56

Figure 3.4 novel TSEN-mediated cleavage sites identified from comPARE are cleaved by recombinant TSEN *in vitro*.

RNAs from approximately 60 nts upstream of the novel TSEN sites to approximately 60 nt downstream were incubated *in vitro* with purified yeast TSEN, expressed in a baculovirus system. As a positive control (left panel) pre-tRNA-Phe (specifically tF(GAA)F) was incubated either in the presence (third lane) or absence (second lane) of recombinant TSEN, or analyzed without any incubation (first lane). As a negative control a distal piece of the *CBP1* mRNA was used (second panel). For panels two to six, the indicated RNA was incubated without recombinant TSEN, with a relatively low concentration of TSEN or a 10-fold higher concentration of TSEN. Products of the expected size are indicated with *. Additional ERV1 products of 35 and 20 nucleotides that are not marked are discussed in the discussion. Each panel is from a gel that also included a pre-tRNA-Phe reaction which provided size markers to identify the expected products. The *COQ5* panel is exposed darker than the other panels to visualize the faint product bands. The table below the gels lists the size of the substrates and expected products. PARE detects two sites in *PKP2*. A single cleavage of the major *PKP2* site results in 75 and 62 nucleotide products, while a second cleavage produces 40 and 35 nts products from the 75 nt fragment, which are indicated in parentheses.

Next we examined if there was a shared sequence or motif around the sites TSEN cleaves. This revealed a motif shared between the mRNA cleavage sites (Figure 3.5A). This motif includes a strong enrichment for an A immediately preceding the cleavage site (the -1 position). There is also a preference for an A in position -2 as well as for G or U at -3. Notably, these preferences are all upstream of the cleavage site and thus not in the PARE sequencing read that starts at +1. As such, these preferences cannot be explained by preferences of T4 RNA ligase or some other aspect of NGS library preparation or sequencing, but must reflect TSEN specificity. We tested the importance of this motif by mutating the -1A of *CBP1* to C. Specifically, we changed the -1As for all three prominent PARE peaks in endogenous *CBP1* to C, generating a *CBP1-3AC* mutant, and analyzed the effects both *in vivo* and *in vitro*.

To analyze the requirement for -1A *in vivo*, we expressed either wild-type *CBP1* or *CBP1-3AC* from a GAL promoter in an *xrn1*Δ strain. *xrn1*Δ stabilizes the 3' cleavage product to detectable levels, as described (Tsuboi et al., 2015). Northern blot analysis revealed that the *CBP1-3AC* mutant reproducibly accumulated less of the cleavage fragment (Figure 3.5B). To quantitate the effect on cleavage we normalized cleaved *CBP1* levels to that of full length *CBP1* mRNA. In four biological replicates, cleavage of *CBP1-3AC* was reduce to an average of 0.33 (+/- 0.16 standard deviation) relative to the normal *CBP1* mRNA (Figure 3.5C). Similarly, mutations that inactivate the cytoplasmic exosome, such as *ski7*Δ, stabilize the 3' cleavage product to detectable levels, as described (Tsuboi et al., 2015). The abundance of this fragment was reduced to 0.41 (+/- 0.09) for the *CBP1-3AC* mRNA (Figure 3.5D). A one sample t-test indicates that these reductions in both cleavage products are statistically significant ($p<0.005$ for each). Note that the *CBP1-3AC* allele has the -1 nucleotide for the three most prominent PARE sites mutated, but in the context of the overexpression construct used, additional PARE peaks are detected (SI Appendix Fig. S1 in publication (Hurtig et al., 2021)). Therefore, the cleavage product that remains in the *CBP1-3AC* mutant likely includes

cleavage products only seen in the overexpressed *CBP1*. These results indicate that TSEN recognizes an A at -1 for efficient cleavage *in vivo*.

To analyze the requirement for A at -1 *in vitro*, we used a 75 nucleotide substrate RNA that was previously shown to be cleaved by TSEN partially purified from yeast (Tsuboi et al., 2015). When we incubated the same RNA with recombinant TSEN it was cleaved at the expected sites (Figure 3.5E, SI Appendix Fig. S2 in publication (Hurtig et al., 2021)). PARE analysis indicates that *CBP1* is cleaved *in vivo* after nucleotides 669, 715, and 719 with the latter cleaved less efficiently. We thus expected major fragments of 46, 18, and 11 nucleotides (and perhaps minor products of 50 and 7 nucleotides). This is in good agreement with the major band produced from wild-type *CBP1* substrate migrating slightly slower that the pre-tRNA-Phe exons of 38 and 39 nts, a second band comigrating with the 18 nucleotide pre-tRNA intron, and a third even smaller band. When we used a substrate with extended 5' and 3' ends it also produced the 46 nucleotide product, confirming that this is an internal fragment, but it produced longer terminal fragments as expected (~60 nts instead of 18 and 11). Importantly, production of the 46 nucleotide product was reduced more than 10-fold for the *CBP1-3AC* RNA, and instead a product of approximately 57 nucleotides was prominent. This 57 nt product is consistent with cleavage only at 669, and shows striking similarity to *in vitro* products of the enzyme with a *sen2-H297A* mutation (Tsuboi et al., 2015) (see discussion). In addition to the change in major product from 46 to 57 nucleotides, the *CBP1-3AC* mutant was cleaved approximately 2-fold less (13% versus 6%, when considering the 46 and 57 nts products cumulatively, and correcting for the number of labeled U residues). This overall reduction in cleavage is in good agreement with the 2 to 3-fold reduction seen *in vivo*. Thus, the *in vitro* results indicate that cleavage at nucleotide 715 is strongly reduced in the *CBP1-3AC* mutant.

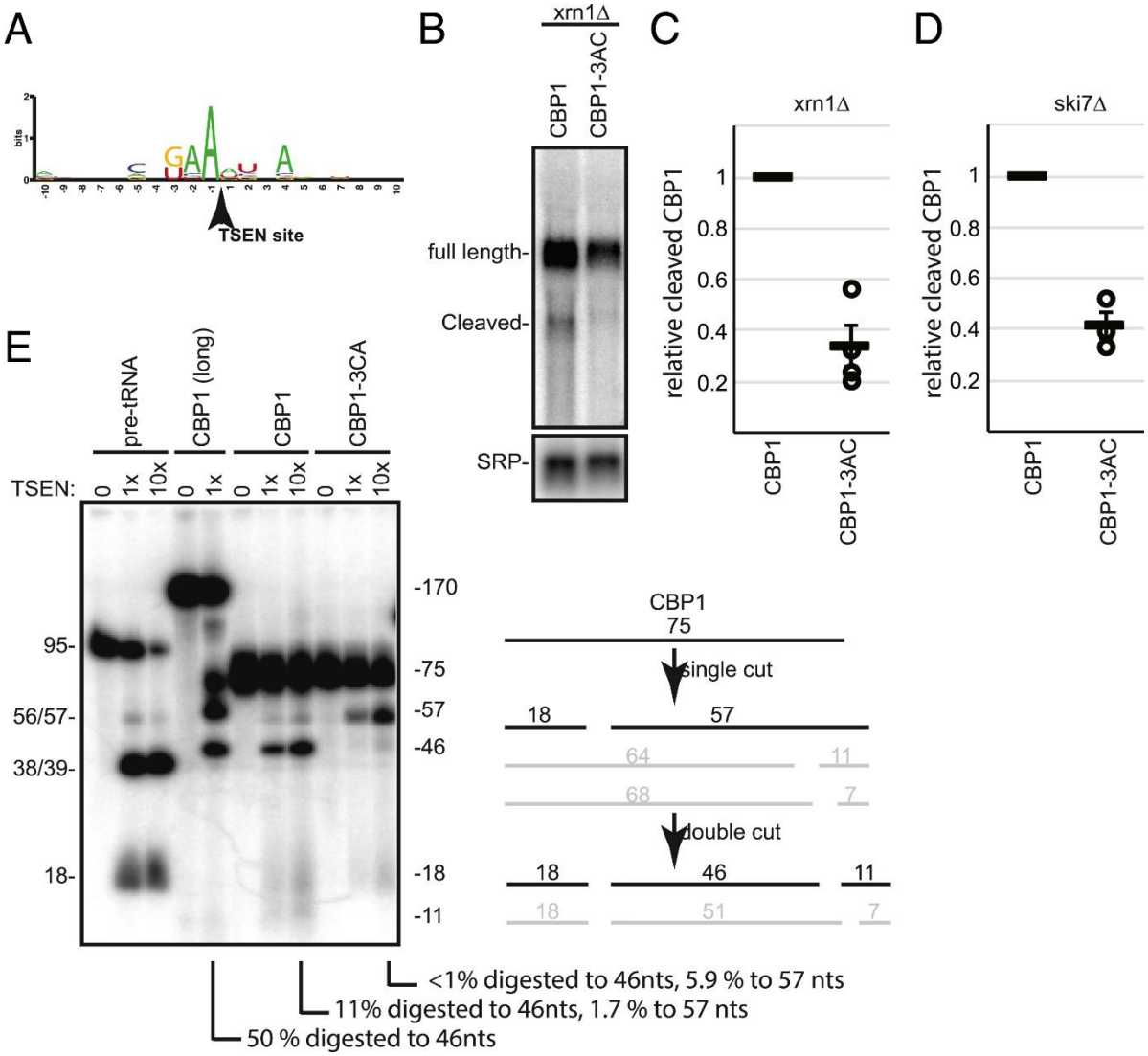
A
TSEN site
B
xrn1Δ
CBP1
CBP1-3AC
full length-
Cleaved-
SRP-
C
xrn1Δ
relative cleaved CBP1
CBP1
CBP1-3AC
D
ski7Δ
relative cleaved CBP1
CBP1
CBP1-3AC
E
pre-tRNA
CBP1 (long)
CBP1
CBP1-3CA
TSEN:
0
1x
10x
95-
56/57-
38/39-
18-
-170
-75
-57
-46
-18
-11
CBP1
75
single cut
18
57
64
11
68
7
double cut
18
46
11
18
51
7
<1% digested to 46nts, 5.9 % to 57 nts
11% digested to 46nts, 1.7 % to 57 nts
50 % digested to 46nts

Figure 3.5: TSEN recognizes an A residue immediately 5' of the cleavage site.

A). Shown is a sequence logo of the top cleavage sites from Figure 3.3, indicating that TSEN has some sequence specificity. **B).** Northern blot analysis of wild-type *CBP1* or a mutant with the -1A nucleotide for the three most prominent TSEN cleavage sites mutated to C (*CBP1-3AC*). In *xrn1*Δ, the 3' cleavage products are detectable for CBP1, but are reduced for the *CBP1-3AC* mutant. This panel shows a representative blot. **C).** and **D).** The level of the cleaved mRNA relative to full length mRNA was quantitated and normalized in *xrn1*Δ (panel C) and *ski7*Δ (panel D) mutants. The values for individual biological replicates are plotted (circles) as is the average (horizontal bar) and standard deviation (error bar). The 3' cleavage product that accumulates in *xrn1*Δ is quantitated in panel C and the 5' cleavage product that accumulates in *ski7*Δ is quantitated in panel D. **E).** Wild-type *CBP1* is efficiently cleaved by recombinant TSEN *in vitro*, but this cleavage is strongly reduced for the *CBP1-3AC* mutant. The numbers below the gel indicate % substrate cleaved in this experiment, which is representative of triplicates. Note that the 46 nts substrate contains fewer labeled nucleotides than the 170 and 75 nts substrates which explains why the product bands appear lighter than the same amount of substrate. Numbers to the left are sizes of the pre-tRNA-Phe (specifically tF(GAA)F) substrate and products (18nt intron, 38 and 39 nt exons, 56 and 57 singly cut RNAs consisting of intron and one exon). Numbers and schematic to the right is a summary of product size expected for the 75 nt substrate based on the *in vivo* cleavage sites (see Table 2.3). Predicted products depicted as black lines are prominent in the gel, while products depicted in gray are not. Shown is a representative gel. A replicate with an independently purified second batch of enzyme and RNA is shown in SI Appendix Fig. S2 in publication (Hurtig et al., 2021).

The Sen2 catalytic histidine is required for cleavage at all sites *in vivo*.

TSEN contains two catalytic sites with catalytic histidine residues in Sen2 (His297) and Sen34 (His217). *In vitro*, *sen2-H297A* prevents cleavage between the 5' exon and intron (5' site) of pre-tRNA, while *sen34-H217A* prevents cleavage of the 3' site (Trotta et al., 2006). In contrast, *in vivo sen2-H297A* causes accumulation of pre-tRNAs that are end-matured but contain both exons and the intron (Dhungel and Hopper, 2012), suggesting that *sen2-H297A* prevents cleavage at both the 5' and 3' sites *in vivo*. To investigate the role of Sen2-H297 more broadly, we repeated PARE analysis. For this analysis we used the *sen2-ts xrn1*Δ strain used above, and transformed it with either a wild-type *SEN2* plasmid, a *sen2-H297A* plasmid, or an empty vector. RNA was extracted from duplicate cultures, and all six RNA samples were analyzed by PARE. We then calculated the comPARE scores for all known TSEN sites, including the 5' and 3' sites of all pre-tRNA introns and the sites in the *CBP1*, *MIS1*, *ERV1*, *COQ5* and *PKP2* mRNAs. In these comPARE analyses, we compared the strain containing the wild-type *SEN2* plasmid to either the strain with the *sen2-H297A* plasmid or the empty vector strain. In Figure 3.6A the comPARE scores of known TSEN sites for replicate 1 of *sen2-H297A* are plotted against the comPARE scores for empty vector, revealing a strong correlation with a slope near 1. This indicates that *in vivo* the *sen2-H297A* complementing plasmid is defective in cleaving both 5' sites and 3' sites in pre-tRNA as well as mRNA sites. Figure 3.6B shows the correlation coefficients for each of the replicates of *sen2-H297A* and empty vector, indicating that the comPARE scores for *sen2-H297A* and empty vector are as strongly correlated with each other as with their biological replicate. Thus, we conclude that Sen2-H297 is required for all TSEN-mediated cleavages *in vivo*, possibly because it has a role in substrate binding in addition to its catalytic role (see discussion).

A

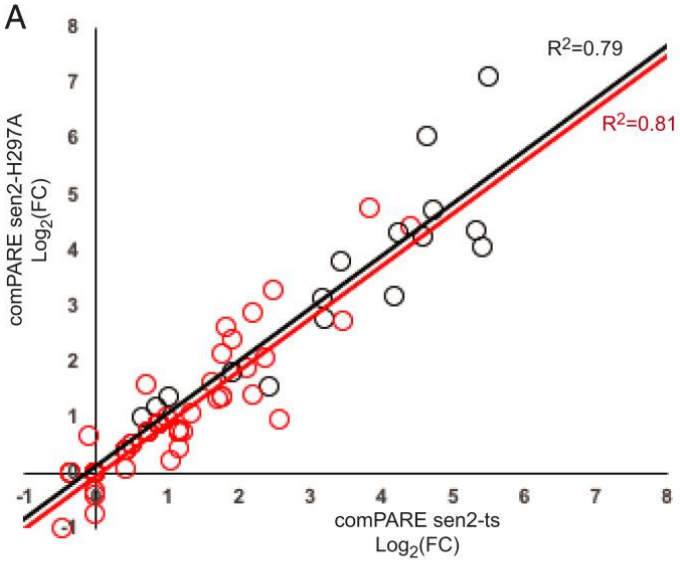

B

	sen2-H297A rep 1	*sen2-H297A* rep 2	*sen2-ts* rep 1
sen2-H297A rep 2	0.78		
sen2-ts rep 1	0.92	0.80	
sen2-ts rep 2	0.82	0.94	0.83

Figure 3.6: All TSEN-dependent cleavages detected by comPARE require Sen2-H297.

A). Plotted are the comPARE scores for one biological replicate of *xrn1*Δ *sen2*-ts with an empty vector plotted against the comPARE score of the same strain with a sen2-H297A plasmid. Data from pre-tRNA splice sites are in red, while data from mRNA sites from Figure 3.3 are in black. Cleavage sites requiring Sen2-H297 fall along a line with slope 1, while Sen2-H297 independent (and presumably Sen34-H217 dependent) sites should fall along the x-axis. The data points cluster along the diagonal and are correlated with a R^2=0.79 for all the mRNA sites and R^2=0.81 for all the pre-tRNA splice sites **B).** Correlation coefficients of two biological replicates of empty vector and two biological replicates of sen2-H297A indicate that essentially all in vivo detected TSEN-dependent cleavages require the His297 residue of Sen2. The correlation coefficients include both the pre-tRNA and mRNA sites.

TSEN cleaves the same mRNAs during fermentative and respiratory growth.

Yeast has two main metabolic growth states that differ greatly by their mitochondrial activity. In the presence of glucose, yeast ferments glucose to ethanol, with mitochondrial respiration being largely inactive. Genes such as *CBP1* and *COQ5* are nonessential under these conditions (yeastgenome.org). The above PARE analysis was performed in either YEP (Figures 3.1 and 3.3) or SC-LEU media (Figure 3.6) both containing glucose. Alternatively, when provided with carbon sources that cannot be fermented (such as glycerol) yeast will grow by respiration, mitochondria are more numerous and more active, and *CBP1* and *COQ5* are essential (yeastgenome.org). Because TSEN is localized to the outside of mitochondria and appears to target mRNAs that encode mitochondrial proteins, we repeated PARE analysis of the *xrn1*Δ and *xrn1*Δ *sen2-ts* strains grown in YEP+2% glycerol. This analysis revealed that TSEN targeted mRNAs are cleaved in both growth conditions (Figure 3.7; SI Appendix Fig. S1 and 3 in publication (Hurtig et al., 2021)).

We next generated a list of genes that scored high in a majority of the seven comPARE datasets by filtering sites that had a PARE score >1 in the *xrn1*Δ sample and a comPARE score >3 when compared to the matching *xrn1*Δ *sen2* sample in at least four of the seven comPARE datasets (Figure 3.7A and SI Appendix Table S1 in publication (Hurtig et al., 2021)). This list contains five pre-tRNA splice sites in four different pre-tRNAs (Figure 3.7A). Two of these are 5' sites and three are 3' sites. Also included in the recurrent sites were 33 sites in 22 different ORFS, as well as one site in the intergenic region between *PAN6* and *ATG32*. Ten of these sites had a comPARE score >3 in all seven datasets, and a good match to the sequence motif in Figure 3.5A and thus the corresponding mRNAs are high confidence TED targets (*CBP1, COQ5, PKP2, DLD1, and ERV1*; SI Appendix Table S1 in publication (Hurtig et al., 2021)). These five mRNAs each encode mitochondrial proteins (Dubreuil et al., 2019; Huh et al., 2003; Kumar et al., 2002). Three other mRNAs have comPARE scores >3

in six of the seven data sets and match well to the sequence motif (*MIS1, YHR033W, MDL1*). *MIS1* appears to be not expressed in the 7th dataset, while *YHR033W* and *MDL1* have comPARE scores of 2.96 and 2.87 in one of the datasets, just barely below the applied cutoff of 3. The Mis1, Mdl1, and YHR033W proteins are also mitochondrial (Dubreuil et al., 2019; Huh et al., 2003; Kumar et al., 2002). Thus, we conclude that these eight mRNAs are very likely TED targets. Some of the other mRNAs in Figure 3.7A may also be TED targets, but some of them may be false positives (*e.g.* YBL059W) even though they had comPARE scores >3 in at least half of the datasets.

GO analysis (https://yeastgenome.org/goTermFinder) of the 22 ORFs from Figure 3.7A for enrichment in cellular components revealed an enrichment for mitochondrial proteins. 13 of the 22 ORFs are annotated with the GO term “mitochondria” (P=0.0011; Figure 3.7A). Nine of these are annotated with “mitochondrial envelope” (P=0.00028). Several similar GO categories were also enriched (e.g. mitochondrial part, mitochondrial membrane, organelle envelope). However, there are 1237 genes annotated with “mitochondria” and 457 with “mitochondrial envelope”, indicating that TED targets only a small subset of them. Similar GO analysis for enrichment in functional categories revealed an enrichment for “nucleotide binding” (ten proteins, p=0.0086), while no particular process category was enriched. Of the ten “nucleotide binding” proteins seven were mitochondrial. Overall, qualitative comparison of these seven comPARE datasets suggests that the same mRNAs that code for mitochondrial proteins are reproducibly cleaved by TSEN under various conditions.

Finally, we used PARE signals to compare the contributions of TED and decapping to mRNA decay. Both TED and decapping products accumulate as 5’ phosphorylated products in the *xrn1*Δ strain. Thus, we used the PARE peaks upstream of ORFs as a measure of decapping and compared the TSEN-dependent PARE peaks to these putative decapping PARE peaks for the eight highest confidence TED targets. Figure 3.7B shows the fraction of

TSEN products relative to the total degradome (TSEN cleavage plus decapping) for these genes. This revealed two trends. First, as we expected the contribution of TED to mRNA degradation varied between mRNAs. When the signals for the four glucose grown samples were averaged (horizontal bars in Figure 3.7B), for *CBP1*, *ERV1* and *PKP2* the PARE signal from TED was similar to the decapping PARE signal, suggesting that both pathways contribute approximately equally to their degradation. For the five other high confidence TED targets, TSEN products were less abundant than decapping products under these conditions, contributing less than 30% of the total mRNA degradome. However, even for these genes the TSEN product made a substantial contribution to the overall degradome. Second, in the glycerol sample, the prominence of TED was reduced relative to decapping for all eight high confidence TED targets when compared to the average of the glucose samples (Figure 3.7B, compare the red dots to the bars). Determining whether this reduced contribution of TED reflects the difference between respiratory and fermentative growth will require additional studies, but it does suggest that the quantitative contribution of TED to mRNA decay varies between conditions. Overall, this comparison between TED and decapping activities suggests that the contribution of TED to mRNA decay is considerable but varies both between mRNAs and conditions (see discussion).

A

Gene	compare sen2-ts rep 1	compare sen2-ts rep 2	compare sen2-ts rep 3	compare sen2-ts rep 4	compare sen2-H297A rep 1	compare sen2-H297A rep 2	compare sen2-ts glycerol
CBP1	7.61	7.04	5.50	8.27	7.12	7.79	4.71
COQ5	6.17	5.55	4.66	4.83	6.04	4.81	6.40
CBP1	5.71	4.47	4.25	5.72	4.30	5.72	7.65
tP(UGG)M	6.65	5.64	3.83	5.62	4.77	4.06	6.42
CBP1	6.26	5.14	4.31	4.10	3.90	4.51	6.86
tL(UAG)L1	5.15	5.15	4.41	4.60	4.41	4.20	6.91
PKP2	4.41	4.98	4.58	5.29	4.23	4.24	5.58
CBP1	4.99	3.94	5.43	4.54	4.03	3.68	3.60
DLD1	3.77	3.62	3.75	3.91	3.75	3.95	7.40
PEX3	-1.01	6.84	0.13	7.95	8.15	7.95	0.00
COQ6	2.79	2.33	5.12	3.31	5.37	3.71	6.56
PKP2	4.71	4.17	4.19	3.65	3.17	4.29	4.99
pan6 3'UTR	4.41	4.77	4.29	3.99	3.68	3.58	4.17
PKP2	3.55	2.70	5.33	5.49	4.34	4.10	2.90
MIS1	5.01	5.44	4.73	3.95	4.73	3.95	0.00
YHR033W	4.55	3.73	2.96	3.86	3.05	4.37	5.15
MDL1	3.44	4.22	3.91	3.35	4.37	2.87	5.00
tP(UGG)O1	2.84	3.71	3.47	4.60	2.72	4.12	5.35
BUD32	3.96	2.73	3.80	3.80	3.44	4.09	4.57
SWT1	3.13	3.58	2.92	4.68	3.18	3.96	4.95
COQ6	1.13	3.29	5.84	2.96	5.23	3.83	2.84
KTR3	3.66	2.70	3.10	3.01	3.19	3.05	6.41
ERV1	4.39	3.68	3.19	3.07	3.13	3.47	4.05
YIR016W	1.55	1.58	3.01	3.87	3.05	3.39	8.30
TAH11	3.53	2.77	3.40	2.85	2.88	3.38	5.35
VMS1	2.57	2.67	3.20	4.79	2.60	3.43	4.79
TUF1	2.75	3.36	2.81	3.83	3.48	3.36	3.93
tP(UGG)O1	3.20	3.50	2.13	4.65	1.86	4.65	3.30
PHB2	1.38	3.12	3.52	4.01	3.21	2.44	5.23
COQ5	3.75	2.68	3.43	2.58	3.79	2.04	4.23
TUF1	3.24	2.14	2.55	3.82	3.35	3.35	3.96
ABP1	4.00	2.88	3.05	4.30	3.99	2.70	1.39
PKP2	3.10	2.30	3.21	4.15	2.74	4.02	2.22
NAT1	4.47	2.80	3.01	2.11	3.21	1.21	4.68
MIS1	3.43	3.75	3.16	2.92	3.16	2.44	0.54
tY(GUA)F1	2.42	3.24	2.49	3.82	3.29	3.82	0.00
PEX3	-0.28	4.77	-0.11	4.48	4.62	4.08	0.00
YBL059W	-1.40	7.62	-7.02	7.27	-6.86	8.92	3.30
RPS14A	-4.62	-0.48	3.08	3.18	3.16	3.63	1.45

B

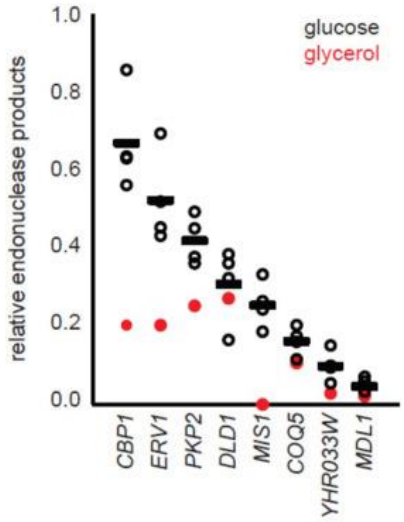

Figure 3.7: Summary of seven comPARE datasets from different conditions.

A). Shown are 39 sites that in the majority (at least 4 of 7) of the datasets had a PARE score >1 and a comPARE score >3. comPARE scores are shown and shaded from high (dark green) to low (dark red). The 39 sites are listed in order of average comPARE score. Yellow highlighted genes encode mitochondrial proteins, while cyan highlighted genes encode intron containing pre-tRNAs. A more extensive version is included as SI Appendix Table S1 in the publication (Hurtig et al., 2021). **B).** Endonuclease cleavage contributes substantially to mRNA decay. To estimate the contribution of TSEN to mRNA degradation the major PARE signals attributable to endonucleolytic cleavage were compared to the total degradome signal (PARE peaks attributable to TSEN plus PARE peaks attributable to decapping). Thus a value of 1 would reflect exclusive degradation by TSEN, while a value of 0.5 reflects equal contributions of TSEN and decapping to mRNA decay.

Chapter Conclusions

PARE was developed to identify endonuclease cleavage sites and has been used to identify the mRNA degradome that accumulates upon deletion or depletion of *XRN1*. Here we use this strategy to characterize the function of two endoribonucleases, the RNA exosome and TSEN, by identifying PARE scores reduced in the corresponding mutant. Because the RNA exosome is both nuclear and cytoplasmic, we used an *xrn1*Δ *rat1-1* double mutant. Notably this is the first characterization of the nuclear degradome available to the community, but we still were unable to identify any convincing endonuclease cleavage sites for the PIN domain of the RNA exosome. In contrast, we identified novel and known TSEN cleavage sites. One possible explanation is that the RNA exosome may have a lower specificity for specific positions than the TSEN complex, which exhibits strong preference to cleave specific sites. In addition, PARE is designed to detect poly-adenylated products, and the PIN domain of the RNA exosome may cleave unadenylated substrates. We further developed a simple bio-informatic pipeline (comPARE) that identifies cleavage sites with single nucleotide precision. comPARE should be readily implementable by RNA biologists studying a variety of processes. Through the powerful method of PARE and comPARE we provide an expanded understanding of TSEN function.

TSEN was initially discovered as an endonuclease with a dedicated function in tRNA splicing (Peebles et al., 1983, 1979), and was studied for many years for this role (Figure 3.8A). Here we show that TSEN cleaves multiple mRNAs that encode mitochondrial proteins and propose to name this pathway tRNA Endonuclease-initiated Decay (TED; Figure 3.8B). One puzzling aspect of yeast TSEN was that it localized to the outside of mitochondria, which provides no obvious advantage for a nuclease dedicated to pre-tRNA splicing. Furthermore, although TSEN is assembled more efficiently in its native location, it is able to assemble and effectively splice tRNAs when artificially localized into the nucleus (Dhungel and Hopper,

2012; Wan and Hopper, 2018). The role of TSEN in cleaving mRNAs that encode mitochondrial proteins provides the first rational explanation for its localization.

We note that archaeal TSEN also cleaves at least one mRNA (Yoshinari et al., 2006), suggesting that TED may be an ancient conserved pathway. The targets of TED are likely to differ in different organisms. For example, archaeal TSEN targets the cbf5 mRNA (Yoshinari et al., 2006), which we did not detect as a yeast target. Unlike yeast TSEN, human TSEN is a nuclear enzyme (Paushkin et al., 2004), and thus it appears unlikely that human TED targets mRNAs that encode mitochondrial proteins. Instead, if human TSEN cleaves mRNAs, the target mRNAs are likely to differ from the ones in yeast.

While TSEN produces 5’ hydroxyl RNAs, Xrn1 only degrades 5’ monophosphate RNAs, and PARE only detects RNAs that have a 5’ monophosphate. This implies that there must be some kinase that phosphorylates TED targets. Based on its known function in other kinase-dependent mRNA decay pathways, Trl1 appears the most likely candidate (Cherry et al., 2019; Peach et al., 2015), but its role will require further investigation (Figure 3.8B). Interestingly, human TSEN associates with the polynucleotide kinase CLP1 (Paushkin et al., 2004; Popow et al., 2011; Ramirez et al., 2008). While the human pre-tRNA splicing mechanism does not require a polynucleotide kinase step, if human TSEN also cleaves other RNAs to initiate their degradation by XRN1 or XRN2, this would require a polynucleotide kinase such as CLP1.

Remarkably, mutations in either human TSEN or CLP1 cause pontocerebellar hypoplasia (Budde et al., 2008; Karaca et al., 2014; Schaffer et al., 2014). Based on several observations we speculate that a defect in TED may be more relevant to this disease than tRNA splicing. First, human tRNA splicing also requires the ligase RTCB (Figure 3.8A), but mutations in *RTCB* have not been found in pontocerebellar hypoplasia patients. Second, as mentioned, TED requires both TSEN and a polynucleotide kinase such as CLP1 but the

distinct human tRNA splicing pathway does not require phosphorylation of an intermediate RNA (Figure 3.8A). Third, fibroblasts and induced neurons of PCH patients with CLP1 mutations accumulated higher levels of some intron-containing pre-tRNAs compared to unaffected controls, but other intron-containing pre-tRNAs were less abundant in patient cells (Schaffer et al., 2014). Thus, pre-tRNA levels were not consistently affected in CLP1 PCH patient cells, consistent with the absence of a RNA phosphorylation step in the human pre-tRNA splicing pathway. Whether a defect in TED indeed underlies pontocerebellar hypoplasia will be difficult to test, but a strategy similar to ours should be able to identify the substrates for such a pathway.

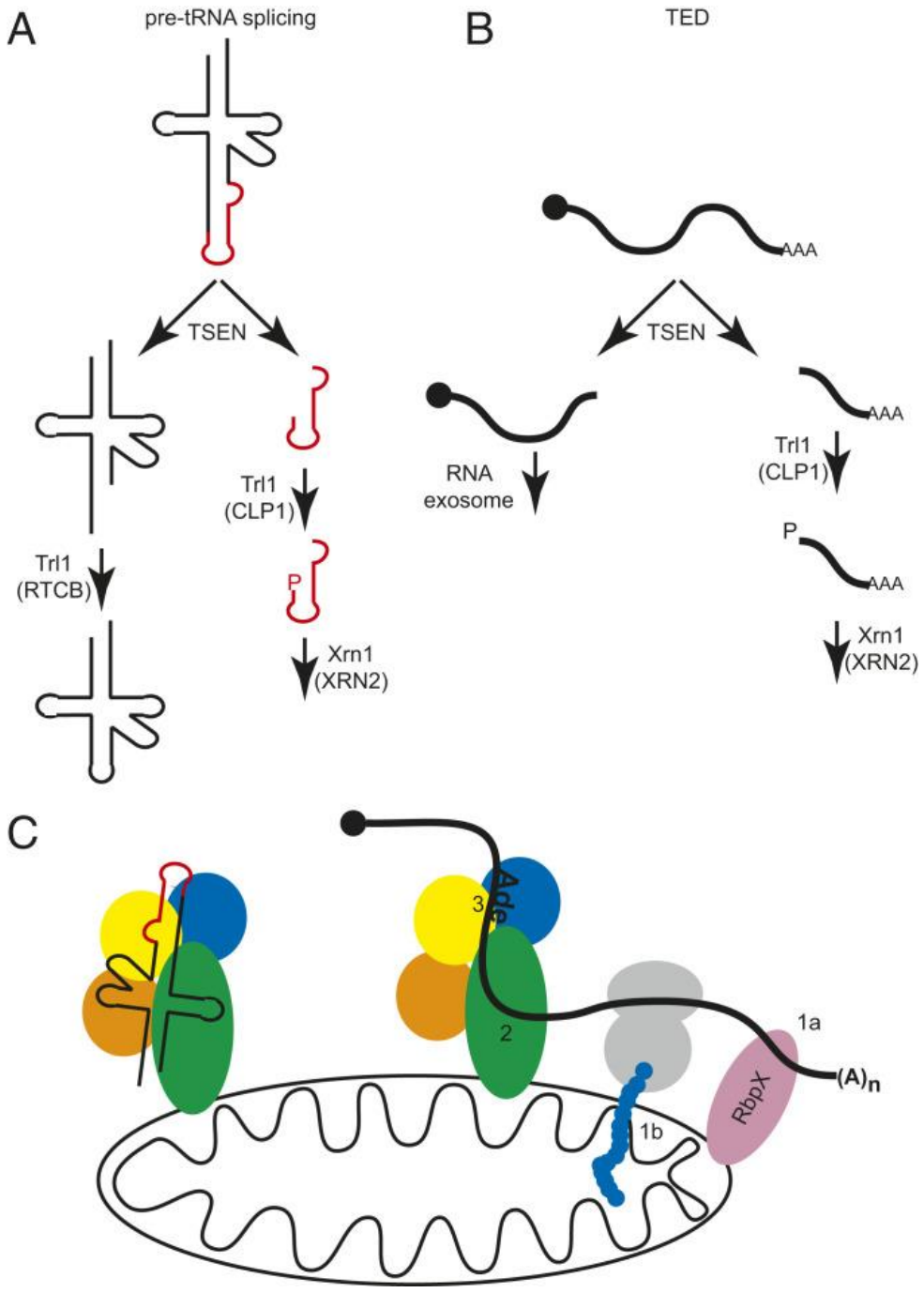
A
pre-tRNA splicing
TSEN
Trl1
(CLP1)
P
Trl1
(RTCB)
Xrn1
(XRN2)
B
TED
AAA
TSEN
RNA
exosome
AAA
Trl1
(CLP1)
P
AAA
Xrn1
(XRN2)
C
3
Ade
2
1a
(A)n
RbpX
1b

Figure 3.8: An expanded view of TSEN function.

A). The pre-tRNA splicing pathway is depicted. TSEN cleaves the pre-tRNA. In yeast, the resulting exons (black lines) are ligated by Trl1 in multiple steps, while in humans this is carried out in a single step by RTCB. The released yeast introns (red lines) are degraded by Xrn1 after phosphorylation by Trl1. In humans this presumably is carried out by CLP1 and XRN2. **B).** The TED pathway is depicted, which includes cleavage by TSEN, degradation of the 5' product by the RNA exosome, and degradation of the 3' product by Xrn1 (XRN2 in humans) after phosphorylation by Trl1 (CLP1 in humans (Wu and Hopper, 2014)). **C).** Shown on the left is the previously proposed ruler model, where Sen54 recognizes tRNA structure at sites distant from the actual cleavage sites. Sen 54 has also been proposed to be required for targeting to the mitochondrial outer membrane. The evidence that both roles are carried out by Sen54 is incomplete and other subunits may also contribute. Shown on the right is that mRNAs are known to be localized to the mitochondrial membrane either by RNA binding proteins (RbpX) binding to their 3' UTR (marked 1a), or through co-translational import of the nascent protein (marked 1b). We propose that this colocalization is required but not sufficient for TSEN-mediated cleavage. The cleavage sites are proposed to be determined by additional interactions between TSEN (perhaps Sen54) and mRNA features distal from the cleavage sites (marked 2) and interaction between the active sites of Sen2 and Sen15 and mRNA features proximal to the cleavage sites (marked 3), including an A at -1 (indicated as Ade).

We suspect that our high-confidence list of TED targets might be incomplete. As discussed, the standard implementation of PARE focused on poly(A)+ RNAs that have a 5' monophosphate, and library prep includes a size selection step. Thus, TSEN could produce some cleavage products that either lack a poly(A) tail, are not 5' phosphorylated after cleavage, or are too small for this RNA isolation and sequencing strategy. We also suspect that the stringent cut-offs we used limit the detection of some sites. For example, we note that in addition to the high confidence site in *ERV1* there is a lower scoring site 35 nucleotides upstream (SI Appendix Fig. S3 in publication (Hurtig et al., 2021)) that is detectable in the *SEN2* strain, but reduced in the *sen2-ts* strain, with an average comPARE score of 2.4. Strikingly, cleavage at this site could explain the *in vitro* cleavage product of about 35 and 26 nucleotides in Figure 3.4. We thus speculate that this is an authentic TSEN site *in vivo* and *in vitro* and other similar sites remain to be determined.

We suspect that the cleavage of the mRNAs we identified is not the unknown essential function of TSEN. TSEN inactivation would result in overexpression of TED targets, but none of the TED targets are known to be lethal when individually overexpressed (Makanae et al., 2013). We therefore conclude that cleavage/degradation of the mRNAs we identified is an unlikely explanation for the lethality of TSEN inactivation. *ERV1* is the only essential gene we identified as a TED target, but its sole intron is a typical spliceosomal intron and TSEN does not appear to have a function in splicing *ERV1* pre-mRNA. Thus, TSEN is unlikely to be required for Erv1 expression. While it is known that TSEN mutations (likely indirectly) affect rRNA processing (Dhungel and Hopper, 2012), none of the targets we discovered seem to be involved in pre-rRNA processing. Overall, we conclude that although we have expanded our understanding of TSEN function, our knowledge remains incomplete and the unknown essential function of TSEN remains to be determined.

In the absence of structural information, substrate recognition by eukaryotic TSEN remains poorly understood. Biochemical studies have revealed multifaceted recognition of pre-tRNAs that combines proximal and distal recognition sites. Specifically, pre-tRNA cleavage requires a basepair between the anticodon loop and intron (the A-I basepair) (Baldi et al., 1992; Bufardeci et al., 1993; Fabbri et al., 1998; Fruscoloni et al., 2001), but is also determined by the distance between the cleavage site and the body of the tRNA (Greer et al., 1987; Reyes and Abelson, 1988). This has led to the proposal of a ruler model, where the overall structure of tRNA is recognized by TSEN, perhaps by the Sen54 subunit, and cleavage occurs at a specific distance from this recognition site (Figure 3.8C, left). Archaeal and eukaryotic TSEN also recognize a short helix within its targets (Fruscoloni et al., 2001; Yoshihisa, 2014). TSEN was also hypothesized to recognize a stem loop structure in *CBP1* (Tsuboi et al., 2015) but the stem loop was solely proposed based on mFOLD prediction, and its importance was not tested through compensatory mutations. In our hands mFOLD, RNAfold, and TurboFold did not suggest convincing structures for any of the TED substrates. We therefore suggest that future *in vivo* and *in vitro* experiments are needed to fully understand the structures of pre-tRNA and mRNA that are recognized by TSEN.

For TED, we propose a model that explains most of our and previously published data (Figure 3.8C, right) and shares aspects with the ruler model for pre-tRNA cleavage. In this modified ruler model, recognition of substrate mRNAs occurs in at least three steps. First, TED requires that target mRNAs are localized with TSEN on the outside of mitochondria (step 1 in Figure 3.8C). mRNAs can be localized to mitochondria through interactions with RNA binding proteins that bind simultaneously to their target mRNAs and mitochondria (step 1a) or through the co-translational recognition of the nascent peptide by the TOM protein import machinery (step1b) (Eliyahu et al., 2010; Gadir et al., 2011; Golani-Armon and Arava, 2016). Similarly, translation of the CBP1 transit peptide has been shown to be required for TED

(Tsuboi et al., 2015). This co-localization contributes to which mRNAs are cleaved, but not what sites are cleaved. Second, we suspect that mRNAs are recognized by a distal substrate recognition site and cleaved some distance away. This would explain why several TED targets are cleaved at a small number of clustered sites: recognizing one distal site may allow cleavage at a cluster of sites. Furthermore, this explains why overexpressed *CBP1* is cleaved at sites that are not efficiently cleaved in the endogenous mRNA. Such distal recognition also explains why a 170nt *CBP1* fragment was cleaved more efficiently than a shorter substrate *in vitro* (Figure 3.5E). Whether distal recognition of mRNAs requires the same binding site on TSEN as for the tRNA ruler mechanism remains to be determined. Finally, interactions between the substrate and enzyme near the catalytic center position the phosphodiester backbone precisely in the active site (step 3). This appears to involve an interaction between the -1A base and the enzyme. Remarkably, mutating the -1A bases in *CBP1* (Figure 3.5D) has a very similar effect to mutating Sen2-His297 *in vitro* (Tsuboi et al., 2015). A possible explanation is that the -1A nucleotide is recognized in proximity to the Sen2 catalytic histidine. In archaea the equivalent His is stacked onto base +1 of the substrate RNA (Xue et al., 2006). We therefore suggest that Sen2-H297 and the -1A both contribute to substrate recognition, but do not directly interact with each other. A role of Sen2-H297 in substrate binding also explains our observation and previous observations (Dhungel and Hopper, 2012) that the *sen2-H297A* mutation prevents cleavage at all TSEN sites *in vivo*.

Although the overall ruler model for pre-tRNA recognition can be extended to TED, the details of substrate recognition are likely to differ. Specifically, we find a preference for A at -1 for mRNA cleavage, that has not been described for pre-tRNA splice sites. Instead the 5' pre-tRNA splice sites appear to have very little if any sequence specificity (SI Appendix Fig. S4 in publication (Hurtig et al., 2021)). Extensive biochemical and structural approaches will be needed to fill in these details of substrate recognition.

Because TSEN has a critical role in tRNA production, regulation of TED by changing the activity of TSEN is unlikely under most conditions. However, slower growth requires lower rates of tRNA synthesis and splicing. A possibly lower amount of TSEN, combined with increased expression of mitochondrial proteins, may be related to our initial analysis that suggests that TED might be less active during slower respiratory growth on glycerol, but more research will be needed to establish how this occurs.

Our proposed multistep substrate recognition model (Figure 3.8C, right) has several additional implications for TED regulation. First, although mRNAs that encode mitochondrial proteins are enriched on the outside of the mitochondria, these mRNAs are also present diffusely in the cytoplasm. For any given gene, TED can only cleave the subset of mRNA molecules that are localized near the mitochondria, while decapping is likely to degrade the more diffuse mRNA molecules from the same gene. It seems likely that co-translational import of proteins into the mitochondria is more efficient than post-translational import of diffusely produced protein. Thus, while TED and decapping may overall contribute similarly to the degradation of TED mRNA targets such as *CBP1*, *ERV1* and *PKP2* (Figure 3.7B), by targeting the localized mRNA, TED might have a disproportionate impact on protein levels by degrading mRNAs actively involved in co-translational import.

A second implication of our model is that any physiological condition that affects the localization of TED targets also is likely to alter the balance between TED and decapping. Similarly, alterations in TED target structure or in protein binding near TSEN recognition sites are likely to alter the balance between TED and decapping. This may explain condition-specific differences in TSEN-mediated and decapping-mediated decay (Figure 3.7B).

A third implication of our model is that *in vitro* cleavage assays only reflect steps 2 and 3 of the model and do not reflect the contribution of co-localization to substrate specificity. This co-localization and the multiple interactions between TSEN, mitochondria, and TED targets is likely to increase the avidity of TSEN for TED targets *in vivo*. In contrast to TED

targets, pre-tRNAs are not known to be actively targeted to the mitochondria. Thus, one reason why mRNA substrates are a poorer substrate *in vitro* when compared to pre-tRNA may be that the *in vitro* system is missing an important aspect of *in vivo* mRNA avidity but the same *in vitro* conditions may fully reflect the affinity for pre-tRNAs.

Several aspects of TED are similar to the ER-localized RIDD pathway. First, mRNA degradation is initiated by an endonuclease that is bound to a specific membrane (the ER membrane and the mitochondrial outer membrane). Second, mRNAs are targeted in part due to their co-localization with the enzyme, and this mRNA localization depends partially on the co-translational import of the encoded nascent protein into the organelle. Third, the endonuclease shows some, but limited sequence specificity (UGC at -2 to +1 for RIDD) (Kimmig et al., 2012). Fourth, the resulting fragments are degraded by the RNA exosome and Xrn1 (Hollien and Weissman, 2006; Kimmig et al., 2012). Fifth, the endoribonuclease cleavage produces a 5’ hydroxyl which is converted to a 5’ monophosphate that allows degradation by Xrn1 *in vivo* and that is exploited by PARE. Given the similarities between the two pathways, we speculate that other mRNA decay pathways initiated by localized endonucleases remain to be discovered. Possible locations for these pathways include the chloroplast outer membrane and highly polarized cell projections such as those found in neurons of Metazoa and hyphae of Fungi.

4) An unknown essential function of tRNA splicing endonuclease is linked to the integrated stress response and intron debranching

This chapter is from the resubmitted paper Hurtig JE, van Hoof A. An unknown essential function of tRNA splicing endonuclease is linked to the integrated stress response and intron debranching. Resubmitted to Genetics. 2023 February 10.

Chapter Introduction

tRNA splicing endonuclease (TSEN) is a multi-subunit RNase with multiple functions that are not completely known (Abelson et al., 1998; Cherry et al., 2018; Dhungel and Hopper, 2012; Hurtig et al., 2021; Rauhut et al., 1990; Tsuboi et al., 2015). TSEN consists of four different subunits; Sen2, Sen15, Sen34 and Sen54 (or TSEN2, TSEN15, TSEN34 and TSEN54 in human) (Trotta et al., 1997). Mutations in any of the four subunits of human TSEN lead to pontocerebellar hypoplasia (PCH), which results in atrophy of the cerebellum and pons, overall microcephaly, developmental disorders, respiratory failure, and childhood death (Battini et al., 2014; Bierhals et al., 2013; Breuss et al., 2016; Budde et al., 2008; Maraş-Genç et al., 2015; Namavar et al., 2011b, 2011a; Sepahvand et al., 2020; van Dijk et al., 2018). Recent results suggest that the single amino acid changes that cause PCH affect the assembly or stability of the complex, and/or its interactions with other proteins (Hayne et al., 2022a; Sekulovski et al., 2022). Whether this causes a defect in tRNA splicing that has brain specific consequences or causes a defect in some other RNA processing or degradation pathway is currently unclear. An important step in understanding PCH is to understand all the functions of this enzyme.

As its name implies, the canonical function of TSEN is to remove introns from pre-tRNAs (Abelson et al., 1998; Peebles et al., 1979; Rauhut et al., 1990; Trotta et al., 1997). Most, if not all, eukaryotic genomes include intron-containing tRNA genes, although these introns are only present in a subset of tRNA genes (http://gtrnadb.ucsc.edu/). 20% of yeast tRNA genes, encoding ten different tRNAs, and 5% of human tRNA genes, encoding four different tRNAs, contain introns that must be removed to generate a complete set of tRNAs required for translation and viability (http://gtrnadb.ucsc.edu/). Consistent with the widespread presence of tRNA introns, homologs of TSEN are present throughout eukaryotes and some archaea, and the tRNA splicing function is thought to be conserved (Fabbri et al., 1998;

Fujishima and Kanai, 2014; Paushkin et al., 2004; Yoshihisa, 2014). Sen2 and Sen34 are the catalytic subunits of TSEN and cleave the 5' and 3' end of the tRNA intron, respectively (Greer et al., 1987; Peebles et al., 1979; Reyes and Abelson, 1988; Trotta et al., 1997). It has been suggested that Sen54 acts as a ruler and "measures" the distance between conserved structural features of tRNA and the intron to correctly orient the complex to cut at the correct sites (Reyes and Abelson, 1988). After both the 5' and 3' sites are cleaved, the exons are ligated together (by Trl1 in yeast or RtcB in Metazoa) (Greer et al., 1983; Popow et al., 2011). Some characterization of PCH-causing TSEN mutations has been attempted in cell culture and zebrafish embryos (Breuss et al., 2016; Kasher et al., 2011). Most studies report a buildup of tRNA precursors and less mature tRNA. However, it is not clear whether these tRNA effects cause the PCH pathology.

In addition to pre-tRNA cleavage, TSEN also cleaves some mRNAs in both archaea and eukaryotes (Hurtig et al., 2021; Tsuboi et al., 2015; Yokobori et al., 2009). This was initially shown for a single eukaryotic mRNA, yeast *CBP1,* but a subsequent transcriptome-wide study showed that approximately nine mRNAs that encode mitochondrial proteins are cleaved by TSEN at specific sites to initiate their degradation (Hurtig et al., 2021; Tsuboi et al., 2015). Whether this mRNA cleavage function is conserved in humans, and whether this contributes to PCH pathology remains to be determined.

Besides these characterized roles, two previous experiments indicate that TSEN has an essential but unidentified function in yeast. First, all four TSEN subunits, as well as the ligase Trl1 and Tpt1, a phosphatase that removes the phosphate that remains after ligation, are essential (Phizicky et al., 1992; Séron et al., 1999; Trotta et al., 1997). Importantly, artificial expression of ten intronless tRNA genes can suppress the lethality of *trl1*Δ and *tpt1*Δ, but not the lethality of *sen2*Δ, *sen15*Δ *sen34*Δ, and *sen54*Δ (Cherry et al., 2018). Thus, these intronless tRNA genes can supply functional tRNAs, independent of splicing as the ligation

machinery is no longer essential. Conversely, this experiment shows that TSEN has a tRNA-splicing independent essential function as the complex remains essential when tRNA splicing is bypassed. Second, yeast TSEN normally localizes to the outside of the mitochondria. However, when TSEN is artificially localized into the nucleus, it is still able to cleave introns from pre-tRNAs but the cell is not viable (Dhungel and Hopper, 2012). This implies that TSEN has an important function in the cytoplasm that is currently unknown and unrelated to tRNA splicing. Interestingly, while many PCH patients with mutations in TSEN have been identified, mutations in other genes required for tRNA splicing are not known to cause PCH. This includes the *RTCB* and *ARCH* genes that are required in the ligation step of the splicing reaction (Desai et al., 2014; Popow et al., 2011). However, mutations in human CLP1, which encodes a polynucleotide kinase that associates with the TSEN complex, have been found to cause PCH (type 10) (Karaca et al., 2014; Monaghan et al., 2021; Schaffer et al., 2014; Ramirez et al., 2008). Interestingly CLP1 is known to have other functions in RNA processing but does not seem to be required for tRNA processing (Hayne et al., 2020; Monaghan et al., 2021; Paushkin et al., 2004; Weitzer et al., 2015). This suggests that CLP1 participates in another function of TSEN in humans, and that this function may be critical for PCH pathology.

To investigate the other essential function of yeast TSEN, we performed genetic screens to identify high-copy and spontaneous suppressors of a *sen2* mutation. The high-copy suppressor screen shows that overexpression of *SEN54* can compensate for point mutations in *SEN2*, possibly by stabilizing the complex. Since PCH causing mutations also have been suggested to destabilize the human complex (Breuss et al., 2016), our results suggest that overexpressing one of the other subunits may be able to compensate for some of these mutations and/or that natural variation in expression of other TSEN subunits could modulate disease severity. In our spontaneous suppressor screen we found two different mutations in *DBR1*, which encodes the intron debranching enzyme for spliceosomal splicing.

RNA-seq on *sen2* mutant strains shows that the Gcn4 integrated stress response pathway is activated. We further showed that *dbr1*Δ partially restored this Gcn4 dysregulation. Both the activation of the integrated stress response in *sen2* and its partial suppression by *dbr1* are independent of a role in tRNA splicing, suggesting Gcn4 is activated by the loss of the other essential function of TSEN. Overall, these results further characterize the other essential function of TSEN.

Results

Overexpression of Sen54 suppresses destabilized Sen2 protein

We performed a high-copy suppressor screen to identify genes whose overexpression can affect the unknown essential function of TSEN mutation. We used a temperature sensitive *sen2* allele (*sen2-ts)* that is functional at room temperature but lethal at 37 °C. This Sen2-ts protein has previously been shown to be destabilized (Metzger et al., 2020). To differentiate between novel functions and the tRNA processing role, a plasmid containing ten intronless tRNA genes was added to the *sen2-ts* strain. Thus, this *sen2-ts* [intronless tRNA] is unable to grow at 37 °C because of a defect in the unknown essential function of TSEN. This strain was then transformed with the Yeast Genome Tiling collection (Jones et al., 2008), which contains high-copy plasmids covering the yeast genome, and plated at 37 °C (Figure 4.1A).

The plasmid was extracted from transformants able to grow at 37 °C and sequenced to determine the suppressor. We recovered two different plasmids that suppressed at 37 °C. As expected, one of these plasmids contain the *SEN2* gene, validating the screen. Sequencing the other revealed *SEN54* as a suppressor.

Because it has previously been shown that the *sen2-ts* protein is unstable (Metzger et al., 2020), we speculated that *SEN54* overexpression may suppress *sen2-ts* by stabilizing the protein. This postulate makes several predictions. First, it predicts that *SEN54* overexpression

would suppress *sen2-ts* both in the absence or presence of the intronless tRNA genes. We therefore compared growth of the *sen2-ts* strain with either an empty vector or the *SEN54* overexpression plasmid. As shown in Figure 4.1B, the *SEN54* plasmid indeed improved growth at 37 °C even in the absence of the intronless tRNA gene plasmid. Second, our postulate predicts that while *SEN54* can suppress *sen2-ts* it should not be able to suppress *sen2*Δ or a point mutation in the catalytic histidine residue of Sen2 (H297A or *sen2-cat*). Indeed, plasmid shuffling assays showed that *SEN54* suppression was specific to the *sen2-ts* mutation. In this assay, a *sen2*Δ strain expressing the wild-type *SEN2* gene on a *URA3* plasmid and a *sen2-cat,* vector*,* or *SEN2 LEU2* plasmid was transformed with either the *SEN54* plasmid or an empty vector and tested for growth on 5FOA. 5FOA selects for cells that have lost the *URA3* plasmid with wild-type *SEN2*. Only strains with the *SEN2-LEU2* plasmid were able to grow (Figure 4.1C) showing that *SEN54* overexpression does not suppress either *sen2*Δ or *sen2-cat*. Together, these results indicate that *SEN54* overexpression suppresses all the functional defects of *sen2-ts* and is not specific for the unknown essential function.

To determine whether the stabilizing effect of Sen54 on Sen2 is limited to yeast or more widely applicable, we knocked down the expression of each subunit in human cells (MCF7) with two different siRNAs and assessed the levels of the other subunits (Figure 4.1D,E). TSEN54 knockdown reduced the level of TSEN2 protein, while TSEN34 was largely unaffected. Conversely, knockdown of TSEN2 also reduced TSEN54 protein, but not TSEN34. This does appear to be specific to TSEN2 and TSEN54 as knockdown of TSEN34 or TSEN15 did not have a pronounced effect on the levels of TSEN2 or TSEN54. Using linear regression, we determined the levels of TSEN54 and TSEN2 are positively correlated in this experiment while the levels of the other subunits are either not correlative (TSEN2 compared to TSEN34; teal) or negatively correlated (TSEN34 compared to TSEN54; green) (Figure

4.1E). These results combined with our yeast data are consistent with an assembly pathway that includes a dimer of TSEN2 and TSEN54 (Figure 4.1F).

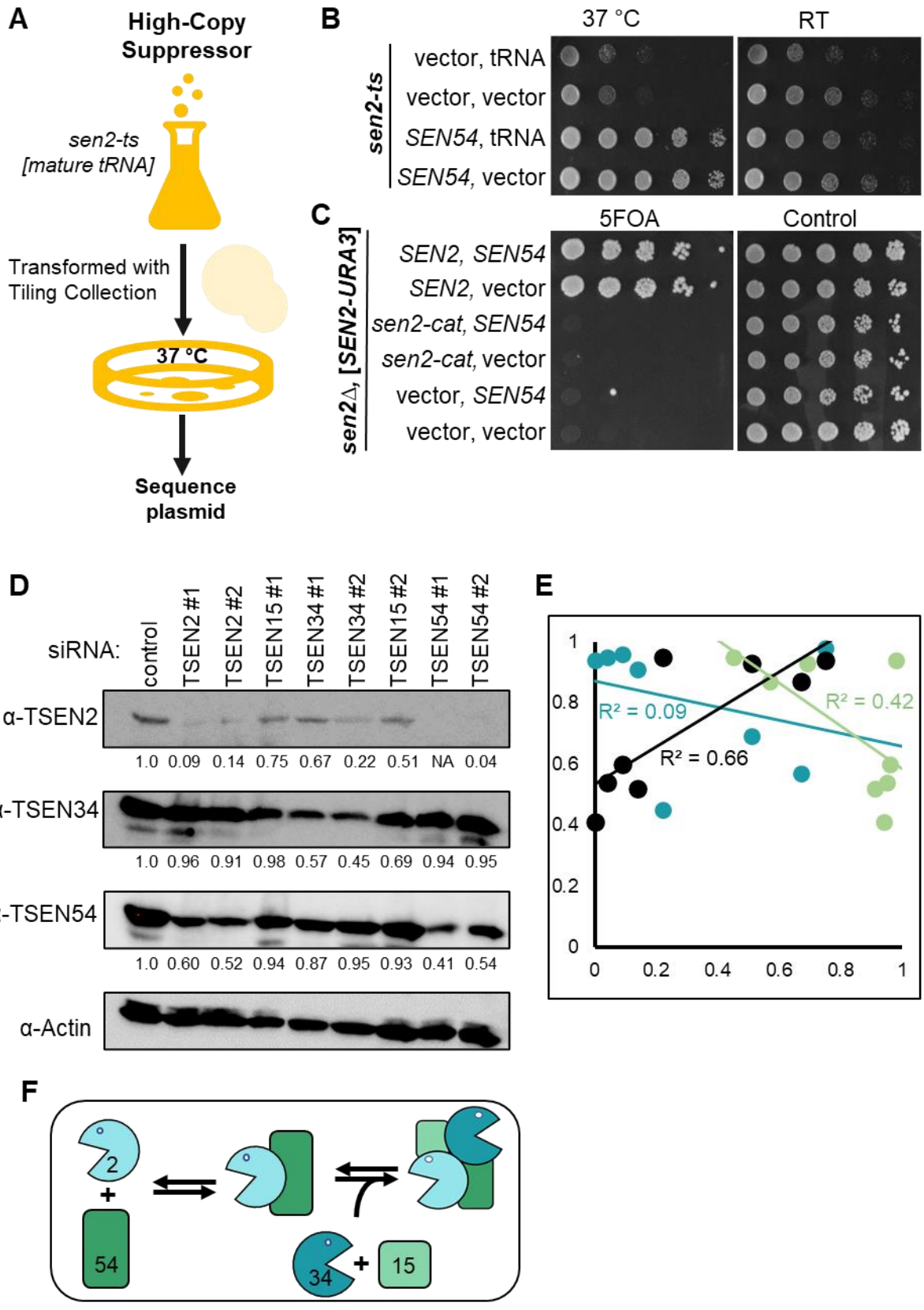
A
High-Copy Suppressor
sen2-ts [mature tRNA]
Transformed with Tiling Collection
37 °C
Sequence plasmid
B
37 °C
RT
sen2-ts
vector, tRNA
vector, vector
SEN54, tRNA
SEN54, vector
C
5FOA
Control
sen2Δ, [SEN2-URA3]
SEN2, SEN54
SEN2, vector
sen2-cat, SEN54
sen2-cat, vector
vector, SEN54
vector, vector
D
siRNA:
control
TSEN2 #1
TSEN2 #2
TSEN15 #1
TSEN34 #1
TSEN34 #2
TSEN15 #2
TSEN54 #1
TSEN54 #2
α-TSEN2
1.0 0.09 0.14 0.75 0.67 0.22 0.51 NA 0.04
α-TSEN34
1.0 0.96 0.91 0.98 0.57 0.45 0.69 0.94 0.95
α-TSEN54
1.0 0.60 0.52 0.94 0.87 0.95 0.93 0.41 0.54
α-Actin
E
R² = 0.09
R² = 0.42
R² = 0.66
F
2
54
34
15

Figure 4.1: *SEN54* is a high-copy suppressor of *sen2-ts.*

A). Schematic of the high-copy suppressor screen. The *sen2-ts* with intronless tRNA was transformed with the genome tiling collection and plated on selective media at 37 °C. The plasmids from colonies that grew were extracted and sequenced. **B).** Overexpression of *SEN54* suppresses all essential functions of *sen2-ts*. This overexpression allows growth of *sen2-ts* at 37 °C with or without expressing artificial intronless tRNA genes (rows 3 and 4, respectively). Growth assays of *sen2-ts* with and without *SEN54* overexpression in the presence or absence of intronless tRNAs are shown. **C).** *SEN54* overexpression does not suppress catalytic inactivation or complete deletion of *SEN2* even when intronless tRNAs are artificially expressed. Shown are growth assays with *sen2*Δ overexpressing *SEN54* or empty vector complemented with empty vector, a catalytic dead Sen2 (H298A), or *SEN2*. This was done both with and without the intronless tRNA plasmid. **D).** In MCF7 cells, the level of human TSEN2 or TSEN54 is reduced when its partner is depleted. A Western blot of human TSEN subunits when each subunit was depleted using siRNA. The blots shown are representative of three independent biological replicates. **E).** Quantification of Western blot in D. Linear regression analysis was performed on TSEN2, TSEN34, and TSEN54 across the siRNA depletions. Black compares TSEN2 to TSEN54; teal compares TSEN2 to TSEN34; green compares TSEN34 to TSEN54. **F).** Model for a possible assembly of TSEN depicting that TSEN2, TSEN54 and their dimer are in equilibrium. Overexpressing TSEN54 shifts the equilibrium to generate more dimer intermediate and thereby favor complete assembly. This model is also consistent with specific yeast two hybrid interactions between Sen2 and Sen15 and between Sen15 and Sen34, but not the other subunits (Trotta et al., 1997) and with the recently solved structures of human TSEN (Hayne et al., 2022a; Sekulovski et al., 2022). The absence of one subunit apparently triggers the degradation of its partner. Conversely, if a structural/folding mutation is introduced into Sen2, adding more Sen54 appears to stabilize its partner.

Mutations in debranching enzyme specifically suppress unknown tRNA independent function of TSEN

To complement the high-copy suppressor screen, we performed a spontaneous suppressor screen. The *sen2-ts* [intronless tRNA] strain was grown at 30 °C for ~40 generations and then plated at 37 °C (Figure 4.2A). Four colonies, from independent repeats, grew at 37 °C. The *SEN2* gene was PCR amplified from these four colonies and sequenced to determine whether they were revertants (changing *sen2-ts* back to wild-type *SEN2*), intragenic suppressors (containing additional mutation in *SEN2*), or extragenic suppressors (still containing the *sen2-ts* allele). Two of the colonies had partial reversions in *SEN2*: the *sen2-ts* allele has four amino acid changes (M72I, Q134R, L220P, and F300C). One of the revertants had reverted P220 back to L while the other revertant had reverted I72 back to M (Figure 4.2B). Therefore, both the mutations at residues 220 and 72 are required for the temperature sensitivity of the strain. Whether the mutations at residues 134 and 300 also contribute to the temperature sensitive phenotype cannot be inferred from these data. The other two colonies maintained all four *sen2-ts* mutations and lacked any additional mutations that could be intragenic suppressors. Thus, our spontaneous suppressor screen identified two partial revertants and two extragenic suppressors.

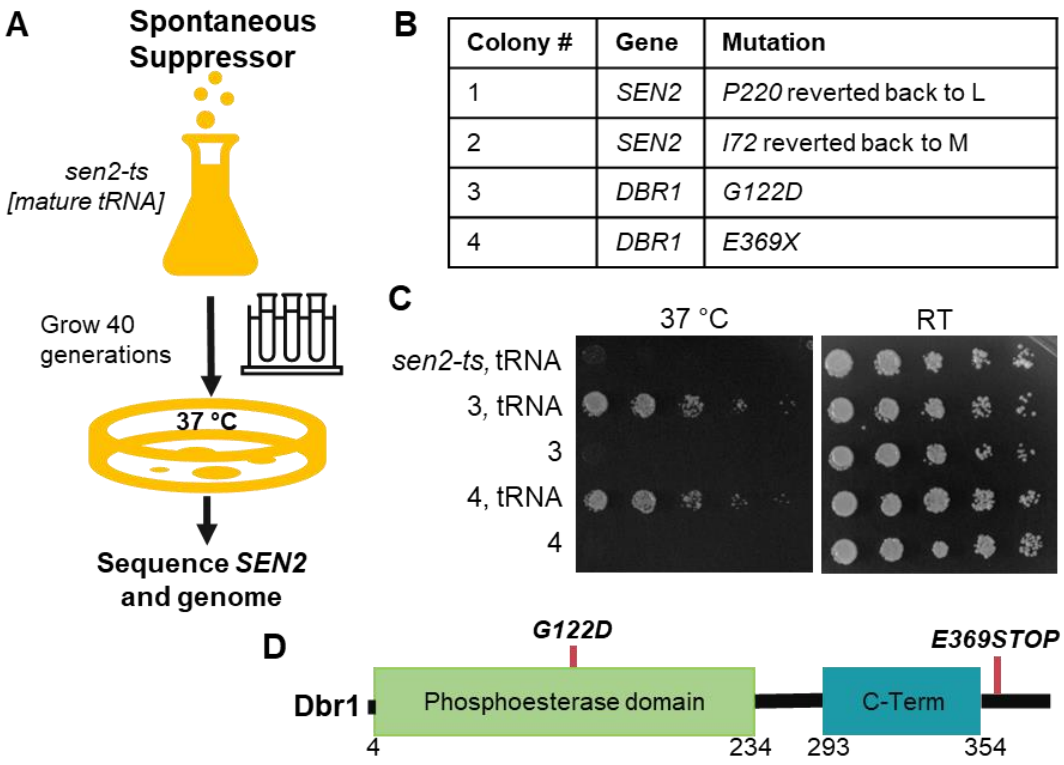

Colony #	Gene	Mutation
1	*SEN2*	*P220* reverted back to L
2	*SEN2*	*I72* reverted back to M
3	*DBR1*	*G122D*
4	*DBR1*	*E369X*

Figure 4.2: **Mutations in *DBR1* suppress *sen2-ts* only in the presence of tRNA.**

A). Schematic of the spontaneous suppressor screen. The *sen2-ts* strain with artificial intronless tRNA genes was grown in liquid culture for 40 generations at 30 °C and a portion was plated at 37 °C after every 10 generations. Colonies that grew were screened for *SEN2* revertants by PCR amplifying this gene and Sanger sequencing. Two colonies that still contained the *sen2-ts* allele were analyzed by whole genome sequencing. **B).** Mutations identified by Sanger sequencing (colonies 1 and 2) and whole genome sequencing (colonies 3 and 4). **C).** The suppressor in colonies 3 and 4 specifically affect the unknown other function of TSEN and do not restore tRNA splicing. A growth assay on colonies 3 and 4 with and without the plasmid artificially expressing intronless tRNAs is shown. **D)**. Colonies 3 and 4 each contain a mutation in *DBR1*. Schematic of Dbr1 with the mutations found in colonies 3 and 4 is denoted. The mutations are in the highly conserved phosphoesterase domain or truncate the protein, respectively.

To characterize the two extragenic suppressors we first determined whether they were general, like the *SEN54* overexpression, or specific for the unknown essential function. The intronless tRNA plasmid was lost from the suppressor strains and growth was assayed at 37 °C. Both *sen2-ts* strains with suppressors lost the ability to grow at 37 °C after loss of the intronless tRNA plasmid (Figure 4.2C). We conclude that these two suppressors have mutations that only suppress the other essential function of TSEN and are unable to suppress the tRNA splicing function.

We used whole genome sequencing to identify the suppressor mutations as previously described (Kim and van Hoof, 2020). The results indicated both suppressors we identified had mutations in *DBR1*. Dbr1 is the lariat debranching enzyme for spliceosomal introns. The spliceosome removes introns from pre-mRNAs (or ncRNAs) and releases them as lariats that contain a 2’5’ linkage (Mohanta and Chakrabarti 2021). This linkage is broken by Dbr1, linearizing the intron and allowing its degradation by exoribonucleases. One of our suppressor strains had a missense mutation, G122D, in the phosphodiesterase domain of Dbr1, which is part of a metallophosphatase superfamily and a well-conserved domain across eukaryotes (Figure 4.2D). Based on the crystal structure of Dbr1 from another eukaryote (Ransey et al., 2017) and the AlphaFold model of yeast Dbr1, G122 is in the core of the protein and changing this to a bulkier and charged residue is likely detrimental (SIFT score 0.01; https://sift.bii.a-star.edu.sg/index.html). The other suppressor had a premature stop codon, deleting the last 37 residues from the protein. Although these 37 residues are not as conserved as the phosphodiesterase domain, they are significantly conserved in other budding yeast species (Saccharomycetaceae). The nature and location of the suppressor mutations suggested they cause loss of Dbr1 function.

To confirm that the *DBR1* loss of function suppresses *sen2-ts,* we tested whether a complete deletion of *DBR1* also suppresses *sen2-ts*. Growth assays showed a *dbr1*Δ *sen2-ts*

strain could grow at 37 °C, comparable to the suppressor strains, but again only in the presence of intronless tRNA plasmid (Figure 4.3B). This shows that loss of Dbr1 function is responsible for the suppression. Notably, there does not appear to be any difference in the accumulation of pre-tRNA species between the *sen2-ts* and the *sen2-ts dbr1*Δ mutant confirming this suppression is tRNA independent (Figure 4.4).

As previously mentioned, Dbr1 has a catalytic phosphoesterase domain that linearizes lariat introns, a crucial step for intron degradation. We wondered if loss of this function was needed for the suppression effect on *sen2-ts* or whether Dbr1 could have some role independent of its known catalytic function. We therefore tested a N85A mutation (*dbr1-cat*) (Figure 4.3A). This mutation has previously been shown to inactivate debranching activity but not affect protein expression level (Khalid *et al.* 2005). Our analysis showed that it too suppressed *sen2-ts* (Figure 4.3C) and thus suppression of the unknown essential function of TSEN is linked to the catalytic activity of Dbr1.

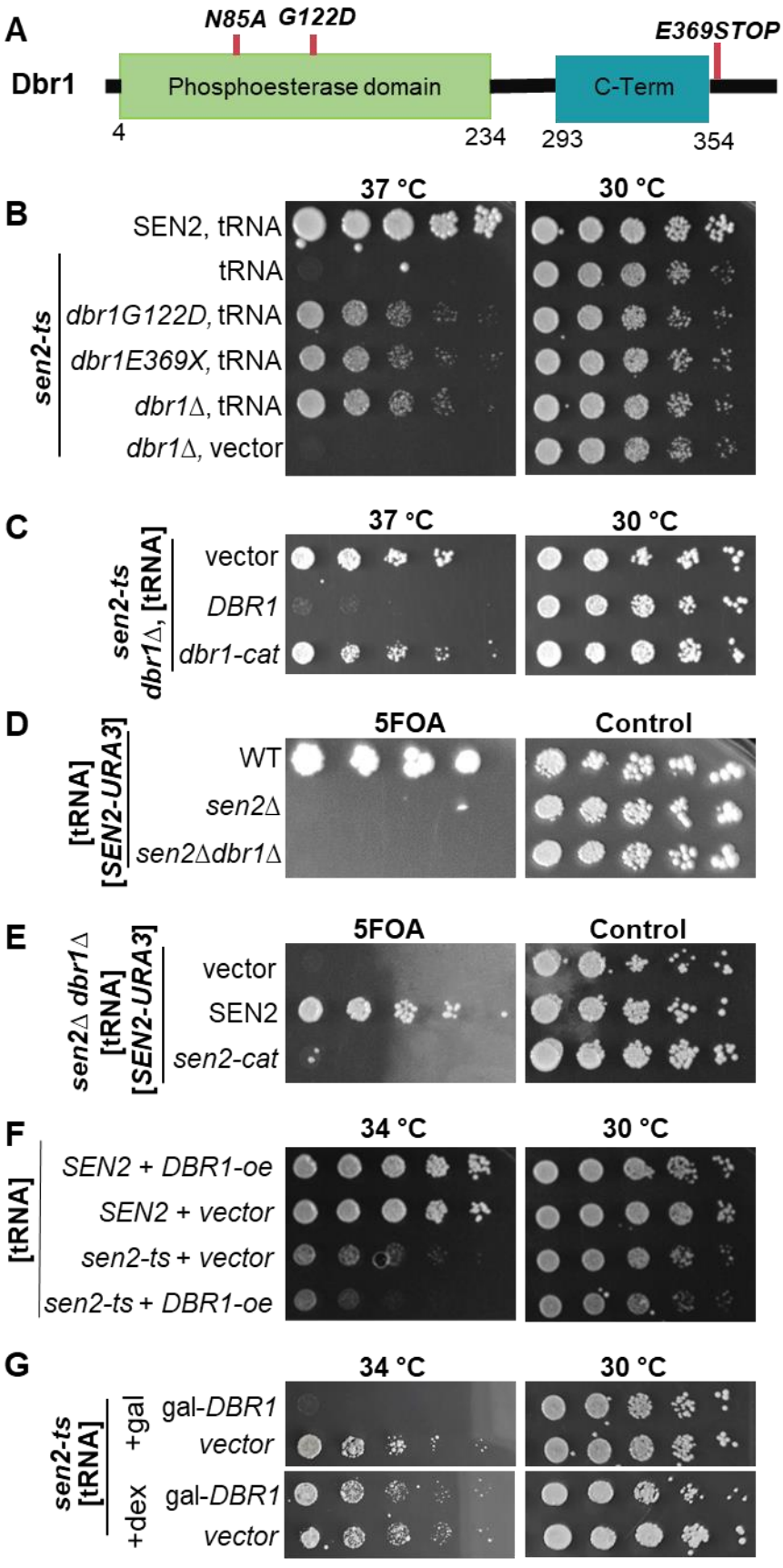
A
N85A
G122D
E369STOP
Dbr1
Phosphoesterase domain
C-Term
4
234
293
354
B
37 °C
30 °C
SEN2, tRNA
tRNA
dbr1G122D, tRNA
dbr1E369X, tRNA
dbr1Δ, tRNA
dbr1Δ, vector
sen2-ts
C
37 °C
30 °C
sen2-ts dbr1Δ, [tRNA]
vector
DBR1
dbr1-cat
D
5FOA
Control
[tRNA] [SEN2-URA3]
WT
sen2Δ
sen2Δdbr1Δ
E
5FOA
Control
sen2Δ dbr1Δ [tRNA] [SEN2-URA3]
vector
SEN2
sen2-cat
F
34 °C
30 °C
[tRNA]
SEN2 + DBR1-oe
SEN2 + vector
sen2-ts + vector
sen2-ts + DBR1-oe
G
34 °C
30 °C
sen2-ts [tRNA]
+gal
gal-DBR1
vector
+dex
gal-DBR1
vector

Figure 4.3*:* Inactivation of *DBR1 specifically* suppresses *sen2-ts* but not a catalytic mutant or *sen2* deletion*.*

A). Diagram of the catalytic mutation N85A in the phosphoesterase domain of Dbr1. **B).** *dbr1*Δ can suppress *sen2-ts* when intronless tRNA genes are artificially expressed. Shown is a growth assay of colonies 3 and 4, which contain *dbr1* point mutations, compared to a *dbr1*Δ with and without the intronless tRNA plasmid. **C).** A catalytic point mutant in *DBR1* suppresses *sen2-ts*. Growth assay of a *dbr1*Δ *sen2-ts* complemented with empty vector, *DBR1, or dbr1-cat* (N85A). Restoring *DBR1* results in loss of suppression while addition of the catalytic mutant of empty vector has no effect. **D).** *dbr1*Δ cannot suppress *sen2*Δ. Growth assay of a wild-type, *sen2*Δ*, or sen2*Δ *dbr1*Δ strain complemented with a *SEN2-URA3* plasmid. 5FOA selects for cells that have lost the SEN2-URA3 plasmid. **E).** *dbr1*Δ cannot suppress a *sen2-cat* mutation. Growth assay of *sen2*Δ *dbr1*Δ*, SEN2 dbr1*Δ*, and sen2-cat dbr1*Δ *strains.* 5FOA selects for cells that have lost the SEN2-URA3 plasmid. **F).** Overexpression of *Dbr1* enhances the growth defect of *sen2-ts* at intermediate temperatures. Shown is a growth assay of wild-type or *sen2-ts* strains with a *DBR1* high copy plasmid (2µ*DBR1*) or empty vector. **G).** Galactose-induced overexpression of *DBR1* severely reduces growth of *sen2-ts* at intermediate temperatures. The *sen2-ts* with intronless tRNA plasmid expressed either an empty vector or pGAL-*DBR1* plasmid and was grown on dextrose or galactose media at the indicated temperatures. The plates at 34 °C were imaged on day 5 and the plates at 30 °C on day 3.

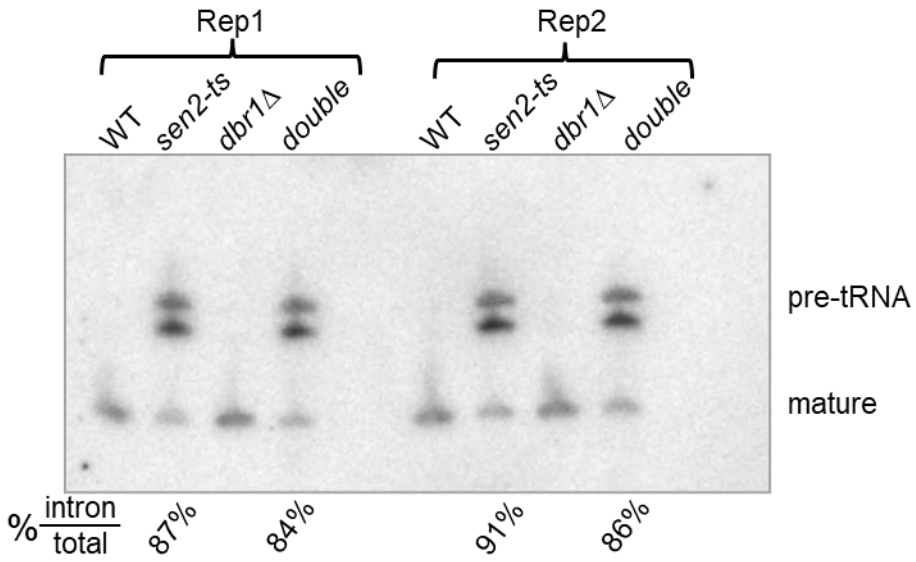

Figure 4.4: pre-tRNA accumulates in *sen2-ts* and the *sen2-ts dbr1*Δ to similar levels.

RNA from the indicated samples were run on a polyacrylamide/urea gel, transferred to a membrane for Northern blotting, probed for Leu(CAA) tRNA and quantified using ImageQuant. The contribution of signal for the two pre-tRNA bands to the total signal is indicated below the blot.

Loss of debranching enzyme suppresses *sen2-ts* but not *sen2*Δ

Because *dbr1* mutations can suppress a *sen2-ts* mutation, we wondered if it could suppress a complete loss of *SEN2*. We assessed this in strains expressing intronless tRNA genes and a wild-type *SEN2* on a selectable *URA3* plasmid (Figure 4.3D). A *SEN2* strain was able to lose the *SEN2* plasmid on 5FOA while a *sen2*Δ strain expressing the same plasmids could not grow on 5FOA as expected. The double mutant, *dbr1*Δ *sen2*Δ, also was not able to lose the *SEN2* plasmid and presents the same phenotype on 5FOA as the *sen2*Δ. Therefore, *dbr1*Δ cannot suppress *sen2*Δ. Similarly, *dbr1*Δ mutation could not suppress the loss of Sen2 catalytic activity (Figure 4.3E).

Because *dbr1*Δ can improve the growth of *sen2-ts*, we wondered whether overexpression had the opposite effect. We performed a growth assay of both *SEN2* and *sen2-ts* strains with intronless tRNA plasmid also expressing either *DBR1* on a high-copy plasmid or an empty vector control at temperatures from room temperature to 37 °C. At 34 °C, the *sen2-ts* strain with empty vector had a growth defect that became reproducibly more pronounced upon *DBR1* overexpression (Figure 4.3F). The control *SEN2* strain was not affected at any temperature by *DBR1* overexpression. As an additional approach, we overexpressed *DBR1* from a relatively strong galactose inducible promotor. This plasmid, or an empty vector control, was introduced into a *sen2-ts* strain with the intronless tRNA plasmid. Strikingly, at 34 °C on galactose, we observed the strain with the *pGAL-DBR1* plasmid had a severe growth defect compared to the vector control (Figure 4.3G). No growth defect was observed on dextrose containing media, which represses the *pGAL* promotor. In both the high copy *DBR1* and *pGAL-DBR1* experiments there was no noticeable effect when the strains were grown at room temperature or 30 °C when *sen2-ts* is functional, or at 37 °C when *sen2-ts* fails to grow and thus cannot be made to grow slower. These results demonstrate that *dbr1* mutations increase growth and *DBR1* overexpression is detrimental in the *sen2-ts* strain.

Altogether, these data suggest that some catalytic activity of TSEN is needed for the *dbr1* suppression effect. This also suggests *dbr1* does not bypass the other function of TSEN, but most likely participates in the same pathway. Furthermore, the observation that *DBR1* overexpression reduces *sen2-ts* growth suggests the possibility that TSEN and Dbr1 compete for a common substrate.

TSEN mutation activates the integrated stress response

Our results so far indicate that Dbr1 and TSEN most likely participate in the same pathway. To gain insight into the nature of this pathway, we performed RNA-seq. RNA from three replicates of wild-type, *sen2-ts*, *dbr1*Δ, and *dbr1*Δ *sen2-ts* yeast all expressing intronless tRNA genes was analyzed. Principle component analysis of the expression levels of all genes and introns indicated that the biological triplicates clustered close together indicating our RNA-seq experiment was highly reproducible (Figure 4.5A). Furthermore, it showed that *sen2-ts* and *dbr1* had distinct and largely orthologous effects with PC1 separating the six *DBR1* samples from the six *dbr1*Δ samples and PC2 separating *SEN2* samples from *sen2-ts*. Interestingly, along PC2, the *dbr1*Δ *sen2-ts* mutant is slightly closer to the *SEN2* samples than the *sen2-ts* single mutant, consistent with the *dbr1*Δ suppressor partially restoring the transcriptome disturbance caused by *sen2-ts*.

To identify individual genes affected by *sen2-ts* and/or *dbr1*Δ, we used DESeq2 (Love et al., 2014). As expected, many introns strongly accumulated in the *dbr1*Δ strain (compared to wild type; Figure 4.5B) and the *dbr1*Δ *sen2-ts* strain (compared to *sen2-ts*; Figure S3 in publication (Hurtig and van Hoof, 2023), with some introns being >100-fold more abundant. The only gene DESeq2 identified as being significantly less expressed in *dbr1*Δ was *DBR1* itself. Other than these expected results, we did not identify interesting differences between *dbr1*Δ and the wild-type strain.

We next examined differences between the wild-type and *sen2-ts* strain (Figure 4.5C). Roughly five times as many genes were upregulated more than 2-fold in the *sen2-ts* when compared to the number of down-regulated genes. The two genes that increased the most were *SNO1* and *SNZ1* with >100-fold change in expression (Figure 4.5C). *SNO1* and *SNZ1* are vitamin biosynthesis genes expressed from the same promotor on opposite strands. Gene-Ontology analysis of the 380 genes significantly upregulated in the *sen2-ts* strain identified an enrichment for amino acid synthesis and related biosynthetic processes. Many amino acid synthesis genes as well as *SNO1* and *SNZ1* are known to be transcriptionally regulated by Gcn4, the master regulator of the integrated stress response in yeast. We therefore compared the genes significantly upregulated in our *sen2-ts* dataset to Gcn4 targets previously identified using RNA-seq (Gaikwad et al., 2021) and ChIP-seq (Rawal et al., 2018) (Figure 4.5D). Over 50% of the genes upregulated in *sen2-ts* had previously been identified as a Gcn4 target in one or both studies. We analyzed the GO-terms of the remaining 174 genes in our dataset and found enrichment for biosynthesis and transport genes. We therefore suspect that these 174 genes include many additional targets of Gcn4 targets that were not identified in the other two studies. Therefore, the results of our RNA-seq suggest the Gcn4 response is activated in the *sen2-ts* strain.

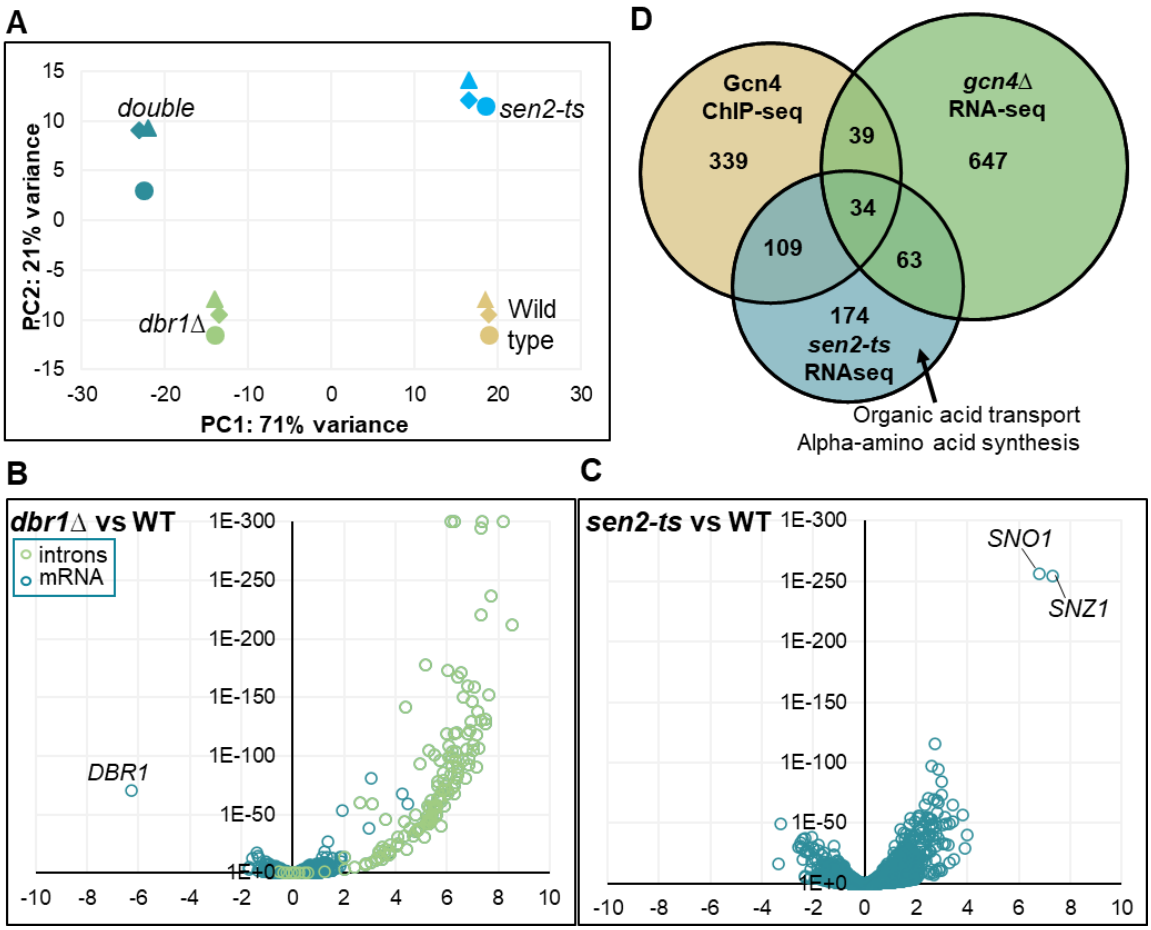
A
double
sen2-ts
dbr1Δ
Wild type
PC2: 21% variance
PC1: 71% variance
D
Gcn4 ChIP-seq
339
gcn4Δ RNA-seq
647
39
34
109
63
174
sen2-ts RNAseq
Organic acid transport
Alpha-amino acid synthesis
B
dbr1Δ vs WT
introns
mRNA
DBR1
C
sen2-ts vs WT
SNO1
SNZ1

Figure 4.5: RNA-seq analysis of *sen2-ts dbr1*Δ

A). Principle component analysis plot showing variance between RNA-seq samples and replicates. The three biological replicates all grouped closely together. PC1 separates the *DBR1* strains from the *dbr1* mutants. PC2 separates the *SEN2* strains from the *sen2-ts* mutants. **B).** Volcano plot from RNA-seq data showing genes and intron that are differentially expressed between *dbr1*Δ and wild type with introns shown in green and mRNAs in blue. As expected, almost all introns accumulate in *dbr1*Δ, but very few mRNAs are affected. **C).** Volcano plot from RNA-seq data showing genes that are differentially expressed between *sen2-ts* and wild type. The top hits, *SNO1* and *SNZ1* are labeled. **D).** More than half of the genes significantly overexpressed in *sen2-ts* are Gcn4 targets previously identified by RNA-seq or ChIP-seq. GO terms for the mRNAs upregulated in *sen2-ts* but not identified in the previous Gcn4 studies are indicated and are similar to Gcn4 targets.

*dbr1*Δ suppresses the integrated stress response activation of *sen2-ts*

As mentioned above, PCA suggested that *dbr1*Δ partially restored the transcriptome disturbance caused by *sen2-ts*. However, PCA does not identify whether a few genes are fully restored, or many genes are partially restored. To distinguish between these possibilities, we compared the fold change between the wild type and *sen2-ts* to the change between the *dbr1*Δ and *dbr1*Δ *sen2-ts*. If *dbr1*Δ restored expression of only a few genes, these few genes would fall along the x-axis while the majority of the genes would fall along a line with slope 1. On the other hand, if *dbr1*Δ partially restored the expression of many genes, these genes would fall on a diagonal line with a slope <1. In this analysis, most genes fell along a line with a slope of 0.67 (as determined by linear regression; green dashed line in Figure 4.6A). Thus, d*br1*Δ returns the levels of genes upregulated in the *sen2-ts* closer to that of wild type. This trend included *SNO1* and *SNZ1* (Figure 4.6B) as well as other known Gcn4 targets. These data suggest that the Gcn4 response is activated in *sen2-ts* and that *dbr1*Δ partially attenuates this effect.

The Gcn4 response is very well characterized (Hinnebusch, 2005). Gcn4 is a transcription factor that activates many amino acid biosynthesis genes while expression of Gcn4 itself is mostly regulated by translation in response to various cues. The *GCN4* mRNA contains four small ORFs upstream of the Gcn4-encoding ORF. Under uninduced conditions the upstream ORFs limit translation of the coding ORF, while under inducing conditions the translation of the uORFs is reduced and the main ORF is translated more. To assay Gcn4 translation we used a previously described *Gcn4-lacZ* reporter (Yang *et al.* 2000) that contains the promoter, 5'UTR, and beginning of the coding region of *GCN4* fused in frame to LacZ. The translation of this *GCN4* reporter was similar between wild type and *dbr1*Δ*,* while *sen2-t*s increases *GCN4-lacZ* reporter translation 2-3 fold (Figure 4.6C). The *dbr1*Δ *sen2-ts* had significant (p=0.02; unpaired t-test) reduction in *GCN4-lacZ* translation compared to the single

sen2-ts mutant with levels similar to the wild-type strain. This confirms our RNA-seq findings that Gcn4 is activated in *sen2-ts* and attenuated in the *dbr1*Δ *sen2-ts* strain.

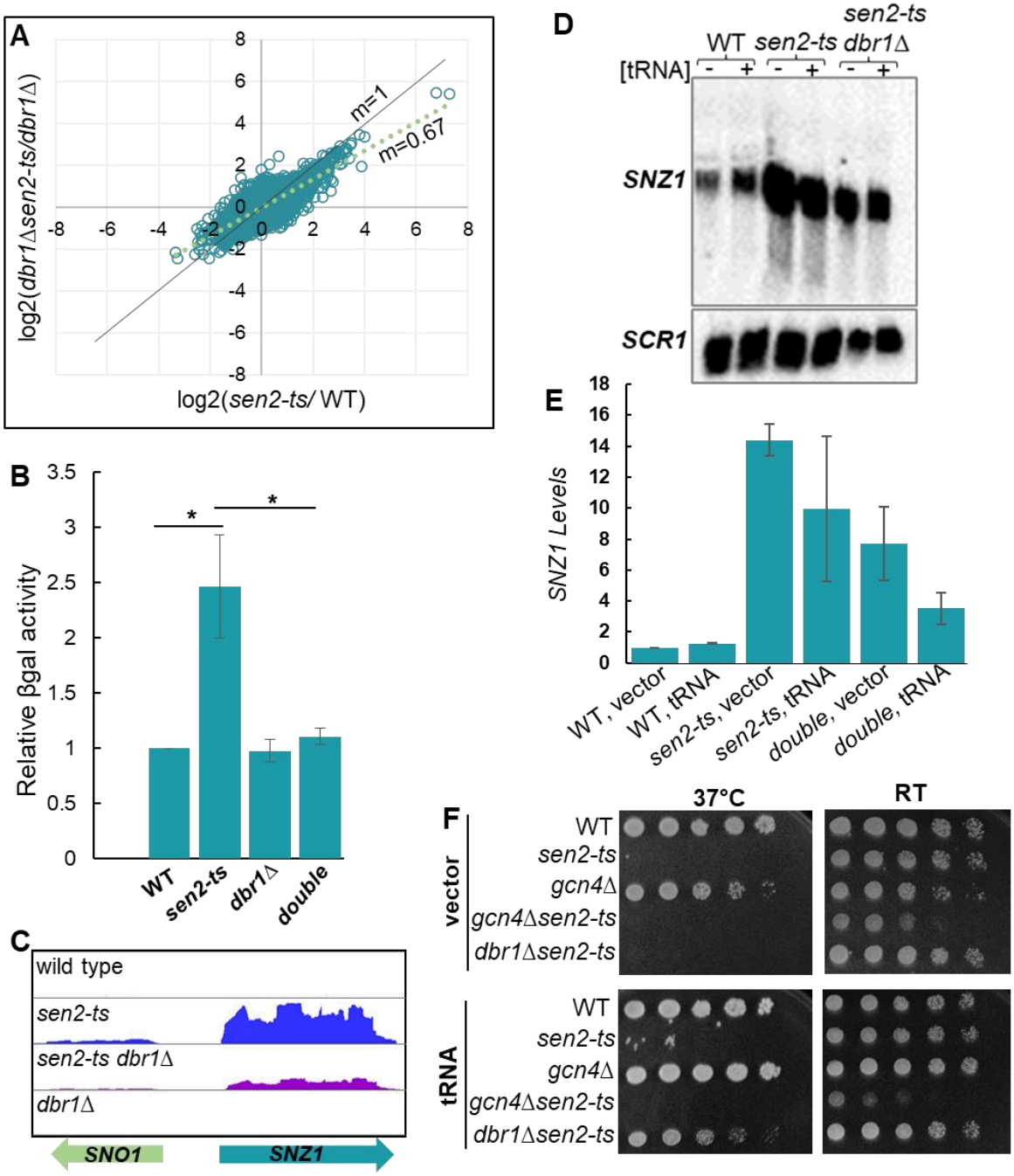
A
log2(dbr1Δsen2-ts/dbr1Δ)
log2(sen2-ts/ WT)
m=1
m=0.67
B
Relative βgal activity
WT
sen2-ts
dbr1Δ
double
C
wild type
sen2-ts
sen2-ts dbr1Δ
dbr1Δ
SNO1
SNZ1
D
sen2-ts
WT sen2-ts dbr1Δ
[tRNA]
SNZ1
SCR1
E
SNZ1 Levels
WT, vector
WT, tRNA
sen2-ts, vector
sen2-ts, tRNA
double, vector
double, tRNA
F
37°C
RT
vector
tRNA
WT
sen2-ts
gcn4Δ
gcn4Δsen2-ts
dbr1Δsen2-ts

Figure 4.6*:* The Gcn4 response is activated in *sen2-ts* and reduced by *dbr1*Δ.

A). mRNAs accumulating in *sen2-ts* are reduced by also deleting *DBR1*. The $\log_2$(fold change) between *SEN2* and *sen2-ts* is plotted on the x-axis. The $\log_2$(fold change) between *SEN2 dbr1*Δ and *sen2-ts dbr1*Δ is plotted on the x-axis. Linear regression analysis of the data reveals a line with a slope of 0.67 (green dotted line). Also indicated is a line with slope 1 (black solid line), which would be expected if *dbr1*Δ had no effect on genes affected by *sen2-ts*. **B).** The expression of both *SNO1 and SNZ1* are elevated in the *sen2-ts* mutant and closer to wild-type levels in the double mutant. Shown is RNA-seq read-coverage of these two genes for a representative technical replicate. **C).** Gcn4 expression is induced by *sen2-ts* and reduced by *dbr1*Δ. A β-galactosidase reporter assay to assesses Gcn4 expression was performed. The data are presented relative to the wild-type strain. The *sen2-ts* strain expresses the Gcn4 reporter significantly more than the wild type (p=0.02; unpaired t-test.) or double mutant (p=0.02; unpaired t-test.). **D).** The expression of both *SNO1 and SNZ1* are elevated in the *sen2-ts* mutant and closer to wild-type levels in the double mutant, in the presence and absence of a plasmid artificially expressing tRNAs from intronless genes. The full image of this Northern is available in the supplement (Figure S4 in publication (Hurtig and van Hoof, 2023)). **E.)** As D, but the quantification averaged over two biological replicates is shown. Shown is the average (bar) and spread of the individual replicates (whiskers). **F).** Gcn4 activation improves growth of a *sen2-ts* strain. Shown is a growth assay of single and double mutants. The *gcn4*Δ *sen2-ts* double mutant strain grows worse at room temperature than the *sen2-ts* single mutant strain.

Activation of the integrated stress response by *sen2-ts* is independent of its tRNA function

We then wanted to confirm these data using a Northern blot analysis (Figure 4.6D). In addition, we also wanted to determine whether the Gcn4 response was related to the tRNA splicing function of TSEN. Therefore, we tested strains either containing the intronless tRNA genes on a plasmid or lacking this plasmid. RNA from wild-type, *sen2-ts* and *dbr1*Δ *sen2-ts* strains was analyzed by Northern blot (Figure 4.6D,E). We saw our RNA-seq results recapitulated in the Northern blot, as *sen2-ts* both with empty vector and intronless tRNA genes increased *SNZ1* expression >10 fold. The *dbr1*Δ *sen2-ts* strain had intermediate levels of *SNZ1* which matches the RNA-seq data. The fold change in *SNZ1* accumulation between the wild type and the *sen2-ts* mutant seemed to be greater in the RNAseq than in the Northern blot. We speculated that this could be due to differences in media as the Northern samples were grown on SC-HIS compared to YPD for the RNAseq samples. To test this, we performed Northern blot analysis on the same RNA samples used in RNAseq, probing for *SNZ1* (Figure S4 in publication (Hurtig and van Hoof 2023)). *SNZ1* mRNA levels in wild-type or *dbr1*Δ were undetectable when grown in YPD, but clearly higher when grown in SC-HIS. This difference in basal levels explains the variation in *SNZ1* fold change between the different experiments. Importantly, these Northern blot analyses show that *SNZ1* induction was independent of the tRNA splicing function as very similar results were obtained with both the intronless tRNA plasmid and the empty vector.

We considered two possible models for the Gcn4 activation in *sen2-ts*. First, it is possible that *sen2-ts* inappropriately over-activates Gcn4, which contributes to its death. Alternatively, Gcn4 is activated in response to some stress caused by *sen2-ts* to compensate for the lack of the other essential function of TSEN. If the Gcn4 response is inappropriate and causes cell death, then *gcn4*Δ should suppress the *sen2-ts* mutation. In contrast, if the Gcn4 response is appropriate and relieves stress, *gcn4*Δ should further reduce growth of *sen2-ts*.

To distinguish between these possibilities, we compared growth of the *gcn4*Δ *sen2-ts* double mutant to that of *sen2-ts* and *gcn4*Δ single mutants both at 37 °C and room temperature. At 37°C the *sen2-ts* strain fails to grow and this was not suppressed by *gcn4*Δ. Importantly, at room temperature, neither the *sen2-ts* not the *gcn4*Δ have a substantial effect on growth. However, the double mutant grows poorly at room temperature (and all other temperatures tested; Figure 4.6F). Notably, the presence of intronless tRNA genes did not affect the growth defect of the *gcn4*Δ *sen2-ts* mutant at room temperature. These results show that activation of the Gcn4 response is not responsible for killing the *sen2-ts* strain but instead is a response that helps the cell survive. Further, this response does not seem to be mediated by the tRNA splicing function of TSEN but instead is likely activated by lack of TSEN's unknown essential function.

Chapter Conclusions

We used a yeast genetics approach to gain further insight into TSEN function. These experiments used a *sen2-ts* strain that causes the protein to be destabilized (Metzger et al., 2020). PCH is caused by single amino acid changes that similarly destabilize the TSEN subunits (Sekulovski et al., 2021). Our results provide new insight into the physiological consequences of TSEN mutations in yeast, including an unanticipated activation of the integrated stress response. Future efforts to test whether human TSEN mutations in PCH patients cause similar physiological consequences may provide insight into the pathological mechanism of this disease.

<u>Sen54 overexpression suppresses all defects of *sen2-ts* likely due to structural stabilization</u>

Using a high-copy suppressor screen, *SEN54* was identified as a high-copy suppressor of the *sen2-ts* allele. This suppression was independent of the presence of intronless tRNA genes showing *SEN54* overexpression suppresses all the defects of essential

functions in *sen2-ts*, instead of being specific to the other essential function. This suppression was however dependent on Sen2 being present and possessing an intact active site. When *SEN2* was deleted or the catalytic H297 was mutated, *SEN54* overexpression no longer suppressed. The western blot on human TSEN demonstrated the reliance of TSEN2 on the presence of TSEN54 as when TSEN54 was knocked down with two different siRNAs, TSEN2 was also depleted. The reverse may also be true, as when TSEN2 was knocked down, TSEN54 levels were also reduced. The single amino acid changes that cause PCH most likely affect the stability of subunits rather than the catalytic activity (Sekulovski et al., 2021). Presumably more severe mutations would not allow embryonic development. It is not understood why some PCH patients have more severe disease than others. Our data suggest that variability in expression of one subunit can affect the levels of the mutated partner, potentially influencing disease severity.

Dbr1 mutations specifically suppress the other essential function of TSEN

The suppression of *sen2-ts* by overexpression of *SEN54*, though interesting, did not provide mechanistic insight into the other essential function of TSEN. Therefore, we complemented this screen with a spontaneous suppressor screen. After several repeats of the selection, we found a total of four colonies that were able to grow at 37 °C. Sanger sequencing of the *SEN2* gene revealed that two colonies had independently reverted one of the four mutated amino acids back to the wild-type allele resulting in loss of temperature sensitivity. The other two colonies had different mutations in the same gene, *DBR1*. We believe our screen approaches saturation because we found two reversions and two suppressors in the same gene. Similar to *SEN54* overexpression, *dbr1*Δ suppresses *sen2-ts*, it does not suppress the full deletion of *SEN2* or the catalytic inactivation of the subunit. As such, when we performed similar spontaneous and high-copy suppressor screens with a *sen2*Δ*,* we were unsuccessful in finding suppressors. This suggests that there is no way for

the cell to fully bypass the tRNA independent functions of TSEN. The loss of the debranching catalytic activity of Dbr1 is also necessary and sufficient for the suppression mechanisms because *dbr1-cat* also suppressed *sen2-ts*. It is also important to emphasize that the *dbr1* mutations only suppressed with the presence of intronless tRNA. When this plasmid was lost, the suppression no longer occurred. Our data therefore show that mutations in *dbr1* only suppress the unknown essential function of TSEN and not the tRNA splicing function, which was confirmed by Northern blotting (Figure 4.4). Thus, this mechanism of suppression does not restore all of TSEN function and is distinct from the repression by *SEN54* overexpression.

Loss of TSEN's other essential function activates the Gcn4 response

By performing RNA-seq, we found genes involved in amino acid synthesis and other biological synthesis pathways were upregulated in *sen2-ts* but closer to wild-type levels in *dbr1*Δ *sen2-ts*. When we compared the upregulated genes to previous literature, we noted significant overlap between our hits and Gcn4 targets. A β-galactosidase assay for Gcn4 translation confirmed that Gcn4 was translated 2.5-fold more in the *sen2-ts* compared to the wild-type and *dbr1*Δ *sen2-ts* strains. Because the Gcn4 stress response is activated in *sen2-ts* but less so in the *dbr1*Δ *sen2-ts* it follows that Gcn4 could be killing the *sen2-ts* mutant. However, when we made the double *gcn4*Δ *sen2-ts* mutant, the opposite proved to be true. Instead of killing the cell, the Gcn4 response is protective of the *sen2-ts* strain.

The activation of Gcn4 in response to amino acid starvation is very well characterized genetically, but the exact molecular mechanisms are not fully determined (Hinnebusch, 2005; Masson, 2019). It is clear that a key step in the response is the activation of the Gcn2 kinase by Gcn1 and Gcn20. One possibility is that Gcn2 directly senses uncharged tRNAs, Which is supported by in vitro binding and kinase assays (Dong et al., 2000; Inglis et al., 2019; Wek et al., 1995). However, purified ribosomes are more potent than uncharged tRNAs in activating human Gcn2 (Inglis et al., 2019) and structural analysis clearly shows that Gcn1 and Gcn20

bind to stalled ribosomes (Pochopien et al., 2021). This suggest the possibility that amino acid starvation results in stalled ribosomes, which in turn activates Gcn2. Given the remaining uncertainties in the molecular mechanisms by which amino acid starvation results in Gcn2 and Gcn4 activation, it is unclear how Dbr1 affects this mechanism. However, there does not appear to be any difference in the accumulation of pre-tRNA species between the *sen2-ts* and the *sen2-ts dbr1*Δ mutant (Figure 4.4). This clarifies that the decrease in the Gcn4 response in *sen2-ts dbr1*Δ is not due to the *dbr1*Δ somehow reducing uncharged pre-tRNA levels.

Inactivation of the debranching enzyme seems to allow an unstable TSEN to perform some function independent of tRNA splicing which suppresses the Gcn4 stress response. The yeast Gcn4 response is homologous to the integrated stress response in humans so it will be interesting to test whether the integrated stress response is activated in PCH, which could provide mechanistic insight into the disease.

Dbr1 and TSEN may compete for a common substrate.

We show that *dbr1*Δ suppresses *sen2-ts* only when intronless tRNAs are artificially expressed, while *SEN54* overexpression suppresses in both the absence and presence of the intronless tRNA plasmid. Thus the two suppression mechanisms are distinct. The most likely explanation for the Sen54 mechanism is that it restores levels of functional TSEN through structural stabilization of *sen2-ts*. Because *dbr1*Δ does not restore the tRNA splicing function of TSEN, we propose a model where Dbr1 and Sen2 compete for some common substrate.

In normal conditions, we propose that TSEN and Dbr1 compete for the same substrate, with TSEN processing that substrate into an essential RNA and Dbr1 directing the substrate to some other fate, perhaps degradation. When TSEN is compromised, Dbr1 diverts the substrate and TSEN cannot make the essential product. When Dbr1 is subsequently

deleted or inactivated, this increases the substrate availability so that even an impaired TSEN can produce its essential product (Figure 4.7).

This model is supported by several observations. First, overexpression of *DBR1* specifically reduces growth of the *sen2-ts* at 34 °C. The observation that inactivation of *DBR1* improves growth of *sen2-ts*, but overexpression of *DBR1* impairs growth of *sen2-ts* would be expected if the two enzymes act on a common substrate. Second, the loss of Dbr1 catalysis is critical for this suppression as demonstrated by the fact that *dbr1-cat* mutation also suppresses *sen2-ts*. Third, the suppression mechanism only acts on a partially impaired TSEN as neither *sen2*Δ nor *sen2-cat* can be suppressed by *dbr1*Δ.

Because TSEN and Dbr1 both act on RNA, it appears likely that the shared substrate is an RNA. However, there is no overlap between the known substrates of TSEN and Dbr1. Dbr1 initiates the degradation of most excised introns by opening the lariat structure they form during splicing. We can rule out the possibility that one of the excised annotated introns is processed into an essential RNA because none of the annotated yeast introns are essential (Parenteau et al., 2019). For nine introns, Dbr1 initiates processing of the intron into a mature snoRNA instead of initiating complete degradation. These snoRNAs however are not essential and even in a *dbr1*Δ strain these snoRNAs are largely functional (Bailey et al., 2022). Besides at annotated introns, splicing occurs at over 150 “protointrons” (Talkish et al., 2019) in the yeast genome. In some cases only the first step of splicing occurs, creating a lariat that contains the intron and 3’ exon (Volanakis et al., 2013). Perhaps the common substrate of Dbr1 and TSEN is one of these excised protointrons. It is also possible that Dbr1 has some other substrate that does not originate from an intron. Interestingly, such lariats have been reported for yeast retrotransposons and shown to be Dbr1 substrates (Menees, 2020). Dbr1 can debranch small Y-shaped RNAs in vitro (as small as a 5 nts RNA with a 2nt 2’ branch), and can even catalyze the breakdown of other phosphodiesters such as bis-p-

nitrophenylphosphate (Schwer *et al.* 2016; Katolik *et al.* 2017). While RNA-seq should have revealed any annotated introns as common substrates, this would not be the case for “proto-introns”, small RNAs, or other molecules. Thus, any of these molecules could be the common substrate of Dbr1 and TSEN.

Dbr1 mutations have been reported to have other effects that are not fully understood. Dbr1 increases the toxicity of TDP-43 expression in yeast (Armakola et al., 2012), and mutations in *DBR1* cause increased susceptibility to viral encephalitis in human patients (Zhang et al., 2018). Further studies towards a complete understanding of Dbr1 function are needed to clarify how these effects of Dbr1 relate to each other and, according to our data, the essential function of TSEN.

Taken together, we propose competition between Dbr1 and TSEN as the most likely model. TSEN creates an essential product and without this product the cell senses stress and activates the Gcn4 response. If Dbr1 is inhibited, the substrate becomes more abundant, and an impaired TSEN can make sufficient amounts of the essential product. As stated before, this common substrate is likely an RNA as the only known functions of Sen2 and Dbr1 are to process RNA. In any case, our results suggest new avenues for research into PCH. We also found the levels of the dimer partners that form the TSEN complex can affect one another. This may affect disease severity and potentially lead to future therapeutics. The Gcn4 stress response is activated in yeast when TSEN is impaired and therefore the homologous human pathway, the integrated stress response, could be activated in PCH patients and elicit some of the disease mechanism. Finally, reducing Dbr1 activity could also suppress human TSEN functions which might provide another novel approach to PCH treatment.

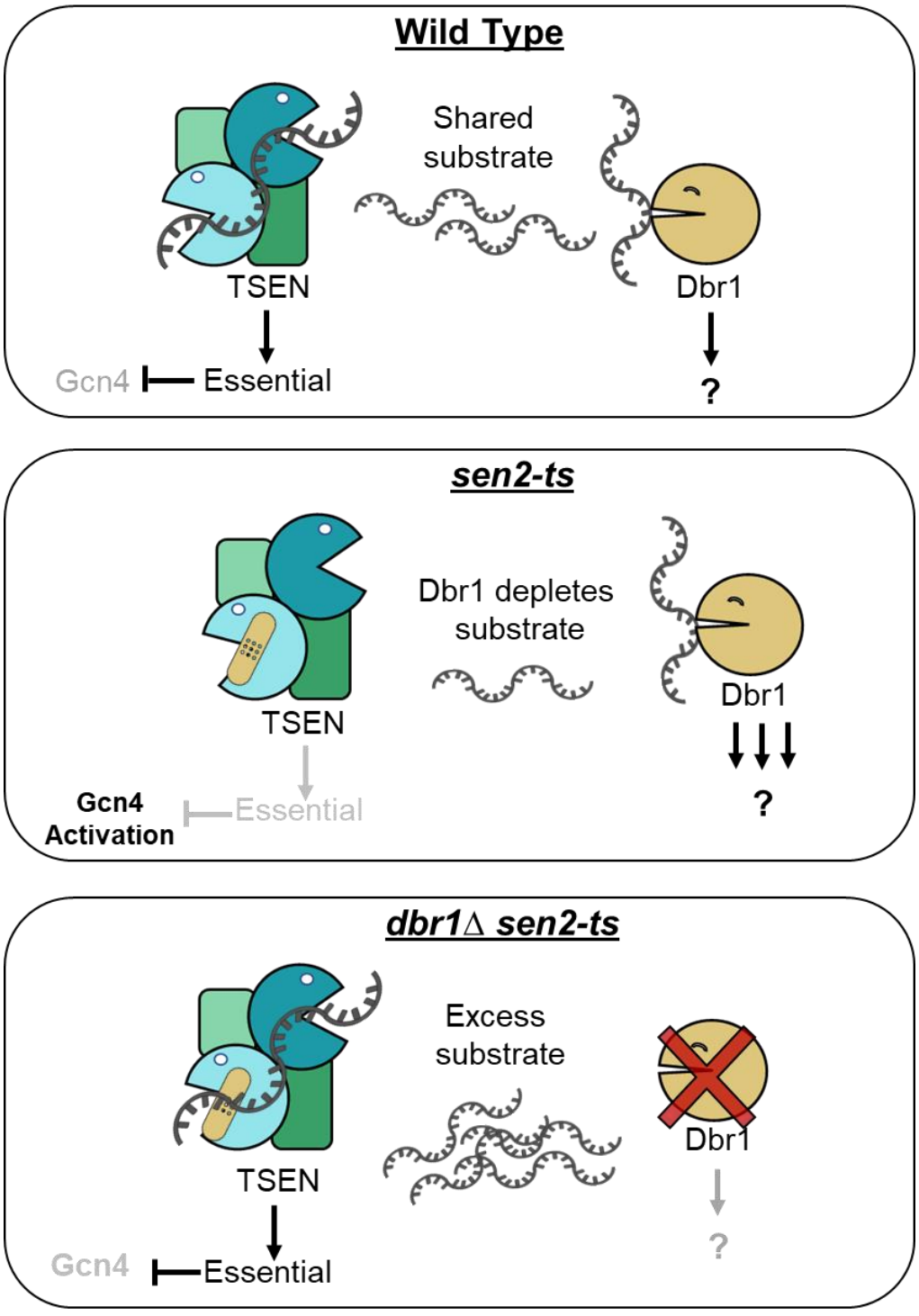
Wild Type
Shared substrate
TSEN
Dbr1
Gcn4
Essential
?
sen2-ts
Dbr1 depletes substrate
TSEN
Dbr1
Gcn4 Activation
Essential
?
dbr1Δ sen2-ts
Excess substrate
TSEN
Dbr1
Gcn4
Essential
?

Figure 4.7: Model for competition between TSEN and Dbr1.

Our data suggest that TSEN and Dbr1 compete for a common substrate that TSEN processes to an essential RNA. See discussion for details.

5) Yeast Dxo1 is required for 25S rRNA maturation and acts as a transcriptome-wide distributive exonuclease

This chapter is from the publication Hurtig JE, van Hoof A. Yeast Dxo1 is required for 25S rRNA maturation and acts as a transcriptome-wide distributive exonuclease. RNA. 2022 May;28(5):657-667. *RNA* allows authors to use their articles in dissertations if they acknowledge the journal (rnajournal.cshlp.org/site/misc/terms).

Chapter Introduction

The maturation and degradation of mRNAs and ncRNAs are multistep processes that are crucial throughout all forms of life. Eukaryotic pre-mRNAs must be spliced, polyadenylated, and capped before they can be utilized in translation. rRNA processing utilizes at least a dozen ribonucleases, including endoribonucleases that separate the 25S, 18S, and 5.8S rRNAs from their common precursor (Henras et al., 2014; Woolford and Baserga, 2013). After this separation, each RNA molecule is further processed by other ribonucleases (endoribonucleases, 5' exoribonucleases, and/or 3' exoribonucleases) to produce mature ribosomes (Henras et al., 2014; Tomecki et al., 2017; Woolford and Baserga, 2013). These ribonucleases often have multiple functions, although in many cases their *in vivo* functions have not been fully defined. For example, the 5' exoribonuclease Rat1 and the 3' exoribonuclease the RNA exosome are both required for rRNA maturation, but they also have many other substrates, including released mRNA introns and aberrant RNAs (Dhoondia et al., 2021; Januszyk and Lima, 2014; Wasmuth and Lima, 2012). Yeast has proven to be a powerful eukaryotic system to initially identify ribonuclease functions, most of which are conserved in other eukaryotes, including humans. Mutations in ribonucleases cause many human genetic diseases (Morton et al., 2018; van Dijk et al., 2018; Weskamp and Barmada, 2018; Wolin and Maquat, 2019), further underscoring the relevance of these enzymes and the overall importance of RNA processing.

The activity and structure of the Rai1/Dxo1/DXO family of enzymes has been well characterized *in vitro* and is suggested to be important for the removal of aberrant caps from mRNAs as well as for other pathways of RNA degradation. This family of enzymes can act on a variety of RNA ends, and removes pyrophosphates, NpN dinucleotides, and aberrant caps such as Gpp, NAD, FAD, and coA (Chang et al., 2012; Doamekpor et al., 2020b; Zhang et al., 2020). Importantly, aberrant caps cannot be removed by the conventional decapping enzyme,

Dcp2, or its homologs. Some family members can also remove mononucleotides and thus act as 5’ exonucleases (Chang et al., 2012; Doamekpor et al., 2020a). In all the above cases, Rai1/Dxo1/DXO enzymes produce an RNA with a 5’ monophosphate that is further degraded by the nuclear 5’ exoribonuclease Rat1 or its cytoplasmic homolog Xrn1. However, it is not fully understood which of these catalytic capacities of Rai1/Dxo1/DXO are important *in vivo*. The human genome only encodes one of these enzymes (DXO), while fungal genomes have been found to encode one or more of the family members. For example, *Schizosaccharomyces pombe* has a single gene (*RAI1*), while *Saccharomyces cerevisiae* and *Kluyveromyces lactis* each have two genes (*RAI1* and *DXO1*).

Mammalian DXO is one of the most well-studied family members. DXO has 5’ exonuclease activity, and thus can remove various cap structures and degrade uncapped transcripts (Doamekpor et al., 2020b; Jiao et al., 2013). DXO products may then be degraded by XRN1 or RAT1 as DXO has been reported to be either a nuclear or cytoplasmic protein (Lynch, 2019; Picard-Jean et al., 2018; Zheng et al., 2011). One *in vitro* activity of human DXO is its ability to convert an RNA with a 5’ hydroxyl to one with a 5’ monophosphate by removing the first two nucleotides (NpN) from the 5’ end of the RNA (Doamekpor et al., 2020a). This is particularly interesting because some endonucleases produce a 5’ hydroxyl that must be converted to a 5’ monophosphate in order for the RNA to be degraded by Xrn1 (Calvin and Li, 2008; Cherry et al., 2019; Navickas et al., 2020). DXO could participate in this pathway, which would provide an explanation for how 5’ hydroxylated endonuclease cleavage products are eventually degraded by Xrn1 and/or Rat1 (Nagarajan et al., 2013; Peach et al., 2015).

Rai1 was initially identified as a Rat1 interacting and stabilizing protein, which allows for efficient 5’ to 3’ degradation by Rat1 in the nucleus (Xue et al., 2000). A key study ascertained the structure of Rai1 and noted a putative active site (Xiang et al., 2009). This observation led to the discovery that Rai1 has catalytic functions independent of stabilizing

Rat1 (Xiang et al., 2009). The catalytic activities of Rai1 have most extensively been characterized for the *S. pombe* enzyme and include the removal of FAD, CoA, NAD, unmethylated, or incomplete caps (Chang et al., 2012; Jiao et al., 2010; Zhang et al., 2020).

In contrast to the nuclear Rai1, *S. cerevisiae* Dxo1 (ScDxo1) localizes to the cytoplasm and appears to act independently of other exonucleases, as ScDxo1 is unable to form a complex with either Rat1 or its cytoplasmic equivalent, Xrn1 (Chang et al., 2012; Huh et al., 2003; Wang et al., 2015). The catalytic activities of ScDxo1 have not been characterized, but Dxo1 from *K. lactis* (KlDxo1) has increased exonuclease activity *in vitro* compared to Rai1 and DXO (Wang et al., 2015). This increased exonuclease activity is due to several amino acid substitutions near the active site (Chang et al., 2012). These same mutations also reduced the decapping activity of Dxo1, indicating a tradeoff between exonuclease and decapping activities. The *in vivo* function of ScDxo1 has been partially characterized. Dxo1 has been identified as a minor contributor to 5' exonuclease activity in No-Go Decay and the unfolded protein response (Cherry et al., 2019; Navickas et al., 2020). During No-Go decay, ribosomes stall on an RNA transcript resulting in cleavage of the trapped mRNA. Similarly, during the unfolded protein response (UPR), the *HAC1* intron is removed by Ire1-mediated endoribonucleolytic cleavage. In both cases, Xrn1 is primarily responsible for degradation of the cleaved mRNA/intron. However, when Xrn1 is deleted, Dxo1 can less efficiently degrade at least a few bases of the mRNA/Hac1 intron (Cherry et al., 2019; Navickas et al., 2020). It remains unclear whether these Dxo1 functions in No-Go decay and the UPR reflect a more global role.

In this paper, we seek to understand the roles of ScDxo1 more completely. Because all the biochemical activities of Dxo1 produce similar 5' monophosphate RNAs that are degraded by Xrn1, we reason that 5' monophosphate RNAs that accumulate in an *xrn1*Δ strain but are absent in *xrn1*Δ*dxo1*Δ are likely the products of Dxo1. We used Parallel Analysis of

RNA Ends (PARE), an RNA sequencing strategy specific for 5' monophosphate ends (Addo-Quaye et al., 2008; German et al., 2008), to identify such products of Dxo1. We found that Dxo1 acts as a transcriptome-wide distributive exonuclease, consistent with its known functions in No-Go decay and the UPR, but greatly expanding the scope of its exonuclease activity. Surprisingly, we also identified Dxo1 as the enzyme primarily responsible for the maturation of 25S rRNA from a 25S' intermediate. The 25S' to the 25S rRNA processing step is well described, but the enzyme responsible had not been convincingly identified (Geerlings et al., 2000; Oeffinger et al., 2009; Thomson and Tollervey, 2010; Tomecki et al., 2017). Overall, this study provides the first global understanding of the function of Dxo1 *in vivo*.

Results

Sequence divergence of Dxo1 and Rai1 suggest functional differences

As a first step in understanding how ScDxo1 differs from its paralog ScRai1, we sought to determine when the duplication occurred and what sequence changes occurred when the two proteins diverged. We found two loci corresponding to Dxo1/Rai1 in the genomes of most Saccharomycetaceae and the very closely related Saccharomycodaceae. This includes species that diverged both before and after the well-characterized whole genome duplication in the *Saccharomyces* lineage (Figure 5.1). In contrast, the more distant budding yeasts of the Phaffomycetaceae, Dipodascaceae, and Lipomycetaceae each contained a single gene, which we will refer to as Rai1/Dxo1. This suggests that Dxo1 and Rai1 arose by gene duplication in a shared ancestor of the Saccharomycetaceae and Saccharomycodaceae.

Next, we compared the sequences of Rai1 and Dxo1 by multiple sequence alignment to determine how the two proteins diverged (Figure S1 in publication (Hurtig and van Hoof, 2022)). Importantly, both proteins retain the catalytic residues of the active site (Figure 5.1B, black letters). One noteworthy change is that amino acid residues known to be important for

Rat1 interaction (Xiang et al., 2009) were lost from one copy (hereafter Dxo1 proteins; Figure 5.1B, red letters). These Dxo1 proteins also gained a short N-terminal extension that is absent from Rai1 and Rai1/Dxo1 proteins (Figure 5.1B). This extension is predicted to be unstructured (www.pondr.com), consistent with the crystal structure of KlDxo1 (Chang et al., 2012). The Dxo1 proteins also consistently had a $xRHx_3D$ motif replacing the ΩRGx_3K motif (Ω being an aromatic residue) of Rai1 and Rai1/Dxo1 proteins (Figure 5.1B, blue letters). This change was shown to enhance the 5' exonuclease activity and reduce the decapping activity of KlDxo1 (Chang et al., 2012). Although the biochemical activities of ScDxo1 have not been directly characterized, the sequence conservation suggests to us that, like KlDxo1, it has robust 5' exonuclease activity and reduced decapping activity.

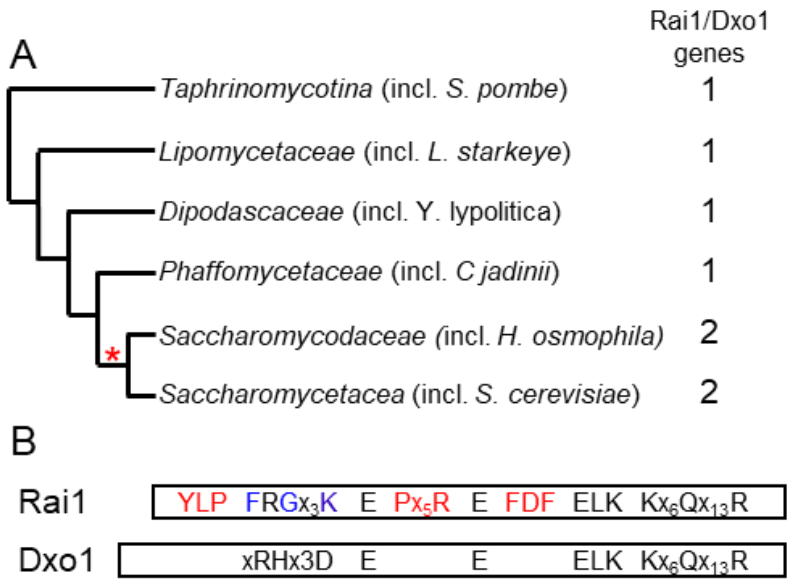

Figure 5.1*:* Dxo1 and Rai1 are duplicated genes that arose in a common ancestor of the Saccharomycetaceae and Saccharomycodaceae and subsequently diverged.

A). Evolutionary tree representing the relationship between different budding yeast families. The number on the right indicates the number of Rai1/Dxo1/DXO genes per genome. The red asterisk indicates the Rai1/Dxo1 duplication that predates the well characterized whole genome duplication in a subset of Saccharomycetaceae. **B).** Conserved sequence motifs of duplicated Rai1s and Dxo1s suggests functional differences between the two enzymes. Catalytic residues are retained in both and indicated in black letters. Residues important for Rat1 interaction are in red and are lost in Dxo1s. The Dxo1s also have a xRHx3D motif replacing the WRGx$_3$K motif of Rai1 in blue, with W being an aromatic residue. This change enhances the 5' exonuclease activity and reduces decapping activity.

Dxo1 can act as a distributive exonuclease on many different RNAs

Next we wanted to determine the *in vivo* function of ScDxo1. To investigate this, we performed PARE in *dxo1*Δ*xrn1*Δ and *xrn1*Δ strains. We have previously used the same strategy to characterize the highly specific activity of the tRNA splicing endonuclease (TSEN). In contrast to the few changes in the PARE profile caused by TSEN inactivation, we saw thousands of PARE signals increase and decrease as a result of Dxo1 inactivation, indicating that Dxo1 has transcriptome-wide effects (Supplemental Figure S2 in publication (Hurtig and van Hoof, 2022)). This included Dxo1 activities downstream of known endonucleases (Cherry et al., 2019; Hurtig et al., 2021), decapping (Harigaya and Parker, 2012), and spliceosome-mediated decay (Harigaya and Parker, 2012; Volanakis et al., 2013).

We first examined one of the most well-studied examples of an endonucleolytic cut in an mRNA, Ire1-mediated cleavage of *HAC1* mRNA. The two cleavage sites in *HAC1* are precisely known, but PARE identified clear peaks in *xrn1*Δ that were shifted a few nucleotides 3' of the actual cleavage sites (Figure 5.2A). In contrast, in *xrn1*Δ*dxo1*Δ, the peak at the actual cleavage site of *HAC1* became more prominent, while the peaks just 3' disappeared (Figure 5.2A). We observed this pattern at both cleavage sites, and both products are known to be degraded by Xrn1 (Cherry et al., 2019). Our results confirm that when Xrn1 is absent, these RNAs can be partially degraded by Dxo1 (Cherry et al., 2019).

We next looked at a *bona fide* TSEN target, *CBP1*. TSEN cleaves the *CBP1* mRNA, facilitating further degradation by Xrn1 (Hurtig et al., 2021; Tsuboi et al., 2015). We examined the peaks within *CBP1* and found a similar trend to that of *HAC1*: *xrn1*Δ showed three major peaks as we previously reported, with smaller peaks one or a few nucleotides downstream. In *xrn1*Δ*dxo1*Δ, peaks 1 and 2 become sharper, and the peaks just downstream disappear (Figure 5.2B). Interestingly, while peak 2 becomes more predominant, peak 3 (five nts downstream of peak 2) almost completely disappears in *dxo1*Δ*xrn1*Δ. We conclude that *CBP1*

is cleaved in only two positions, and the sharper peaks 1 and 2 reflect the direct cleavage products. Peak 3 and smaller peaks downstream of peaks 1 and 2 result from Dxo1 digestion of these direct cleavage products. We previously reported that *CBP1* was cleaved by recombinant TSEN *in vitro* and were initially puzzled that only sites 1 and 2 are robustly cleaved by TSEN (Hurtig et al., 2021). The conclusion that site 3 is the product of Dxo1 and only an indirect product of TSEN provides a probable explanation for the discrepancy between our previous *in vivo* and *in vitro* sites.

Spliceosome-mediated mRNA degradation refers to a decay pathway initiated by the first step of splicing (Volanakis et al., 2013). Instead of being used in the second step of splicing, the lariat intermediate (containing the intron, exon 2, and the polyA tail) is debranched and degraded by Xrn1. A previous degradome study in yeast showed that this occurred in a subset of intron-containing mRNAs (Harigaya and Parker, 2012), and we observed the same spliceosome-mediated decay targets in our dataset. However, in both the previous study and our *xrn1*Δ strain, the 5' monophosphate ends were often one to three nucleotides downstream of the known 5' splice site. One example of this is *OST5*. When examining the *xrn1*Δ PARE data, we observed the same group of peaks downstream of the 5' splice site as was reported previously (Harigaya and Parker, 2012). In contrast, *xrn1*Δ*dxo1*Δ accumulates 5' monophosphate ends that precisely match the 5' splice site (Figure 5.2C). This indicates that Dxo1 not only processes introns from atypical splicing events like *HAC1*, but it also processes spliceosomal introns. Both our data and the degradome sequencing of Harigaya and Parker use poly(A) plus RNA, which enriches for the products of spliceosome-mediated decay. Conversely, when both steps of splicing are completed, the intron is released without a poly(A) tail and rapidly degraded by Rat1. *ACT1* is an example of an efficiently spliced transcript and, as such, neither our study nor the previous study detected abundant 5' monophosphate ends on the intron (Figure 5.2D). Overall, these results suggest that Dxo1

can act downstream of several endoribonucleases, including Ire1, TSEN, and the spliceosome.

The major cytoplasmic mRNA degradation pathway involves removal of the 5' cap structure by Dcp2 and degradation of the decapped mRNA by Xrn1. Therefore, 5' monophosphorylated decapped mRNAs accumulate in *xrn1*Δ strains, but not a *dcp2*Δ *xrn1*Δ strain (Harigaya and Parker, 2012; Hurtig et al., 2021). In our PARE data, the products of Dcp2 are represented by peaks located at the beginning of the 5' UTRs (e.g. *ACT1* and *PGK1*; Figure 5.2D and 5.E) in *xrn1*Δ. When only Xrn1 is deleted, we detect these decapped products as clusters of peaks, similar to what was seen for the endonuclease products. In *dxo1*Δ*xrn1*Δ, these clusters of peaks are replaced by fewer, sharper peaks (Figure 5.2D, E). For example, the *xrn1*Δ sample shows a prominent peak 110 nts upstream of the start codon of *ACT1*, and smaller peaks at -109 and -108. Similarly, there are peaks at -40, -39 and -38 of *PGK1*. In comparison, the *xrn1*Δ*dxo1*Δ strain produced sharper peaks at -110 and -40, respectively. These *dxo1*Δ*xrn1*Δ peaks match exactly those seen in previously published TL-seq, a genome wide-mapping method of capped 5' ends (Arribere and Gilbert, 2013), and are absent in previously published PARE data from a *dcp2*Δ*xrn1*Δ strain (Harigaya and Parker 2012). The most likely explanation for these data is that Dxo1 acts on the Dcp2 product and removes 1 or 2 nucleotides. A possible alternative explanation is that Dxo1-mediated removal of canonical 7mGpppN or aberrant (GpppN, NAD or FAD) caps would also produce peaks 1 nt downstream of the cap. However, the additional signal 2 nts downstream is not readily explained by such decapping activity. Though our data cannot completely rule out this alternative scenario, the homology studies of ScDxo1 also suggest this enzyme is a better exonuclease than decapping enzyme (Figure 5.1).

Overall, based on the general pattern that *xrn1*Δ strains often have smaller peaks just downstream of a main peak and that these diffuse peaks sharpen to a single main peak in

*xrn1*Δ*dxo1*Δ, we conclude that in the absence of Xrn1, Dxo1 can act as a distributive exonuclease that removes a few nucleotides from the 5' end of a wide variety of transcripts (Figure 5.2F). All of the Dxo1 substrates mentioned above have previously been shown to be stabilized by *xrn1*Δ, suggesting that in a wild-type strain, Xrn1 is the major exoribonuclease while Dxo1 makes minor contributions. Importantly, by sharpening peaks, our *xrn1*Δ*dxo1*Δ data set increases the mapping precision for decapping and cleavage sites, and thus serves as a useful resource that complements past and future degradome studies.

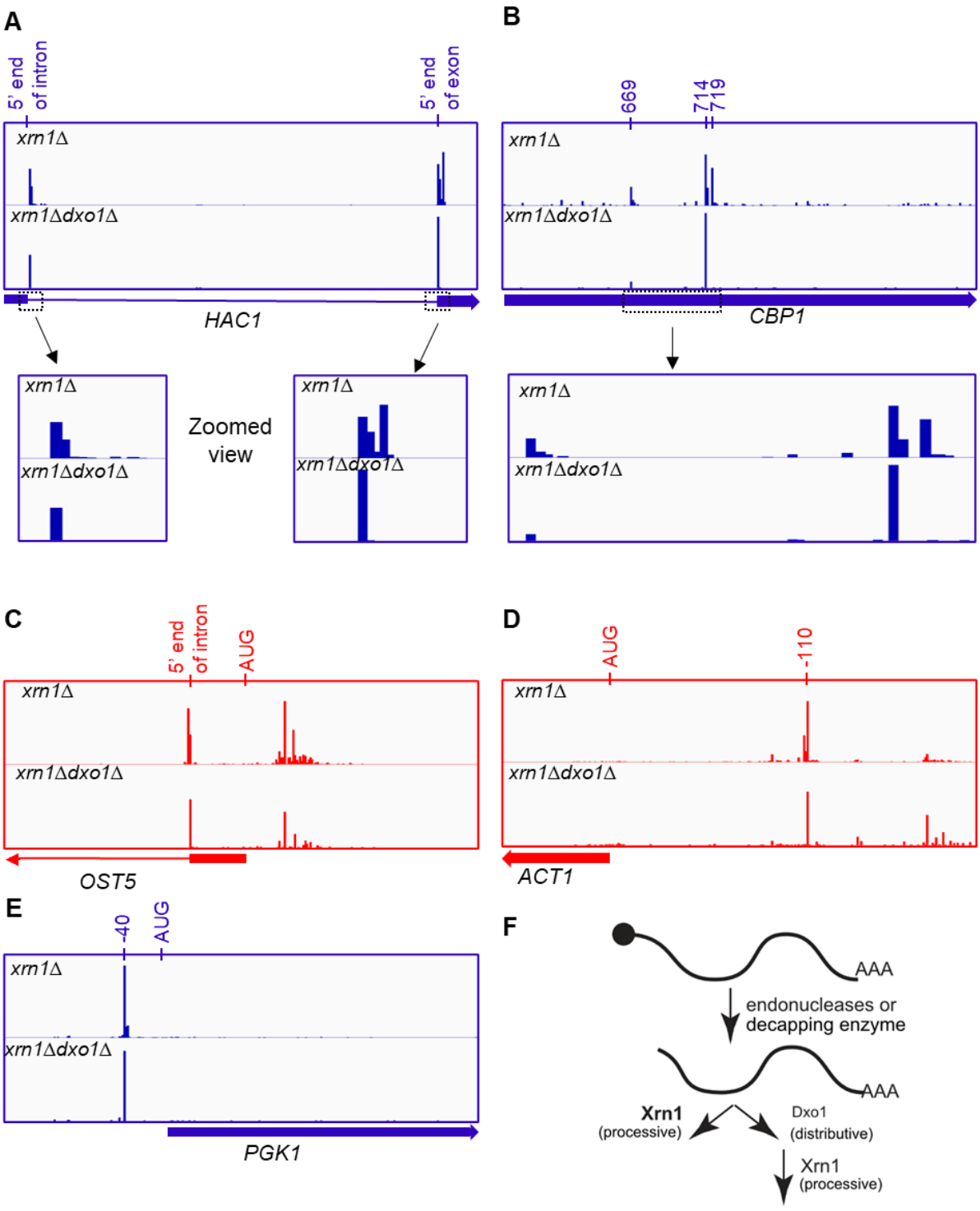
A
5' end of intron
5' end of exon
xrn1Δ
xrn1Δdxo1Δ
HAC1
Zoomed view
B
669
714
719
CBP1
C
5' end of intron
AUG
OST5
D
AUG
-110
ACT1
E
-40
AUG
PGK1
F
AAA
endonucleases or decapping enzyme
Xrn1 (processive)
Dxo1 (distributive)
Xrn1 (processive)

Figure 5.2*:* Dxo1 is a distributive exonuclease that acts downstream of decapping and endonuclease cleavage.

A-E). Read maps of PARE data on *xrn1*Δ and *xrn1*Δ*dxo1*Δ yeast showing the accumulation of 5' monophosphorylated RNA ends as peaks in the mRNAs *HAC1*, *CBP1*, *OST5*, *ACT1* and *PGK1*. For each gene a single representative PARE repeat is shown. The y-axes are linear with the range indicated in the top right. Each endonuclease site results in a single sharp peak in the *xrn1*Δ*dxo1*Δ strain, but a cluster of peaks in xrn1Δ. This pattern is highlighted in the zoomed in areas in A and B. Decapping of *OST5*, *ACT1* and *PGK1* also results in fewer peaks in *xrn1*Δ*dxo1*Δ than in *xrn1*Δ, but a few peaks remain which likely reflects multiple transcription start sites. The main capping sites for *ACT1* at -110 and *PGK1* at -40 are indicated above the graphs and the coding regions (boxes) and introns (lines) below the graphs. **F)**. Model showing the distributive activity of Dxo1. After endonuclease cleavage or decapping, Dxo1 can act as a distributive exonuclease before or in the absence of complete processive degradation by Xrn1.

Dxo1 is required for 25S rRNA maturation

One of the most prominent differences we noticed in *xrn1*Δ*dxo1*Δ was a shift in the 5' end of 25S rRNA. In the *xrn1*Δ PARE data, the 25S rRNA 5' end usually produces the most abundant signal. 25S rRNA has a 5' monophosphate end and an internal A-rich sequence that causes incomplete depletion by oligo(dT) beads (Roy and Chanfreau, 2020). In *xrn1*Δ*dxo1*Δ, we saw prominent peaks two and seven nts upstream of the normal 25S rRNA 5' end, with an almost complete loss of the normal 5' end, suggesting a defect in 25S 5' end processing.

In the 5' end processing pathway of 25S rRNA, Las1 cleaves the 35S precursor into a 27S intermediate (Gasse et al., 2015; Henras et al., 2014; Schillewaert et al., 2012; Woolford and Baserga, 2013). Then, Rat1 processes the 27S intermediate to 25S', which has a 5' extension of several nucleotides (Geerlings et al., 2000; Henras et al., 2014; Woolford and Baserga, 2013). The enzyme responsible for 25S' to 25S processing has not been definitively assigned. It has been suggested that Rat1 may continue removing nucleotides when it reaches 25S' to produce the 25S , though slower than in the previous step (Geerlings et al., 2000). Alternatively, it has been suggested that Rrp17 may be responsible for the final step in producing 25S rRNA. However, both *rat1* and *rrp17* mutants accumulate earlier rRNA processing intermediates, not specifically the 25S' (Geerlings et al., 2000; Oeffinger et al., 2009). Therefore, previous data suggesting that either Rat1 or Rrp17 is responsible for 25S' to 25S processing is inconclusive.

To further analyze the possible role of Dxo1 in rRNA processing, we also performed PARE in wild type (*XRN1+ DXO1+*) and *dxo1*Δ single mutants (Figure 5.3A). In both the wild type and *xrn1*Δ single mutant, we observe a large peak at the mature 25S 5' end. This indicates that Xrn1 is not required for 25S 5' end processing. On the other hand, the *dxo1*Δ and *xrn1*Δ*dxo1*Δ mutants show the accumulation of two peaks at -2 and -7 relative to the

normal 25S 5' end, which corresponds to the 25S' intermediate (Figure 5.3A). We did not see a similar shift in the mature 18S rRNA 5' end (Figure 5.3B). These findings indicate that Dxo1 is required for processing 25S' to the mature 25S rRNA. The effect of Dxo1 on 25S rRNA seems to be highly specific since we observed no notable differences for other ncRNAs with 5' monophosphate mature ends in the *dxo1*Δ PARE data. Thus, in the presence of Xrn1, Dxo1 does not appear to have transcriptome-wide effects, but rather is highly specific for 25S' to 25S rRNA processing.

To confirm that Dxo1 is required for 25S 5' end formation, we performed Northern blot analysis with a probe designed to hybridize to 25S' but not 25S rRNA. As shown in Figure 5.3C and quantitated in Figure 5.3D, we detected a large increase in 25S' rRNA in *dxo1*Δ and *dxo1*Δ*xrn1*Δ. Thus, *dxo1*Δ is the first mutant known to specifically accumulate 25S' rRNA and almost completely lack the mature 25S rRNA. Remarkably, this processing defect does not cause marked growth defect (see below), indicating that ribosomes with 25S' rRNA are largely functional. This is similar to 3' extended 5.8S and 5S rRNA that are largely functional under standard lab conditions (Briggs et al., 1998; Faber et al., 2002; van Hoof et al., 2000).

These observations suggest that the processing of 27S to 25S is initiated by Rat1 but completed by Dxo1 (Figure 5.3E). Analogous cases of hand-off RNA processing reactions have been described for yeast 3' exonucleases, including those involved in 5.8S rRNA 3' end formation (Thomson and Tollervey, 2010; van Hoof et al., 2000). We speculate that both Dxo1 and Rat1 are required for mature 25S formation due to the processivity/affinity of Rat1/Xrn1 enzymes (Jinek et al., 2011; Nagarajan et al., 2013). Processivity requires that the enzyme remain bound to the substrate between subsequent rounds of catalysis. An X-ray structure of Xrn1 bound to an RNA substrate indicates that the enzyme binds three nucleotides at a time, and *in vitro* assays show that Xrn1 activity requires a three nucleotide single stranded overhang (Jinek et al., 2011; Nagarajan et al., 2013). While a short single stranded 5'

overhang is critical for processive 5' nucleases, the mature 5' end of 25S rRNA forms a double stranded structure with 5.8S rRNA. This effectively prevents final 5' end maturation by Xrn1/Rat1 and necessitates hand-off to a distributive enzyme. Consistent with our findings of hand-off, *in vitro* studies of Rat1 have shown that it can process pre-ribosomal subunits to 25S' but not to the mature 25S rRNA (Fromm et al., 2017; Gasse et al., 2015). Because the processivity of Xrn1/Rat1 is highly conserved, we hypothesize that this cooperative processing of 25S rRNA may also be conserved. Indeed, human 28S rRNA processing produces an intermediate analogous to 25S' (Mullineux and Lafontaine, 2012).

As previously mentioned, Dxo1 is primarily cytoplasmic (Huh et al., 2003). Because 25S 5' end maturation appears to be a major function of Dxo1, this implies that the final maturation of 25S rRNA occurs in the cytoplasm. While the initial steps of rRNA maturation are carried out (cotranscriptionally) in the nucleolus, the final step in 5.8S and 18S rRNA maturation are cytoplasmic as well (Fatica et al., 2004, 2003; Thomson and Tollervey, 2010). Furthermore, the 25S' intermediate co-immunoprecipitates with Arx1, a factor that is co-exported with the ribosomal subunit (Thomson and Tollervey, 2010), which is consistent with cytoplasmic final maturation of 25S rRNA.

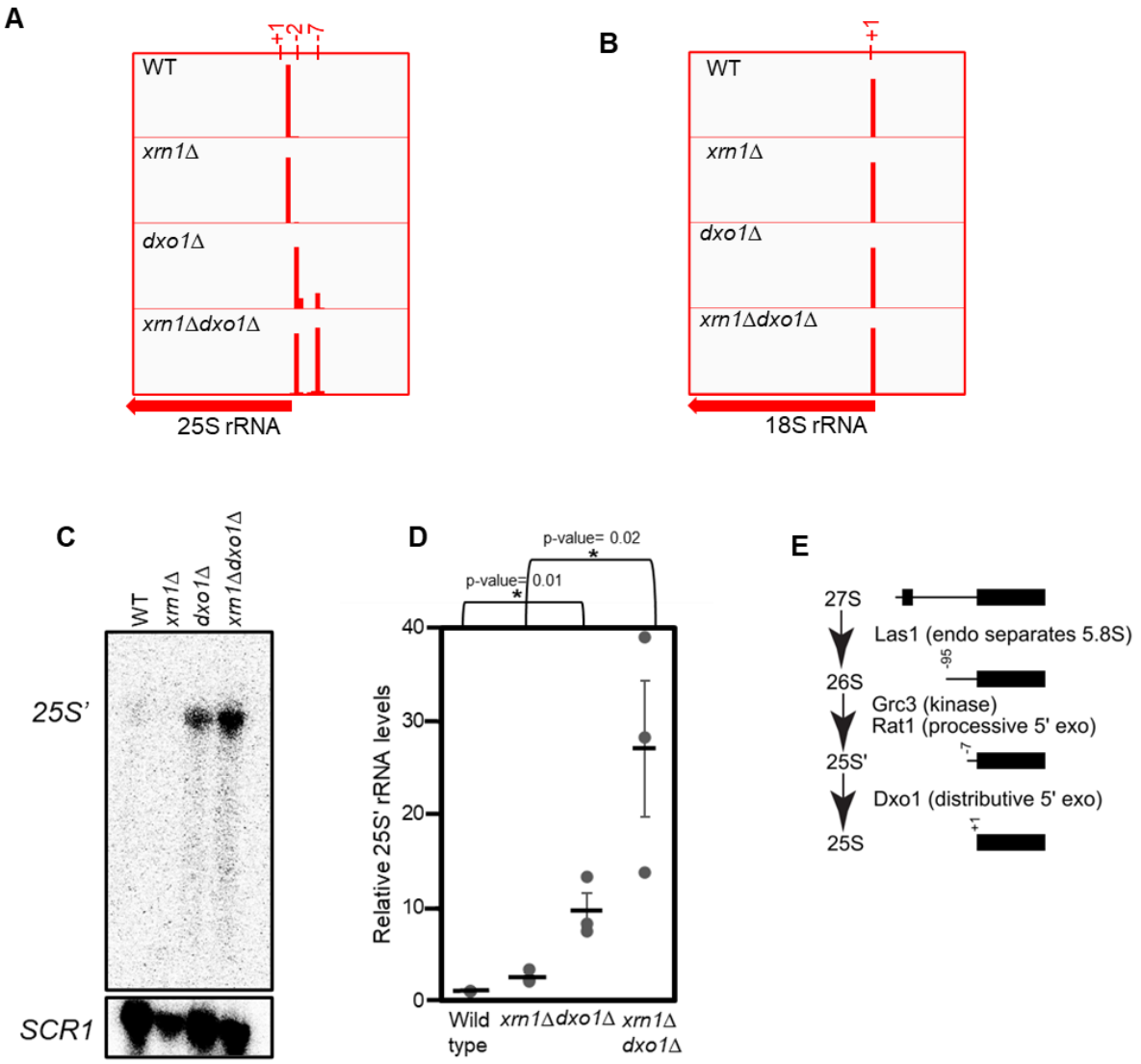
A
+1
+2
-7
WT
xrn1Δ
dxo1Δ
xrn1Δdxo1Δ
25S rRNA
B
+1
WT
xrn1Δ
dxo1Δ
xrn1Δdxo1Δ
18S rRNA
C
WT
xrn1Δ
dxo1Δ
xrn1Δdxo1Δ
25S'
SCR1
D
p-value= 0.02
p-value= 0.01
Relative 25S' rRNA levels
40
30
20
10
0
Wild type
xrn1Δdxo1Δ
xrn1Δ dxo1Δ
E
27S
Las1 (endo separates 5.8S)
-95
26S
Grc3 (kinase)
Rat1 (processive 5' exo)
-7
25S'
Dxo1 (distributive 5' exo)
+1
25S

Figure 5.3: Dxo1 processes the 25S' intermediate to 25S rRNA.

A,B). Read maps of PARE data from wild-type, *xrn1*Δ, *dxo1*Δ, and *xrn1*Δ*dxo1*Δ yeast showing the accumulation of 5' monophosphorylated RNA ends as peaks in rRNA. The y-axes are linear with the range indicated in the top right. The scale of the y-axes is different between samples, reflecting some variability in the efficiency of rRNA removal. A). When Dxo1 is deleted, the peak for mature 25S is replaced by peaks 2 and 7 nts upstream that correspond to the 25S' intermediate. B). The 18S rRNA 5' end is not affected by Dxo1, demonstrating the specificity of Dxo1 to 25S' processing. **C).** Representative Northern blot of the same strains measuring 25S' accumulation. *SCR1* is used as a loading control. **D).** Quantification of Northern blots of three biological replicates normalized to the *SCR1* control and presented relative to the wild type strain. Mean and standard error are indicated. Significance was determined by a two-tailed t-test**. E).** Model showing rRNA processing steps including the new finding that Dxo1 processes the 25S' to the 25S rRNA.

*dxo1*Δ suppresses the *xrn1*Δ growth defect

Because Xrn1 and Dxo1 both act as cytoplasmic 5' exoribonucleases, we were curious whether the double mutant had a more severe growth defect than either single mutant. As previously reported (Larimer and Stevens, 1990; Tishkoff et al., 1991), *xrn1*Δ causes a growth defect, while *dxo1*Δ does not have a notable effect on growth. However, contrary to our expectation, the *dxo1*Δ*xrn1*Δ strain had improved growth compared to the single *xrn1*Δ (Figure 5.4A). The growth of the *xrn1*Δ*dxo1*Δ strain is not restored to wild-type levels but seems to present an intermediate phenotype. To confirm this observation, we introduced either a *DXO1* plasmid or empty vector control plasmid into the *dxo1*Δ*xrn1*Δ and *xrn1*Δ strains. We then quantified the doubling time of these strains to more precisely assess their growth. Figure 5.4B shows that deleting *DXO1* from the *xrn1*Δ strain decreased the doubling time approximately 20% (p=0.01) and re-introducing *DXO1* to *dxo1*Δ*xrn1*Δ returned the doubling time to the level of *xrn1*Δ (p=0.01), confirming that *dxo1*Δ suppresses the *xrn1*Δ growth defect.

It has long been unclear why *xrn1*Δ mutants grow slowly. Canonically, the main function of Xrn1 is to degrade largely untranslated mRNAs that are decapped and deadenylated (Johnson, 1997; Nagarajan et al., 2013). It is not clear why the accumulation of these seemingly inert mRNAs would negatively affect cell growth. A novel hypothesis is that Dxo1 converts some unknown Xrn1 substrate into a toxic RNA, but in the absence of data we can only speculate on the identify of that toxic RNA. An alternative possibility is that *dxo1*Δ somehow affects the activity of the cytoplasmic RNA exosome. In the absence of Xrn1, the RNA exosome degrades mRNAs and thus becomes essential (Johnson and Kolodner, 1995). Thus, if *dxo1*Δ increases cytoplasmic exosome activity or the accessibility of RNAs to the exosome, this would also explain the improved growth of *dxo1*Δ*xrn1*Δ.

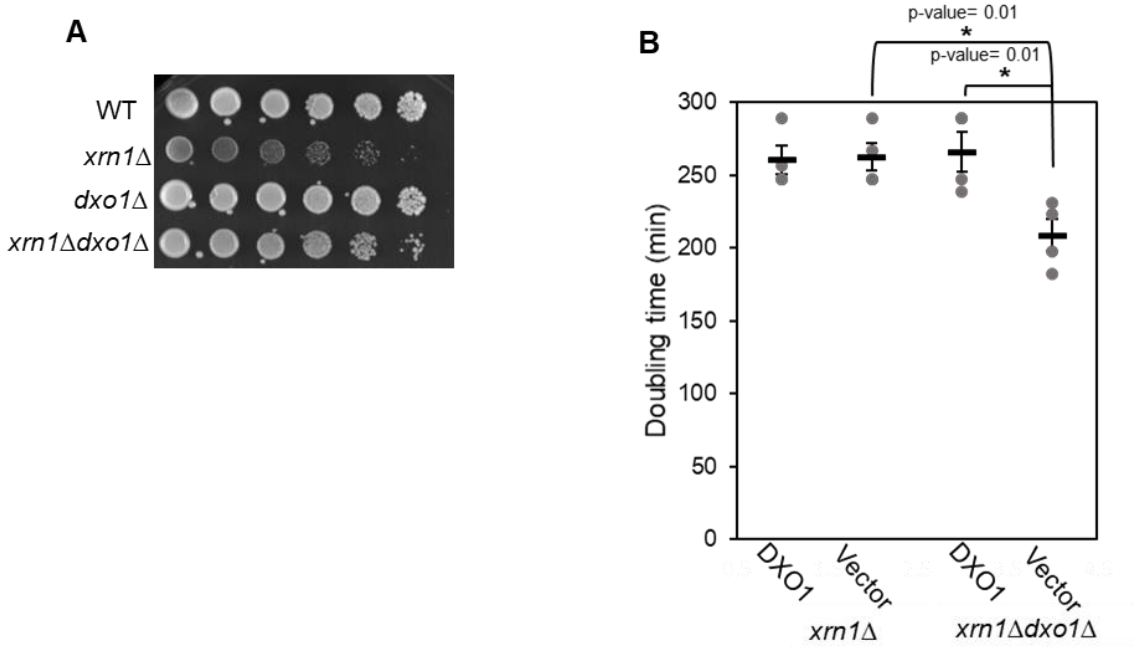

Figure 5.4: Deletion of Dxo1 partially restores the slow growth of *xrn1*Δ.

A). The indicated yeast strains were serially diluted for the growth assay and plated on YPD at 30°C for 3 days. **B).** Doubling time of the indicated strains was determined in biological triplicates. Mean and standard error are indicated and significance was calculated using a two-tailed t-test. *dxo1*Δ*xrn1*Δ and *xrn1*Δ strains. We then quantified the doubling time of these strains to more precisely assess their growth. Figure 5.4B shows that deleting *DXO1* from the *xrn1*Δ strain decreased the doubling time approximately 20% (p=0.01) and re-introducing *DXO1* to *dxo1*Δ*xrn1*Δ returned the doubling time to the level of *xrn1*Δ (p=0.01), confirming that *dxo1*Δ suppresses the *xrn1*Δ growth defect.

Chapter Conclusions

While the biochemical activity of KlDxo1 has been carefully characterized (Chang et al., 2012), neither the biochemical activity nor *in vivo* functions of ScDxo1 were well studied. Here we show that Dxo1 is a conserved enzyme that is related to, but distinct from, Rai1 and that it arose in a common ancestor of the Saccharomycetaceae and Saccharomycodaceae. This duplication may have allowed specialization, with Rai1 better suited to remove various aberrant caps in the nucleus and Dxo1 better suited for distributive exonuclease activity in the cytoplasm. In species that do not have a duplicated Rai1/Dxo1, one enzyme may have to carry out both decapping and exonuclease activity. Optimal decapping and exonuclease activity require mutually exclusive sequence motifs (Chang et al., 2012) (Figure 5.1), so such a bifunctional decapping and exonuclease enzyme is likely suboptimal for both. We expect that similar duplication may have occurred in other eukaryotes, but we have not extensively tested that possibility. We did notice that a subset of *Candida* species independently duplicated this gene, with orf19.8253 more closely resembling Dxo1 and orf19.13690 more closely resembling Rai1. More extremely, the *C. elegans* genome includes as many as nine Rai1/Dxo1/DXO genes.

In this study, we identify *in vivo* Dxo1 products by PARE and show that in the absence of Xrn1, Dxo1 can act as transcriptome-wide distributive 5' exonuclease. However, in the presence of Xrn1, Dxo1 appears to be specifically required to convert 25S' pre-rRNA to the mature 25S rRNA, a known step for which the enzyme had not been conclusively identified. Our results, combined with previous work (Thomson and Tollervey, 2010), imply that the large ribosomal subunit is exported while containing 6S and 25S' rRNA intermediates that are subsequently matured in the cytoplasm. While several examples of hand-off from one 3' exoribonuclease to another have been reported (Allmang et al., 1999b; Faber et al., 2002; Tucker et al., 2001; van Hoof et al., 2000; Zuo and Deutscher, 2002), we expand this concept

to 5’ exoribonucleases. We further speculate that distributive exonucleases may be needed to generate precise structured ends on a variety of ncRNAs.

Three types of reactions have now been ascribed to Dxo1: 25S rRNA processing, removal of aberrant cap structures, and distributive transcriptome wide 5’ exonuclease activity (Figure 5.5). Because aberrant caps are thought to be added in the same positions as the more abundant canonical caps, the PARE reads derived from aberrant decapping likely only form a minor fraction of the reads mapped to mRNA start sites and thus the aberrant decapping activity cannot be distinguished by PARE. These three functions raise the question: Which is the primary function of Dxo1? Dxo1 removes 7 nucleotides from 25S’ for each of the 2,000 ribosomes synthesized per minute in a growing yeast cell, which amounts to 14,000 catalytic cycles per minute per cell (Warner, 1999). A rapidly growing yeast cell also produces approximately 1,000 mRNAs per minute (Pelechano et al., 2010). Most of these receive a canonical cap, but an unknown fraction receives an aberrant cap. It appears unlikely that as much as 10% of the caps are aberrant, but even with this high estimate, the 100 aberrant decapping events per minute would be more than two orders of magnitude lower than the 14,000 catalytic cycles to form the mature 25S rRNA. Finally, while in the absence of Xrn1, a 5’ exonucleolytic role in mRNA decay becomes detectable, this role is limited in the presence of Xrn1 because *xrn1*Δ is known to stabilize most mRNAs. Thus we predict this mRNA decay role of Dxo1 is also minor when compared to 25S rRNA processing. Overall, we conclude that Dxo1 has several functions with its primarily role being 25S rRNA processing.

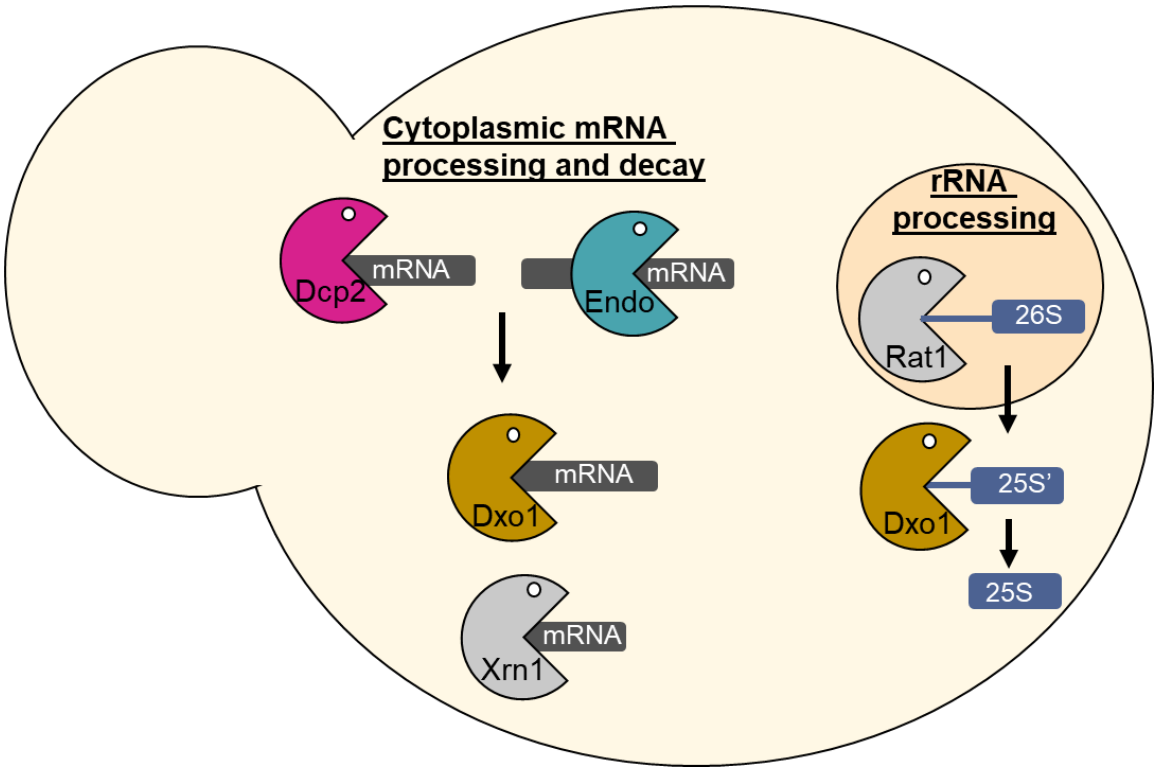

Figure 5.5: The multiple functions of Dxo1.

Dxo1 has several functions in *S. cerevisiae* including 'nibbling' downstream of decapping and endonuclease enzymes. The most prominent function of Dxo1 is processing the 25S' to the 25S rRNA in the cytoplasm. See discussion for further details.

6) Trl1 functions in kinase-mediated mRNA decay

Chapter Introduction

Splicing is an essential process in which introns are removed from pre-RNAs. Splicing allows multiple isoforms to be produced from the same RNA which can produce proteins with varying functions, adding to the diversity of life. In particular, viruses have limited amounts of genetic material which makes splicing critical to produce the necessary proteins for host invasion. Though the spliceosome catalyzes the majority of splicing in eukaryotes, several critical splicing events including tRNA and *HAC1* splicing, are performed by other enzymes.

In yeast tRNA splicing, the tRNA splicing endonuclease (TSEN) cleaves either side of the intron, excising it from the anticodon loop. The two halves of the tRNA are then ligated together by the tRNA ligase (Trl1) and the tRNA phosphotransferase (Tpt1) (Abelson et al., 1998). Trl1 has three different active sites with three separate functions, all of which are necessary to properly splice the tRNA (Greer et al., 1983; Sawaya et al., 2003). TSEN cleavage results in a 2'3' cyclic phosphate on the 5' exon and a 5' hydroxyl on the 3' exon (Ho et al., 1990). The phosphodiesterase activity of Trl1 opens this 2'3' phosphate ring to create a 2' phosphate and 3' hydroxyl. On the 3' exon, the kinase domain of Trl1 phosphorylates the 5' end to a 5' phosphate. The ligase domain of Trl1 then has the necessary substrates and joins the 5' phosphate and 3' hydroxyl together, ligating the two exons (Greer et al., 1983; Phizicky et al., 1992). Tpt1 then resolves the remaining 2' phosphate to create the fully spliced tRNA (Culver et al., 1997). tRNA splicing is an essential process in yeast and therefore TSEN, Trl1, and Tpt1 are all essential enzymes.

Removal of the intron from *HAC1* mRNA is another example of non-spliceosomal splicing. *HAC1* encodes a transcription factor that controls the unfolded protein response (UPR). *HAC1* is transcribed with an inhibitory intron and during normal growth, this full-length

transcript is degraded by Xrn1 and the RNA exosome. However, when the endoplasmic reticulum (ER) senses misfolded proteins, the inhibitory intron of *HAC1* is removed allowing the transcript to be translated into a transcription factor which regulates the expression of many genes in order to begin the UPR (Cox et al., 1993; Gonzalez et al., 1999; Mori et al., 1996, 1993). The intron of *HAC1* is removed by the ER localized endonuclease Ire1. Ire1 spans the ER membrane with the endonuclease domain in the cytoplasm (Cox et al., 1993; Mori et al., 1993). Ire1 activity is low under optimal growth conditions but activated when unfolded proteins accumulate inside the ER. Activated Ire1 then cleaves on either side of the Hac1 intron (Cox et al., 1993; Gonzalez et al., 1999; Mori et al., 1993). Similar to TSEN cleavage, Ire1 cleavage also produces a in a 2'3' phosphate and 5' hydroxyl (Gonzalez et al., 1999; Shigematsu et al., 2018). The ligation of the two exons is then handed off to Trl1. Just as with tRNA exon ligation, Trl1 phosphorylates the 5' end and opens the 2'3' ring to produce compatible ends which Trl1 ligates together (Sidrauski et al., 1996). Trl1 functions in both non-coding and mRNA splicing, and its activity also encourages degradation of the excised introns (Wu and Hopper, 2014). In both Hac1 and tRNA splicing, the intron is also left with a 5' hydroxyl which Trl1 phosphorylates to initiate degradation of the intron by Xrn1. With such different substrates, we speculate that Trl1 could have other targets in which it either splices, or similar to introns, facilitates transcript degradation.

Another component of the tRNA splicing pathway, TSEN, also has other functions. TSEN can participate in endonuclease decay of the transcript *CBP1* (Tsuboi et al., 2015) and as described in chapter 3, other mitochondrial protein encoding mRNAs in a process we termed TED (tRNA endonuclease decay). The 3' cleavage products of TSEN are stabilized by deletion of Xrn1, however studies of Xrn1 activity in vitro show that the exonuclease strongly prefers 5' phosphates and has little to no activity on the 5' hydroxyls that result from TSEN cleavage (Nagarajan et al., 2013; Stevens and Poole, 1995). A kinase like Trl1 could

be required to produce a 5’ phosphate before Xrn1 degradation. As shown in chapter 5, Dxo1 can “nibble” at some of the cleavage fragments of TSEN but this is not required for degradation by Xrn1. TSEN and Trl1 may also work together in endonuclease decay, in which Trl1 processes the ends of the cleavage products to encourage decay by exonucleases.

In metazoans and *S. pombe*, Ire1 cleavage induces mRNA decay in a process termed RIDD (regulated Ire1-dependent decay) (Hollien and Weissman, 2006; Kimmig et al., 2012). RIDD has a variety of physiological roles depending on the cell type and conditions. In drosophila, RIDD is necessary for photoreceptor differentiation. Ire1 degrades an mRNA encoding a fatty acid transporter which prevents buildup of fatty acids in the cell to allow development of the photoreceptor (Dourlen et al., 2012). Ire1 degradation can also be an important component of maintaining cell homeostasis in some cell types. Ire1 acts as mediator between the mRNA and the protein folding and secretory pathways in the ER (Metcalf et al., 2020). During homeostasis, RIDD couples the amount of mRNA and the capacity of the ER folding machinery by degrading mRNAs so the ER is not overwhelmed (Metcalf et al., 2020). Under ER stress like the UPR, RIDD can become more active to further reduce the work load for the ER. If the stress is too extreme, RIDD can trigger apoptosis by degrading resident ER mRNAs (Han et al., 2009). One way RIDD seems to control apoptosis is through depression of caspases. Ire1 degrades mRNAs and miRNAs that normally inhibit caspase activation, resulting in apoptosis (Upton et al., 2012). Similar to TED, Xrn1 and the RNA exosome degrade metazoan Ire1 cleaved RIDD targets (Hollien and Weissman, 2006). However, it is unknown if there is an intermediate step to resolve the 5’ hydroxyl before XRN1 cleavage and what enzyme would mediate this step.

RIDD in *S. pombe* also aids in the maintenance of homeostasis. Similar to metazoan RIDD, Ire1 cleaves mRNAs that are translated by ribosomes on the ER membrane. Ire1 regulates the input of mRNA to the ER translation, folding, and secretory machinery (Kimmig

et al., 2012). RIDD targets include the mRNAs encoding ER membrane proteins themselves and may be degraded to control the lipid levels of the ER membrane (Volmer and Ron, 2015). One difference between S. pombe and metazoans is the involvement of No-Go decay (Guydosh et al., 2017). S. pombe Ire1 cleaves within the coding region and causes ribosomes to stall. The No-Go decay machinery including Dom34, the Ski complex, and the RNA exosome resolve the stalls and degrade the mRNA transcript (Guydosh et al., 2017). Interestingly, Ire1 *S. pombe* does not have *HAC1/XBP1* homolog nor does Ire1 seem to participate in mRNA splicing and instead regulates homeostasis and the UPR exclusively through RIDD (Kimmig et al., 2012; Niwa et al., 2004). Conversely, *S. cerevisiae* Ire1 is only known to splice *HAC1* with no in vivo characterized RIDD pathway. Previous literature has shown *Sc*Ire1 can cleave some yeast mRNAs such as Dap2 in vitro but these results have not been reproducible in vivo (Tam et al., 2014).

In this chapter, I seek to understand the degradation of endonuclease mediated decay products by Xrn1 and elucidate the role, if any, Trl1 plays in this process. As in chapter 3 and 5, I employed Parallel Analysis of RNA Ends (PARE) to determine targets of Trl1. I found that Trl1 acts downstream of some TED targets though it may not be essential for the degradation of the cleavage products by Xrn1. However, it seems that Trl1 is the only kinase that acts on these TED targets eliminating the possibility of another kinase acting on the products before Xrn1 degradation. I also performed PARE on *ire1* deletion strains to find potential targets of RIDD in *S. cerevisiae*. The deletion of Ire1 proved to cause many changes within the transcriptome which made determining genuine cleavage peaks difficult. Instead, I used both the Ire1 and Trl1 data to look for shared targets that could be RIDD targets that are phosphorylated by Trl1. Through this, I found that Trl1 and Ire1 both act on a few substrates. I hypothesize that these targets may be in vivo evidence of RIDD in *S. cerevisiae*. Overall, I speculate that Trl1 can act downstream of both RIDD and TED as the sole kinase to

phosphorylate the 5’ hydroxyl after endonuclease cleavage. In the case of TED, this does not seem to be necessary for degradation of all the cleavage products by Xrn1, implying there is a 5’ monophosphate-independent but Xrn1-dependent mechanism for their degradation.

Results

Parallel analysis of RNA ends identifies known targets of Trl1

To identify novel targets of Trl1 phosphorylation, I used PARE (Parallel analysis of RNA ends), a specialized type of RNAseq that detects RNAs with 5’ phosphates (German et al., 2009, 2008; Harigaya and Parker, 2012). I hypothesized that Trl1 acts as a kinase downstream of endonuclease cleavage to promote degradation of the cleavage fragments by Xrn1, similar to its role in *HAC1* and tRNA intron degradation. Therefore, if Trl1 does phosphorylate the 5’ hydroxyls resulting from endonuclease cleavage, the adaptor can be ligated to the 5’ phosphate and amplified in RNAseq, resulting in a peak. If Trl1 is the only kinase that acts on a cleavage product, the cleaved RNA will persist in a 5’ hydroxylated form that cannot be ligated and amplified in PARE and this peak will disappear in the PARE data. Because its kinase cleavage products are likely degraded, I performed PARE in an *xrn1*Δ background.

Trl1 has three different active sites for its three distinct functions: kinase, ligase, and phosphodiesterase. I transformed a *trl1*Δ*xrn1*Δ strains with plasmids containing Trl1 with mutations K404A/T405A or D425A which have been previously shown to disrupt kinase activity (Sawaya et al., 2003), along with an empty vector and wild-type control. Deletion and catalytic mutations in Trl1 are lethal as mature tRNAs cannot be produced. Therefore, the *E. coli* tRNA ligase RtcB was also expressed in these strains. The data were filtered for a PARE score of greater than 2 in the Trl1 expressing strain meaning that peaks with at least 2 cpm reads indicate a piece of RNA with a 5’ phosphate. This filter step eliminates background

noise of RNAseq reads that are dispersed throughout the genome. To determine potential sites of 5' end phosphorylation by Trl1, I also filtered for a comPARE score between the empty vector and Trl1 expressing strain of 1 in both replicates which only returns sites with at least twice as many reads in the Trl1 expressing strains as in the vector mutants.

Using linear regression, I compared the similarity of the PARE scores (peak heights) of replicates at these potential sites to assess reproducibility and degree of similarity between the mutants (Figure 6.1). The replicates were similar to one another (Figure 6.1A), with R^2 values between 0.74 and 0.89. I then compared replicate 1 of vector, K404A/T405A, and D425A strains. Each of these is an independent assay to identify Trl1-kinase dependent peaks, and they were all well related with R^2 values between 0.75 and 0.89 (Figure 6.1B). The correlation between the wild type and empty vector was expectantly low with an R^2 of 0.20 as I selected for differences between these strains by filtering the comPARE score. The kinase mutants were equally dissimilar to the wild type showing that even with filtering by just the comPARE score for the vector, the data for the kinase mutants showed the same trend. Taken together this indicates that our data are reproducible and the kinase point mutants and deletion (vector) of *trl1* have similar effects on the degradome.

A).

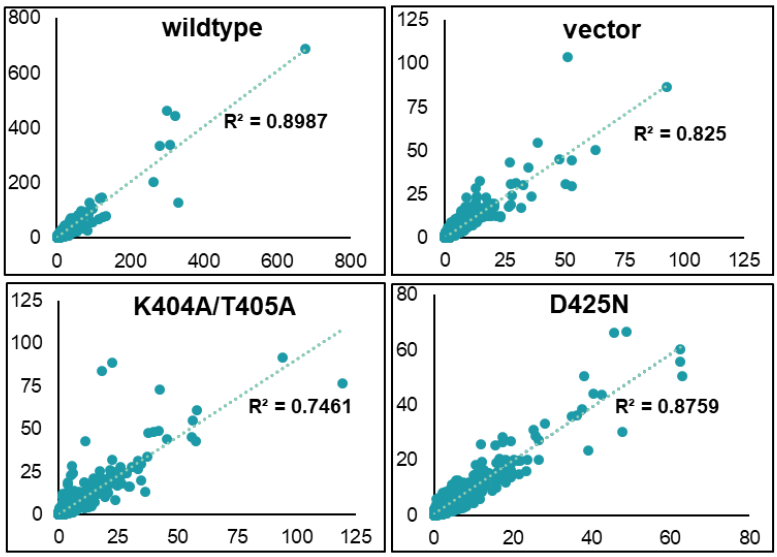
wildtype
R² = 0.8987
vector
R² = 0.825
K404A/T405A
R² = 0.7461
D425N
R² = 0.8759

B).

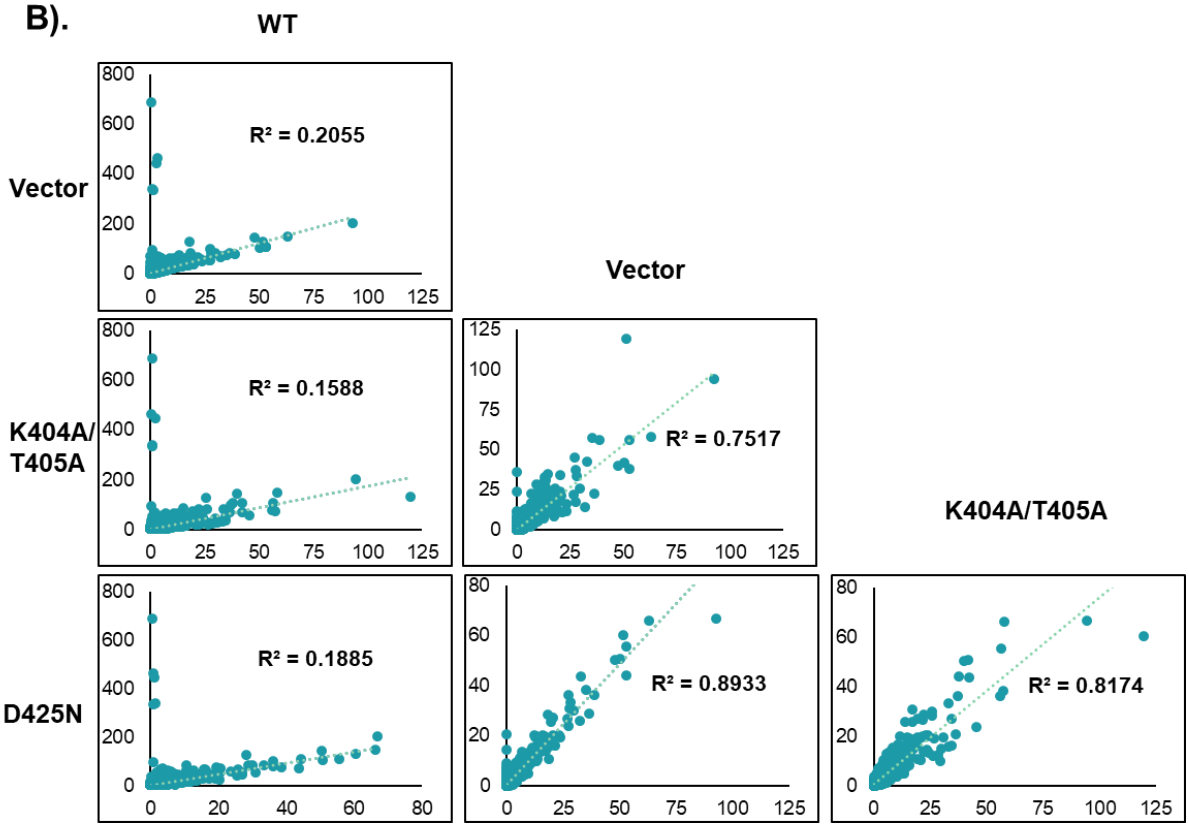
WT
Vector
R² = 0.2055
Vector
K404A/
T405A
R² = 0.1588
R² = 0.7517
K404A/T405A
D425N
R² = 0.1885
R² = 0.8933
R² = 0.8174

Figure 6.1. *trl1*Δ and Trl1 kinase point mutants have similar effects on the RNA degradome.

A). Biological replicates of Trl1 PARE are similar to each other as shown by linear regression analysis. The data were filtered by a PARE score of greater than 2 in the *TRL1* dataset and a comPARE score in the WT/ [vector] dataset of greater than 1. The R^2 value is shown. B). Three different Trl1 alleles have similar effects in the PARE data. Using the same filters as in A, the mutants within one replicate were compared to one another by linear regression. Though the data were filtered for sites that are different between the wildtype and vector, the other mutants are equally dissimilar to the wild type. The mutants are also closely related under these filters.

Next, I examined the PARE data for known targets of Trl1 to ensure our method can capture phosphorylation by Trl1. Hac1 is one of the best characterized targets of Trl1 with the exons being ligated following phosphorylation, and the intron being degraded. I performed comPARE analysis in which the peaks were compared between the wild type and each of the three mutants. HAC1 had the highest comPARE score or change between the wild type and mutants. When examining the read map of the Trl1 expressing strain in IGV, peaks can be observed corresponding to ligation of the adaptor to a 5' phosphate at the end of both the intron and 3' exon, corresponding to phosphorylation (Figure 6.2A). In all three mutants, these peaks disappeared indicating loss of phosphorylation. I note that the peaks appear in clusters due to the distributive exonuclease activity of Dxo1 as described in chapter 5. Though PARE enriches for PolyA+ RNAs, the phosphorylation of some intron containing tRNAs was still detectable. Specifically, PARE detected *tP(UGG)O1* and *tK(UUU)L* which were reduced at least 16-fold (comPARE score>4) (Figure 6.2B,C). Peaks corresponding to phosphorylation of the 3' exons were abolished in all three mutants. Overall, these data show that PARE can detect targets of Trl1 kinase activity and all three mutants abolish this activity similarly.

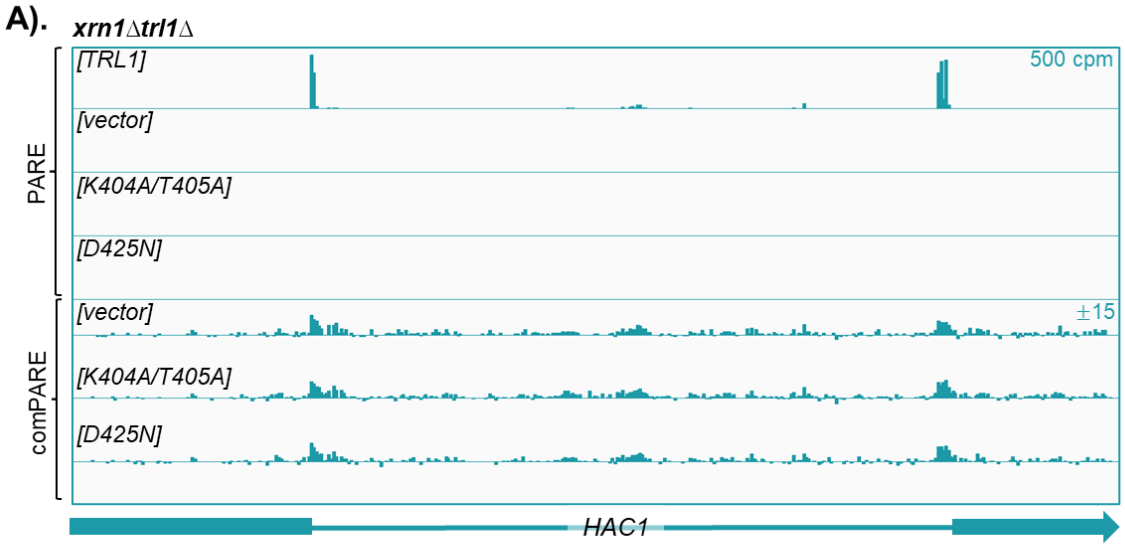
A).
xrn1Δtrl1Δ
[TRL1]
500 cpm
[vector]
[K404A/T405A]
[D425N]
PARE
[vector]
±15
[K404A/T405A]
[D425N]
comPARE
HAC1

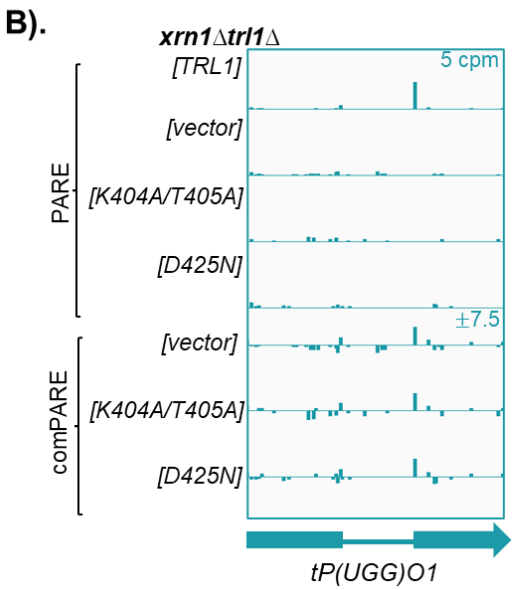
B).
xrn1Δtrl1Δ
[TRL1]
5 cpm
[vector]
[K404A/T405A]
[D425N]
PARE
±7.5
[vector]
[K404A/T405A]
[D425N]
comPARE
tP(UGG)O1

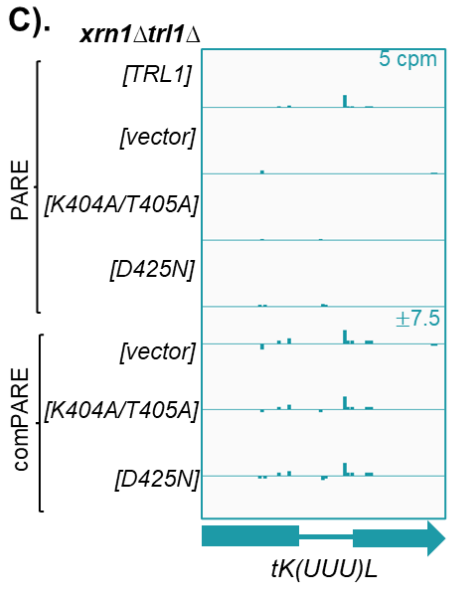
C).
xrn1Δtrl1Δ
[TRL1]
5 cpm
[vector]
[K404A/T405A]
[D425N]
PARE
±7.5
[vector]
[K404A/T405A]
[D425N]
comPARE
tK(UUU)L

Figure 6.2: PARE can detect known targets of Trl1.

Read accumulation of **A).** *HAC1*, **B).** *tP(UGG)O1*, and **C).** *tK(UUU)L* showing the presence of a 5' phosphate in the *TRL1* strain that is decreased in the mutants. Reads are plotted on the yeast genome with peaks corresponding to the sites where Trl1 has added a 5' phosphate, enabling ligation of the adaptor and amplification for RNAseq. Both the read count (PARE score in cpm) for each strain and the fold change (comPARE score) for the wildtype compared to each mutant are plotted. The scale for the graphs is given to the left. Arrows indicate the direction of the transcript and display position of intron.

PARE identifies novel targets of Trl1 including activity downstream of TED

I next wanted to search for novel targets of Trl1. I first looked at known endonuclease sites to determine if Trl1 phosphorylates endonuclease cleavage products to facilitate degradation or ligation. One site that I identified was downstream of cleavage by the TSEN complex in *CBP1* (Figure 6.3A). The van Hoof lab and others have established that this cleavage likely leads to degradation in a process the van Hoof lab previously termed TED. We observed peaks in the Trl1 expressing strain that corresponded to the same three sites we identified in PARE of the TSEN complex. These three peaks disappeared in the three *trl1* mutants. Similarly, I detected kinase activity on the TED target *COQ5* (Figure 6.3B). This identified Trl1 as the polynucleotide kinase that converts the 5' hydroxyls of TSEN cleaved mRNAs to 5' monophosphates.

I next looked at the top comPARE scores within the Trl1 datasets. I identified *CBR1* and *TCP1* mRNAs as potential targets of Trl1 though it is unknown if any endonuclease cleaves within these transcripts (Figure 6.3C,D). Novel potential targets are not limited to mRNAs as an unknown RNA that is antisense to *DGR2* also had high PARE and comPARE scores (Figure 6.3E). This target had consistently high comPARE scores >4 when the wild type was compared to any of the three mutants and across both replicates. These results show that PARE was able to identify possible novel kinase targets of Trl1 including the TED targets *CBP1* and *COQ5*. I hypothesized that Trl1 acts downstream of TSEN to phosphorylate the 5' end of the 3' cleavage product to allow degradation by Xrn1. More data are needed to confirm *CBR1*, *TCP1*, and *DGR2* as targets of Trl1 as well as how, when, and why they are cleaved and phosphorylated.

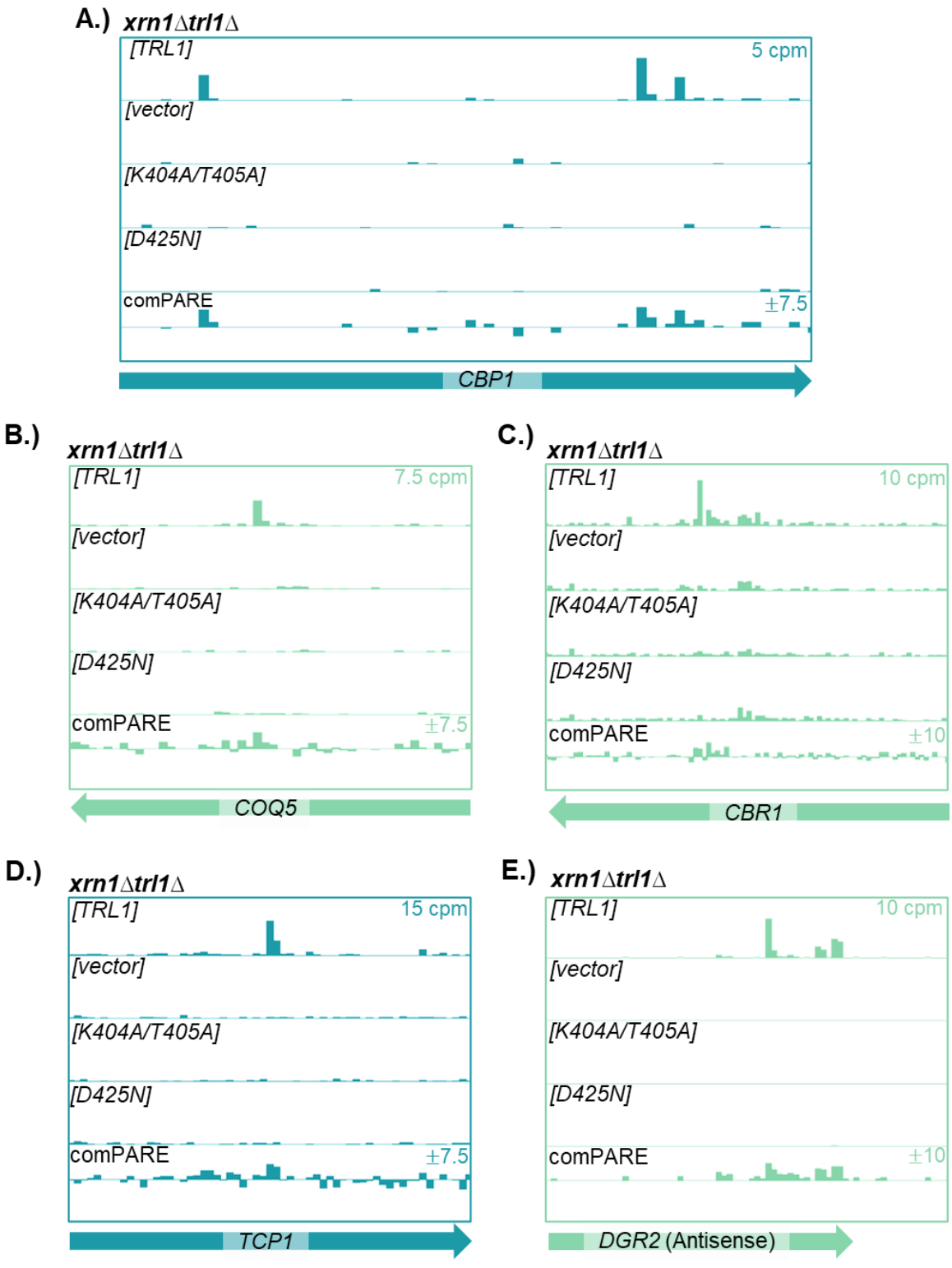
A.) xrn1Δtrl1Δ
[TRL1]
5 cpm
[vector]
[K404A/T405A]
[D425N]
comPARE
±7.5
CBP1
B.) xrn1Δtrl1Δ
[TRL1]
7.5 cpm
[vector]
[K404A/T405A]
[D425N]
comPARE
±7.5
COQ5
C.) xrn1Δtrl1Δ
[TRL1]
10 cpm
[vector]
[K404A/T405A]
[D425N]
comPARE
±10
CBR1
D.) xrn1Δtrl1Δ
[TRL1]
15 cpm
[vector]
[K404A/T405A]
[D425N]
comPARE
±7.5
TCP1
E.) xrn1Δtrl1Δ
[TRL1]
10 cpm
[vector]
[K404A/T405A]
[D425N]
comPARE
±10
DGR2 (Antisense)

Figure 6.3: Trl1 has other targets including some downstream of TSEN cleavage.

Read maps for **A).** *CBP1*, **B).** *COQ5*, **C).** *CBR1*, **D).** *TCP1*, and **E).** *DGR2* showing the accumulation of peaks in the *TRL1* strain that disappeared in all three mutants. The comPARE score is displayed for the *TRL1* compared to the vector. Arrows show the direction of the transcript and the color corresponds to the strand (green is reverse and blue is forward).

Trl1 is not required for CBP1 degradation downstream of TED

I found that Trl1 acts downstream of TSEN cleavage on the TED target *CBP1*. As previously mentioned, I knew that these cleavage products are degraded by the RNA exosome and Xrn1. To assess if Trl1 is necessary for degradation by the downstream exonucleases, I performed a Northern blot for CBP1. In a *ski7*Δ strain where the cytoplasmic RNA exosome is inactivated, I observed the accumulation of the 5' cleavage product resulting from TSEN cleavage of CBP1 (Figure 6.4A). This was not visible in the wild type, indicating Ski7 and the RNA exosome is necessary for degradation of this product. When compared to a *trl1*Δ strain, I observed little accumulation of the cleavage product indicating that the RNA exosome can still degrade this product even without Trl1. The 3' cleavage product showed similar results. In the *xrn1*Δ mutant, I observed the clear accumulation of the cleavage product that was not present in the wild type (Figure 6.4B). This indicates that Xrn1 is necessary for the degradation of the 3' cleavage product. In the *trl1*Δ mutant, I did not observe the accumulation of the cleavage product suggesting that Trl1 phosphorylation is not necessary for degradation by Xrn1.

I previously found that the distributive 5' to 3' exonuclease Dxo1 can also act on CBP1 downstream of TSEN cleavage. Like Trl1, processing by Dxo1 is not necessary for the degradation of the 3' product of CBP1 as I did not see accumulation of the cleavage product in the *dxo1*Δ mutant. Since both Trl1 and Dxo1 act on CBP1 but neither alone is necessary for degradation of the cleavage product, I thought that the two enzymes could function redundantly in processing the 5' hydroxyl. However, a *dxo1*Δ*trl1*Δ also did not accumulate the 3' cleavage product indicating that both enzymes are unnecessary for degradation by Xrn1 (6.4B). Of note, Trl1 does seem to be the only enzyme that phosphorylates the 3' cleavage product of CBP1. In the PARE data, I observed no residual peaks when Trl1 was deleted

indicating the 5’ end of this fragment was not phosphorylated at all (Figure 6.3A). I speculate that Xrn1 can degrade cleaved *CBP1* even in the absence of a 5’ monophosphate.

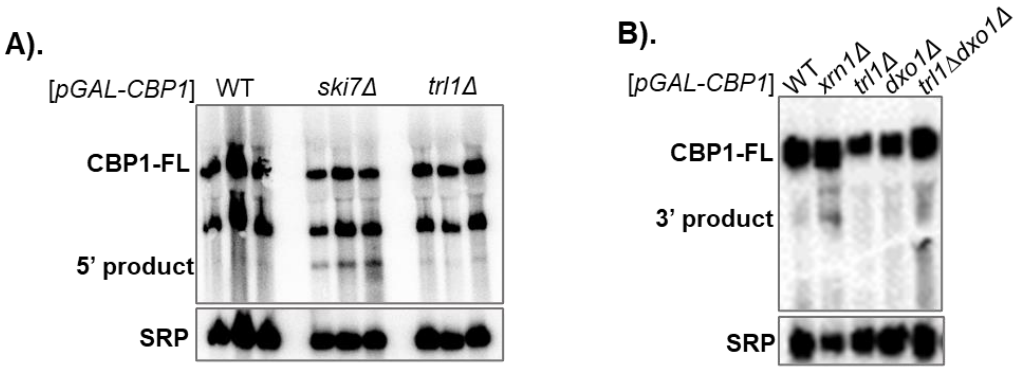

Figure 6.4: Trl1 is not required for degradation of *CBP1* cleavage fragments.

Northern blots of the A). 5’ and B). 3’ cleavage products of CBP1 following cleavage by TSEN in exonuclease mutants and *trl1*Δ yeast backgrounds. A). The RNA exosome (*ski7*) but not Trl1 is required for degradation of the 5’ cleavage fragment. B). Xrn1 is required for the 3’ product degradation but neither the exonuclease Dxo1 nor Trl1 are required for this degradation. SRP was used as a loading control.

Ire1 and Trl1 share common substrates and may participate in RIDD together in yeast in vivo

One of the novel targets of Trl1 I identified was *NPL4*. Npl4 is involved in endoplasmic reticulum associated degradation (ERAD) and destruction of ER membrane proteins (Hitchcock et al., 2001). Because Npl4 is involved in protein regulation in the ER, I hypothesized that this mRNA could be a target of Ire1 endonuclease cleavage that is phosphorylated by Trl1 before degradation, like the *HAC1* intron. I performed PARE to determine if *NPL4* and any other mRNAs are targets of both Ire1 and Trl1. To do this, I generated *ire1*Δ*xrn1*Δ and *xrn1*Δ strains that were then treated with tunicamycin according to previous literature to induce ER stress with the expectation that this would increase Ire1 endonuclease activity (Cherry et al., 2019). Duplicate cultures of each of these four conditions (*ire1*Δ/*IRE1* and +/- tunicamycin) were analyzed by PARE. I then compared the top comPARE hits between the Trl1 expressing and vector control strain with the *IRE1* and *ire1*Δ strains which correspond to sites with peaks in both wildtype datasets that were decreased when *trl1* and *ire1* were deleted. Like in the Trl1 dataset, *HAC1* was among the top comPARE hits for Ire1, with peaks at the 5' end of both the intron and 3' exon in the wild type in both the control DMSO treatment and the tunicamycin treatment (Figure 6.5A). *HAC1* cleavage and splicing is known to be induced by tunicamycin. However, the PARE signal, which is a complex product of nuclease digestion, phosphorylation, and ligation rates, actually decreased somewhat, perhaps indicating that phosphorylation or splicing rate may also be increased upon tunicamycin treatment. Another complicating factor is that *HAC1* transcription is induced by tunicamycin treatment in an Ire1 independent manner (Leber et al., 2004). Importantly however, the peaks at 5' end of the intron and 3' exon both strongly decreased in *ire1*Δ in both the presence and absence of tunicamycin and in both replicates (Figure 6.5A). Thus, PARE and comPARE successfully detected the two known Ire1 sites in the RNA degradome.

With confirmation that I could identify shared targets of Ire1 and Trl1 within our PARE data, I next examined *NPL4.* I indeed identified a strong peak in both the *TRL1* and *IRE1* strains that disappeared in the vector control or deletion, respectively (Figure 6.5B). These data suggest that *NPL4* is cleaved by Ire1 and phosphorylated by Trl1. *NPL4* has no intron so it seems likely that cleavage by Ire1 could be involved in the degradation of the transcript. This could be the first in vivo evidence of RIDD in *S. cerevisiae*. Several attempts at in vitro characterization of *S. cerevisiae* Ire1 RIDD targets have been made but none have been able to be confirmed in vivo. I also looked through our Ire1 and Trl1 data for indications of possible cleavage in the mRNAs *DAP2* and *mFα2* which one in vitro study suggested to be RIDD targets (Tam et al., 2014) but found no peaks in either the *TRL1* or *IRE1* strains (regardless of tunicamycin treatment) datasets.

I also found a few other mRNAs that could also be targets of RIDD as they have peaks in both the Trl1 and Ire1 datasets, though less striking than *NPL4.* The antisense strand of *MOT3* seems to have many comPARE peaks in both the *IRE1* and *TRL1* datasets (Figure 6.5C). The fact that the peaks are so dispersed and this apparent cleavage is of the antisense strand makes this a less likely target for RIDD even though the comPARE scores were among the top hits in both datasets. In vitro or low throughput methods will need to be utilized to confirm these data before beginning to decern its biological significance. *EFT1* and *EFT2* were both found to have comPARE peaks in the *IRE1* and *TRL1* datasets (Figure 6.5D,E). *EFT1* and *EFT2* are paralogs resulting from the whole genome duplication. The *EFT1* and *EFT2* mRNAs are virtually identical with only four nucleotide differences in the 2529 nucleotide coding regions. Therefore, this PARE signal may reflect cleavage of one or both paralogs. The Eft1 and Eft2 proteins are identical and function as elongation factors required for protein synthesis (Perentesis et al., 1992). It is unclear if this would put the mRNAs in spatial contact with Ire1 for cleavage; however, degradation of these mRNAs could be involved in arresting

translation which fits with previous findings that RIDD tends to downregulate translation to reduce the load for the protein folding machinery in the ER. More data are needed to determine if these are cleavage targets of Ire1, if they are degraded downstream of cleavage, and if the degradation is dependent on Trl1. Overall, I speculate that Ire1 and Trl1 share targets that could be in vivo evidence of RIDD in *S. cerevisiae.*

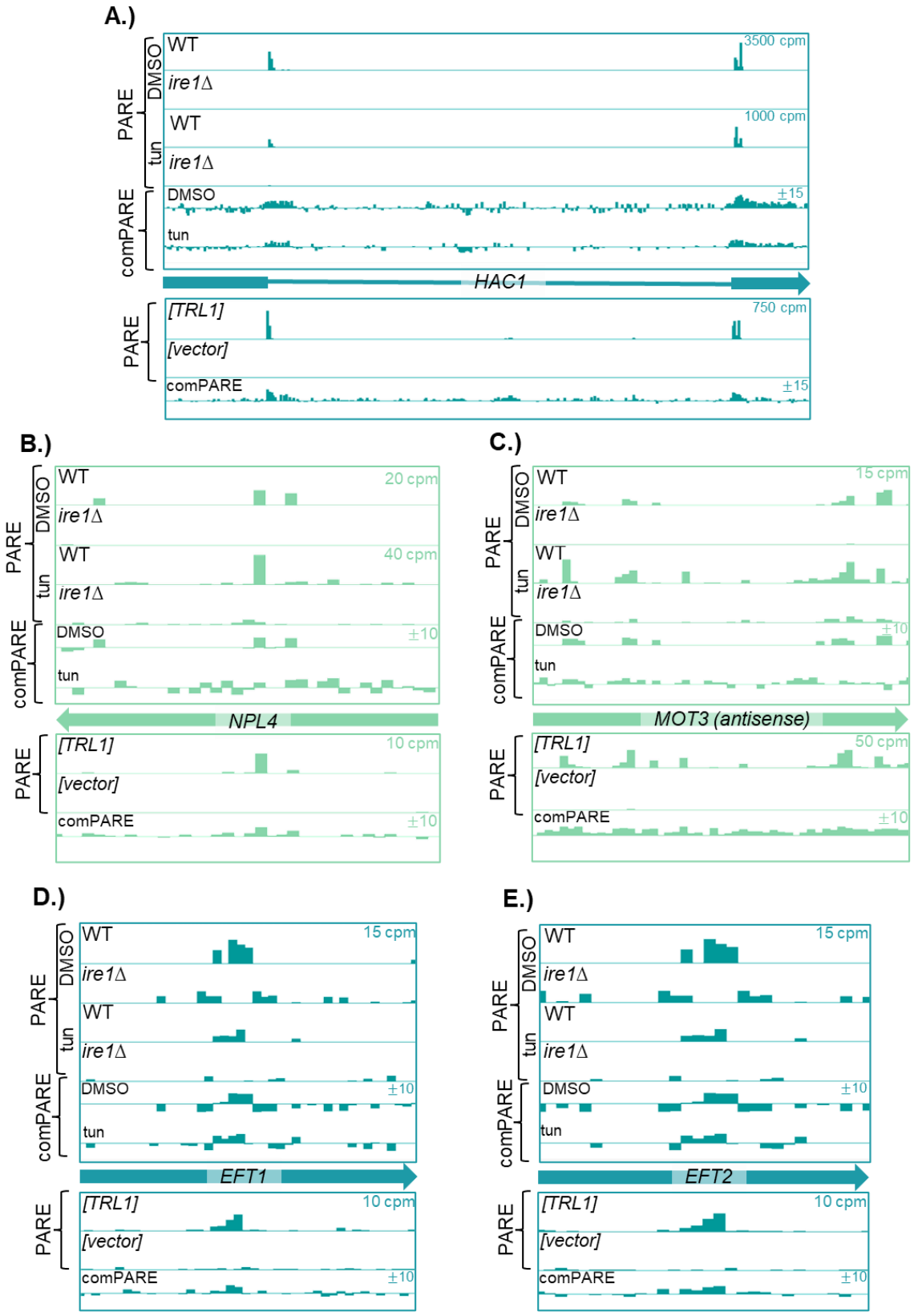
A.)
PARE
DMSO
WT
ire1Δ
tun
WT
ire1Δ
comPARE
DMSO
tun
3500 cpm
1000 cpm
±15
HAC1
PARE
[TRL1]
[vector]
comPARE
750 cpm
±15
B.)
PARE
DMSO
WT
ire1Δ
tun
WT
ire1Δ
comPARE
DMSO
tun
20 cpm
40 cpm
±10
NPL4
PARE
[TRL1]
[vector]
comPARE
10 cpm
±10
C.)
PARE
DMSO
WT
ire1Δ
tun
WT
ire1Δ
comPARE
DMSO
tun
15 cpm
±10
MOT3 (antisense)
PARE
[TRL1]
[vector]
comPARE
50 cpm
±10
D.)
PARE
DMSO
WT
ire1Δ
tun
WT
ire1Δ
comPARE
DMSO
tun
15 cpm
±10
EFT1
PARE
[TRL1]
[vector]
comPARE
10 cpm
±10
E.)
PARE
DMSO
WT
ire1Δ
tun
WT
ire1Δ
comPARE
DMSO
tun
15 cpm
±10
EFT2
PARE
[TRL1]
[vector]
comPARE
10 cpm
±10

Figure 6.5: Ire1 and Trl1 share targets; evidence of RIDD in *S. cerevisiae*.

PARE and comPARE data from Ire1 and Trl1 datasets show sites where peaks are present in the IRE1 and TRL1 strains and reduced in the *ire1*Δ and *trl1* mutants. The Ire1 dataset yeast were grown in the presence of tunicamycin or DMSO. Read maps for the shared targets **A).** *HAC1*, **B).** *NPL4*, **C).** *MOT3*, **D).** *EFT1*, and **E).** *EFT2* are shown.

Complex effects of Ire1 and tunicamycin on the transcriptome complicate the interpretation of *ire1*Δ PARE data

Using PARE, I hoped to identify other direct targets of Ire1 that could be involved in RIDD or the UPR. This proved to be difficult, however. There were thousands of sites with a comPARE score above 4. Many of those appeared within the 5' UTR, and these likely correspond to genes that are transcriptionally regulated by Hac1. In an attempt to exclude these hits, I filtered our comPARE to only coding regions. Even with this filtering, thousands of hits remained with many located in genes with these 5' UTR clusters. This made it difficult to distinguish between direct signals resulting from endonuclease cleavage and indirect signals resulting from expression changes. Globally, the number of comPARE scores >4 was much larger than the number of scores < -4 (Figure 6.6A). This is encouraging as the peaks corresponding with cleavage would have to have a positive comPARE score. However, the sheer number of suspected indirect effects made it difficult to identify direct endonuclease targets.

Another compounding aspect of this Ire1 PARE study was the tunicamycin treatment. As can be seen in Figure 6.6B, the majority of sites that are unaffected by *ire1*Δ in both tunicamycin and DMSO conditions are clustered around the origin. However, there were also a large number of sites that were affected under both conditions, but unexpectedly the magnitude of the effect of *ire1*Δ tended to be smaller in the tunicamycin treated samples than in the control treated samples (slope <1 in Figure 6.6B), mirroring what I described above for *HAC1* cleavage. I expected more cleavage or transcriptional changes when the UPR was induced, however this suggests the opposite. This reflects a complicated biological response to tunicamycin. The PARE data clearly showed that tunicamycin affected its well-known target gene *KAR2* both in the *IRE1* and *ire1*Δ suggesting that tunicamycin has Ire1-independent effects (Figure 6.6C). Furthermore, the *IRE1* strain turns on *HAC1* and the UPR to limit the

damage of tunicamycin, while the *ire1*Δ strain does not have this capacity. Overall, using the Trl1 comPARE hits, I was able to identify possible shared targets that could be in vivo evidence of RIDD in *S. cerevisiae*. I was unable to systematically identify targets of Ire1 transcriptome-wide due to the prevalence of indirect effects in the dataset. In the discussion, I propose a few ways to remedy this.

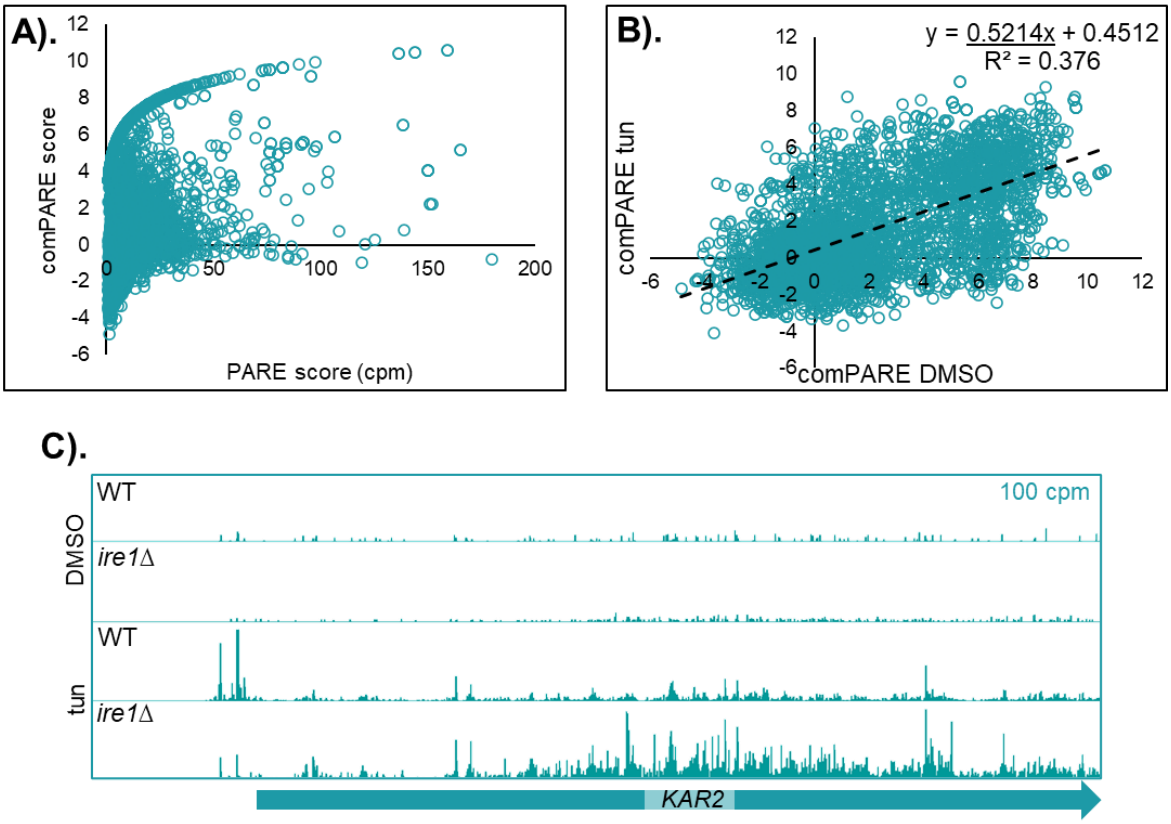

Figure 6.6: Trends within the Ire1 data.

A). Scatterplot of sites with a PARE score of greater than 1 but less than 200 (in order to get a better zoom on the data) are graphed based on their PARE and comPARE score. Overall, the data are enriched for positive comPARE scores. **B).** Linear regression of the comPARE scores of the *IRE1* vs the *ire1*Δ of yeast treated with tunicamycin or DMSO show the tunicamycin caused less change between the wildtype and mutant than the DMSO treatment. The slope is displayed in the upper left corner. **C).** Read map of *KAR2* demonstrating that tunicamycin affects the transcriptome in an Ire1-independent manner. Increased read accumulation is seen in both the 5' UTR and throughout the gene with tunicamycin treatment.

Chapter Conclusions

Using PARE, I investigated the substrates and functions of the multi-domain enzyme Trl1, and its potential role in endonuclease-mediated mRNA decay. When some endonucleases cleave including TSEN and Ire1, the resulting 3' cleavage product has a 5' hydroxyl that is not a canonical substrate of Xrn1. How these 3' cleavage products are eventually degraded by Xrn1 is unknown which led to our hypothesis that Trl1 phosphorylates the 5' hydroxyl to allow Xrn1 degradation. Both a full deletion (vector) and two different kinase dead Trl1 mutants, K404A/T405A and D425N were assessed and found to have similar effects on Trl1 activity within the PARE data as the mutants were as close to one another as they were to their own replicates. I confirmed our PARE analysis was effective at capturing Trl1 targets by verifying known substrates within our data. *HAC1* and tRNAs with introns both showed peaks that were present in the *TRL1* strain and that were reduced in all three mutants. Using comPARE, novel targets can be deduced from these data. *CBP1*, a TED target, has peaks that were present in the *TRL1* that were reduced in the mutants. These peaks also match with our previously published PARE data for TED targets. *COQ5* is another TED target that may also be phosphorylated by Trl1. I propose that Trl1 acts downstream of TSEN cleavage to phosphorylate the resulting 5' hydroxyl to a phosphate that can then be degraded by Xrn1. This is similar to how the tRNA intron is degraded after cleavage by TSEN. Several other potential targets were identified such as *CBR1*, *DGR2* antisense strand, and *TCP1*. These targets are not known to be cleaved by an endonuclease so the function of potential Trl1 phosphorylation is not known. In vitro or low-throughput assays need to be performed to determine if these are genuine targets of the Trl1 kinase domain and if this occurs downstream of some type of cleavage.

Previous data from our lab showed that *CBP1* is also a target of the distributive exonuclease, Dxo1. Since it seems that both Dxo1 and Trl1 act downstream of cleavage, I

investigated if one or both enzymes are necessary for *CBP1* cleavage product degradation. Through Northern blot analysis, I showed that neither phosphorylation by the Trl1 kinase domain nor "nibbling" from Dxo1 are required for degradation of the 3' cleavage product. The PARE data suggest that there is no other kinase converting the 5' hydroxyl to a phosphate on *CBP1* as the peaks were absent in the *trl1* mutants. Another possibility is that a distributive 5' to 3' exonuclease can remove the 5' hydroxyls. In humans, DXO can remove 5' hydroxyls but if *S. cerevisiae* Dxo1 can process 5' hydroxyls, which is unlikely based on sequence similarity (Chapter 5), it is not necessary for the degradation of *CBP1* by Xrn1. The last scenario that I propose is that there is no intermediate step and Xrn1 can process 5' hydroxyls itself, though less efficiently than its preferred 5' phosphate substrate. Several publications show that Xrn1 rapidly degrades 5' phosphates while having little to no activity on 5' hydroxyls. However, most of these studies were in vitro. In vivo, it is possible that Xrn1 eventually removes the 5' hydroxyl which would then leave a 5' phosphate allowing it to quickly degrade the rest of the cleavage product. Xrn1 may also have some sequence specificity. Catherine Stuart confirmed Trl1 is not required for degradation of the 5' hydroxyl fragment of *CBP1* resulting from TSEN cleavage but is required for Xrn1 mediated decay of the 5' hydroxyl product of a hammerhead ribozyme (Stuart and van Hoof unpublished data). Kinetic analysis of Xrn1 on specific TED targets like *CBP1* with 5' hydroxyls would be needed to confirm that Xrn1 can have activity on 5' hydroxyls.

I identified *NPL4* as a possible substrate of Trl1. Npl4 is involved in ERAD, which led me to the hypothesis that this mRNA may initially be cleaved by Ire1 before Trl1 phosphorylation, as is the case with *HAC1*. If *NPL4* is a target of Ire1 and phosphorylated by Trl1 before degradation by Xrn1, this could be the first in vivo evidence of RIDD in *S. cerevisiae*. I then performed PARE on an *ire1*Δ*xrn1*Δ mutant to identify novel targets of Ire1. Indeed, *NPL4* seems to be a target of both Ire1 and Trl1. Npl4 functions in ERAD, a pathway

to remove damaged and unfoldable proteins from the ER back to the cytosol for degradation (Hitchcock et al., 2001). Perhaps Npl4 grants not yet folded proteins more time to fold when the cell experiences a defect in the folding machinery. Other potential targets of both Ire1 and Trl1 included *EFT1/2*, which are involved in protein synthesis specifically in ribosomal translocation during translation elongation (Perentesis et al., 1992). Downregulating these proteins upon ER folding stress may function to reduce the load of proteins coming into the ER. For the other targets identified, the biological function of cleavage is less clear. For example, an RNA antisense to *MOT3* had one of the highest comPARE scores in both the Trl1 and Ire1 datasets but the nature and function of this antisense RNA are unclear. Additionally, the peaks were diffuse with what looks like several clusters spanning ~20 nucleotides. More work will need to be conducted to ensure these are targets of Ire1 and Trl1 and possible examples of RIDD.

Previous studies have shown that Ire1 is more active with addition of tunicamycin which causes ER stress. However, the PARE results showed that tunicamycin addition reduced the *HAC1* cleavage product accumulation. This could be due to rapid ligation by Trl1 but that does not explain why the intron also had less signal as it is not a target of ligation. One possibility is that in S*. cerevisiae,* more RIDD occurs as demonstrated by the larger *NPL4* peak in the tunicamycin treated condition. However, the rest of our proposed RIDD targets like *EFT1/2* had stronger peaks in the DMSO control treatment making this scenario unlikely. I looked at the global changes between the comPARE of DMSO and tunicamycin treatments. The slope revealed that the changes between the wild type and *ire1*Δ deletion were more extreme with the DMSO treatment than the tunicamycin treatment, suggesting that the *HAC1* and potential novel targets followed this global trend. It should be noted that this experiment was only performed in duplicate and thus while these trends are noticeable, further replicates and rigorous statistical analysis would be needed to draw firm conclusions.

In general, my Ire1 PARE data did not clearly identify all the targets of Ire1. As previously stated in the results, there were thousands of mRNAs with clusters of peaks in the 5' UTR. This likely corresponds to an overall change in transcription and/or mRNA decapping, and the observed peaks are due to more decapping occurring on more abundant transcripts. I tried to filter for coding regions, but I still had many peaks that clustered to genes that were likely differentially expressed between the wild type and *ire1*∆ deletion. Decapping peaks are prominent in PARE data, but previously, most decapping peaks have been the same between the wild type and mutants, preventing them from being called during the comPARE analysis. The fact that the expression of so many genes changes is likely the reason these data are dominated by indirect signals. The overall trend of the data suggests that the majority of peaks are higher in the *IRE1* strain and reduced in the *ire1*∆. This is promising as a cleavage site is expected to have a positive comPARE score indicating PARE likely captured Ire1 targets, and reducing the indirect effects should clarify these sites. I propose three future approaches to more effectively find Ire1 cleavage targets rather than relying on shared targets with Trl1. First, I could compare our PARE data to RNAseq data and filter out genes that are known to have expression changes when *ire1* is deleted. Unfortunately, I was unable to locate a suitable dataset in SRA. In any case, it might be preferable to perform RNAseq and PARE on the same RNA samples rather than using the existing published RNAseq data to eliminate as many confounding variables as possible. Second, using a catalytic Ire1 mutant rather than full deletion of *ire1* may also limit expression changes. Ire1 has both endonuclease and protein kinase domains. The protein kinase domain is thought to solely function to activate the nuclease activity (Shamu and Walter, 1996), but it is possible that it phosphorylates some other proteins, which may affect gene expression in an unknown manner. The endonuclease mutant of Ire1 still has active kinase domain and is still incorporated into the ER membrane. Thus, comparing this mutant to *IRE1* would eliminate effects that are solely kinase dependent. Third, the major target of Ire1 is *HAC1* which when spliced translates into the major

transcription factor that regulates the UPR. Thus, in the *ire1*∆ the mutant the Hac1 protein is not translated and the UPR target genes are not induced. If the comPARE analysis was repeated in a *hac1*∆ background, this would eliminate these indirect effects and narrow down potential cleavage sites.

Overall, I was able to use PARE to find potential targets of the kinase domain of Trl1. These data were much less confounded by indirect effects likely due to complementation of the *trl1* mutant strains with RtcB. *TRL1* is essential due to its role in tRNA splicing; so in order to make viable kinase mutants, this function had to be bypassed by the expression of *E. coli* RtcB. This also likely restores some *HAC1* mRNA splicing, and thus in our *trl1* strains, the UPR is largely functional. *CBP1* is among the Trl1 targets that I identified which is also a TED target. Trl1 phosphorylates the residual 5' hydroxyl to a phosphate that is then detectable by PARE. However, this cleavage product can still be degraded without Trl1. I also identified *NPL4* as at least one potential *S. cerevisiae* RIDD target. These data need validation with other methods, mutants, and replicates. However, I hope that these data generate excitement for further exploration of RIDD and endonuclease mediated decay in *S. cerevisiae*.

7) Discussion

TSEN participates in a novel endonuclease decay pathway

Yeast TSEN has an essential function independent of tRNA processing (Cherry et al., 2018; Dhungel and Hopper, 2012). Previous research established TSEN cleaves *CBP1* mRNA (Tsuboi et al., 2015) and led to my hypothesis that TSEN may cleave other mRNAs which could be an essential function of TSEN. We utilized PARE to detect TSEN cleavage sites within the yeast transcriptome. As I had little bioinformatic experience, I needed a user-friendly way to analyze PARE data and as a result, developed the comPARE pipeline on the Galaxy server. Notably, my pipeline specifically calls single peaks that correspond to cleavage sites while traditional RNAseq analysis reports signals based on the read count of the whole gene. Using comPARE I identified several novel mRNA targets encoding mitochondrially localized proteins. TSEN cleaves pre-tRNA based on structure, length, and sequence features including a key basepair between the anticodon and the intron (the A-I basepair). Within mRNA targets, I showed TSEN cleaves after adenosines and mutation of these leads to reduced cleavage. Because TSEN is localized to the mitochondrial membrane and has mRNA localized targets, I tested if forcing respiration with the non-fermentable sugar glycerol would affect TSEN cleavage targets or frequency but found no distinctive differences. We also performed PARE on cells expressing a catalytic mutant of Sen2 to probe which subunit is responsible for cleavage at each mRNA site. However, I observed a total loss of cleavage similar to the temperature sensitive mutant likely because this mutation may disrupt the structure or RNA binding of the TSEN complex as a whole.

One of the future goals of this project is to determine which subunit is responsible for which mRNA cleavage sites. Since the catalytic mutant of Sen2 interfered with Sen34 activity, a different residue of Sen2 needs to be selected that specifically affects Sen2 while leaving

Sen34 function intact. We examined growth and tRNA processing of strains with substitutions of residues thought to be involved in RNA binding and catalysis, as well as homologous mutations found in PCH patients (Figure 7.1, 7.2, and Table 7.1). One mutant, *G293E*, results in viable cells at room temperature (Figure 7.1) (published as a cold sensitive mutant (Ho et al., 1990)) but still causes defects in tRNA processing (7.2B,C). In this strain, the exon1-intron intermediate, corresponding to precursor cleaved only at the 3' site by Sen34 (Figure 7.2A), accumulates in both pre-tRNAs tested. There is no buildup of full pre-tRNA nor a decrease in mature tRNA suggesting this mutant maintains Sen34 and some Sen2 function. This mutant may be a good choice for PARE in the future as only Sen2 function appears to be affected, allowing differentiation of Sen34 and Sen2 targets. However, the absence of a growth phenotype suggests that the Sen2 catalytic site and activity only have a minor defect. This mutant may not have enough of a defect in mRNA cleavage to generate significant comPARE scores. In vitro cleavage assays on known TED targets could also differentiate subunit specificity as the Sen34 sites will be cleaved at normal levels while those of Sen2 will be reduced. Among other mutations tested, three PCH mutations (*F230C, Y266C,* and *P233R*) and candidate residues that are expected to stack with RNA bases (*W348A* and *W370A*), did not cause a growth defect or affect tRNA cleavage (Figure 7.1, 7.2, and Table 7.1). *Y289F* (catalytic base, See Figure 1.3 for details of catalysis), *R321A* (RNA interaction), and *K238A* (transition-state stabilizer) all caused growth defects and had varying effects on tRNA cleavage. Like the vector control and *H298A* (catalytic acid), these mutations impaired both 5' and 3' tRNA cleavage as there was an accumulation of pre-tRNA and less mature tRNA produced (Figure 7.2). 3' cleavage was less affected than 5' cleavage as the exon1-intron intermediate accumulated in at least the *Y289F* and *K328A*. Interestingly, the *R321A* mutant accumulated intron-exon2 intermediate corresponding to Sen34 impairment with more Sen2 5' cleavage but only with tryptophan pre-tRNA and not the leucine pre-tRNA (Figure 7.2). I hypothesized that at least for tryptophan pre-tRNA processing, *R321A* is important for Sen34

function in some way. Previous in vitro work showed that this residue did not affect Sen34 function despite the homologous residue of Sen34 impairing Sen2 function (Trotta et al., 2006). These in vivo data suggest more work needs to be done on the interaction between Sen2 and Sen34. The recently determined structure of human TSEN will be helpful in further understanding the role of individual amino acid residues in catalysis and complex assembly.

To summarize these data (Table 7.1), the *G293E* mutant likely has the least disruption of Sen34 cleavage while still reducing Sen2 activity. *Y289F* and *K328A* produce similar effects as the *H298A* mutant in that both Sen2 and Sen34 cleavage are reduced, leading to less mature tRNA overall. R321 contributes to Sen34 cleavage at the 3' site of at least the tryptophan pre-tRNA, but the mutant has a similar effect to the empty vector on the leucine tRNA with little cleavage at either site. These data show residues in Sen2 can contribute to Sen34 cleavage in some way which disputes previous in vitro data. This also shows different residues may be more important for cleavage on certain pre-tRNAs. I hypothesize that this is due to the differences in the structure of pre-tRNAs with differing positions of the A-I pairing creating differing bulge-helix-bulge structures. I hope that these data inform future work on TSEN catalysis and demonstrate that there are differences in how TSEN interacts not only with different types of RNA, but even within pre-tRNAs, which will need further study.

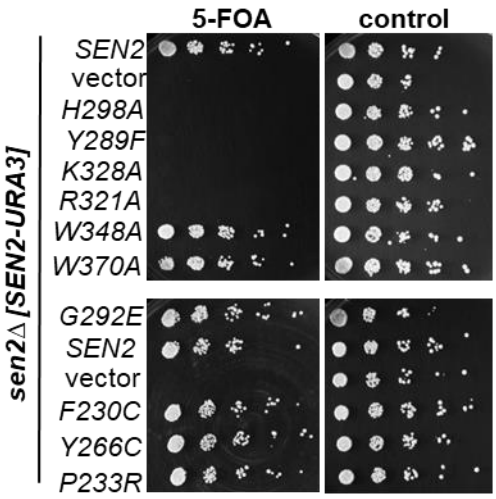

Figure 7.1: Mutations in *SEN2* can cause growth defects.

Growth assay of plasmid shuffle with *sen2*Δ yeast transformed with *SEN2-URA3* plasmid and mutant plasmids on a *LEU2*-vector. The *SEN2-URA3* plasmid was selected against on 5-FOA to reveal the growth defect caused by the mutant *LEU* plasmids. The mutations were selected based on proposed function or homologous PCH mutations (Table 7.1). The yeast were grown at 30 °C for 3 days and imaged. The image shown is representative of two replicates.

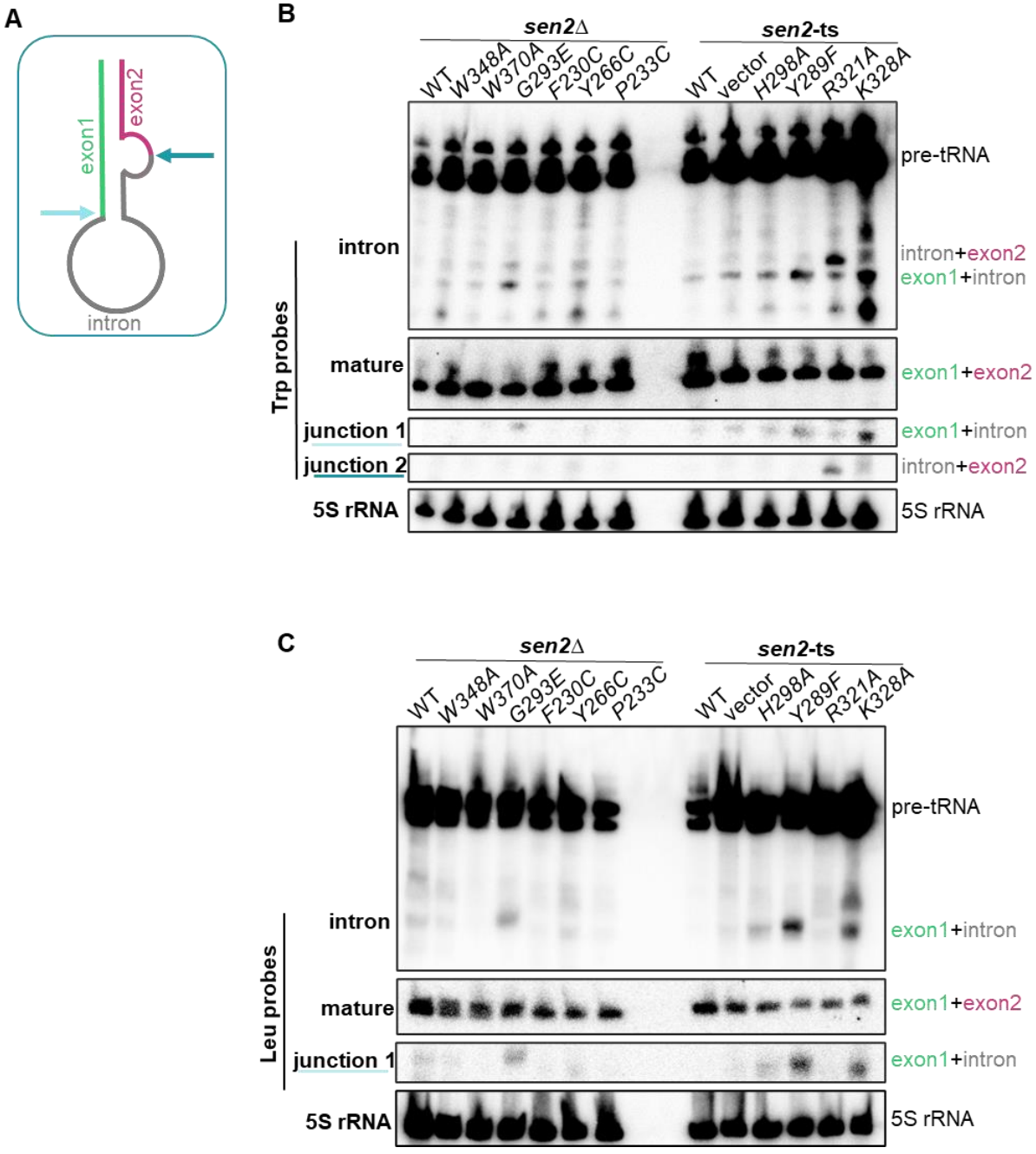
A
exon1
exon2
intron
B
sen2Δ
sen2-ts
WT
W348A
W370A
G293E
F230C
Y266C
P233C
WT
vector
H298A
Y289F
R321A
K328A
pre-tRNA
intron
intron+exon2
exon1+intron
Trp probes
mature
exon1+exon2
junction 1
exon1+intron
junction 2
intron+exon2
5S rRNA
5S rRNA
C
sen2Δ
sen2-ts
WT
W348A
W370A
G293E
F230C
Y266C
P233C
WT
vector
H298A
Y289F
R321A
K328A
pre-tRNA
intron
exon1+intron
Leu probes
mature
exon1+exon2
junction 1
exon1+intron
5S rRNA
5S rRNA

Figure 7.2: Residues of SEN2 are important for both 5' and 3' cleavage of tRNAs.

A). Schematic of the exon-intron junctions of pre-tRNAs. The arrows point to the 5' and 3' cleavage sites. Polyacrylamide Northern blot analysis of B). tryptophan pre-tRNA W(UUG) and C). leucine pre-tRNA L(CAA) with probes spanning the indicated region (left side) of the tRNA. See Table 2.3 for sequences. The tRNA species are labeled on the left and color coordinated to the introns and exons in the schematic. The mutant plasmids were expressed in a *sen2*Δ background if the mutation was not lethal (Figure 7.1) or a *sen2-ts* background for lethal mutants. 5S rRNA was used as a loading control.

Table 7.1: Summary *sen2* mutations and their effect on growth (Figure 7.1) and tRNA processing (Figure 7.2).

mutation	feature	growth	exon1+ intron	intron+ exon2	full precursor	mature tRNA
W348A	stacking	alive	none	none	normal	normal
W370A	stacking	alive	none	none	normal	normal
G293E	no 5' cleave	alive	present	none	normal	normal
F230C	PCH	alive	none	none	normal	normal
Y266C	PCH	alive	none	none	normal	normal
P233C	PCH	alive	none	none	normal	normal
H298A	cat acid	dead	present	none	increased	reduced
Y289F	cat base	dead	present	none	increased	reduced
R321A	stacking	dead	present	only Trp	increased	reduced
K328A	transition stabilizer	dead	present	none	increased	reduced

Though the in vivo Sen2 mutagenesis data show the essentiality and overall tRNA processing effects of individual residues, how each residue contributes to TSEN function, RNA binding, and overall structure has not been determined. Why these residues are important would become easier to interpret by generating a cryo-EM structure of yeast TSEN. Two cryo-EM structures of human TSEN have been generated and all of the residues in the active sites are conserved between yeast and humans. Both these structures only have pre-tRNA Arg(TCT), which has a shorter intron (13-15 nucleotides), bound to the complex. As the tRNA cleavage data shows, generating structures with a variety of pre-tRNAs will likely change some interactions, revealing other important residues. The human structure fails to clearly resolve the TSEN2-5'splice site interaction suggesting this part of the complex is more flexible (Hayne et al., 2022a; Sekulovski et al., 2022). Though there are no known mRNA targets of human TSEN, the authors hypothesize this flexibility could be needed to accommodate binding of other substrates like mRNAs in the complex. Studying the TSEN structure with an mRNA, such as yeast *CBP1*, could help elucidate how TSEN cleavage and substrate recognition differs between mRNAs and tRNAs.

Another future direction includes determining substrates for human TSEN. TSEN is likely to be essential as no patients with two null alleles have been identified and short-term siRNA-mediated knock down of TSEN subunits led MCF7 cells to die. This essentiality limits the experimental approaches one can take for target identification. The RNAseq data from yeast *sen2-ts* revealed many indirect effects but not the direct targets. Likewise, RNAseq on human cells depleted of TSEN is unlikely to be informative. One possibility is to perform PARE in human cells, specifically neuronal cells. Identifying mRNA targets of human TSEN would be groundbreaking data, giving insight into RNA processing in neurons as well as the molecular pathology of PCH. This experiment poses some technical problems. XRN1 has been successfully knocked out/down in HEK cells which is expected to stabilize cytoplasmic

cleavage products (Gilbertson et al., 2018). However, the localization of human TSEN is still debated with newer data showing TSEN is localized to the cytoplasm while older data suggests TSEN is nuclear. Due to this conflict, both cytoplasmic XRN1 and nuclear XRN2 should be knocked down or depleted to ensure stabilization of TSEN cleavage products, regardless of where the complex is localized. The nuclear XRN2 is likely to be essential. Thus one gene XRN1 would need to be knocked out and two would need to be knocked down (XRN2 and a TSEN subunit) which is time consuming to both generate and confirm efficient depletion or knockdown of each gene. An alternative is to perform CLIP-seq with either TSEN2 or TSEN34 catalytic mutants to identify RNAs that are bound to the catalytic subunits of TSEN. Yet another possibility is to look for substrates that human TSEN can cleave in vitro. One approach would be to incubate total human RNA with and without purified human TSEN and the identify 5’ hydroxyl or 2’3’ cyclic phosphate ends in the TSEN treated sample that are absent in the mock treated sample. These suggested experiments would contribute to our understanding of the TSEN complex structure, function, and substrate specificity, endonuclease decay, and neuronal disease.

Chapter three defines a novel endonuclease decay pathway, TED, and emphasizes that endonucleases can significantly contribute to mRNA decay. I hope these studies have laid the groundwork for not only studying TSEN targets and functions, but for utilizing PARE and comPARE to identify novel endonucleases or targets and expand upon the role of these enzymes in mRNA cleavage and degradation. TED likely occurs in other organisms such as humans and could play some role in PCH. If my study were expanded into mammalian cell lines or even patient cells, the molecular consequences of TSEN mutations that drive the PCH phenotype could be uncovered. I hope that my study inspires others to look beyond tRNA as a cause for PCH and investigate other functions of TSEN and its effect on neuronal development and human disease.

Genetic analysis of TSEN functions

Despite identifying novel TSEN targets, PARE did not obviously clarify the other essential function of TSEN. Therefore in chapter 4, I switched from a high-throughput RNAseq approach to utilizing classical genetic yeast screens to define other functions of TSEN. The high-copy suppressor assay identified *SEN54* as a suppressor of *sen2-ts,* and I further showed this overexpression only suppressed the *ts* allele, not a full deletion nor catalytic mutant. This led to the hypothesis that *SEN54* overexpression stabilizes *sen2-ts,* which is supported by previous literature that suggests these two subunits form a dimer within the full TSEN tetramer. This hypothesis was further supported by human TSEN subunit levels as when TSEN54 was knocked down in MCF7 cells, the protein levels of TSEN2 also decreased. This also seemed to be true for the reverse; when SEN2 was knocked down the levels of SEN54 also decreased. The protein levels of TSEN34 are unaffected by TSEN54 knockdown suggesting this phenomenon is specific to the dimer partners. Many PCH mutations are thought to destabilize the mutated protein (Hayne et al., 2022a; Sekulovski et al., 2022). It would be interesting to test whether overexpressing another subunit could stabilize the complex, analogous to the high copy suppression I found. I speculate that TSEN54 overexpression may stabilize TSEN2 and vice versa and that TSEN15 overexpression may stabilize TSEN34 and vice versa. I would like to test whether temperature sensitive alleles of yeast *SEN15, SEN34,* and *SEN54* can be suppressed by overexpressing another subunit but temperature sensitive alleles have not been reported for these three subunits.

My spontaneous suppressor analysis found mutations in Dbr1, the lariat debranching enzyme, suppressed a *sen2-ts* mutation. Like *SEN54* overexpression, this was only true for the *ts* mutant and not the catalytic dead nor the full deletion of *SEN2*. The fact that some TSEN must be active and the loss of *dbr1* catalytic activity was necessary for this suppression led us to believe that they may compete for a common substrate. In further support of this

hypothesis, I found that overexpression of *DBR1* in *sen2-ts* yeast causes a more severe growth defect at intermediate temperatures. This suggests an increase in Dbr1 sequesters more of the shared substrate, inhibiting TSEN from performing an essential function. We also considered that Dbr1 could be producing a toxic product from the shared substrate, but if this were the case, the suppression of the *dbr1*Δ would have occurred with the *sen2-cat* and *sen2*Δ*.* Using RNAseq, I identified that the Gcn4 response is activated in the *sen2-ts* mutant and closer to wildtype levels in the *sen2-ts dbr1*Δ mutant. A growth assay with *sen2-ts* and *gcn4*Δ double mutants showed that the increased Gcn4 response in the *sen2-ts* mutant was not killing the cells but was actually protective. These data suggest the Gcn4 response is activated because of a defect in the other essential function of TSEN and the response is decreased in the *sen2-ts dbr1*Δ mutant because TSEN can perform more of its essential function when Dbr1 is absent or inactivated and no longer competing for substrate.

Of course, many questions remain about the essential function of TSEN, primarily, what it is. I propose that identifying common substrates between Dbr1 and TSEN using RIP-seq or CRAC, in which RNA bound to enzymes is pulled down and sequenced, would further resolve the other essential function of TSEN. In some archaea, the TSEN homolog EndA cleaves pre-rRNAs that form stem loop structures to produce the 16S and 23S rRNAs (Schwarz et al., 2020). Additionally, one study suggested TSEN may play a role in yeast rRNA processing, though maybe only indirectly (Dhungel and Hopper, 2012). I tried to replicate these yeast results but was unable to find differences in rRNA processing in *sen2-ts* mutants. Still, this is an avenue that deserves further exploration.

Future directions for this research should focus on human TSEN. I would like to confirm these yeast data in human cells starting with determining if human TSEN even has another essential function. This could be addressed by recreating the Hesselberth yeast tRNA processing bypass experiment in human cells (Cherry et al., 2018). Cells would be transfected

with intronless tRNA genes and then subjected to knockdown or depletion of TSEN or the human ligase RtcB. If the bypass is successful, tRNA processing should no longer be essential and the cells should survive without RtcB. If TSEN has another essential function, knockdown of TSEN even with successful tRNA processing bypass would still be lethal. Interestingly, it has been shown that introducing intronless tRNA genes can bypass the essentiality of tRNA ligase in trypanosomes (Lopes et al., 2016), but similar results have not been reported for TSEN.

Though DBR1 is likely essential in mice (Zhang et al., 2018; Zheng et al., 2015), it may be interesting to knockdown both TSEN and DBR1 to see if loss of both proteins improves the phenotype. Loss of DBR1 has already been found to suppress one neuronal disease. In ALS, TDP-43 mutants form aggregates but loss of DBR1 catalytic activity suppresses this phenotype (Armakola et al., 2012). The TDP-43 aggregates are sequestered by the lariat introns, preventing mutant TDP-43 from interfering with vital cellular functions. When performing cell culture analysis with siRNA, I found knockdown of TSEN2, 34, and 54 with at least one of the two tested siRNAs resulted in a growth defect. Knocking down both TSEN and DBR1 either with siRNA or degron-depletion would show if the interaction between the two enzymes found in yeast is conserved in humans. Finally, because the Gcn4 response is activated in *sen2-ts* mutants the same could be true in PCH patients. Measuring activation of the homologous human Gnc4 response, the integrated stress response, in mammalian cell lines with PCH mutations or even patient cells could elucidate some of the molecular mechanisms of PCH. These experiments will further our understanding of TSEN function in yeast and humans and further define the connection between RNA processing and neuronal disease.

Overall, the work presented in chapter 4 positions the field closer to finding the other essential function of TSEN. I hypothesize that Dbr1 and TSEN share a common substrate

which specifies a future avenue to explore the other essential function of the complex. I also found that the Gcn4 response is activated by a lack of the other essential function of TSEN and provides protection in the mutant cells. One way to characterize the essential function of TSEN is to determine how *GCN4* translation is activated. The canonical pathway is that Gcn2 phosphorylates eIF2α (Hinnebusch, 2005; Masson, 2019). It would be interesting to test if eIF2α is phosphorylated and if Gcn2 is required for Gcn4 response activation in the *sen2-ts* mutant. If Gcn2 does phosphorylate eIf2α in *sen2-ts* mutants, Gcn2 activation mechanisms become more interesting and lead to more questions including whether Gcn1 and Gcn20 (Hinnebusch, 2005; Masson, 2019) are required for Gcn4 activation in *sen2-ts.*

If the integrated stress response is also activated in PCH, this could explain some of the symptoms that occur in the condition and suggest possible treatments to reduce symptoms. The data generated in chapter four could not only lead to further understanding of the mechanisms and symptoms of PCH, but also guide therapeutic development. I hope that these data lead to further understanding of the TSEN complex and lay a foundation for future PCH research.

Dxo1 is a distributive exonuclease; 'nibbling' both mRNA and rRNA

After finding new targets of TSEN and characterizing the TED pathway, I wanted to know what enzymes function downstream of TSEN after mRNA cleavage to degrade these TED targets in *S. cerevisiae*. One candidate that could degrade the 5' hydroxyl resulting from TSEN cleavage is Dxo1. In humans, its homolog DXO can process 5' hydroxyls to the XRN1 preferred 5' phosphates by removing two nucleotides from the end of the RNA (Doamekpor et al., 2020a). By examining the sequence similarity of Dxo1 and other Rai1/DXO/Dxo1 enzymes across species, I found that *S. cerevisiae* Dxo1 differs from nuclear Rai1 in that Dxo1 has more exonuclease than decapping activity. Rai1 also interacts with Rat1 to aid the

major nuclear 5' to 3' exonuclease, but Dxo1 has lost these residues making it unlikely to interact with Rat1 or Xrn1. Based on these observations, I suspected Dxo1 as a cytoplasmic exonuclease. I used PARE to investigate possible targets of Dxo1 and determine if Dxo1 degrades endonuclease cleavage products. In previous PARE data, many of the endonuclease and decapping peaks were clustered together but when Dxo1 was deleted, these clusters sharpened into one defined peak. This led me to the conclusion that Dxo1 functions downstream of endonuclease and decapping enzymes as a distributive exonuclease, 'nibbling' a few bases off the ends of some products. In *xrn1*Δ PARE, *CBP1* has three major peaks corresponding to three TSEN cleavage sites, but in the *xrn1*Δ*dxo1*Δ data, only two cleavage sites are observed. This corroborates in vitro data that shows that TSEN only cleaves *CBP1* in two places. I also found that Dxo1 trims the 25S' rRNA to the 25S. The enzyme that performs this step in *S. cerevisiae* was never identified but was always thought to be nuclear. Not only do these data identify the responsible enzyme but also suggest that this step occurs in the cytoplasm. Finally, I made the unexpected observation that *dxo1*Δ partially suppresses an *xrn1*Δ growth defect. The reason for this suppression is unclear but I speculate that in the absence of Xrn1, Dxo1 interferes with the degradation of RNAs by more efficient processive exonucleases.

The role of Dxo1 in *S. cerevisiae* rRNA processing is a novel function for the Rai1/DXO/Dxo1 family of enzymes. I wondered if this activity is conserved in other organisms. To investigate if DXO processes human rRNA, I performed PARE on DXO knockout HEK cells, kindly provided by Mike Kiledjian (Rutgers University). The data showed that DXO does not participate in 28S rRNA processing nor affect processing of any other rRNA in human cells. This was not an unexpected result as human DXO is primarily nuclear and the active site looks quite different from that of Dxo1. When examining the rest of the transcriptome, I found many hits in the DXO PARE dataset with most peaks being in intergenic or intronic

regions. In the future, these data along with more replicates, could be used to find novel functions of human DXO.

Next, I examined an organism that is evolutionarily closer to *S. cerevisiae*, *S. pombe*. Like humans, *S. pombe* has only one family member in the Rai1DXO/Dxo1 family, Din1 (also called Rai1). We performed PARE on *din1*∆ and wildtype *S. pombe* strains (provided by Ke Zhang Reid at Wake Forest University) to assess if Din1 processes rRNA like *S. cerevisiae* Dxo1. Like human DXO, Din1 does not process rRNA in *S. pombe*. So how and when did this function evolve? To investigate this, I plan on assessing the ability of different Rai1/Dxo1 family members across budding yeast species to process 25S rRNA. *S. cerevisiae* Rai1 and Dxo1 are homologs resulting from a gene duplication leading us to two theories. Either the Rai1/Dxo1 single gene ancestor could perform the functions of both Rai1 and Dxo1 and the duplication resulted in sub-functionalization, or the duplication resulted in Dxo1 taking on a completely novel function in rRNA processing (neo-functionalization). I will test the rRNA processing ability of both Rai1 and Dxo1 from *K. lactis* as the enzymes from this species seem to have resulted from the same gene duplication. I also plan on testing *C. albicans* which also has both Rai1 and Dxo1 enzymes. This duplication appears to be a different event from that which resulted in *S. cerevisiae*/*K. lactis* Rai1/Dxo1 duplication. Lastly, I will test relatives of *C. albicans* and *S. cerevisiae* with only one Rai1/Dxo1 family member, *C. auris* and *W. ciferrii,* respectively. Characterizing Rai1/Dxo1 family members across these species will reveal if the rRNA processing function of Dxo1 is a new role following duplication or if duplication of a bifunctional gene resulted in Dxo1 and Rai1 specializing in their respective functions and losing the other function. As for assessing the role of *S. cerevisiae* Dxo1 in endonuclease mediated decay, one important experiment would be to determine if Dxo1 can process 5’ hydroxyls, as well as to study the kinetics of Dxo1 on different types of 5’ ends. Studying the interaction between Xrn1 and Dxo1 and the mechanism behind the partial suppression of

*dxo1*Δ on the *xrn1*Δ growth could lead to the discovery of other exonucleases or RNA decay mechanisms. Together these experiments will help elucidate the evolution and functions of Dxo1/Rai1/DXO functions.

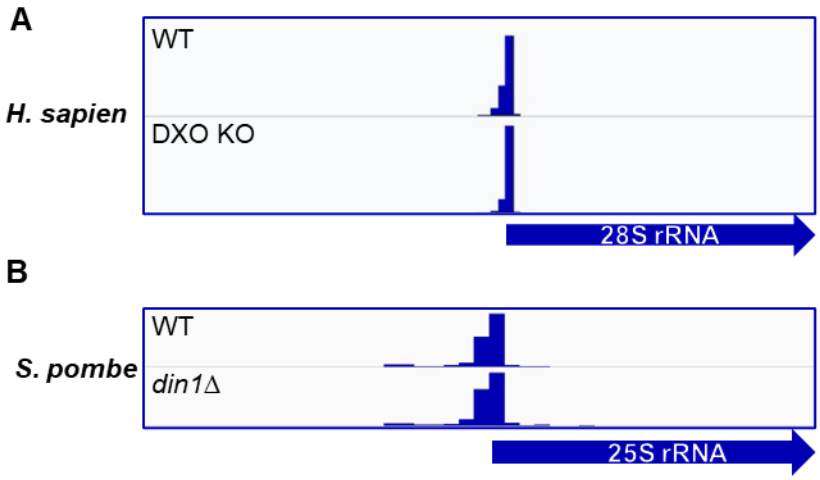

Figure 7.3: Human and *S. pombe* Rai1/DXO enzymes do not process the 28S/25S rRNA. PARE data of A). wildtype and DXO knockout HEK 293T cells and B). wildtype and *din1*Δ *S. pombe* cells. Reads are mapped to the rDNA locus of the organism with the peaks corresponding to sites in the transcriptome with 5' phosphates.

This research elucidated novel roles of *S. cerevisiae* Dxo1 as an exonuclease. Dxo1 can 'nibble' on many transcripts downstream of decapping and endonuclease cleavage explaining the clustering of peaks observed in previous PARE data. To identify endonuclease cleavage sites more precisely, it may be better to conduct PARE in a *xrn1*Δ *dxo1*Δ background instead of a *xrn1*Δ mutant. The *xrn1*Δ *dxo1*Δ also has the added benefit of faster growth than the *xrn1*Δ. Whether this 'nibbling' has a purpose or only occurs in the absence of Xrn1 is unknown. The major role of Dxo1 is in processing the abundant 25S rRNA. Rat1 processes the 26S to 25S' RNA in the nucleus and I have now shown that the 25S' rRNA is then passed to Dxo1 in the cytoplasm to trim the intermediate to the 25S rRNA. I hope that future endeavors elucidate how this rRNA processing function evolved and provide insight into the overall evolution of RNA processing.

Trl1 acts downstream of endonucleases; new evidence for RIDD in *S. cerevisiae*

Another enzyme that could participate in TED and other endonuclease decay pathways is Trl1. Trl1 acts on both mRNA and tRNA downstream of endonuclease cleavage (Abelson et al., 1998; Sidrauski et al., 1996). We hypothesized Trl1 phosphorylates the 5' hydroxyl resulting from endonuclease cleavage which allows Xrn1 to degrade the cleavage product. Using PARE, I identified several novel targets of Trl1 kinase including the TED targets *CBP1* and *COQ5*. This suggests Trl1 participates in the TED pathway by phosphorylating the cleavage product before degradation by Xrn1. We found that although both Trl1 and the exonuclease Dxo1 can act on *CBP1* cleavage products, neither enzyme is required for degradation of the 3' *CBP1* product by Xrn1. The PARE data also suggest that Trl1 is the only kinase that acts on the 3' *CBP1* cleavage product. I propose that Xrn1 itself may be able to slowly remove the 5' hydroxyl, bypassing the need for an intermediate step in the absence of Trl1 phosphorylation. Characterizing the kinetics of Xrn1 in vitro, specifically its activity on endonuclease products with 5' hydroxyls would test this hypothesis. The observation from

Catherine Stuart in our lab that Trl1 is required to degrade the 5' hydroxylated RNA resulting from hammerhead-ribozyme cleavage suggests that this Xrn1 activity may be sequence or structure dependent, which should also be investigated in vitro.

I also identified *NPL4* as a target of Trl1. Because Npl4 is involved in the ER and stress response (Hitchcock et al., 2001), I hypothesized that this transcript is cleaved by the endonuclease Ire1 upstream of Trl1 phosphorylation. I performed PARE to determine if *NPL4* and other transcripts phosphorylated by Trl1 are also targets of Ire1. The data showed that *NPL4* is cleaved by Ire1 at the same site as Trl1 phosphorylation. *NPL4* does not have any introns leading me to hypothesize that Ire1 and Trl1 act in the degradation of this transcript. This could be the first in vivo evidence of RIDD in *S. cerevisiae*. Unfortunately, the Ire1 data were complicated by many transcriptome wide changes that occurred with the deletion of Ire1, hindering efforts to identify genuine direct cleavage sites. Therefore, I could only identify shared Trl1 and Ire1 targets including *NPL4* which I propose could be an example of RIDD.

The results of this chapter are preliminary. The Trl1 targets I proposed need to be confirmed using low-throughput or in vitro methods. Some of the Trl1 targets identified are not known endonuclease targets. What occurs upstream of Trl1 phosphorylation, such as cleavage by potentially novel endonucleases, should be investigated. Candidate endonucleases that leave a 5' OH in addition to TSEN and Ire1 include Las1, Rny1, and Cue2 and its paralog Ypl199c. Of these Las1 and Rny1 are largely nuclear and vacuolar, respectively, and thus appear less likely to be in the same pathway as Trl1 (MacIntosh et al., 2001; Schillewaert et al., 2012). Cue2 and Trl1 have both been implicated in no-go decay, but the targets I highlighted above have not been identified as no-go substrates (D'Orazio et al., 2019; Navickas et al., 2020). Nonetheless, PARE on a *cue2*Δ *ypl199c*Δ mutant might identify some Trl1 targets as no-go substrates. To further investigate Ire1 targets and hopefully identify more vivo examples of RIDD, I plan to redo these experiments in a *hac1*Δ deletion or *hac1-*

intronless background. This will hopefully negate the transcriptome wide changes resulting from the deletion of Ire1, as I think most of the confounding signal was due to the downstream effects of the Hac1 transcription factor. To determine the fate of these transcripts after endonuclease cleavage and Trl1 phosphorylation, I could look at the sites in an *XRN1* background. If these peaks are not present in this data, the cleavage products are likely degraded by Xrn1. If the cleavage products are degraded like those in the TED pathway, this would further support the idea of RIDD in *S. cerevisiae* as well as the existence of novel endonuclease decay pathways. To confirm that Ire1 has Hac1 independent functions it would also be informative to perform RNAseq on *hac1*Δ and *hac1*Δ*ire1*Δ strains.

Though in the early stages, these data may have identified at least one in vivo example of RIDD in *S. cerevisiae*. In vitro characterization of *S. cerevisiae* RIDD has been attempted in the past but in vivo research has failed to replicate these targets. This chapter also expanded the known role and targets of Trl1. Not only does Trl1 function as a kinase in the heal-and seal-ligation pathway but also acts downstream of endonucleases contributing to degradation of the 3' product. We hope that this generates further interest in endonuclease decay pathways such as TED and RIDD. in *S. cerevisiae* and other organisms.

Overall implications TSEN function and endonuclease decay pathways

In this thesis, I strived to elucidate the other essential role of TSEN, define novel targets of TSEN, and investigate the mechanisms involved in endonuclease decay. I found TSEN is involved in a novel decay pathway, termed TED (Figure 7.4). After TSEN cleavage, these TED targets are processed by Dxo1 and Trl1 though neither of these enzymes are essential for degradation of the 3' cleavage product by Xrn1. We also investigated the existence of the RIDD endonuclease decay pathway in *S. cerevisiae* and defined possible targets of Ire1 cleavage that are then phosphorylated by Trl1. Though it is unclear if TED is

an essential function of TSEN, I found Dbr1 and TSEN likely compete for some RNA substrate and cleavage of this RNA by TSEN is essential (Figure 7.4).

In the future, research should be conducted on the interaction between Dbr1 and TSEN to identify their common substrate and discover the other essential function of TSEN. It is still unknown if human TSEN also has another essential function or if the functions identified in yeast are conserved in humans. The structure of the human complex suggests that the RNA binding pocket around TSEN2 is flexible and could allow targets other than tRNA, supporting the idea that human TSEN likely has other functions. In addition to investigating other functions, more research is needed to determine where human TSEN is localized as the current evidence is mixed. Investigating the roles TSEN may help elucidate how mutations in TSEN cause PCH and eventually lead to some answers or at least hope for patients.

Work in this thesis also suggests RIDD may occur in *S. cerevisiae* though this requires further investigation before any conclusions can be definitively made. In addition to TED and RIDD it would be interesting to explore what other endonucleases play a role in mRNA decay. Another area of research is determining what happens to these cleavage products after endonuclease cleavage and the steps involved in their degradation. We found *S. cerevisiae* Dxo1 processes the 25S rRNA (Figure 7.4) and this could be relatively specific to budding yeast as neither the humans DXO nor *S. pombe* Din1 perform a similar function. Researching this family of enzymes in other organisms will give insight into how the rRNA processing function of Dxo1 evolved and lead to further understanding of the evolution of RNA processing pathways.

Though I failed to identify the other essential function of TSEN, the data generated in this thesis offers a novel starting point to TSEN function discovery. I have defined a novel endonuclease decay pathway and clarified routes through which these targets are degraded

downstream of endonuclease cleavage. In addition, I have defined methods for generating and analyzing novel endonuclease targets. Overall, this thesis demonstrates RNA processing enzymes can have multiple roles, including endonuclease-mediated decay, a complex process that contributes significantly to mRNA decay.

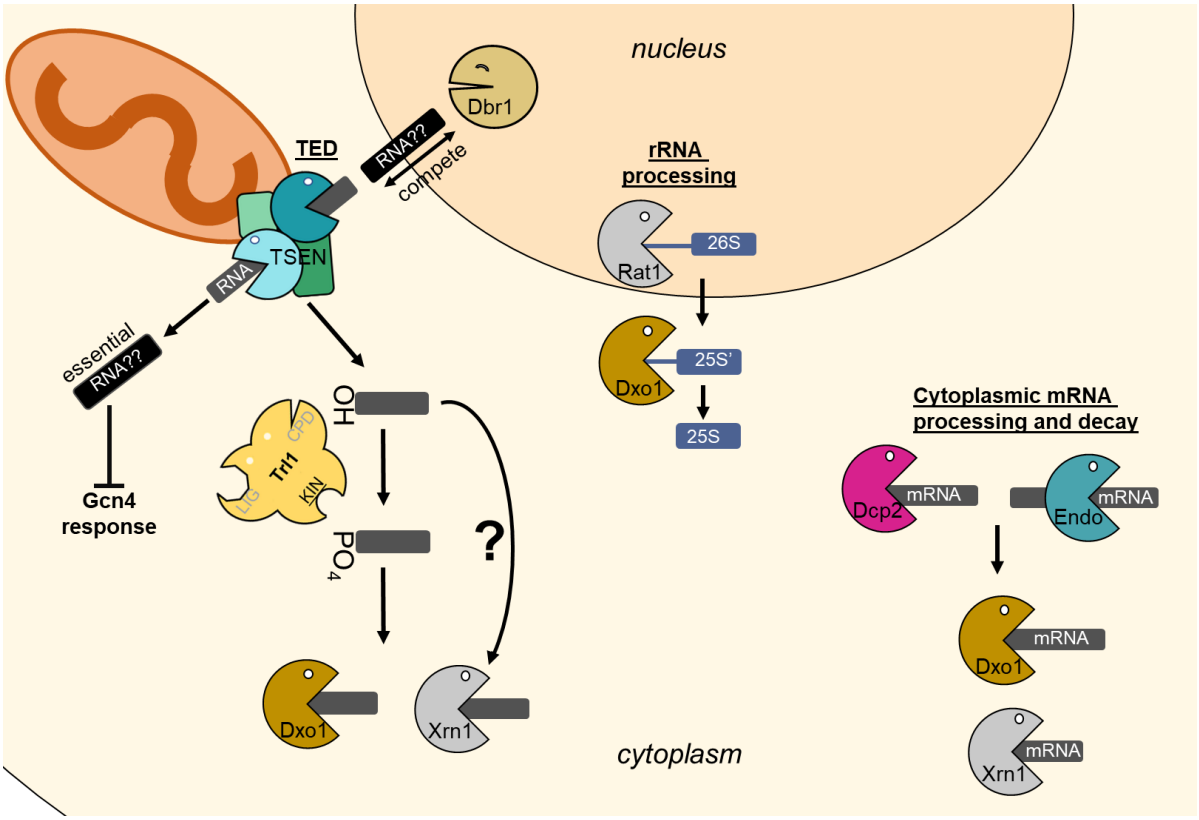

Figure 7.4: Functions of the TSEN complex and other adventures in RNA processing.

TSEN cleaves mRNAs within the cytoplasm to initiate RNA decay in a process we termed TED. In addition to this novel function, we also found evidence that Dbr1 and TSEN compete for a common substrate. If TSEN fails to produce this product, the Gcn4 response is activated. After TSEN cleavage, a product with a 5' hydroxyl is produced that can be phosphorylated by Trl1, though this is not necessary for degradation by Xrn1. These phosphorylated TED products along with other mRNA cleavage products with 5' phosphates can be processed by the exonuclease Dxo1. Dxo1 can 'nibble' a few bases from these 5' phosphate ends, though the biological implications of this function are unknown. The main function of Dxo1 is processing the 5' end of the 25S' rRNA to the 25S rRNA in the cytoplasm.

8) References

Abelson, J., Trotta, C.R., Li, H., 1998. tRNA splicing. J. Biol. Chem. 273, 12685–12688.

Addo-Quaye, C., Eshoo, T.W., Bartel, D.P., Axtell, M.J., 2008. Endogenous siRNA and miRNA targets identified by sequencing of the Arabidopsis degradome. Curr. Biol. CB 18, 758–762. https://doi.org/10.1016/j.cub.2008.04.042

Akiyama, Y., Lyons, S.M., Abe, T., Anderson, P.J., Ivanov, P., 2022. Cytoplasmic processing of human transfer RNAs. https://doi.org/10.1101/2022.04.28.489951

Allmang, C., Kufel, J., Chanfreau, G., Mitchell, P., Petfalski, E., Tollervey, D., 1999a. Functions of the exosome in rRNA, snoRNA and snRNA synthesis. EMBO J. 18, 5399–5410. https://doi.org/10.1093/emboj/18.19.5399

Allmang, C., Petfalski, E., Podtelejnikov, A., Mann, M., Tollervey, D., Mitchell, P., 1999b. The yeast exosome and human PM–Scl are related complexes of 3′ → 5′ exonucleases. Genes Dev. 13, 2148–2158.

Amberg, D.C., Burke, D.J., Strathern, J.N., 2006. Assay of β-Galactosidase in Yeast: Permeabilized Cell Assay. Cold Spring Harb. Protoc. 2006, pdb.prot4158. https://doi.org/10.1101/pdb.prot4158

Anderson, J.S., Parker, R.P., 1998. The 3’ to 5’ degradation of yeast mRNAs is a general mechanism for mRNA turnover that requires the SKI2 DEVH box protein and 3’ to 5’ exonucleases of the exosome complex. EMBO J. 17, 1497–1506. https://doi.org/10.1093/emboj/17.5.1497

Armakola, M., Higgins, M.J., Figley, M.D., Barmada, S.J., Scarborough, E.A., Diaz, Z., Fang, X., Shorter, J., Krogan, N.J., Finkbeiner, S., Farese, R.V., Gitler, A.D., 2012. Inhibition of RNA lariat debranching enzyme suppresses TDP-43 toxicity in ALS disease models. Nat. Genet. 44, 1302–1309. https://doi.org/10.1038/ng.2434

Arribere, J.A., Gilbert, W.V., 2013. Roles for transcript leaders in translation and mRNA decay revealed by transcript leader sequencing. Genome Res. 23, 977–987. https://doi.org/10.1101/gr.150342.112

Bailey, A.D., Talkish, J., Ding, H., Igel, H., Duran, A., Mantripragada, S., Paten, B., Ares, M., 2022. Concerted modification of nucleotides at functional centers of the ribosome revealed by single-molecule RNA modification profiling. eLife 11, e76562. https://doi.org/10.7554/eLife.76562

Baldi, M.I., Mattoccia, E., Bufardeci, E., Fabbri, S., Tocchini-Valentini, G.P., 1992. Participation of the intron in the reaction catalyzed by the Xenopus tRNA splicing endonuclease. Science 255, 1404–1408.

Battini, R., D'Arrigo, S., Cassandrini, D., Guzzetta, A., Fiorillo, C., Pantaleoni, C., Romano, A., Alfei, E., Cioni, G., Santorelli, F.M., 2014. Novel mutations in TSEN54 in pontocerebellar hypoplasia type 2. J. Child Neurol. 29, 520–525. https://doi.org/10.1177/0883073812470002

Ben-Aroya, S., Coombes, C., Kwok, T., O'Donnell, K.A., Boeke, J.D., Hieter, P., 2008. Toward a Comprehensive Temperature-Sensitive Mutant Repository of the Essential Genes of Saccharomyces cerevisiae. Mol. Cell 30, 248–258. https://doi.org/10.1016/j.molcel.2008.02.021

Bierhals, T., Korenke, G.C., Uyanik, G., Kutsche, K., 2013. Pontocerebellar hypoplasia type 2 and TSEN2: review of the literature and two novel mutations. Eur. J. Med. Genet. 56, 325–330. https://doi.org/10.1016/j.ejmg.2013.03.009

Bizzari, S., Hamzeh, A.R., Mohamed, M., Al-Ali, M.T., Bastaki, F., 2019. Expanded PCH1D phenotype linked to EXOSC9 mutation. Eur. J. Med. Genet. https://doi.org/10.1016/j.ejmg.2019.01.012

Boczonadi, V., Müller, J.S., Pyle, A., Munkley, J., Dor, T., Quartararo, J., Ferrero, I., Karcagi, V., Giunta, M., Polvikoski, T., Birchall, D., Princzinger, A., Cinnamon, Y.,

Lützkendorf, S., Piko, H., Reza, M., Florez, L., Santibanez-Koref, M., Griffin, H., Schuelke, M., Elpeleg, O., Kalaydjieva, L., Lochmüller, H., Elliott, D.J., Chinnery, P.F., Edvardson, S., Horvath, R., 2014. EXOSC8 mutations alter mRNA metabolism and cause hypomyelination with spinal muscular atrophy and cerebellar hypoplasia. Nat. Commun. 5, 4287. https://doi.org/10.1038/ncomms5287

Breuss, M.W., Sultan, T., James, K.N., Rosti, R.O., Scott, E., Musaev, D., Furia, B., Reis, A., Sticht, H., Al-Owain, M., Alkuraya, F.S., Reuter, M.S., Abou Jamra, R., Trotta, C.R., Gleeson, J.G., 2016. Autosomal-Recessive Mutations in the tRNA Splicing Endonuclease Subunit TSEN15 Cause Pontocerebellar Hypoplasia and Progressive Microcephaly. Am. J. Hum. Genet. 99, 228–235. https://doi.org/10.1016/j.ajhg.2016.05.023

Briggs, M.W., Burkard, K.T., Butler, J.S., 1998. Rrp6p, the yeast homologue of the human PM-Scl 100-kDa autoantigen, is essential for efficient 5.8 S rRNA 3' end formation. J. Biol. Chem. 273, 13255–13263. https://doi.org/10.1074/jbc.273.21.13255

Budde, B.S., Namavar, Y., Barth, P.G., Poll-The, B.T., Nürnberg, G., Becker, C., Ruissen, F. van, Weterman, M.A.J., Fluiter, K., Beek, E.T. te, Aronica, E., Knaap, M.S. van der, Höhne, W., Toliat, M.R., Crow, Y.J., Steinlin, M., Voit, T., Roelens, F., Brussel, W., Brockmann, K., Kyllerman, M., Boltshauser, E., Hammersen, G., Willemsen, M., Basel-Vanagaite, L., Krägeloh-Mann, I., Vries, L.S. de, Sztriha, L., Muntoni, F., Ferrie, C.D., Battini, R., Hennekam, R.C.M., Grillo, E., Beemer, F.A., Stoets, L.M.E., Wollnik, B., Nürnberg, P., Baas, F., 2008. tRNA splicing endonuclease mutations cause pontocerebellar hypoplasia. Nat. Genet. 40, 1113–1118. https://doi.org/10.1038/ng.204

Bufardeci, E., Fabbri, S., Baldi, M.I., Mattoccia, E., Tocchini-Valentini, G.P., 1993. In vitro genetic analysis of the structural features of the pre-tRNA required for determination of the 3' splice site in the intron excision reaction. EMBO J. 12, 4697–4704.

Burns, D.T., Donkervoort, S., Müller, J.S., Knierim, E., Bharucha-Goebel, D., Faqeih, E.A., Bell, S.K., AlFaifi, A.Y., Monies, D., Millan, F., Retterer, K., Dyack, S., MacKay, S., Morales-Gonzalez, S., Giunta, M., Munro, B., Hudson, G., Scavina, M., Baker, L., Massini, T.C., Lek, M., Hu, Y., Ezzo, D., AlKuraya, F.S., Kang, P.B., Griffin, H., Foley, A.R., Schuelke, M., Horvath, R., Bönnemann, C.G., 2018. Variants in EXOSC9 Disrupt the RNA Exosome and Result in Cerebellar Atrophy with Spinal Motor Neuronopathy. Am. J. Hum. Genet. 102, 858–873. https://doi.org/10.1016/j.ajhg.2018.03.011

Calvin, K., Li, H., 2008. RNA-splicing endonuclease structure and function. Cell. Mol. Life Sci. 65, 1176–1185. https://doi.org/10.1007/s00018-008-7393-y

Cassandrini, D., Biancheri, R., Tessa, A., Di Rocco, M., Di Capua, M., Bruno, C., Denora, P.S., Sartori, S., Rossi, A., Nozza, P., Emma, F., Mezzano, P., Politi, M.R., Laverda, A.M., Zara, F., Pavone, L., Simonati, A., Leuzzi, V., Santorelli, F.M., Bertini, E., 2010. Pontocerebellar hypoplasia: clinical, pathologic, and genetic studies. Neurology 75, 1459–1464. https://doi.org/10.1212/WNL.0b013e3181f88173

Chang, J.H., Jiao, X., Chiba, K., Oh, C., Martin, C.E., Kiledjian, M., Tong, L., 2012. Dxo1 is a novel eukaryotic enzyme with both decapping and 5′-3′ exoribonuclease activity. Nat. Struct. Mol. Biol. 19, 1011–1017. https://doi.org/10.1038/nsmb.2381

Chapman, K.B., Boeke, J.D., 1991. Isolation and characterization of the gene encoding yeast debranching enzyme. Cell 65, 483–492. https://doi.org/10.1016/0092-8674(91)90466-c

Chapman, R.E., Walter, P., 1997. Translational attenuation mediated by an mRNA intron. Curr. Biol. CB 7, 850–859. https://doi.org/10.1016/s0960-9822(06)00373-3

Chatterjee, K., Nostramo, R.T., Wan, Y., Hopper, A.K., 2018. tRNA dynamics between the nucleus, cytoplasm and mitochondrial surface: Location, location, location. Biochim.

Biophys. Acta Gene Regul. Mech. 1861, 373–386. https://doi.org/10.1016/j.bbagrm.2017.11.007

Chen, H., Li, N., Xu, Y., Li, G., Song, C., Yao, R.-E., Yu, T., Wang, J., Yang, L., 2022. Novel compound heterozygous variant of TOE1 results in a mild type of pontocerebellar hypoplasia type 7: an expansion of the clinical phenotype. Neurogenetics 23, 11–17. https://doi.org/10.1007/s10048-021-00675-0

Cherry, P.D., Peach, S.E., Hesselberth, J.R., 2019. Multiple decay events target HAC1 mRNA during splicing to regulate the unfolded protein response. eLife 8, e42262. https://doi.org/10.7554/eLife.42262

Cherry, P.D., White, L.K., York, K., Hesselberth, J.R., 2018. Genetic bypass of essential RNA repair enzymes in budding yeast. RNA N. Y. N 24, 313–323. https://doi.org/10.1261/rna.061788.117

Chlebowski, A., Lubas, M., Jensen, T.H., Dziembowski, A., 2013. RNA decay machines: The exosome. Biochim. Biophys. Acta BBA - Gene Regul. Mech., RNA Decay Mechanisms 1829, 552–560. https://doi.org/10.1016/j.bbagrm.2013.01.006

Coller, J., Parker, R., 2004. EUKARYOTIC mRNA DECAPPING. Annu. Rev. Biochem. 73, 861–890. https://doi.org/10.1146/annurev.biochem.73.011303.074032

Cox, J.S., Shamu, C.E., Walter, P., 1993. Transcriptional induction of genes encoding endoplasmic reticulum resident proteins requires a transmembrane protein kinase. Cell 73, 1197–1206. https://doi.org/10.1016/0092-8674(93)90648-a

Culver, G.M., McCraith, S.M., Consaul, S.A., Stanford, D.R., Phizicky, E.M., 1997. A 2'-phosphotransferase implicated in tRNA splicing is essential in Saccharomyces cerevisiae. J. Biol. Chem. 272, 13203–13210. https://doi.org/10.1074/jbc.272.20.13203

Delan-Forino, C., Schneider, C., Tollervey, D., 2017. Transcriptome-wide analysis of alternative routes for RNA substrates into the exosome complex. PLOS Genet. 13, e1006699. https://doi.org/10.1371/journal.pgen.1006699

Desai, K.K., Cheng, C.L., Bingman, C.A., Phillips, G.N., Raines, R.T., 2014. A tRNA splicing operon: Archease endows RtcB with dual GTP/ATP cofactor specificity and accelerates RNA ligation. Nucleic Acids Res. 42, 3931–3942. https://doi.org/10.1093/nar/gkt1375

Dhoondia, Z., Elewa, H., Malik, M., Arif, Z., Pique-Regi, R., Ansari, A., 2021. A termination-independent role of Rat1 in cotranscriptional splicing. Nucleic Acids Res. 49, 5520–5536. https://doi.org/10.1093/nar/gkab339

Dhungel, N., Hopper, A.K., 2012. Beyond tRNA cleavage: novel essential function for yeast tRNA splicing endonuclease unrelated to tRNA processing. Genes Dev. 26, 503–514. https://doi.org/10.1101/gad.183004.111

Doamekpor, S.K., Gozdek, A., Kwasnik, A., Kufel, J., Tong, L., 2020a. A novel 5′-hydroxyl dinucleotide hydrolase activity for the DXO/Rai1 family of enzymes. Nucleic Acids Res. 48, 349–358. https://doi.org/10.1093/nar/gkz1107

Doamekpor, S.K., Grudzien-Nogalska, E., Mlynarska-Cieslak, A., Kowalska, J., Kiledjian, M., Tong, L., 2020b. DXO/Rai1 enzymes remove 5′-end FAD and dephospho-CoA caps on RNAs. Nucleic Acids Res. 48, 6136–6148. https://doi.org/10.1093/nar/gkaa297

Dong, J., Qiu, H., Garcia-Barrio, M., Anderson, J., Hinnebusch, A.G., 2000. Uncharged tRNA Activates GCN2 by Displacing the Protein Kinase Moiety from a Bipartite tRNA-Binding Domain. Mol. Cell 6, 269–279. https://doi.org/10.1016/S1097-2765(00)00028-9

D'Orazio, K.N., Wu, C.C.-C., Sinha, N., Loll-Krippleber, R., Brown, G.W., Green, R., 2019. The endonuclease Cue2 cleaves mRNAs at stalled ribosomes during No Go Decay. eLife 8, e49117. https://doi.org/10.7554/eLife.49117

Dourlen, P., Bertin, B., Chatelain, G., Robin, M., Napoletano, F., Roux, M.J., Mollereau, B., 2012. Drosophila Fatty Acid Transport Protein Regulates Rhodopsin-1 Metabolism and Is Required for Photoreceptor Neuron Survival. PLOS Genet. 8, e1002833. https://doi.org/10.1371/journal.pgen.1002833

Dubreuil, B., Sass, E., Nadav, Y., Heidenreich, M., Georgeson, J.M., Weill, U., Duan, Y., Meurer, M., Schuldiner, M., Knop, M., Levy, E.D., 2019. YeastRGB: comparing the abundance and localization of yeast proteins across cells and libraries. Nucleic Acids Res. 47, D1245–D1249. https://doi.org/10.1093/nar/gky941

Dufey, E., Bravo-San Pedro, J.M., Eggers, C., González-Quiroz, M., Urra, H., Sagredo, A.I., Sepulveda, D., Pihán, P., Carreras-Sureda, A., Hazari, Y., Sagredo, E.A., Gutierrez, D., Valls, C., Papaioannou, A., Acosta-Alvear, D., Campos, G., Domingos, P.M., Pedeux, R., Chevet, E., Alvarez, A., Godoy, P., Walter, P., Glavic, A., Kroemer, G., Hetz, C., 2020. Genotoxic stress triggers the activation of IRE1α-dependent RNA decay to modulate the DNA damage response. Nat. Commun. 11, 2401. https://doi.org/10.1038/s41467-020-15694-y

Eberle, A.B., Lykke-Andersen, S., Mühlemann, O., Jensen, T.H., 2009. SMG6 promotes endonucleolytic cleavage of nonsense mRNA in human cells. Nat. Struct. Mol. Biol. 16, 49–55. https://doi.org/10.1038/nsmb.1530

Eliyahu, E., Pnueli, L., Melamed, D., Scherrer, T., Gerber, A.P., Pines, O., Rapaport, D., Arava, Y., 2010. Tom20 Mediates Localization of mRNAs to Mitochondria in a Translation-Dependent Manner. Mol. Cell. Biol. 30, 284–294. https://doi.org/10.1128/MCB.00651-09

Fabbri, S., Fruscoloni, P., Bufardeci, E., Di Nicola Negri, E., Baldi, M.I., Attardi, D.G., Mattoccia, E., Tocchini-Valentini, G.P., 1998. Conservation of substrate recognition mechanisms by tRNA splicing endonucleases. Science 280, 284–286.

Faber, A.W., Van Dijk, M., Raué, H.A., Vos, J.C., 2002. Ngl2p is a Ccr4p-like RNA nuclease essential for the final step in 3'-end processing of 5.8S rRNA in Saccharomyces cerevisiae. RNA N. Y. N 8, 1095–1101. https://doi.org/10.1017/s1355838202021027

Fatica, A., Oeffinger, M., Dlakić, M., Tollervey, D., 2003. Nob1p Is Required for Cleavage of the 3′ End of 18S rRNA. Mol. Cell. Biol. 23, 1798–1807. https://doi.org/10.1128/MCB.23.5.1798-1807.2003

Fatica, A., Tollervey, D., Dlakić, M., 2004. PIN domain of Nob1p is required for D-site cleavage in 20S pre-rRNA. RNA 10, 1698–1701. https://doi.org/10.1261/rna.7123504

Feddersen, A., Dedic, E., Poulsen, E.G., Schmid, M., Van, L.B., Jensen, T.H., Brodersen, D.E., 2012. Saccharomyces cerevisiae Ngl3p is an active 3'-5' exonuclease with a specificity towards poly-A RNA reminiscent of cellular deadenylases. Nucleic Acids Res. 40, 837–846. https://doi.org/10.1093/nar/gkr782

Frischmeyer, P.A., Hoof, A. van, O'Donnell, K., Guerrerio, A.L., Parker, R., Dietz, H.C., 2002. An mRNA Surveillance Mechanism That Eliminates Transcripts Lacking Termination Codons. Science 295, 2258–2261. https://doi.org/10.1126/science.1067338

Fromm, L., Falk, S., Flemming, D., Schuller, J.M., Thoms, M., Conti, E., Hurt, E., 2017. Reconstitution of the complete pathway of ITS2 processing at the pre-ribosome. Nat. Commun. 8, 1787. https://doi.org/10.1038/s41467-017-01786-9

Fruscoloni, P., Baldi, M.I., Tocchini-Valentini, G.P., 2001. Cleavage of non-tRNA substrates by eukaryal tRNA splicing endonucleases. EMBO Rep. 2, 217–221. https://doi.org/10.1093/embo-reports/kve040

Fujishima, K., Kanai, A., 2014. tRNA gene diversity in the three domains of life. Front. Genet. 5. https://doi.org/10.3389/fgene.2014.00142

Gadir, N., Haim-Vilmovsky, L., Kraut-Cohen, J., Gerst, J.E., 2011. Localization of mRNAs coding for mitochondrial proteins in the yeast Saccharomyces cerevisiae. RNA 17, 1551–1565. https://doi.org/10.1261/rna.2621111

Gaikwad, S., Ghobakhlou, F., Young, D.J., Visweswaraiah, J., Zhang, H., Hinnebusch, A.G., 2021. Reprogramming of translation in yeast cells impaired for ribosome recycling favors short, efficiently translated mRNAs. eLife 10, e64283. https://doi.org/10.7554/eLife.64283

Garneau, N.L., Wilusz, J., Wilusz, C.J., 2007. The highways and byways of mRNA decay. Nat. Rev. Mol. Cell Biol. 8, 113–126. https://doi.org/10.1038/nrm2104

Garrison, E., Marth, G., 2012. Haplotype-based variant detection from short-read sequencing. https://doi.org/10.48550/arXiv.1207.3907

Gasse, L., Flemming, D., Hurt, E., 2015. Coordinated Ribosomal ITS2 RNA Processing by the Las1 Complex Integrating Endonuclease, Polynucleotide Kinase, and Exonuclease Activities. Mol. Cell 60, 808–815. https://doi.org/10.1016/j.molcel.2015.10.021

Geerlings, T.H., Vos, J.C., Raué, H.A., 2000. The final step in the formation of 25S rRNA in Saccharomyces cerevisiae is performed by 5'-->3' exonucleases. RNA 6, 1698–1703.

German, M.A., Luo, S., Schroth, G., Meyers, B.C., Green, P.J., 2009. Construction of Parallel Analysis of RNA Ends (PARE) libraries for the study of cleaved miRNA targets and the RNA degradome. Nat. Protoc. 4, 356–362. https://doi.org/10.1038/nprot.2009.8

German, M.A., Pillay, M., Jeong, D.-H., Hetawal, A., Luo, S., Janardhanan, P., Kannan, V., Rymarquis, L.A., Nobuta, K., German, R., De Paoli, E., Lu, C., Schroth, G., Meyers, B.C., Green, P.J., 2008. Global identification of microRNA-target RNA pairs by

parallel analysis of RNA ends. Nat. Biotechnol. 26, 941–946. https://doi.org/10.1038/nbt1417

Getz, M.A., Weinberg, D.E., Drinnenberg, I.A., Fink, G.R., Bartel, D.P., 2020. Xrn1p acts at multiple steps in the budding-yeast RNAi pathway to enhance the efficiency of silencing. Nucleic Acids Res. 48, 7404–7420. https://doi.org/10.1093/nar/gkaa468

Giaever, G., Chu, A.M., Ni, L., Connelly, C., Riles, L., Véronneau, S., Dow, S., Lucau-Danila, A., Anderson, K., André, B., Arkin, A.P., Astromoff, A., El-Bakkoury, M., Bangham, R., Benito, R., Brachat, S., Campanaro, S., Curtiss, M., Davis, K., Deutschbauer, A., Entian, K.-D., Flaherty, P., Foury, F., Garfinkel, D.J., Gerstein, M., Gotte, D., Güldener, U., Hegemann, J.H., Hempel, S., Herman, Z., Jaramillo, D.F., Kelly, D.E., Kelly, S.L., Kötter, P., LaBonte, D., Lamb, D.C., Lan, N., Liang, H., Liao, H., Liu, L., Luo, C., Lussier, M., Mao, R., Menard, P., Ooi, S.L., Revuelta, J.L., Roberts, C.J., Rose, M., Ross-Macdonald, P., Scherens, B., Schimmack, G., Shafer, B., Shoemaker, D.D., Sookhai-Mahadeo, S., Storms, R.K., Strathern, J.N., Valle, G., Voet, M., Volckaert, G., Wang, C., Ward, T.R., Wilhelmy, J., Winzeler, E.A., Yang, Y., Yen, G., Youngman, E., Yu, K., Bussey, H., Boeke, J.D., Snyder, M., Philippsen, P., Davis, R.W., Johnston, M., 2002. Functional profiling of the Saccharomyces cerevisiae genome. Nature 418, 387–391. https://doi.org/10.1038/nature00935

Gietz, R.D., Schiestl, R.H., 2007. High-efficiency yeast transformation using the LiAc/SS carrier DNA/PEG method. Nat. Protoc. 2, 31–34. https://doi.org/10.1038/nprot.2007.13

Gilbertson, S., Federspiel, J.D., Hartenian, E., Cristea, I.M., Glaunsinger, B., 2018. Changes in mRNA abundance drive shuttling of RNA binding proteins, linking cytoplasmic RNA degradation to transcription. eLife 7, e37663. https://doi.org/10.7554/eLife.37663

Golani-Armon, A., Arava, Y., 2016. Localization of nuclear-encoded mRNAs to mitochondria outer surface. Biochem. Mosc. 81, 1038–1043. https://doi.org/10.1134/S0006297916100023

Goldstein, A.L., McCusker, J.H., 1999. Three new dominant drug resistance cassettes for gene disruption in Saccharomyces cerevisiae. Yeast Chichester Engl. 15, 1541–1553. https://doi.org/10.1002/(SICI)1097-0061(199910)15:14<1541::AID-YEA476>3.0.CO;2-K

Gonzalez, T.N., Sidrauski, C., Dörfler, S., Walter, P., 1999. Mechanism of non-spliceosomal mRNA splicing in the unfolded protein response pathway. EMBO J. 18, 3119–3132. https://doi.org/10.1093/emboj/18.11.3119

Greer, C.L., Peebles, C.L., Gegenheimer, P., Abelson, J., 1983. Mechanism of action of a yeast RNA ligase in tRNA splicing. Cell 32, 537–546.

Greer, C.L., Söll, D., Willis, I., 1987. Substrate recognition and identification of splice sites by the tRNA-splicing endonuclease and ligase from Saccharomyces cerevisiae. Mol. Cell. Biol. 7, 76–84. https://doi.org/10.1128/mcb.7.1.76

Guydosh, N.R., Kimmig, P., Walter, P., Green, R., 2017. Regulated Ire1-dependent mRNA decay requires no-go mRNA degradation to maintain endoplasmic reticulum homeostasis in S. pombe. eLife 6, e29216. https://doi.org/10.7554/eLife.29216

Hamamy, H., 2012. Consanguineous marriages. J. Community Genet. 3, 185–192. https://doi.org/10.1007/s12687-011-0072-y

Han, D., Lerner, A.G., Walle, L.V., Upton, J.-P., Xu, W., Hagen, A., Backes, B.J., Oakes, S.A., Papa, F.R., 2009. IRE1α Kinase Activation Modes Control Alternate Endoribonuclease Outputs to Determine Divergent Cell Fates. Cell 138, 562–575. https://doi.org/10.1016/j.cell.2009.07.017

Harigaya, Y., Parker, R., 2012. Global analysis of mRNA decay intermediates in Saccharomyces cerevisiae. Proc. Natl. Acad. Sci. 109, 11764–11769. https://doi.org/10.1073/pnas.1119741109

Hayashi, S., Mori, S., Suzuki, Takeo, Suzuki, Tsutomu, Yoshihisa, T., 2019. Impact of intron removal from tRNA genes on Saccharomyces cerevisiae. Nucleic Acids Res. 47, 5936–5949. https://doi.org/10.1093/nar/gkz270

Hayne, C.K., Butay, K.J.U., Stewart, Z.D., Krahn, J.M., Perera, L., Williams, J.G., Petrovitch, R.M., Deterding, L.J., Matera, A.G., Borgnia, M.J., Stanley, R.E., 2022a. Structural Basis for pre-tRNA Recognition and Processing by the Human tRNA Splicing Endonuclease Complex. https://doi.org/10.1101/2022.09.02.506201

Hayne, C.K., Lewis, T.A., Stanley, R.E., 2022b. Recent insights into the structure, function, and regulation of the eukaryotic transfer RNA splicing endonuclease complex. Wiley Interdiscip. Rev. RNA 13, e1717. https://doi.org/10.1002/wrna.1717

Hayne, C.K., Schmidt, C.A., Haque, M.I., Matera, A.G., Stanley, R.E., 2020. Reconstitution of the human tRNA splicing endonuclease complex: insight into the regulation of pre-tRNA cleavage. Nucleic Acids Res. https://doi.org/10.1093/nar/gkaa438

He, F., Amrani, N., Johansson, M.J.O., Jacobson, A., 2008. Chapter 6. Qualitative and quantitative assessment of the activity of the yeast nonsense-mediated mRNA decay pathway. Methods Enzymol. 449, 127–147. https://doi.org/10.1016/S0076-6879(08)02406-3

Henras, A., Plisson-Chastang, C., O'Donohue, M.-F., Chakraborty, A., Gleizes, P.-E., 2014. An overview of pre-ribosomal RNA processing in eukaryotes. Wiley Interdiscip. Rev. RNA 6. https://doi.org/10.1002/wrna.1269

Hinnebusch, A.G., 2005. Translational regulation of GCN4 and the general amino acid control of yeast. Annu. Rev. Microbiol. 59, 407–450. https://doi.org/10.1146/annurev.micro.59.031805.133833

Hitchcock, A.L., Krebber, H., Frietze, S., Lin, A., Latterich, M., Silver, P.A., 2001. The conserved npl4 protein complex mediates proteasome-dependent membrane-bound transcription factor activation. Mol. Biol. Cell 12, 3226–3241. https://doi.org/10.1091/mbc.12.10.3226

Ho, C.K., Rauhut, R., Vijayraghavan, U., Abelson, J., 1990. Accumulation of pre-tRNA splicing “2/3” intermediates in a Saccharomyces cerevisiae mutant. EMBO J. 9, 1245–1252.

Hollien, J., Lin, J.H., Li, H., Stevens, N., Walter, P., Weissman, J.S., 2009. Regulated Ire1-dependent decay of messenger RNAs in mammalian cells. J. Cell Biol. 186, 323–331. https://doi.org/10.1083/jcb.200903014

Hollien, J., Weissman, J.S., 2006. Decay of endoplasmic reticulum-localized mRNAs during the unfolded protein response. Science 313, 104–107. https://doi.org/10.1126/science.1129631

Hopper, A.K., 2013. Transfer RNA post-transcriptional processing, turnover, and subcellular dynamics in the yeast Saccharomyces cerevisiae. Genetics 194, 43–67. https://doi.org/10.1534/genetics.112.147470

Huh, W.-K., Falvo, J.V., Gerke, L.C., Carroll, A.S., Howson, R.W., Weissman, J.S., O’Shea, E.K., 2003. Global analysis of protein localization in budding yeast. Nature 425, 686–691. https://doi.org/10.1038/nature02026

Huntzinger, E., Kashima, I., Fauser, M., Saulière, J., Izaurralde, E., 2008. SMG6 is the catalytic endonuclease that cleaves mRNAs containing nonsense codons in metazoan. RNA N. Y. N 14, 2609–2617. https://doi.org/10.1261/rna.1386208

Hurtig, J.E., Steiger, M.A., Nagarajan, V.K., Li, T., Chao, T.-C., Tsai, K.-L., Hoof, A. van, 2021. Comparative parallel analysis of RNA ends identifies mRNA substrates of a tRNA splicing endonuclease-initiated mRNA decay pathway. Proc. Natl. Acad. Sci. 118. https://doi.org/10.1073/pnas.2020429118

Hurtig, J.E., van Hoof, A., 2022. Yeast Dxo1 is required for 25S rRNA maturation and acts as a transcriptome-wide distributive exonuclease. RNA rna.078952.121. https://doi.org/10.1261/rna.078952.121

Inglis, A.J., Masson, G.R., Shao, S., Perisic, O., McLaughlin, S.H., Hegde, R.S., Williams, R.L., 2019. Activation of GCN2 by the ribosomal P-stalk. Proc. Natl. Acad. Sci. U. S. A. 116, 4946–4954. https://doi.org/10.1073/pnas.1813352116

Islas-Osuna, M.A., Ellis, T.P., Marnell, L.L., Mittelmeier, T.M., Dieckmann, C.L., 2002. Cbp1 is required for translation of the mitochondrial cytochrome b mRNA of Saccharomyces cerevisiae. J. Biol. Chem. 277, 37987–37990. https://doi.org/10.1074/jbc.M206132200

Januszyk, K., Lima, C.D., 2014. The eukaryotic RNA exosome. Curr. Opin. Struct. Biol. 24, 132–140. https://doi.org/10.1016/j.sbi.2014.01.011

Jiao, X., Chang, J.H., Kilic, T., Tong, L., Kiledjian, M., 2013. A mammalian pre-mRNA 5’ end capping quality control mechanism and an unexpected link of capping to pre-mRNA processing. Mol. Cell 50, 104–115. https://doi.org/10.1016/j.molcel.2013.02.017

Jiao, X., Xiang, S., Oh, C., Martin, C.E., Tong, L., Kiledjian, M., 2010. Identification of a quality-control mechanism for mRNA 5’-end capping. Nature 467, 608–611. https://doi.org/10.1038/nature09338

Jinek, M., Coyle, S.M., Doudna, J.A., 2011. Coupled 5′ nucleotide recognition and processivity in Xrn1-mediated mRNA decay. Mol. Cell 41, 600–608. https://doi.org/10.1016/j.molcel.2011.02.004

Johnson, A.W., 1997. Rat1p and Xrn1p are functionally interchangeable exoribonucleases that are restricted to and required in the nucleus and cytoplasm, respectively. Mol. Cell. Biol. 17, 6122–6130.

Johnson, A.W., Kolodner, R.D., 1995. Synthetic lethality of sep1 (xrn1) ski2 and sep1 (xrn1) ski3 mutants of Saccharomyces cerevisiae is independent of killer virus and

suggests a general role for these genes in translation control. Mol. Cell. Biol. 15, 2719–2727.

Johnson, P.F., Abelson, J., 1983. The yeast tRNATyr gene intron is essential for correct modification of its tRNA product. Nature 302, 681–687. https://doi.org/10.1038/302681a0

Jones, C.I., Grima, D.P., Waldron, J.A., Jones, S., Parker, H.N., Newbury, S.F., 2013. The 5'-3' exoribonuclease Pacman (Xrn1) regulates expression of the heat shock protein Hsp67Bc and the microRNA miR-277-3p in Drosophila wing imaginal discs. RNA Biol. 10, 1345–1355. https://doi.org/10.4161/rna.25354

Jones, G.M., Stalker, J., Humphray, S., West, A., Cox, T., Rogers, J., Dunham, I., Prelich, G., 2008. A systematic library for comprehensive overexpression screens in Saccharomyces cerevisiae. Nat. Methods 5, 239–241. https://doi.org/10.1038/nmeth.1181

Joyce, G.F., 1989. RNA evolution and the origins of life. Nature 338, 217–224. https://doi.org/10.1038/338217a0

Karaca, E., Weitzer, S., Pehlivan, D., Shiraishi, H., Gogakos, T., Hanada, T., Jhangiani, S.N., Wiszniewski, W., Withers, M., Campbell, I.M., Erdin, S., Isikay, S., Franco, L.M., Gonzaga-Jauregui, C., Gambin, T., Gelowani, V., Hunter, J.V., Yesil, G., Koparir, E., Yilmaz, S., Brown, M., Briskin, D., Hafner, M., Morozov, P., Farazi, T.A., Bernreuther, C., Glatzel, M., Trattnig, S., Friske, J., Kronnerwetter, C., Bainbridge, M.N., Gezdirici, A., Seven, M., Muzny, D.M., Boerwinkle, E., Ozen, M., Baylor Hopkins Center for Mendelian Genomics, Clausen, T., Tuschl, T., Yuksel, A., Hess, A., Gibbs, R.A., Martinez, J., Penninger, J.M., Lupski, J.R., 2014. Human CLP1 mutations alter tRNA biogenesis, affecting both peripheral and central nervous system function. Cell 157, 636–650. https://doi.org/10.1016/j.cell.2014.02.058

Kasher, P.R., Namavar, Y., van Tijn, P., Fluiter, K., Sizarov, A., Kamermans, M., Grierson, A.J., Zivkovic, D., Baas, F., 2011. Impairment of the tRNA-splicing endonuclease subunit 54 (tsen54) gene causes neurological abnormalities and larval death in zebrafish models of pontocerebellar hypoplasia. Hum. Mol. Genet. 20, 1574–1584. https://doi.org/10.1093/hmg/ddr034

Katolik, A., Clark, N.E., Tago, N., Montemayor, E.J., Hart, P.J., Damha, M.J., 2017. Fluorescent Branched RNAs for High-Throughput Analysis of Dbr1 Enzyme Kinetics and Inhibition. ACS Chem. Biol. 12, 622–627. https://doi.org/10.1021/acschembio.6b00971

Khalid, M.F., Damha, M.J., Shuman, S., Schwer, B., 2005. Structure–function analysis of yeast RNA debranching enzyme (Dbr1), a manganese-dependent phosphodiesterase. Nucleic Acids Res. 33, 6349–6360. https://doi.org/10.1093/nar/gki934

Kim, M., van Hoof, A., 2020. Suppressors of mRNA Decapping Defects Restore Growth Without Major Effects on mRNA Decay Rates or Abundance. Genetics 216, 1051–1069. https://doi.org/10.1534/genetics.120.303641

Kimmig, P., Diaz, M., Zheng, J., Williams, C.C., Lang, A., Aragón, T., Li, H., Walter, P., 2012. The unfolded protein response in fission yeast modulates stability of select mRNAs to maintain protein homeostasis. eLife 1, e00048. https://doi.org/10.7554/eLife.00048

Kosmaczewski, S.G., Edwards, T.J., Han, S.M., Eckwahl, M.J., Meyer, B.I., Peach, S., Hesselberth, J.R., Wolin, S.L., Hammarlund, M., 2014. The RtcB RNA ligase is an essential component of the metazoan unfolded protein response. EMBO Rep. 15, 1278–1285. https://doi.org/10.15252/embr.201439531

Kramer, S., McLennan, A.G., 2019. The complex enzymology of mRNA decapping: Enzymes of four classes cleave pyrophosphate bonds. Wiley Interdiscip. Rev. RNA 10, e1511. https://doi.org/10.1002/wrna.1511

Krzyszton, M., Zakrzewska-Placzek, M., Koper, M., Kufel, J., 2012. Chapter Seven - Rat1 and Xrn2: The Diverse Functions of the Nuclear Rat1/Xrn2 Exonuclease, in: Chanfreau, G.F., Tamanoi, F. (Eds.), The Enzymes, Eukaryotic RNases and Their Partners in RNA Degradation and Biogenesis, Part A. Academic Press, pp. 131–163. https://doi.org/10.1016/B978-0-12-404740-2.00007-0

Kumar, A., Agarwal, S., Heyman, J.A., Matson, S., Heidtman, M., Piccirillo, S., Umansky, L., Drawid, A., Jansen, R., Liu, Y., Cheung, K.-H., Miller, P., Gerstein, M., Roeder, G.S., Snyder, M., 2002. Subcellular localization of the yeast proteome. Genes Dev. 16, 707–719. https://doi.org/10.1101/gad.970902

Langmead, B., Trapnell, C., Pop, M., Salzberg, S.L., 2009. Ultrafast and memory-efficient alignment of short DNA sequences to the human genome. Genome Biol. 10, R25. https://doi.org/10.1186/gb-2009-10-3-r25

Lardelli, R.M., Schaffer, A.E., Eggens, V.R.C., Zaki, M.S., Grainger, S.L., Sathe, S., Van Nostrand, E.L., Schlachetzki, Z., Rosti, B., Akizu, N., Scott, E., Heckman, L.D., Rosti, R.O., Dikoglu, E., Gregor, A., Guemez-Gamboa, A., Musaev, D., Mande, R., Widjaja, A., Shaw, T.L., Markmiller, S., Marin-Valencia, I., Davies, J.H., de Meirleir, L., Kayserili, H., Altunoglu, U., Freckmann, M.L., Warwick, L., Chitayat, D., Çağlayan, A.O., Bilguvar, K., Per, H., Fagerberg, C., Kibaek, M., Aldinger, K.A., Manchester, D., Matsumoto, N., Muramatsu, K., Saitsu, H., Shiina, M., Ogata, K., Foulds, N., Dobyns, W.B., Chi, N., Traver, D., Spaccini, L., Bova, S.M., Gabriel, S.B., Gunel, M., Valente, E.M., Nassogne, M.-C., Bennett, E.J., Yeo, G.W., Baas, F., Lykke-Andersen, J., Gleeson, J.G., 2017. Biallelic Mutations in the 3’ Exonuclease TOE1 Cause

Pontocerebellar Hypoplasia and Uncover a Role in snRNA Processing. Nat. Genet. 49, 457–464. https://doi.org/10.1038/ng.3762

Larimer, F.W., Stevens, A., 1990. Disruption of the gene XRN1, coding for a 5′→3′ exoribonuclease, restricts yeast cell growth. Gene 95, 85–90. https://doi.org/10.1016/0378-1119(90)90417-P

Leber, J.H., Bernales, S., Walter, P., 2004. IRE1-Independent Gain Control of the Unfolded Protein Response. PLOS Biol. 2, e235. https://doi.org/10.1371/journal.pbio.0020235

Lebreton, A., Tomecki, R., Dziembowski, A., Séraphin, B., 2008. Endonucleolytic RNA cleavage by a eukaryotic exosome. Nature 456, 993–996. https://doi.org/10.1038/nature07480

Lee, K., Tirasophon, W., Shen, X., Michalak, M., Prywes, R., Okada, T., Yoshida, H., Mori, K., Kaufman, R.J., 2002. IRE1-mediated unconventional mRNA splicing and S2P-mediated ATF6 cleavage merge to regulate XBP1 in signaling the unfolded protein response. Genes Dev. 16, 452–466. https://doi.org/10.1101/gad.964702

Li, H., Trotta, C.R., Abelson, J., 1998. Crystal structure and evolution of a transfer RNA splicing enzyme. Science 280, 279–284.

Lima, W.F., De Hoyos, C.L., Liang, X., Crooke, S.T., 2016. RNA cleavage products generated by antisense oligonucleotides and siRNAs are processed by the RNA surveillance machinery. Nucleic Acids Res. 44, 3351–3363. https://doi.org/10.1093/nar/gkw065

Lopes, R.R.S., Silveira, G. de O., Eitler, R., Vidal, R.S., Kessler, A., Hinger, S., Paris, Z., Alfonzo, J.D., Polycarpo, C., 2016. The essential function of the Trypanosoma brucei Trl1 homolog in procyclic cells is maturation of the intron-containing tRNATyr. RNA 22, 1190–1199. https://doi.org/10.1261/rna.056242.116

Love, M.I., Huber, W., Anders, S., 2014. Moderated estimation of fold change and dispersion for RNA-seq data with DESeq2. Genome Biol. 15, 550. https://doi.org/10.1186/s13059-014-0550-8

Lykke-Andersen, S., Chen, Y., Ardal, B.R., Lilje, B., Waage, J., Sandelin, A., Jensen, T.H., 2014. Human nonsense-mediated RNA decay initiates widely by endonucleolysis and targets snoRNA host genes. Genes Dev. 28, 2498–2517. https://doi.org/10.1101/gad.246538.114

Lynch, E.R., 2019. The Dxo Decapping Exonuclease Is a Restriction Factor for RNA Viruses (Master of Science Thesis). Colorado State University.

MacIntosh, G.C., Bariola, P.A., Newbigin, E., Green, P.J., 2001. Characterization of Rny1, the Saccharomyces cerevisiae member of the T2 RNase family of RNases: Unexpected functions for ancient enzymes? Proc. Natl. Acad. Sci. U. S. A. 98, 1018–1023.

Makanae, K., Kintaka, R., Makino, T., Kitano, H., Moriya, H., 2013. Identification of dosage-sensitive genes in Saccharomyces cerevisiae using the genetic tug-of-war method. Genome Res. 23, 300–311. https://doi.org/10.1101/gr.146662.112

Maraş-Genç, H., Uyur-Yalçın, E., Rosti, R.Ö., Gleeson, J.G., Kara, B., 2015. TSEN54 gene-related pontocerebellar hypoplasia type 2 presenting with exaggerated startle response: report of two cases in a family. Turk. J. Pediatr. 57, 286–289.

Masson, G.R., 2019. Towards a model of GCN2 activation. Biochem. Soc. Trans. 47, 1481–1488. https://doi.org/10.1042/BST20190331

Matera, A.G., Wang, Z., 2014. A day in the life of the spliceosome. Nat. Rev. Mol. Cell Biol. 15, 108–121. https://doi.org/10.1038/nrm3742

Matsuo, Y., Ikeuchi, K., Saeki, Y., Iwasaki, S., Schmidt, C., Udagawa, T., Sato, F., Tsuchiya, H., Becker, T., Tanaka, K., Ingolia, N.T., Beckmann, R., Inada, T., 2017.

Ubiquitination of stalled ribosome triggers ribosome-associated quality control. Nat. Commun. 8, 159. https://doi.org/10.1038/s41467-017-00188-1

Menees, T.M., 2020. RNA Lariat Debranching Enzyme as a Retroviral and Long-Terminal-Repeat Retrotransposon Host Factor. Annu. Rev. Virol. 7, 189–202. https://doi.org/10.1146/annurev-virology-012720-094902

Metcalf, M.G., Higuchi-Sanabria, R., Garcia, G., Tsui, C.K., Dillin, A., 2020. Beyond the cell factory: Homeostatic regulation of and by the UPRER. Sci. Adv. 6, eabb9614. https://doi.org/10.1126/sciadv.abb9614

Metzger, M.B., Scales, J.L., Dunklebarger, M.F., Loncarek, J., Weissman, A.M., 2020. A protein quality control pathway at the mitochondrial outer membrane. eLife 9, e51065. https://doi.org/10.7554/eLife.51065

Mishiba, K., Nagashima, Y., Suzuki, E., Hayashi, N., Ogata, Y., Shimada, Y., Koizumi, N., 2013. Defects in IRE1 enhance cell death and fail to degrade mRNAs encoding secretory pathway proteins in the Arabidopsis unfolded protein response. Proc. Natl. Acad. Sci. 110, 5713–5718. https://doi.org/10.1073/pnas.1219047110

Mitchell, P., Petfalski, E., Shevchenko, A., Mann, M., Tollervey, D., 1997. The Exosome: A Conserved Eukaryotic RNA Processing Complex Containing Multiple 3′→5′ Exoribonucleases. Cell 91, 457–466. https://doi.org/10.1016/S0092-8674(00)80432-8

Mohanta, A., Chakrabarti, K., 2021. Dbr1 functions in mRNA processing, intron turnover and human diseases. Biochimie 180. https://doi.org/10.1016/j.biochi.2020.10.003

Monaghan, C.E., Adamson, S.I., Kapur, M., Chuang, J.H., Ackerman, S.L., 2021. The Clp1 R140H mutation alters tRNA metabolism and mRNA 3' processing in mouse models of pontocerebellar hypoplasia. Proc. Natl. Acad. Sci. U. S. A. 118, e2110730118. https://doi.org/10.1073/pnas.2110730118

Moore, K., Hollien, J., 2015. Ire1-mediated decay in mammalian cells relies on mRNA sequence, structure, and translational status. Mol. Biol. Cell 26, 2873–2884. https://doi.org/10.1091/mbc.E15-02-0074

Mori, K., Kawahara, T., Yoshida, H., Yanagi, H., Yura, T., 1996. Signalling from endoplasmic reticulum to nucleus: transcription factor with a basic-leucine zipper motif is required for the unfolded protein-response pathway. Genes Cells Devoted Mol. Cell. Mech. 1, 803–817. https://doi.org/10.1046/j.1365-2443.1996.d01-274.x

Mori, K., Ma, W., Gething, M.J., Sambrook, J., 1993. A transmembrane protein with a cdc2+/CDC28-related kinase activity is required for signaling from the ER to the nucleus. Cell 74, 743–756. https://doi.org/10.1016/0092-8674(93)90521-q

Morton, D.J., Kuiper, E.G., Jones, S.K., Leung, S.W., Corbett, A.H., Fasken, M.B., 2018. The RNA exosome and RNA exosome-linked disease. RNA 24, 127–142. https://doi.org/10.1261/rna.064626.117

Mu, W., Heller, T., Barañano, K.W., 2021. Two siblings with a novel variant of EXOSC3 extended phenotypic spectrum of pontocerebellar hypoplasia 1B to an exceptionally mild form. BMJ Case Rep. CP 14, e236732. https://doi.org/10.1136/bcr-2020-236732

Mullineux, S.-T., Lafontaine, D.L.J., 2012. Mapping the cleavage sites on mammalian pre-rRNAs: where do we stand? Biochimie 94, 1521–1532. https://doi.org/10.1016/j.biochi.2012.02.001

Nagarajan, V.K., Jones, C.I., Newbury, S.F., Green, P.J., 2013. XRN 5’→3’ exoribonucleases: Structure, mechanisms and functions. Biochim. Biophys. Acta 1829, 590–603. https://doi.org/10.1016/j.bbagrm.2013.03.005

Nagarajan, V.K., Kukulich, P.M., von Hagel, B., Green, P.J., 2019. RNA degradomes reveal substrates and importance for dark and nitrogen stress responses of Arabidopsis XRN4. Nucleic Acids Res. 47, 9216–9230. https://doi.org/10.1093/nar/gkz712

Namavar, Y., Barth, P.G., Kasher, P.R., van Ruissen, F., Brockmann, K., Bernert, G., Writzl, K., Ventura, K., Cheng, E.Y., Ferriero, D.M., Basel-Vanagaite, L., Eggens, V.R.C., Krägeloh-Mann, I., De Meirleir, L., King, M., Graham, J.M., von Moers, A., Knoers, N., Sztriha, L., Korinthenberg, R., Consortium, P.C.H., Dobyns, W.B., Baas, F., Poll-The, B.T., 2011a. Clinical, neuroradiological and genetic findings in pontocerebellar hypoplasia. Brain 134, 143–156. https://doi.org/10.1093/brain/awq287

Namavar, Y., Chitayat, D., Barth, P.G., van Ruissen, F., de Wissel, M.B., Poll-The, B.T., Silver, R., Baas, F., 2011b. TSEN54 mutations cause pontocerebellar hypoplasia type 5. Eur. J. Hum. Genet. EJHG 19, 724–726. https://doi.org/10.1038/ejhg.2011.8

Navickas, A., Chamois, S., Saint-Fort, R., Henri, J., Torchet, C., Benard, L., 2020. No-Go Decay mRNA cleavage in the ribosome exit tunnel produces 5′-OH ends phosphorylated by Trl1. Nat. Commun. 11, 1–11. https://doi.org/10.1038/s41467-019-13991-9

Negri, E.D.N., Fabbri, S., Bufardeci, E., Baldi, M.I., Attardi, D.G., Mattoccia, E., Tocchini-Valentini, G.P., 1997. The Eucaryal tRNA Splicing Endonuclease Recognizes a Tripartite Set of RNA Elements. Cell 89, 859–866. https://doi.org/10.1016/S0092-8674(00)80271-8

NEWBURY, S., WOOLLARD, A., 2004. The 5′–3′ exoribonuclease xrn-1 is essential for ventral epithelial enclosure during C. elegans embryogenesis. RNA 10, 59–65. https://doi.org/10.1261/rna.2195504

Nicholson-Shaw, T., Ajaj, Y., Perelis, M., Fulzele, A., Yeo, G.W., Bennett, E.J., Lykke-Andersen, J., 2022. The 2’,3’ cyclic phosphatase Angel1 facilitates mRNA degradation during human ribosome-associated quality control. https://doi.org/10.1101/2022.04.28.489582

Niwa, M., Patil, C.K., DeRisi, J., Walter, P., 2004. Genome-scale approaches for discovering novel nonconventional splicing substrates of the Ire1 nuclease. Genome Biol. 6, R3. https://doi.org/10.1186/gb-2004-6-1-r3

Oeffinger, M., Zenklusen, D., Ferguson, A., Wei, K.E., El Hage, A., Tollervey, D., Chait, B.T., Singer, R.H., Rout, M.P., 2009. Rrp17p Is a Eukaryotic Exonuclease Required for 5′ End Processing of Pre-60S Ribosomal RNA. Mol. Cell 36, 768–781. https://doi.org/10.1016/j.molcel.2009.11.011

Ohira, T., Suzuki, T., 2011. Retrograde nuclear import of tRNA precursors is required for modified base biogenesis in yeast. Proc. Natl. Acad. Sci. U. S. A. 108, 10502–10507. https://doi.org/10.1073/pnas.1105645108

Orban, T.I., Izaurralde, E., 2005. Decay of mRNAs targeted by RISC requires XRN1, the Ski complex, and the exosome. RNA 11, 459–469. https://doi.org/10.1261/rna.7231505

Parenteau, J., Maignon, L., Berthoumieux, M., Catala, M., Gagnon, V., Abou Elela, S., 2019. Introns are mediators of cell response to starvation. Nature 565, 612–617. https://doi.org/10.1038/s41586-018-0859-7

Paushkin, S.V., Patel, M., Furia, B.S., Peltz, S.W., Trotta, C.R., 2004. Identification of a human endonuclease complex reveals a link between tRNA splicing and pre-mRNA 3’ end formation. Cell 117, 311–321.

Payea, M.J., Hauke, A.C., De Zoysa, T., Phizicky, E.M., 2020. Mutations in the anticodon stem of tRNA cause accumulation and Met22-dependent decay of pre-tRNA in yeast. RNA N. Y. N 26, 29–43. https://doi.org/10.1261/rna.073155.119

Peach, S.E., York, K., Hesselberth, J.R., 2015. Global analysis of RNA cleavage by 5′-hydroxyl RNA sequencing. Nucleic Acids Res. 43, e108. https://doi.org/10.1093/nar/gkv536

Peebles, C.L., Gegenheimer, P., Abelson, J., 1983. Precise excision of intervening sequences from precursor tRNAs by a membrane-associated yeast endonuclease. Cell 32, 525–536. https://doi.org/10.1016/0092-8674(83)90472-5

Peebles, C.L., Ogden, R.C., Knapp, G., Abelson, J., 1979. Splicing of yeast tRNA precursors: a two-stage reaction. Cell 18, 27–35. https://doi.org/10.1016/0092-8674(79)90350-7

Pelechano, V., Chávez, S., Pérez-Ortín, J.E., 2010. A complete set of nascent transcription rates for yeast genes. PloS One 5, e15442. https://doi.org/10.1371/journal.pone.0015442

Perentesis, J.P., Phan, L.D., Gleason, W.B., LaPorte, D.C., Livingston, D.M., Bodley, J.W., 1992. Saccharomyces cerevisiae elongation factor 2. Genetic cloning, characterization of expression, and G-domain modeling. J. Biol. Chem. 267, 1190–1197.

Phizicky, E.M., Consaul, S.A., Nehrke, K.W., Abelson, J., 1992. Yeast tRNA ligase mutants are nonviable and accumulate tRNA splicing intermediates. J. Biol. Chem. 267, 4577–4582.

Phizicky, E.M., Hopper, A.K., 2010. tRNA biology charges to the front. Genes Dev. 24, 1832–1860. https://doi.org/10.1101/gad.1956510

Picard-Jean, F., Brand, C., Tremblay-Létourneau, M., Allaire, A., Beaudoin, M.C., Boudreault, S., Duval, C., Rainville-Sirois, J., Robert, F., Pelletier, J., Geiss, B.J., Bisaillon, M., 2018. 2’-O-methylation of the mRNA cap protects RNAs from decapping and degradation by DXO. PLOS ONE 13, e0193804. https://doi.org/10.1371/journal.pone.0193804

Pinto, P.H., Kroupova, A., Schleiffer, A., Mechtler, K., Jinek, M., Weitzer, S., Martinez, J., 2020. ANGEL2 is a member of the CCR4 family of deadenylases with 2’,3’-cyclic

phosphatase activity. Science 369, 524–530. https://doi.org/10.1126/science.aba9763

Pochopien, A.A., Beckert, B., Kasvandik, S., Berninghausen, O., Beckmann, R., Tenson, T., Wilson, D.N., 2021. Structure of Gcn1 bound to stalled and colliding 80S ribosomes. Proc. Natl. Acad. Sci. 118, e2022756118. https://doi.org/10.1073/pnas.2022756118

Popow, J., Englert, M., Weitzer, S., Schleiffer, A., Mierzwa, B., Mechtler, K., Trowitzsch, S., Will, C.L., Lührmann, R., Söll, D., Martinez, J., 2011. HSPC117 Is the Essential Subunit of a Human tRNA Splicing Ligase Complex. Science 331, 760–764. https://doi.org/10.1126/science.1197847

Powers, K.T., Szeto, J.-Y.A., Schaffitzel, C., 2020. New insights into no-go, non-stop and nonsense-mediated mRNA decay complexes. Curr. Opin. Struct. Biol., Catalysis and Regulation ● Protein Nucleic Acid Interaction 65, 110–118. https://doi.org/10.1016/j.sbi.2020.06.011

Pratt, A.J., MacRae, I.J., 2009. The RNA-induced Silencing Complex: A Versatile Gene-silencing Machine. J. Biol. Chem. 284, 17897–17901. https://doi.org/10.1074/jbc.R900012200

Ramirez, A., Shuman, S., Schwer, B., 2008. Human RNA 5′-kinase (hClp1) can function as a tRNA splicing enzyme in vivo. RNA 14, 1737. https://doi.org/10.1261/rna.1142908

Ransey, E., Paredes, E., Dey, S.K., Das, S.R., Heroux, A., Macbeth, M.R., 2017. Crystal structure of the Entamoeba histolytica RNA lariat debranching enzyme EhDbr1 reveals a catalytic Zn2+ /Mn2+ heterobinucleation. FEBS Lett. 591, 2003–2010. https://doi.org/10.1002/1873-3468.12677

Rauhut, R., Green, P.R., Abelson, J., 1990. Yeast tRNA-splicing endonuclease is a heterotrimeric enzyme. J. Biol. Chem. 265, 18180–18184.

Rawal, Y., Chereji, R.V., Valabhoju, V., Qiu, H., Ocampo, J., Clark, D.J., Hinnebusch, A.G., 2018. Gcn4 binding in coding regions can activate internal and canonical 5′

promoters in yeast. Mol. Cell 70, 297-311.e4. https://doi.org/10.1016/j.molcel.2018.03.007

Reyes, V.M., Abelson, J., 1988. Substrate recognition and splice site determination in yeast tRNA splicing. Cell 55, 719–730. https://doi.org/10.1016/0092-8674(88)90230-9

Ron, D., Walter, P., 2007. Signal integration in the endoplasmic reticulum unfolded protein response. Nat. Rev. Mol. Cell Biol. 8, 519–529. https://doi.org/10.1038/nrm2199

Rong, T., Yao, R., Deng, Y., Lin, Q., Wang, G., Wang, J., Jiang, F., Jiang, Y., 2022. Case Report: A Relatively Mild Phenotype Produced by Novel Mutations in the SEPSECS Gene. Front. Pediatr. 9, 805575. https://doi.org/10.3389/fped.2021.805575

Roy, K.R., Chanfreau, G.F., 2020. Robust mapping of polyadenylated and non-polyadenylated RNA 3' ends at nucleotide resolution by 3'-end sequencing. Methods San Diego Calif 176, 4–13. https://doi.org/10.1016/j.ymeth.2019.05.016

Sakamoto, M., Shiiki, T., Matsui, S., Okamoto, N., Koshimizu, E., Tsuchida, N., Uchiyama, Y., Hamanaka, K., Fujita, A., Miyatake, S., Misawa, K., Mizuguchi, T., Matsumoto, N., 2022. A novel homozygous CHMP1A variant arising from segmental uniparental disomy causes pontocerebellar hypoplasia type 8. J. Hum. Genet. https://doi.org/10.1038/s10038-022-01098-x

Saldanha, R., Mohr, G., Belfort, M., Lambowitz, A.M., 1993. Group I and group II introns. FASEB J. 7, 15–24. https://doi.org/10.1096/fasebj.7.1.8422962

Sánchez-Albisua, I., Frölich, S., Barth, P.G., Steinlin, M., Krägeloh-Mann, I., 2014. Natural course of pontocerebellar hypoplasia type 2A. Orphanet J. Rare Dis. 9, 70. https://doi.org/10.1186/1750-1172-9-70

Sawaya, R., Schwer, B., Shuman, S., 2003. Genetic and Biochemical Analysis of the Functional Domains of Yeast tRNA Ligase. J. Biol. Chem. 278, 43928–43938. https://doi.org/10.1074/jbc.M307839200

Schaeffer, D., Tsanova, B., Barbas, A., Reis, F.P., Dastidar, E.G., Sanchez-Rotunno, M., Arraiano, C.M., Hoof, A. van, 2009. The exosome contains domains with specific endoribonuclease, exoribonuclease and cytoplasmic mRNA decay activities. Nat. Struct. Mol. Biol. 16, 56. https://doi.org/10.1038/nsmb.1528

Schaeffer, D., van Hoof, A., 2011. Different nuclease requirements for exosome-mediated degradation of normal and nonstop mRNAs. Proc. Natl. Acad. Sci. U. S. A. 108, 2366–2371. https://doi.org/10.1073/pnas.1013180108

Schaffer, A.E., Eggens, V.R.C., Caglayan, A.O., Reuter, M.S., Scott, E., Coufal, N.G., Silhavy, J.L., Xue, Y., Kayserili, H., Yasuno, K., Rosti, R.O., Abdellateef, M., Caglar, C., Kasher, P.R., Cazemier, J.L., Weterman, M.A., Cantagrel, V., Cai, N., Zweier, C., Altunoglu, U., Satkin, N.B., Aktar, F., Tuysuz, B., Yalcinkaya, C., Caksen, H., Bilguvar, K., Fu, X.-D., Trotta, C., Gabriel, S., Reis, A., Gunel, M., Baas, F., Gleeson, J.G., 2014. CLP1 Founder Mutation Links tRNA Splicing and Maturation to Cerebellar Development and Neurodegeneration. Cell 157, 651–663. https://doi.org/10.1016/j.cell.2014.03.049

Schillewaert, S., Wacheul, L., Lhomme, F., Lafontaine, D.L.J., 2012. The evolutionarily conserved protein Las1 is required for pre-rRNA processing at both ends of ITS2. Mol. Cell. Biol. 32, 430–444. https://doi.org/10.1128/MCB.06019-11

Schmid, M., Jensen, T.H., 2008. The exosome: a multipurpose RNA-decay machine. Trends Biochem. Sci. 33, 501–510. https://doi.org/10.1016/j.tibs.2008.07.003

Schmidt, C.A., Matera, A.G., 2020. tRNA introns: Presence, processing, and purpose. WIREs RNA 11, e1583. https://doi.org/10.1002/wrna.1583

Schmidt, S.A., Foley, P.L., Jeong, D.-H., Rymarquis, L.A., Doyle, F., Tenenbaum, S.A., Belasco, J.G., Green, P.J., 2015. Identification of SMG6 cleavage sites and a preferred RNA cleavage motif by global analysis of endogenous NMD targets in human cells. Nucleic Acids Res. 43, 309–323. https://doi.org/10.1093/nar/gku1258

Schneider, C., Kudla, G., Wlotzka, W., Tuck, A., Tollervey, D., 2012. Transcriptome-wide Analysis of Exosome Targets. Mol. Cell 48, 422–433. https://doi.org/10.1016/j.molcel.2012.08.013

Schneider, C., Leung, E., Brown, J., Tollervey, D., 2009. The N-terminal PIN domain of the exosome subunit Rrp44 harbors endonuclease activity and tethers Rrp44 to the yeast core exosome. Nucleic Acids Res. 37, 1127–1140. https://doi.org/10.1093/nar/gkn1020

Schneider, C., Tollervey, D., 2013. Threading the barrel of the RNA exosome. Trends Biochem. Sci. 38, 485–493. https://doi.org/10.1016/j.tibs.2013.06.013

Schwarz, T.S., Berkemer, S.J., Bernhart, S.H., Weiß, M., Ferreira-Cerca, S., Stadler, P.F., Marchfelder, A., 2020. Splicing Endonuclease Is an Important Player in rRNA and tRNA Maturation in Archaea. Front. Microbiol. 11.

Schwenzer, H., Jühling, F., Chu, A., Pallett, L.J., Baumert, T.F., Maini, M., Fassati, A., 2019. Oxidative Stress Triggers Selective tRNA Retrograde Transport in Human Cells during the Integrated Stress Response. Cell Rep. 26, 3416-3428.e5. https://doi.org/10.1016/j.celrep.2019.02.077

Schwer, B., Khalid, F., Shuman, S., 2016. Mechanistic insights into the manganese-dependent phosphodiesterase activity of yeast Dbr1 with bis-p-nitrophenylphosphate and branched RNA substrates. RNA. https://doi.org/10.1261/rna.058552.116

Sekulovski, S., Devant, P., Panizza, S., Gogakos, T., Pitiriciu, A., Heitmeier, K., Ramsay, E.P., Barth, M., Schmidt, C., Tuschl, T., Baas, F., Weitzer, S., Martinez, J., Trowitzsch, S., 2021. Assembly defects of human tRNA splicing endonuclease contribute to impaired pre-tRNA processing in pontocerebellar hypoplasia. Nat. Commun. 12, 5610. https://doi.org/10.1038/s41467-021-25870-3

Sekulovski, S., Sušac, L., Stelzl, L.S., Tampé, R., Trowitzsch, S., 2022. Structural basis of substrate recognition by human tRNA splicing endonuclease TSEN. https://doi.org/10.1101/2022.09.03.506465

Sepahvand, A., Razmara, E., Bitarafan, F., Galehdari, M., Tavasoli, A.R., Almadani, N., Garshasbi, M., 2020. A homozygote variant in the tRNA splicing endonuclease subunit 54 causes pontocerebellar hypoplasia in a consanguineous Iranian family. Mol. Genet. Genomic Med. 8, e1413. https://doi.org/10.1002/mgg3.1413

Séron, K., Blondel, M.O., Haguenauer-Tsapis, R., 1999. Disruption of six novel genes from the left arm of chromosome XV of Saccharomyces cerevisiae and basic phenotypic analysis of the generated mutants. Yeast Chichester Engl. 15, 73–79. https://doi.org/10.1002/(SICI)1097-0061(19990115)15:1<73::AID-YEA341>3.0.CO;2-Q

Shamu, C.E., Walter, P., 1996. Oligomerization and phosphorylation of the Ire1p kinase during intracellular signaling from the endoplasmic reticulum to the nucleus. EMBO J. 15, 3028–3039.

Shigematsu, M., Kawamura, T., Kirino, Y., 2018. Generation of 2′,3′-Cyclic Phosphate-Containing RNAs as a Hidden Layer of the Transcriptome. Front. Genet. 9.

Shobuike, T., Tatebayashi, K., Tani, T., Sugano, S., Ikeda, H., 2001. The dhp1+ gene, encoding a putative nuclear 5′→3′ exoribonuclease, is required for proper chromosome segregation in fission yeast. Nucleic Acids Res. 29, 1326–1333.

Sidrauski, C., Cox, J.S., Walter, P., 1996. tRNA Ligase Is Required for Regulated mRNA Splicing in the Unfolded Protein Response. Cell 87, 405–413. https://doi.org/10.1016/S0092-8674(00)81361-6

Sidrauski, C., Walter, P., 1997. The transmembrane kinase Ire1p is a site-specific endonuclease that initiates mRNA splicing in the unfolded protein response. Cell 90, 1031–1039.

Sikorski, R.S., Hieter, P., 1989. A system of shuttle vectors and yeast host strains designed for efficient manipulation of DNA in Saccharomyces cerevisiae. Genetics 122, 19–27. https://doi.org/10.1093/genetics/122.1.19

Slavotinek, A., Misceo, D., Htun, S., Mathisen, L., Frengen, E., Foreman, M., Hurtig, J.E., Enyenihi, L., Sterrett, M.C., Leung, S.W., Schneidman-Duhovny, D., Estrada-Veras, J., Duncan, J.L., Xia, V., Beleford, D., Si, Y., Douglas, G., Treidene, H.E., Hoof, A. van, Fasken, M.B., Corbett, A.H., 2020. Biallelic variants in the RNA exosome gene EXOSC5 are associated with developmental delays, short stature, cerebellar hypoplasia and motor weakness. https://doi.org/10.1101/2020.04.01.839274

Song, J., Markley, J.L., 2007. Three-dimensional structure determined for a subunit of human tRNA splicing endonuclease (Sen15) reveals a novel dimeric fold. J. Mol. Biol. 366, 155–164. https://doi.org/10.1016/j.jmb.2006.11.024

Souret, F.F., Kastenmayer, J.P., Green, P.J., 2004. AtXRN4 degrades mRNA in Arabidopsis and its substrates include selected miRNA targets. Mol. Cell 15, 173–183. https://doi.org/10.1016/j.molcel.2004.06.006

Stevens, A., Poole, T.L., 1995. 5′-Exonuclease-2 of Saccharomyces cerevisiae purification and features of ribonuclease activity with comparison to 5’-exonuclease-1. J. Biol. Chem. 270, 16063–16069. https://doi.org/10.1074/jbc.270.27.16063

Strobel, M.C., Abelson, J., 1986. Effect of intron mutations on processing and function of Saccharomyces cerevisiae SUP53 tRNA in vitro and in vivo. Mol. Cell. Biol. 6, 2663–2673. https://doi.org/10.1128/mcb.6.7.2663-2673.1986

Szweykowska-Kulinska, Z., Senger, B., Keith, G., Fasiolo, F., Grosjean, H., 1994. Intron-dependent formation of pseudouridines in the anticodon of Saccharomyces cerevisiae minor tRNA(Ile). EMBO J. 13, 4636–4644. https://doi.org/10.1002/j.1460-2075.1994.tb06786.x

Takano, A., Endo, T., Yoshihisa, T., 2005. tRNA actively shuttles between the nucleus and cytosol in yeast. Science 309, 140–142. https://doi.org/10.1126/science.1113346

Takaoka, S., Yanagiya, A., Mohamed, H.M.A., Higa, R., Abe, T., Inoue, K., Takahashi, A., Stoney, P., Yamamoto, T., 2021. Neuronal XRN1 is required for maintenance of whole-body metabolic homeostasis. iScience 24, 103151. https://doi.org/10.1016/j.isci.2021.103151

Talkish, J., Igel, H., Perriman, R.J., Shiue, L., Katzman, S., Munding, E.M., Shelansky, R., Donohue, J.P., Ares, M., 2019. Rapidly evolving protointrons in Saccharomyces genomes revealed by a hungry spliceosome. PLoS Genet. 15, e1008249. https://doi.org/10.1371/journal.pgen.1008249

Tam, A.B., Koong, A.C., Niwa, M., 2014. Ire1 Has Distinct Catalytic Mechanisms for XBP1/HAC1 Splicing and RIDD. Cell Rep. 9, 850–858. https://doi.org/10.1016/j.celrep.2014.09.016

Thomson, E., Tollervey, D., 2010. The Final Step in 5.8S rRNA Processing Is Cytoplasmic in Saccharomyces cerevisiae. Mol. Cell. Biol. 30, 976–984. https://doi.org/10.1128/MCB.01359-09

Tishkoff, D.X., Johnson, A.W., Kolodner, R.D., 1991. Molecular and genetic analysis of the gene encoding the Saccharomyces cerevisiae strand exchange protein Sep1. Mol. Cell. Biol. 11, 2593–2608. https://doi.org/10.1128/mcb.11.5.2593-2608.1991

Tomecki, R., Sikorski, P.J., Zakrzewska-Placzek, M., 2017. Comparison of preribosomal RNA processing pathways in yeast, plant and human cells - focus on coordinated action of endo- and exoribonucleases. FEBS Lett. 591, 1801–1850. https://doi.org/10.1002/1873-3468.12682

Trotta, C.R., Miao, F., Arn, E.A., Stevens, S.W., Ho, C.K., Rauhut, R., Abelson, J.N., 1997. The Yeast tRNA Splicing Endonuclease: A Tetrameric Enzyme with Two Active Site

Subunits Homologous to the Archaeal tRNA Endonucleases. Cell 89, 849–858. https://doi.org/10.1016/S0092-8674(00)80270-6

Trotta, C.R., Paushkin, S.V., Patel, M., Li, H., Peltz, S.W., 2006. Cleavage of pre-tRNAs by the splicing endonuclease requires a composite active site. Nature 441, 375–377. https://doi.org/10.1038/nature04741

Tsanova, B., Spatrick, P., Jacobson, A., van Hoof, A., 2014. The RNA exosome affects iron response and sensitivity to oxidative stress. RNA 20, 1057–1067. https://doi.org/10.1261/rna.043257.113

Tsuboi, T., Yamazaki, R., Nobuta, R., Ikeuchi, K., Makino, S., Ohtaki, A., Suzuki, Y., Yoshihisa, T., Trotta, C., Inada, T., 2015. The tRNA Splicing Endonuclease Complex Cleaves the Mitochondria-localized CBP1 mRNA. J. Biol. Chem. 290, 16021–16030. https://doi.org/10.1074/jbc.M114.634592

Tucker, M., Valencia-Sanchez, M.A., Staples, R.R., Chen, J., Denis, C.L., Parker, R., 2001. The transcription factor associated Ccr4 and Caf1 proteins are components of the major cytoplasmic mRNA deadenylase in Saccharomyces cerevisiae. Cell 104, 377–386. https://doi.org/10.1016/s0092-8674(01)00225-2

Upton, J.-P., Wang, L., Han, D., Wang, E.S., Huskey, N.E., Lim, L., Truitt, M., McManus, M.T., Ruggero, D., Goga, A., Papa, F.R., Oakes, S.A., 2012. IRE1α Cleaves Select microRNAs During ER Stress to Derepress Translation of Proapoptotic Caspase-2. Science 338, 818–822. https://doi.org/10.1126/science.1226191

van Dijk, T., Baas, F., Barth, P.G., Poll-The, B.T., 2018. What's new in pontocerebellar hypoplasia? An update on genes and subtypes. Orphanet J. Rare Dis. 13, 92. https://doi.org/10.1186/s13023-018-0826-2

van Hoof, A., Frischmeyer, P.A., Dietz, H.C., Parker, R., 2002. Exosome-mediated recognition and degradation of mRNAs lacking a termination codon. Science 295, 2262–2264. https://doi.org/10.1126/science.1067272

van Hoof, A., Lennertz, P., Parker, R., 2000. Three conserved members of the RNase D family have unique and overlapping functions in the processing of 5S, 5.8S, U4, U5, RNase MRP and RNase P RNAs in yeast. EMBO J. 19, 1357–1365. https://doi.org/10.1093/emboj/19.6.1357

Volanakis, A., Passoni, M., Hector, R.D., Shah, S., Kilchert, C., Granneman, S., Vasiljeva, L., 2013. Spliceosome-mediated decay (SMD) regulates expression of nonintronic genes in budding yeast. Genes Dev. 27, 2025–2038. https://doi.org/10.1101/gad.221960.113

Volmer, R., Ron, D., 2015. Lipid-dependent regulation of the unfolded protein response. Curr. Opin. Cell Biol., Cell regulation 33, 67–73. https://doi.org/10.1016/j.ceb.2014.12.002

Wan, Y., Hopper, A.K., 2018. From powerhouse to processing plant: conserved roles of mitochondrial outer membrane proteins in tRNA splicing. Genes Dev. 32, 1309–1314. https://doi.org/10.1101/gad.316257.118

Wang, V.Y.-F., Jiao, X., Kiledjian, M., Tong, L., 2015. Structural and biochemical studies of the distinct activity profiles of Rai1 enzymes. Nucleic Acids Res. 43, 6596–6606. https://doi.org/10.1093/nar/gkv620

Warner, J.R., 1999. The economics of ribosome biosynthesis in yeast. Trends Biochem. Sci. 24, 437–440. https://doi.org/10.1016/s0968-0004(99)01460-7

Wasmuth, E.V., Lima, C.D., 2012. Structure and activities of the eukaryotic RNA exosome. The Enzymes 31, 53–75. https://doi.org/10.1016/B978-0-12-404740-2.00003-3

Weitzer, S., Hanada, T., Penninger, J.M., Martinez, J., 2015. CLP1 as a novel player in linking tRNA splicing to neurodegenerative disorders. Wiley Interdiscip. Rev. RNA 6, 47–63. https://doi.org/10.1002/wrna.1255

Wek, S.A., Zhu, S., Wek, R.C., 1995. The histidyl-tRNA synthetase-related sequence in the eIF-2 alpha protein kinase GCN2 interacts with tRNA and is required for activation in response to starvation for different amino acids. Mol. Cell. Biol. 15, 4497–4506.

Weskamp, K., Barmada, S.J., 2018. RNA Degradation in Neurodegenerative Disease. Adv. Neurobiol. 20, 103–142. https://doi.org/10.1007/978-3-319-89689-2_5

Wolin, S.L., Maquat, L.E., 2019. Cellular RNA surveillance in health and disease. Science 366, 822–827. https://doi.org/10.1126/science.aax2957

Woolford, J.L., Baserga, S.J., 2013. Ribosome Biogenesis in the Yeast Saccharomyces cerevisiae. Genetics 195, 643–681. https://doi.org/10.1534/genetics.113.153197

Wu, J., Hopper, A.K., 2014. Healing for destruction: tRNA intron degradation in yeast is a two-step cytoplasmic process catalyzed by tRNA ligase Rlg1 and 5'-to-3' exonuclease Xrn1. Genes Dev. 28, 1556–1561. https://doi.org/10.1101/gad.244673.114

Wurm, J.P., Sprangers, R., 2019. Dcp2: an mRNA decapping enzyme that adopts many different shapes and forms. Curr. Opin. Struct. Biol. 59, 115–123. https://doi.org/10.1016/j.sbi.2019.07.009

Xiang, S., Cooper-Morgan, A., Jiao, X., Kiledjian, M., Manley, J.L., Tong, L., 2009. Structure and function of the 5'-->3' exoribonuclease Rat1 and its activating partner Rai1. Nature 458, 784–788. https://doi.org/10.1038/nature07731

Xue, S., Calvin, K., Li, H., 2006. RNA Recognition and Cleavage by a Splicing Endonuclease. Science 312, 906–910. https://doi.org/10.1126/science.1126629

Xue, Y., Bai, X., Lee, I., Kallstrom, G., Ho, J., Brown, J., Stevens, A., Johnson, A.W., 2000. Saccharomyces cerevisiae RAI1 (YGL246c) Is Homologous to Human DOM3Z and Encodes a Protein That Binds the Nuclear Exoribonuclease Rat1p. Mol. Cell. Biol. 20, 4006–4015.

Yang, R., Wek, S.A., Wek, R.C., 2000. Glucose Limitation Induces GCN4 Translation by Activation of Gcn2 Protein Kinase. Mol. Cell. Biol. 20, 2706–2717.

Yang, Xue, Bayat, V., DiDonato, N., Zhao, Y., Zarnegar, B., Siprashvili, Z., Lopez-Pajares, V., Sun, T., Tao, S., Li, C., Rump, A., Khavari, P., Lu, B., 2020. Genetic and genomic studies of pathogenic EXOSC2 mutations in the newly described disease SHRF implicate the autophagy pathway in disease pathogenesis. Hum. Mol. Genet. 29, 541–553. https://doi.org/10.1093/hmg/ddz251

Yang, Xiao-cui, Sun, Y., Aik, W.S., Marzluff, W.F., Tong, L., Dominski, Z., 2020. Studies with recombinant U7 snRNP demonstrate that CPSF73 is both an endonuclease and a 5'-3' exonuclease. RNA rna.076273.120. https://doi.org/10.1261/rna.076273.120

Yokobori, S., Itoh, T., Yoshinari, S., Nomura, N., Sako, Y., Yamagishi, A., Oshima, T., Kita, K., Watanabe, Y., 2009. Gain and loss of an intron in a protein-coding gene in Archaea: the case of an archaeal RNA pseudouridine synthase gene. BMC Evol. Biol. 9, 198. https://doi.org/10.1186/1471-2148-9-198

Yoshihisa, T., 2014. Handling tRNA introns, archaeal way and eukaryotic way. Front. Genet. 5. https://doi.org/10.3389/fgene.2014.00213

Yoshihisa, T., Ohshima, C., Yunoki-Esaki, K., Endo, T., 2007. Cytoplasmic splicing of tRNA in Saccharomyces cerevisiae. Genes Cells Devoted Mol. Cell. Mech. 12, 285–297. https://doi.org/10.1111/j.1365-2443.2007.01056.x

Yoshihisa, T., Yunoki-Esaki, K., Ohshima, C., Tanaka, N., Endo, T., 2003. Possibility of cytoplasmic pre-tRNA splicing: the yeast tRNA splicing endonuclease mainly localizes on the mitochondria. Mol. Biol. Cell 14, 3266–3279. https://doi.org/10.1091/mbc.e02-11-0757

Yoshinari, S., Fujita, S., Masui, R., Kuramitsu, S., Yokobori, S., Kita, K., Watanabe, Y., 2005. Functional reconstitution of a crenarchaeal splicing endonuclease in vitro.

Biochem. Biophys. Res. Commun. 334, 1254–1259. https://doi.org/10.1016/j.bbrc.2005.07.023

Yoshinari, S., Itoh, T., Hallam, S.J., DeLong, E.F., Yokobori, S., Yamagishi, A., Oshima, T., Kita, K., Watanabe, Y., 2006. Archaeal pre-mRNA splicing: A connection to hetero-oligomeric splicing endonuclease. Biochem. Biophys. Res. Commun. 346, 1024–1032. https://doi.org/10.1016/j.bbrc.2006.06.011

Zhang, S.-Y., Clark, N.E., Freije, C.A., Pauwels, E., Taggart, A.J., Okada, S., Mandel, H., Garcia, P., Ciancanelli, M.J., Biran, A., Lafaille, F.G., Tsumura, M., Cobat, A., Luo, J., Volpi, S., Zimmer, B., Sakata, S., Dinis, A., Ohara, O., Garcia Reino, E.J., Dobbs, K., Hasek, M., Holloway, S.P., McCammon, K., Hussong, S.A., DeRosa, N., Van Skike, C.E., Katolik, A., Lorenzo, L., Hyodo, M., Faria, E., Halwani, R., Fukuhara, R., Smith, G.A., Galvan, V., Damha, M.J., Al-Muhsen, S., Itan, Y., Boeke, J.D., Notarangelo, L.D., Studer, L., Kobayashi, M., Diogo, L., Fairbrother, W.G., Abel, L., Rosenberg, B.R., Hart, P.J., Etzioni, A., Casanova, J.-L., 2018. Inborn Errors of RNA Lariat Metabolism in Humans with Brainstem Viral Infection. Cell 172, 952-965.e18. https://doi.org/10.1016/j.cell.2018.02.019

Zhang, Y., Kuster, D., Schmidt, T., Kirrmaier, D., Nübel, G., Ibberson, D., Benes, V., Hombauer, H., Knop, M., Jäschke, A., 2020. Extensive 5'-surveillance guards against non-canonical NAD-caps of nuclear mRNAs in yeast. Nat. Commun. 11, 5508. https://doi.org/10.1038/s41467-020-19326-3

Zheng, D., Chen, C.-Y.A., Shyu, A.-B., 2011. Unraveling regulation and new components of human P-bodies through a protein interaction framework and experimental validation. RNA 17, 1619–1634. https://doi.org/10.1261/rna.2789611

Zheng, S., Vuong, B.Q., Vaidyanathan, B., Lin, J.-Y., Huang, F.-T., Chaudhuri, J., 2015. Non-coding RNA Generated following Lariat Debranching Mediates Targeting of AID to DNA. Cell 161, 762–773. https://doi.org/10.1016/j.cell.2015.03.020

Zuker, M., 2003. Mfold web server for nucleic acid folding and hybridization prediction. Nucleic Acids Res. 31, 3406–3415. https://doi.org/10.1093/nar/gkg595

Zuo, Y., Deutscher, M.P., 2002. The physiological role of RNase T can be explained by its unusual substrate specificity. J. Biol. Chem. 277, 29654–29661. https://doi.org/10.1074/jbc.M204252200

9) Vita

Jennifer E. Hurtig graduated from the College of Wooster in 2017 with a Bachelor of Arts in Biochemistry and Molecular Biology. In the summer of 2016, she was selected for an internship at UT Health Texas Medical Center where she worked under the supervision of James West Ph.D. in the lab of Kevin Morano, Ph.D. In August of 2017 she entered The University of Texas MD Anderson Cancer Center UTHealth Graduate School of Biomedical Sciences. In 2018, the van Hoof lab welcomed her as a fellow yeast bud.